Synthesis of Sterubin, Flavonoid Hybrids, and Curcumin Bioisosteres and Characterization of their Neuroprotective Effects

Synthese von Sterubin, Flavonoid Hybriden und Curcumin Bioisosteren und Charakterisierung ihrer neuroprotektiven Effekte

Doctoral thesis for a doctoral degree
at the Graduate School of Life Sciences,
Julius-Maximilians-Universität Würzburg,
Section Neuroscience
submitted by

Julian Hofmann

from

Steinau an der Straße

Würzburg, 2021

Submitted on: ……

Members of the Thesis Committee

Chairperson: Prof. Dr. Peter Jakob

Primary Supervisor: Prof. Dr. Michael Decker

Supervisor (Second): Prof. Dr. Ulrike Holzgrabe

Supervisor (Third): Prof. Dr. Christian Stigloher

Date of Public Defence: ……

Date of Receipt of Certificates: ……

The presented work has been carried out as a member of the Graduate School of Life Science under the supervision of Professor Dr. Michael Decker at the Chair of Pharmaceutical and Medicinal Chemistry at the Institute for Pharmacy and Food Chemistry of the Julius Maximilian University of Würzburg between May 2018 and December 2021.

List of Publications

Hofmann J.[*]; Fayez, S.[*]; Scheiner, M.; Hoffmann, M.; Oerter, S.; Appelt-Menzel, A.; Maher, P.; Maurice, T.; Bringmann, G.; Decker, M. Sterubin: Enantioresolution and Configurational Stability, Enantiomeric Purity in Nature, and Neuroprotective Activity in Vitro and in Vivo. *Chem. Eur. J.* **2020**, *26* (32), 7299–7308.

Hofmann, J.; Ginex, T.; Espargaró, A.; Scheiner, M.; Gunesch, S.; Aragó, M.; Stigloher, C.; Sabaté, R.; Luque, J.; Decker, M. Azobioisosteres of Curcumin with Pronounced Activity against Amyloid Aggregation, Intracellular Oxidative Stress, and Neuroinflammation. *Chem. Eur. J.* **2021**, *27* (19), 6015–6027.

* These authors contributed equally.

Copyrights

Parts of this work have been published previously and are reproduced, adapted, and/or modified with the permission of:

Hofmann J.; Fayez, S.; Scheiner, M.; Hoffmann, M.; Oerter, S.; Appelt-Menzel, A.; Maher, P.; Maurice, T.; Bringmann, G.; Decker, M. Sterubin: Enantioresolution and Configurational Stability, Enantiomeric Purity in Nature, and Neuroprotective Activity in Vitro and in Vivo. *Chem. Eur. J.* **2020**, *26* (32), 7299–7308.

DOI: 10.1002/chem.202001264

Hofmann, J.; Ginex, T.; Espargaró, A.; Scheiner, M.; Gunesch, S.; Aragó, M.; Stigloher, C.; Sabaté, R.; Luque, J.; Decker, M. Azobioisosteres of Curcumin with Pronounced Activity against Amyloid Aggregation, Intracellular Oxidative Stress, and Neuroinflammation. *Chem. Eur. J.* **2021**, 27 (19), 6015–6027.

DOI: 10.1002/chem.202005263

Declaration of Authorship

Publication: **Hofmann J.**; Fayez, S.; Scheiner, M.; Hoffmann, M.; Oerter, S.; Appelt-Menzel, A.; Maher, P.; Maurice, T.; Bringmann, G.; Decker, M. Sterubin: Enantioresolution and Configurational Stability, Enantiomeric Purity in Nature, and Neuroprotective Activity in Vitro and in Vivo. *Chem. Eur. J.* **2020**, *26* (32), 7299–7308.					
Participated in	**Author Initials,** Responsibility decreasing from left to right				
Study Design Methods Development	JH/SF	GB/MD	PM/TM		
Data Collection	JH/SF	MH/MS/PM	SO		
Data Analysis and Interpretation	JH/SF	GB/MD	PM/TM	SO/AAM	
Manuscript Writing					
Writing of Introduction	JH/SF	GB/MD			
Writing of Materials & Methods	JH/SF	MH			
Writing of Discussion	JH/SF	PM/MH	TM		
Writing of First Draft	JH/SF	GB/MD			

Explanations: shared first authorship

Publication: **Hofmann, J.**; Ginex, T.; Espargaró, A.; Scheiner, M.; Gunesch, S.; Aragó, M.; Stigloher, S.; Sabaté, R.; Luque, J.; Decker, M. Azobioisosteres of Curcumin with Pronounced Activity against Amyloid Aggregation, Intracellular Oxidative Stress, and Neuroinflammation. *Chem. Eur. J.* **2021**, *27* (19), 6015–6027.					
Participated in	**Author Initials,** Responsibility decreasing from left to right				
Study Design Methods Development	JH/JL/MD	TG/RS			
Data Collection	JH	TG	RS/AE	SG	MS/MA
Data Analysis and Interpretation	JH/TG	FJ/MD	RS/AE	CS	
Manuscript Writing					
Writing of Introduction	JH	FJ/TG	MD		
Writing of Materials & Methods	JH	TG	RS		
Writing of Discussion	JH/TG	FJ/MD			
Writing of First Draft	JH				

Explanations: exclusive first authorship

Unpublished manuscript: **Hofmann J.;** Walther R.; Gutmann M.; Decker M. Synthesis and Biological Evaluation of Flavonoid-Cinnamic Acid Amide Hybrids with Distinct Activity in Phenotypic Screening Assays for Neurodegeneration					
Participated in	**Author Initials,** Responsibility decreasing from left to right				
Study Design Methods Development	JH	MD			
Data Collection	JH				
Data Analysis and Interpretation	JH	RW/MG	MD		
Manuscript Writing					
Writing of Introduction	JH	MD			
Writing of Materials & Methods	JH	RW/MG			
Writing of Discussion	JH	MD			
Writing of First Draft	JH				

Explanations: Unpublished manuscript, exclusive first authorship

Publication: **Hofmann J.**; Fayez, S.; Scheiner, M.; Hoffmann, M.; Oerter, S.; Appelt-Menzel, A.; Maher, P.; Maurice, T.; Bringmann, G.; Decker, M. Sterubin: Enantioresolution and Configurational Stability, Enantiomeric Purity in Nature, and Neuroprotective Activity in Vitro and in Vivo. *Chem. Eur. J.* **2020**, *26* (32), 7299–7308.					
Figure	**Author Initials,** Responsibility decreasing from left to right				
1	JH	SF			
2	SF	GB			
3	SF	GB			
4	SF	JH	GB		
5	JH	MD			
6	SF/JH	GB/MD			
7	MH	JH	MD/TG		
8	PM				
Scheme 1	JH	GB			
Scheme 2	JH	GB/MD			
SI-1	SF	GB			
SI-2	SO	AAM			
SI-3	MH	TG			
SI-4	MS	TG			
Scheme SI-1	JH	GB/MD			

Explanations: shared first authorship

Publication: **Hofmann, J.**; Ginex, T.; Espargaró, A.; Scheiner, M.; Gunesch, S.; Aragó, M.; Stigloher, C.; Sabaté, R.; Luque, J.; Decker, M. Azobioisosteres of Curcumin with Pronounced Activity against Amyloid Aggregation, Intracellular Oxidative Stress, and Neuroinflammation. *Chem. Eur. J.* **2021**, *27* (19), 6015–6027.					
Figure	**Author Initials,** Responsibility decreasing from left to right				
1	JH	MD			
2	TG	FJ			
3	JH	CS			
4	TG	FJ			
5	JH	MD			
6	JH	SG	MD		
Table 1	AE	RS			
Table 2	JH	MD			
Scheme 1	JH	MD			
S1	TG	FJ			
S2	TG	FJ			
S3	TG	FJ			
S4	JH	CS			
S5	JH	CS			
S6	JH	SG	MD		
Chromatograms 8a-g	JH	MD			
Table S1	TG	FJ			

Explanations: exclusive first authorship

Unpublished manuscript: **Hofmann J.**; Walther R.; Gutmann M.; Decker M. Synthesis and Biological Evaluation of Flavonoid-Cinnamic Acid Amide Hybrids with Distinct Activity in Phenotypic Screening Assays for Neurodegeneration					
Figure	**Author Initials,** Responsibility decreasing from left to right				
1	JH	MD			
2	JH	MD			
3	JH	MD			
4	JH	MG			
5	JH	MD			
6	JH	MD			
7	JH	RW			
Scheme 1	JH	MD			
Scheme 2	JH	MD			
Table 1	JH	RW			
SI-1	JH	MD			
SI-2	JH	RW			
SI-3	JH	RW			
SI-4	JH	RW			
Scheme SI-1	JH	MD			
Chromatograms 1-6	JH	MD			

Explanations: Unpublished manuscript, exclusive first authorship

The doctoral researcher confirms that he has obtained permission from both the publishers and the co-authors for legal second publication.

The doctoral researcher and the primary supervisor confirm the correctness of the above-mentioned assessment.

Julian Hofmann	07.12.2021	Würzburg	
Doctoral Researcher's Name	Date	Place	Signature
Prof. Dr. Michael Decker	07.12.2021	Würzburg	
Primary Supervisor's Name	Date	Place	Signature

Other Scientific Contributions

Hofmann, J.; Walther R.; Gutmann M.; Holzgrabe U.; Decker M. Flavonoid-Cinnamic Acid Amide Hybrids with Pronounced Activity in Phenotypic Screening Assays Associated with Neurodegeneration. DPhG Annual Meeting, Leipzig (Virtual Meeting), September 28th – October 01st, 2021 (Poster Presentation).

Hofmann J.; Fayez, S.; Scheiner, M.; Hoffmann, M.; Oerter, S.; Appelt-Menzel, A.; Maher, P.; Maurice, T.; Bringmann, G.; Decker, M. Sterubin Enantioresolution and Configurational Stability, Enantiomeric Purity in Nature, and Neuroprotective Activity *in vitro* and *in vivo*. 2nd Autumn School of the M.Sc. “Translational Neuroscience”, Virtual Symposium, October 30th – 31st, 2020 (Poster Presentation).

Hofmann J.; Gunesch S.; Luque F. J.; Stigloher C.; Decker M. Bioisosteres of the Natural Product Taxifolin and their Biological Activity. EUREKA! 14th International GSLS Symposium 2019, Würzburg (Germany), October 09th – 10th 2019 (Poster Presentation).

Hofmann J.; Luque F. J.; Stigloher C.; Decker M. Bioisosteres of the Natural Product Taxifolin and their Impact on Amyloid-β 42 Aggregation and Intracellular Oxidative Stress. DPhG Annual Meeting, Heidelberg (Germany), September 01st – 04th, 2019 (Poster Presentation and Poster Short Talk).

Hofmann J.; Stigloher C.; Decker M. Bioisosteres of the Natural Product Taxifolin and their Impact on Amyloid-β 42 Aggregation and Intracellular Oxidative Stress. GSLS Retreat 2019 Waldmünchen (Germany), May 17th – 19th 2019 (Poster Presentation).

Affidavit

I hereby confirm that my thesis entitled *Synthesis of Sterubin, Flavonoid Hybrids, and Curcumin Bioisosteres and Characterization of their Neuroprotective Effects* is the result of my own work. I did not receive any help or support from commercial consultants. All sources and / or materials applied are listed and specified in the thesis.

Furthermore, I confirm that this thesis has not yet been submitted as part of another examination process neither in identical nor in similar form.

Würzburg,	07.12.2021	
Place	Date	Signature

Eidesstattliche Erklärung

Hiermit erkläre ich an Eides statt, die Dissertation *Synthese von Sterubin, Flavonoid Hybriden und Curcumin Bioisosteren und Charakterisierung ihrer neuroprotektiven Effekte* eigenständig, d.h. insbesondere selbständig und ohne Hilfe eines kommerziellen Promotionsberaters, angefertigt und keine anderen als die von mir angegebenen Quellen und Hilfsmittel verwendet zu haben.

Ich erkläre außerdem, dass die Dissertation weder in gleicher noch in ähnlicher Form bereits in einem anderen Prüfungsverfahren vorgelegen hat.

Würzburg,	07.12.2021	
Ort	Datum	Unterschrift

Acknowledgements/Danksagung

Meine Zeit als Doktorand kommt nun zum Ende und am Schluss möchte mich noch bei einigen bedanken, die mich auf meinem Weg unterstützt und zum Erfolg dieser Arbeit beigetragen haben.

Zunächst vielen Dank an meine Betreuer Prof. Dr. Michael Decker, Prof. Dr. Christian Stigloher und Prof. Dr. Ulrike Holzgrabe für die anregenden Diskussionen in den jährlichen Meetings und die Unterstützung in jeglichen wissenschaftlichen Fragestellungen.

Besonderer Dank an meinen Doktorvater Prof. Dr. Michael Decker für die Möglichkeit diese Arbeit anzufertigen, für die stetige Motivation und das Vertrauen, dass mir im Laufe der Promotion immer stärker entgegengebracht wurde.

Weiterer Dank gilt all meinen Kooperationspartnern, die zum Gelingen der Arbeit beigetragen und mich bei den Veröffentlichungen unterstützt haben. Besonders hervorheben möchte ich an dieser Stelle Prof. Dr. Dr. hc. mult. Gerhard Bringmann und Dr. Shaimaa Fayez für die sehr produktive und lehrreiche Zusammenarbeit im Sterubin Projekt. Des Weiteren Prof. Dr. F. Javier Luque und Dr. Tiziana Ginex für das Verwirklichen des Bioisostere Projektes. An dieser Stelle auch vielen Dank an Prof. Dr. Raimon Sabaté und Dr. Alba Espargaró für die freundliche Aufnahme in ihrem Labor in Barcelona. Für die Unterstützung im dritten Projekt und jeglichen Problemen mit der Zellkultur bedanke ich mich herzlich bei Dr. Markus Gutmann und für die gute Zusammenarbeit in analytischen Fragestellungen vielen Dank an Rasmus Walther. Vielen Dank für diese besondere Zeit an alle ehemaligen und auch aktuellen Mitglieder des Arbeitskreises Decker: Dr. Matze, Dr. Sandra, Dr. Luca, Dr. Matthias, Dr. Christian, Hubert, Philipp, Alex, Thomas, Anna, Diego, Sophie, Eva und Feng. Vielen Dank für die enge Zusammenarbeit, für die offenen Ohren und die schönen Stunden beim Kaffee oder auch Bier trinken.

Ein großes Dankeschön an alle Kollegen in den Arbeitskreisen Holzgrabe, Meinel, Högger, Sotriffer und Scherf-Clavel mit denen man sich rege über Probleme an der LC/MS und auch anderweitig ausgetauscht und unterstützt hat, an das Werkstattteam und Frau Möhler und Frau Weidinger im Sekretariat. Ohne Euch wäre vieles komplizierter gewesen als es teilweise schon war.

Mein tiefster Dank gilt meiner Freundin Franzi, die zwar aktuell den gleichen (Leidens-)Weg durchmacht, aber mich dennoch immer unterstützt, motiviert und geduldig zugehört hat, egal wie viel Stress sie selbst hatte.

Vielen Dank auch ein drittes Mal an meine Familie, meine Eltern Mechthild und Roland sowie mein Tantchen Anette und Onkel Arnold für die Unterstützung auf all meinen Wegen. Ohne euch wäre ich nicht da, wo ich jetzt bin.

Table of content

1. Introduction

1.1 Alzheimer´s Disease and neurodegeneration

According to the World Alzheimer Report 2021, 55 million people worldwide are affected by dementia and about two third of them suffer from Alzheimer´s disease (AD), the most common form of dementia.[1] It is the sixth leading cause of death in the United States and the fifth leading cause of death among the population with the age of 65 and older.[2] AD was firstly described by Alois Alzheimer in 1907 as in illness of the cerebral cortex.[3] The disease progresses over several stages and is thought to begin up to 20 years or more before the first symptoms evolve.[4-9]

The so-called AD continuum is divided into three broad phases: preclinical AD, mild cognitive impairment (MCI), and dementia.[10-13] In the first stage, the disease does not show any symptoms and also in the second stage, MCIs do not interfere with everyday activities and may not be noticed by others than family and friends. The dementia due to AD goes along with language problems and memory loss, difficulties to perform daily activities e.g., clothing, or personal hygiene and in the final stage individuals need around-the-clock care.

Like Parkinson´s disease (PD) or Huntington´s disease, AD is a neurodegenerative disease. Neurodegeneration is a general term, which describes pathological processes leading to neuronal damage and the loss of neurons.[14] Neurodegeneration is driven by several factors including oxidative stress, loss of neurotrophic support, alternations in glucose metabolism, inflammation, and alterations in protein processing.[15-16] The best-known proteins in relation to AD and major hallmarks of the disease are abnormal aggregation of the β-amyloid peptide (Aβ) and tau-protein.[17] Both proteins will be discussed in more detail later on. The pathophysiological changes in the brain occur also while aging, making age besides genetics the greatest risk factor for AD.[18-19]

The temporal sequence and the complex interplay between the different contributors to AD and neurodegeneration is still under discussion and a parallel occurrence of the main events is likely to cause the disease. Therefore, it becomes evident, that addressing only one target within this intertwined network of pathologies of AD is unlikely to alter the disease progression significantly (Fig. 1).

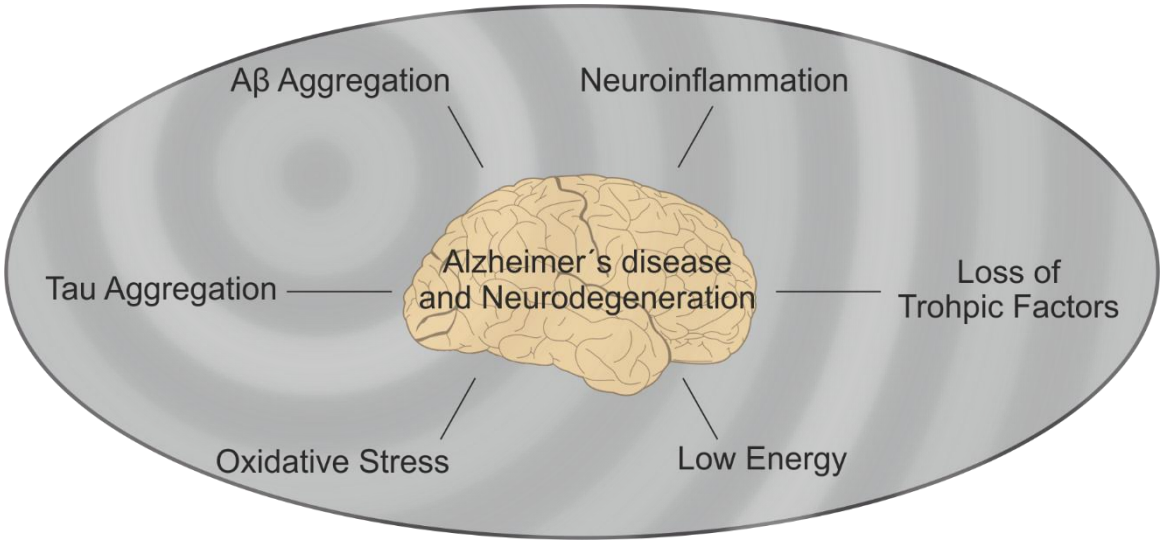

Figure 1: Overview of different AD and neurodegeneration pathologies.

1.2 Amyloid β and Tau Hypothesis

1.2.1 Amyloid β

The probably best-known hallmark of AD is the deposition of senile plaques (SP), which were already described by Alois Alzheimer.[3] SP are associated with the aggregation and deposition of the peptide amyloid-β (Aβ).[20] Aβ also exists in healthy individuals, but its physiological function of is poorly understood.[21] Under normal conditions, the processing of the transmembrane polypeptide amyloid precursor protein (APP) is regulated by α-, β-, and γ-secretase[22] and cleavage products are rapidly degraded.[23] However, miscleavage of APP and insufficient clearance of Aβ results in formation of neurotoxic oligomers.[24]

The amyloid cascade hypothesis was established in 1992[25-28] and claims Aβ as the initial cause of AD followed by a sequence of pathogenic events: microglial and astrocytic activation, disturbed neuronal homeostasis and oxidative injury, altered kinase and phosphatase activities leading to neurofibrillary tangles (NFTs), widespread neuronal and synaptic dysfunction, neuronal loss and in the end dementia.[29] While there is general agreement of the single events within the amyloid cascade and the connection to AD and a large acceptance of this hypothesis supported by genetic and biochemical data, the presence of Aβ plaques in healthy individuals, the uncertain nature of the pathogenic amyloid species and repeated failure of therapeutics targeting Aβ inconsistent with the hypothesis.[30-31]

With a long list of failed drugs targeting Aβ aggregation (tramiprosate[32], tarenflurbil[33], semagacestat[34]) or Aβ clearance (bapineuzumab[35], solanezumab[36]) and the controversial approval of aducanumab[37-38], the one-target strategy for AD was unsuccessful so far. Therefore, a holistic strategy addressing multiple factors of the disease is needed for modifying the disease.

1.2.2 Tau-Protein

Closely related to the Aβ hypothesis and another prominent hallmark of AD are NFTs, which consist of hyperphosphorylated tau protein.[39] The biochemical role of tau is the stabilization of microtubules, particularly in axons.[40] Tau is also involved in neuronal maturation and regulation of synaptic functions.[41-42] Native tau is unfolded, however, abnormal posttranslational modifications mostly represented by hyperphosphorylation lead to aggregation[43-45], which goes a long with impaired axonal transport, synaptic loss and several other factors like oxidative stress and inflammation and ultimately cognitive impairment.[39] Evidence in literature suggests that Aβ oligomers are upstream of NFTs in AD pathogenesis, nevertheless, this is controversially discussed and studies suggest crosstalk between Aβ and tau. Some studies even suggest, these proteins act separately.[17, 46-50]

1.3 Phenotypic Screening reflecting different pathologies of AD

Within multiple approaches for drug discovery the most important are the single target paradigm and phenotypic screening.[15] Addressing one single molecular target in the context of neurodegeneration and AD becomes very difficult if not impossible, because the understanding of the disease is still incomplete and there is no well-validated target yet.[51]

All single target-based efforts have failed in the past.[15] Therefore, the phenotypic screening approach aims on different aspects of AD and reflects single pathological events in cell-based assays with the aim to identify compounds with a pleotropic effect, which address several pathways in parallel.[52] The phenotypic screening assays described below were carried out within this work and should not be considered as a complete set for phenotypic screening. Every assay related to neurodegeneration and AD would gain additional information about the behavior of a desired compound and several additional assays and cell lines are already in use like the PC12 cell differentiation assay[53] or the Aβ expressing MC65 cells.[54]

1.3.1 Oxytosis/Ferroptosis

Oxidative stress describes the imbalance between pro- and antioxidants in cell homeostasis, resulting in the accumulation of reactive oxygen species (ROS) and a number of downstream events, which are associated with cell death and are thought to be driver of synaptic loss and the disease progression of AD.[55-56] A pathway, which is very well studies in this regard is the oxytosis/ferroptosis pathway (Fig. 2). The oxytosis/ferroptosis pathway is a form of oxidative stress-induced programmed cell death showing the morphology of necrosis[57] and biochemical characteristics of apoptosis.[58] Glutamate toxicity was first discovered in 1989[59] and the term oxytosis was established in 2001.[60] Ferroptosis was described over 10 years later[61] and shows similar characteristics to oxytosis, why oxytosis/ferroptosis pathway is probably a more appropriate name for it.[62] The oxytosis/ferroptosis can be assayed in the murine neuronal cell line HT22, a subclone of the hippocampal cell line HT4.[63] The initial step in this pathway is the inhibition of the glutamate/cystine antiporter X_c^- by an excess of glutamate[59], the small molecule erastin[61] or sulfasalazine.[64] Cystine is the oxidized form of cysteine, the rate-limiting amino acid for the production of the tripeptide glutathione (GSH), a key player in cellular redox homeostasis.[65] Hence, the depletion of GSH leads after 6-8 h to an exponential increase in ROS.[66] It is important to note, that high levels of ROS do not lead directly to cell death, however ROS activates further cascades, which participate in cell death.[67] GSH-depletion not only results in increased ROS, but it also results in decreased activity of the GSH dependent enzyme glutathione peroxidase 4 (GPx4).[68] GPx4 reduces lipid hydroperoxides[69] and experimentally, the inhibition of GPx4 is induced by the compound RSL3.[70] Depletion of GSH as well as GPx4 leads to increased lipid peroxidation due to the activation of 12/15 lipid oxygenase (12/15 LOX)[68, 71] and it is still under discussion if the peroxidation in the oxytosis/ferroptosis pathway leads to cell death or is a result of cell death.[72-74] Within the time frame of ROS accumulation, GSH depletion and lipid peroxidation (6-8 h after glutamate treatment), cyclic guanosine monophosphate (cGMP) levels rise, which is mechanistically connected to calcium influx, a requirement for cell death via oxytosis/ferroptosis.[59, 71, 75] Increased Ca^{2+} levels result in the release of apoptotic factors.[76-77] The features of the oxytosis/ferroptosis pathway are observed in neurodegeneration and AD and recent studies could also link amyloid toxicity to the oxytosis/ferroptosis pathway.[78] This close relationship shows the relevance of the oxytosis and ferroptosis assay as laboratory tool for drug screening. The role of every single event of this cascade in context of neurodegeneration and AD is exhaustively discussed in a recent review by Maher et al.[67]

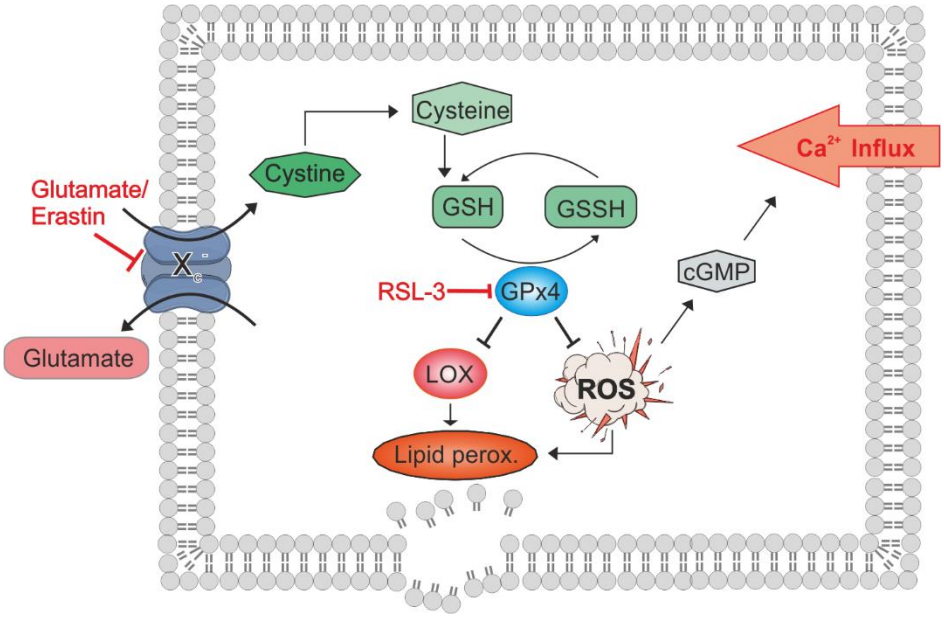

Figure 2: Oxytosis/Ferroptosis pathway. Glutamate and cystine are transported via the X_c^- antiporter. Cystine is converted in cysteine, the rate-limiting amino acid for production of GSH. GSH and GPx4 prevent lipid peroxidation by LOX and ROS. The X_C^- inhibitors as well as the GPx4 inhibitor RSL-3 cause intracellular ROS overproduction, which is besides lipid peroxidation linked to rise of cGMP levels. Elevated cGMP levels are connected to Ca^{2+} influx and cell death.

1.3.2 ATP-depletion

Age is the major risk factor for AD[18-19], therefore aging processes have to be considered in studies related to neurological disorders.[79-80] During aging and also observed in AD, energy metabolism changes, the mitochondrial activity is reduced and consequently adenosine triphosphate (ATP) levels decrease.[81-83] Additionally, it could be shown, that hypoglycaemia impairs cerebral function and cognition.[84] Therefore, compounds which maintain ATP levels are considered to act neuroprotective. The ischemia of ATP can be induced *in vitro* with the well-known irreversible inhibitor iodoacetic acid (IAA) of the glycolytic enzyme glyceraldehyde 3-phosphate dehydrogenase (GAPDH) and is applied within the phenotypic screening approach in HT22 cells.[85]

1.3.3 Neuroinflammation

Emerging evidence suggest an important role of inflammatory processes in the pathogenesis and the progression of AD.[86] A key player in neuroinflammation are microglia, the resident phagocytes of the central nervous system.[87] Microglia are important for pathogen defense[87], as well as for the maintenance and protection of synapses[88] e.g., by the release of neurotrophic factors.[89] Activated microglia initiate an innate immune response leading to

neuroinflammation, which is intended to be protective and beneficial for repairing tissue damage[90], however, a chronic inflammatory response can contribute to neurodegeneration.[91] Chronic inflammation is mediated by cytokines and chemokines.[92-93] The relevance of neuroinflammation in AD can be shown e.g., by elevated levels of the proinflammatory cytokines tumor necrosis factor-alpha (TNF-α) and interleukin 6 (IL-6).[94-96] One laboratory tool to study inflammatory processes is the murine microglia cell line BV-2. The treatment of BV-2 cells with bacterial lipopolysaccharide (LPS) leads to an increased release of nitrogen monoxide (NO), proinflammatory cytokines and several other factors contribution to neuroinflammation and finally neurodegeneration.[97]

1.4 Flavonoids

1.4.1 Chemistry of Flavonoids

Records of the first use of plants for medical purposes are described in the Ebers Papyrus of the Ancient Egypt in 2900 B.C..[98] Plants produce natural products, which are secondary metabolites and usually not important for plant growth or reproduction.[99] Natural products and their derivatives have provided a source for the development of new drugs for a long time[100] and still today it is estimated, that ~25% of all prescribed drugs are derived from secondary plant metabolites.[101] Among a very large number of different natural products is the class of flavonoids. Flavonoids are polyphenolic phytochemicals which can be found in fruits, wine, tea, and seeds. Many studies investigated the pleiotropic effect of flavonoids on neurons and cognition, making them an interesting compound class in the context of neurodegenerative diseases.[102] Chemically, flavonoids consist of a flavan backbone and the major group can be subdivided into six groups: flavanonols, flavonols, flavanones, flavones, flavanols and anthocyanidins (Fig. 3).[103]

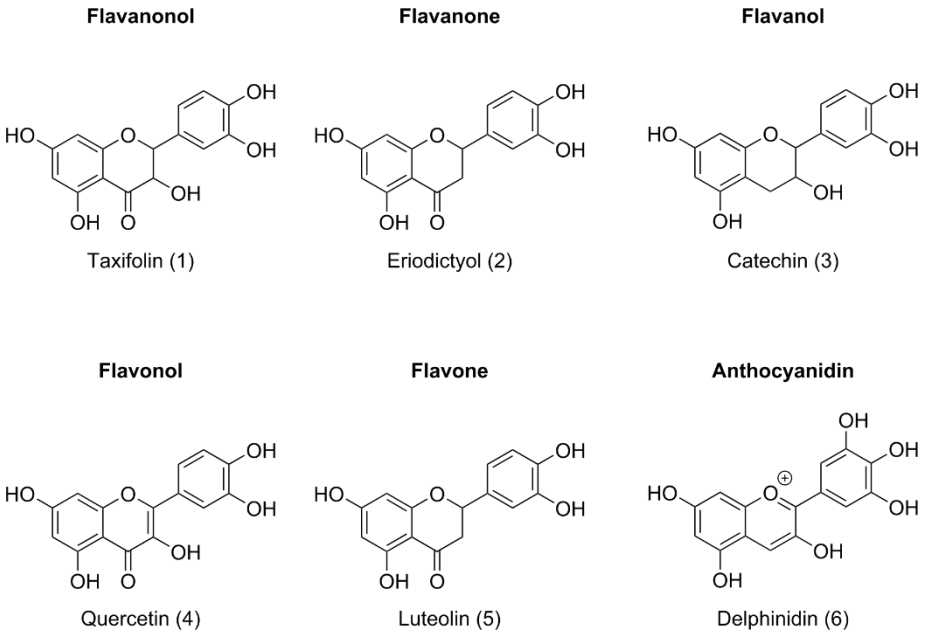

Figure 3: Structure of taxifolin (1), eriodictyol (2), catechin (3) quercetin (4), luteolin (5), and delphinidin (6) as representatives of the major subgroups of flavonoids.

The most important synthetic approach towards different kind of flavonoids is the condensation of 2-hydroxyacetophenones with benzaldehydes resulting in chalcones, which can be cyclized under basic or acidic conditions to the respective flavonoid (Fig. 4).[104]

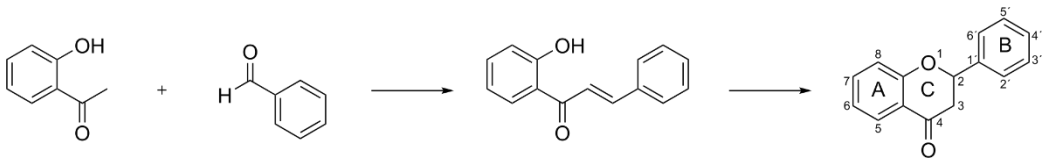

Figure 4: General synthetic approach towards flavonoids.

1.4.2 Flavonoids in the context of neurodegeneration and AD

Epidemiological studies suggest a beneficial impact of flavonoids, especially flavonols, on AD and related dementia[105-106] as well as on Parkinson´s Disease.[107] The epidemiological studies can be supported by countless studies of single flavonoids or plant extracts containing flavonoids as major ingredient on different pathways related to oxidative stress, inflammation, and neurodegeneration. The extensively studied flavonol quercetin for example reduces Aβ toxicity in the neuronal cell line PC12[108], decreases oxidative stress by increasing GSH levels as well as activation of the anti-oxidative glyoxalase pathway.[109] Quercetin also reduces levels of the inflammation marker TNFα and IL-6.[110] Dihydroquercetin, also known as taxifolin, is mitochondrial protective, anti-oxidative, and counteracts Aβ oligomerization.[111] There are also reports on the beneficial effects of luteolin[102], fisetin[112] and eriodictyol[113] in the context of AD and neurodegeneration and the list could be continued, however, those flavonoids are most relevant in context of this work.

Despite the positive effects described for flavonoids they have poor pharmacokinetics and are suspected for low druggability.[114] Flavonoids have poor water solubility and depending on the distinct structure they are poorly bioavailable.[115-116] Flavonoids are rapidly metabolized via first-pass Phase II metabolism[117] and also their ability to reach the central nervous system and cross the blood brain barrier (BBB) is questioned.[118] On the one hand there are reports on flavonoids of blueberry extracts, which could not be found enriched in rat brains after chronic consumption and therefore do not cross the BBB,[119] on the other hand the flavanone naringenin[120] and flavanol (-)-epigallocatechin[121] are penetrating the BBB.

However, many flavonoids, inter alia, luteolin, fisetin and quercetin, have shown disease modifying potential within animal models of AD and PD.[122] One encouraging example of natural products in the context of dementia is the leaf extract of *Ginkgo biloba* (EGB761). It contains glycosides of quercetin, kaempferol, and isorhamnetin and those are with 24% of the total wight the main component of the extract.[123] Several double-blinded, randomized placebo-controlled clinical trials have shown the efficacy of EGb761 against dementia.[124]

2. Scope and Objectives

As highlighted in the introduction, AD is a complex multifactorial disease, and the single-target approach did not lead to a treatment or drug to alter the progression of AD. Natural products hold a special interest as disease modifying agents in the context of neurodegeneration and AD. The scope of this work can be divided into three parts which contained the synthesis and biological evaluation of:

- the flavanone sterubin,
- flavonoid cinnamic acid amide hybrid compounds,
- and bioisosteric compounds of the natural product curcumin.

Sterubin is a known flavanone of the plant *Eriodictyon californicum* and was found to be a very potent neuroprotectant within the screening of a commercial library of plant extracts.[113] The plant extracts were firstly screened in the oxytosis assays and positive hits were further characterized in phenotypic screening assays introduced above. Sterubin carries a stereogenic center at C-2 and the objective within this work was to study the impact of the stereochemistry on the biological activity. Additionally, sufficient amounts of the compound were accessible by synthesis for characterization of disease-modifying effects in an AD mouse model.

Previous studies have shown the drastical increase of the neuroprotective properties of the flavonolignan silibinin[125] or the flavanonol taxifolin[126] by esterification of position 7 with cinnamic acid. To further increase the neuroprotective properties of this kind of compounds, taxifolin was exchanged by flavonoids known to be more active in the phenotypic screening assays than taxifolin. For better druggability, the ester was replaced by an amide, which is more stable towards hydrolysis and finally, the influence of a double bond within the C-ring of the flavonoids was assessed.

The third part comprises the design, synthesis, characterization within the phenotypic screening approach and the influence on aggregation of Aβ and tau by bioisosteres of the natural product curcumin.

3. Sterubin: Enantioresolution and Configurational Stability, Enantiomeric Purity in Nature, and Neuroprotective Activity in Vitro and in Vivo

Chemistry
A European Journal

Chemistry Europe
European Chemical Societies Publishing

Full Paper | Open Access

Sterubin: Enantioresolution and Configurational Stability, Enantiomeric Purity in Nature, and Neuroprotective Activity in Vitro and in Vivo

Julian Hofmann, Dr. Shaimaa Fayez, Matthias Scheiner, Dr. Matthias Hoffmann, Dr. Sabrina Oerter, Dr. Antje Appelt-Menzel, Dr. Pamela Maher, Dr. Tangui Maurice, Prof. Dr. Gerhard Bringmann, Prof. Dr. Michael Decker

First published: 02 May 2020 | https://doi.org/10.1002/chem.202001264 | Citations: 4

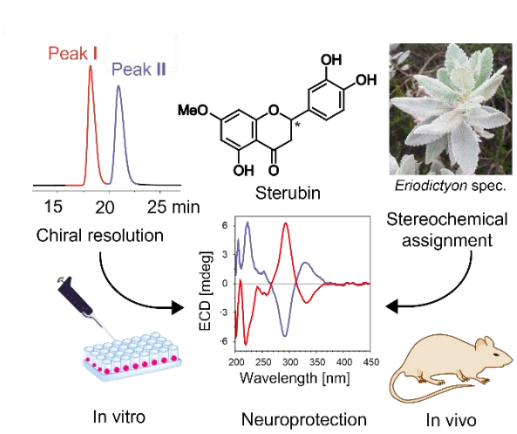

The content of this chapter was previously published and adapted with the permission of Wiley-VCH GmbH.

Hofmann J.*; Fayez, S.*; Scheiner, M.; Hoffmann, M.; Oerter, S.; Appelt-Menzel, A.; Maher, P.; Maurice, T.; Bringmann, G.; Decker, M. Sterubin: Enantioresolution and Configurational Stability, Enantiomeric Purity in Nature, and Neuroprotective Activity in Vitro and in Vivo. *Chem. Eur. J.* **2020**, *26* (32), 7299–7308.

* These authors contributed equally.

Author contributions:

J. Hofmann under supervision of Prof. Dr. Michael Decker designed and synthesized the compounds and performed the biological experiments.

Dr. S. Fayez under supervision of Prof. Dr. Gerhard Bringmann performed extraction of *E. californicum*, chiral resolution of sterubin and HPLC analysis of cell samples.

M. Scheiner and Dr. M. Hofmann under supervision of Dr. T. Maurice performed *in vivo* studies in memory impaired mice.

Dr. Sabrina Oerter and Dr. A. Appelt-Menzel performed toxicity experiments.

Dr. P. Maher performed *in vivo* studies in healthy mice.

3.1 Introduction

Over the past few decades, numerous plant-derived natural products have been investigated for their activities against neurodegenerative hallmarks, including the reduction of oxidative stress, Aβ aggregation, and neuroinflammation.[127] Especially flavonoids hold a huge interest in this regards due to their pleiotropic effects.[52, 128] Recently, Fischer et al. have investigated a plant extract library with a history of use in traditional medicine obtained from Caithness Biotechnologies (Leicester, UK) in age associated phenotypic screening for AD drug candidates.[113] This included the extract of *Eriodictyon californicum*, also known as Yerba santa meaning the "sacred herb". Yerba santa has long been used for medicinal purposes by native inhabitants of California, where the plant is indigenous.[129] The leaves contain different flavonoids (Fig. 5), which are known for their anti-inflammatory acitivites.[130] The study assigned sterubin as the most active compound in the extract of *E. californicum*, showing a remarkably higher *in vitro* activity than the co-existing flavonoids eriodictyol (**2**) or homoeriodictyol (**8**).[113] Sterubin (**7**) is also a known antagonist for the bitter taste receptors T2R[131], why it is used as ingredient in food and pharmaceuticals as bitter-masking agent.[132] The T2R receptor is also present in the brain[133], where its function is presently unknown. Sterubin (**7**) is very well characterized within multiple *in vitro* assays related to neurodegeneration, however, the chirality of sterubin was not taken into consideration making it unclear, which or if a single enantiomer was responsible for the activity. Moreover, nothing has been reported on the *in vivo* activity of sterubin in an AD model so far.

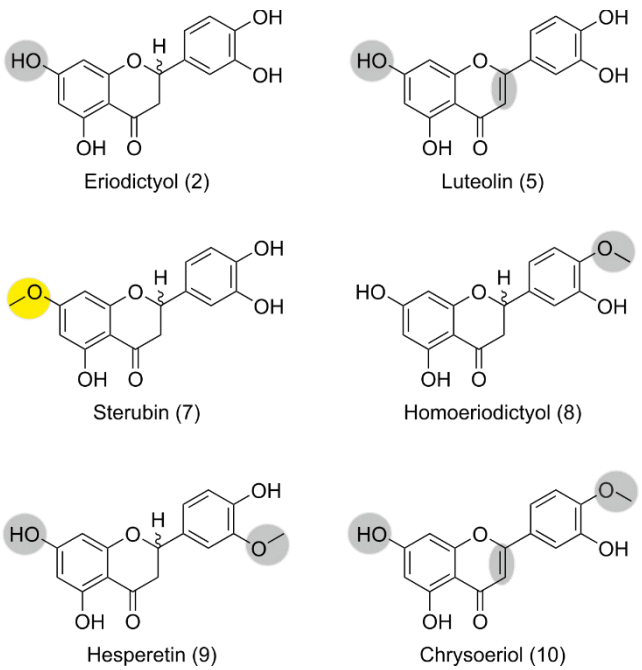

Figure 5: Flavonoids of *E. californicum*: Eriodictyol (**2**), luteolin (**5**), sterubin (**7**), homoeriodictyol (**8**), hesperetin (**9**), chrysoeriol (**10**). Structural differences to sterubin (7-OMe, yellow) are highlighted in grey.

3.2 Chemistry

3.2.1 Synthesis of sterubin and dehydrosterubin

Efforts on the synthesis of flavonoids have a long tradition, and many synthesis procedures are known. The most important for laboratory practice is the condensation of a C_6C_2 unit (mostly represented by a 2-hydroxyacetophenone) and a C_6C_1 unit (represented by an aromatic aldehyde).[104] The synthesis of the acetophenone started with methylation of phloroglucinol (**11**) followed by acetylation and methoxymethyl (MOM) protection of the free hydroxy groups. Phloroglucinol is indeed also an important building block for the A ring of flavonoids in the biosynthesis of plants.[134] For the C-ring, commercially available 3,4-dihydroxybenzaldehyde (**15**) was also MOM-protected before the condensation with acetophenone (**14**) to form the respective chalcone (**17**). Concomitant MOM deprotection and ring closure was achieved by heating compound **17** in 10% $HCl_{(aq.)}$ in MeOH, followed by treatment with sodium acetate to give racemic sterubin (**7**). Dehydrosterubin (**20**), also named hydroxygenkwanin, was needed as reference compound later on. After acetylation of sterubin, dehydrogenation with *N*-bromosuccinimide (NBS) in the presence of catalytic amounts of benzoyl peroxide (BPO) gave the respective dehydro compound. Deprotection was accomplished in 6 M $HCl_{(aq.)}$ in acetonitrile, resulting in dehydrosterubin (**20**).

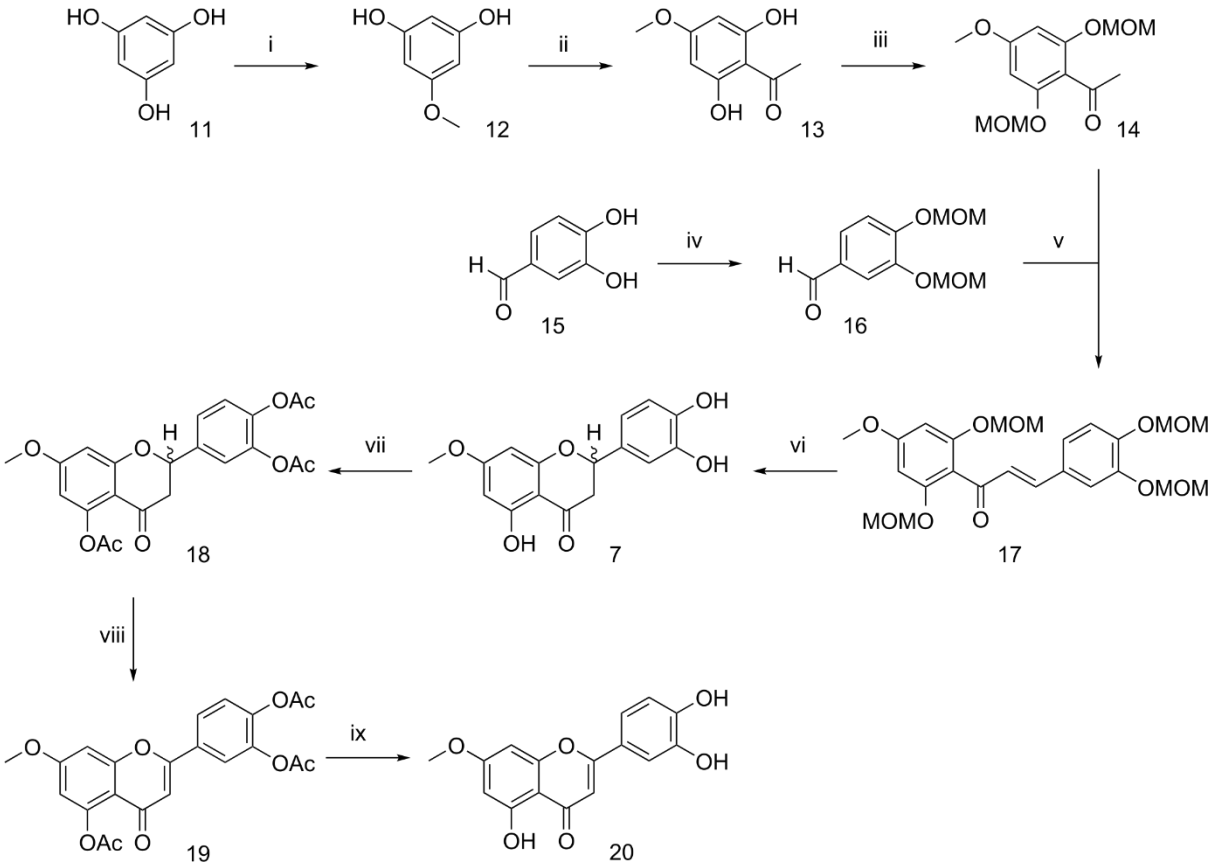

Figure 6: Synthesis of sterubin (**7**) and hydroxygenkwanin (**20**): Reagents and conditions: i) K_2CO_3, Me_2SO_4, acetone, 55 °C, 16 h (82%); ii) CH_3COCl, $AlCl_3$, CH_2Cl_2, 0 °C to r.t., 16 h (54%); iii) NaH, MOM-Cl, DMF, 0° to r.t., 16 h (90%); iv) K_2CO_3, MOM-Cl, acetone, r.t., 16 h (96%); v) KOH, EtOH, 0° to r.t., 16 h (85%); vi) 1. 10% HCl in MeOH, 45 °C, 30 min., 2. NaOAc, MeOH, reflux, 3 h (55%); vii) Ac_2O, I_2, r.t., 2 h (70%); viii) NBS, BPO, $CHCl_3$, reflux, 2 h (63%); ix) 6M HCl, MeCN, reflux, 1.5 h (50%).

3.2.2 Resolution of sterubin enantiomers and configurational assignment

The synthetic racemate of sterubin was successfully resolved on a ChiralPak IA® column (10 x 25 mm, 5 µm) using gradient elution with initial condition from 32% B to 60% B in 29 min and a flow rate of 6 mL/min, where B is 90% acetonitrile in water with 0.05% TFA as a buffer (Fig 7A). Maximum absorption and peak detection were achieved using a PDA detector at λ = 290 nm.

Next, the absolute configuration of the two resolved peaks was assigned online, by HPLC-ECD coupling.[135] By measurement at a single wavelength, 290 nm, the chiroptically opposite behavior of the two peaks was clearly observed (Fig 7B). This was corroborated by the full online ECD spectra showing a first, negative couplet at 330 nm (Peak **I**) and a second, positive one at 290 nm (Peak **II**) for the fast enantiomer and an opposite curve for the slower peak (Fig 7C). The assignment of the two peaks was accomplished by comparison of the ECD

spectra of the two enantiomers with that of the closely related *S*-configured flavanone glycoside hesperidin (**21**) (Fig 7D).[136] The ECD curve of peak **II** showed a good match with the spectrum of **21**, hence the slower enantiomer was *S*-configured. For the faster eluting peak **I** virtually opposite spectra were detected, consequently it is the (*R*)-enantiomer.

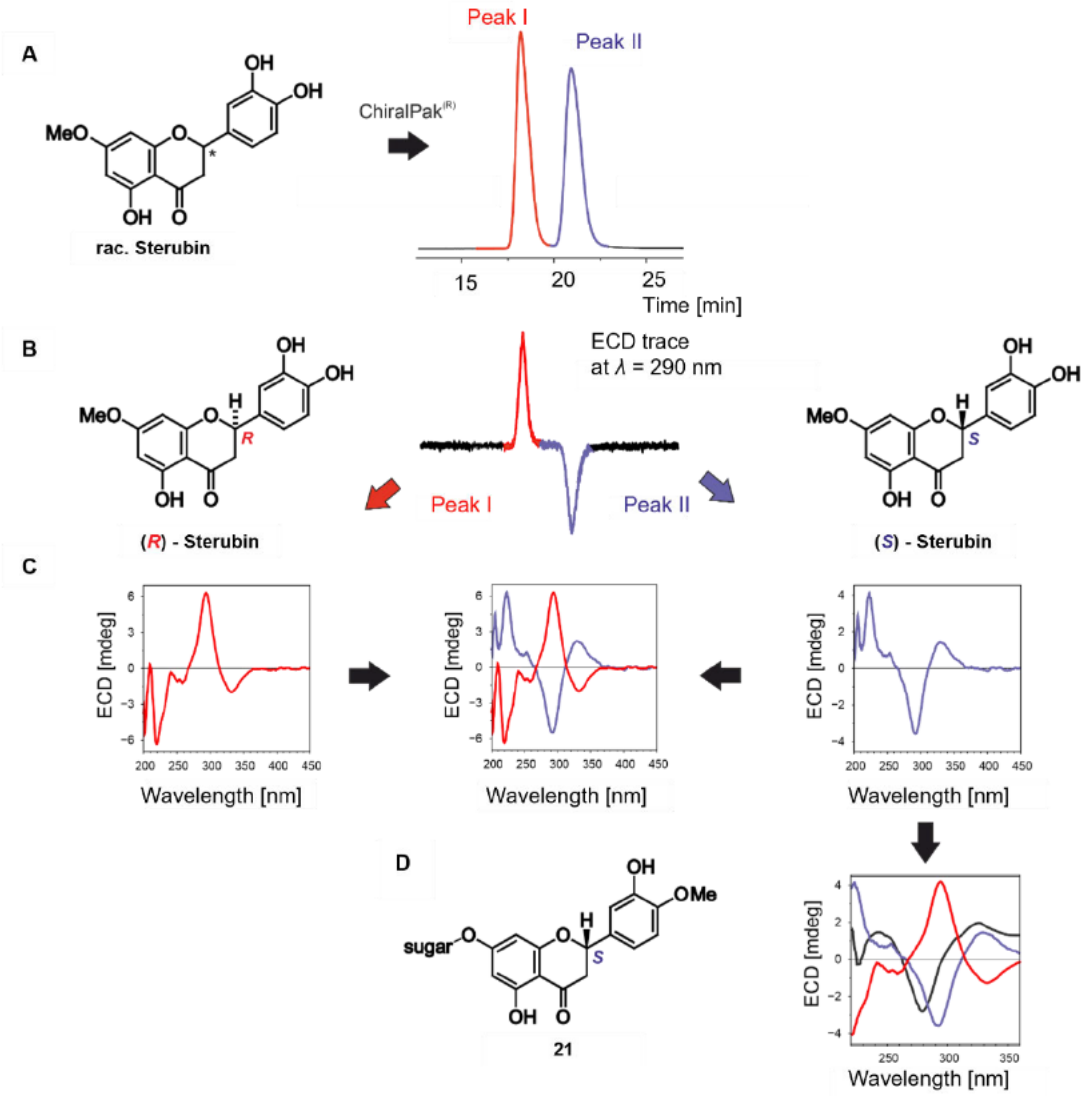

Figure 7: (A) Enantiomeric resolution of racemic sterubin on a ChiralPak IA® column; (B) ECD trace (recorded at λ = 290 nm); (C) online LC-ECD spectra of the two sterubin enantiomers; (D) configurational assignment of the two enantiomers by comparison of their online ECD curves with the offline spectrum reported for the closely related, and configurationally known flavanone glycoside hesperidin (**21**). Sugar = rutinose.

3.2.3 Stability of the pure enantiomers and assignment of enantiomeric purity in *E. californicum*

The pure enantiomers were kept dissolved in methanol at room temperature and the solution was monitored for racemization by HPLC on a ChiralPak IA® column after 2, 20, and 44 h. Under the applied conditions, the two enantiomers proved to be configurationally fully stable over the whole time as seen in figure 8 A-C.

The first isolation of sterubin from *E. californicum* was described by Johnson in 1983.[137] However, nothing was reported regarding enantiomeric purity of sterubin in nature. The most flavonoids produced by plants are in the respective (*S*)-conformation.[138] To investigate the absolute configuration and the enantiomeric purity of sterubin (**7**) in *E. californicum*, dried leaves of the plant were extracted in ethyl acetate assisted by ultrasonication for 30 min at room temperature. Sterubin and related flavanones were enriched by precipitation from the ethyl acetate crude extract after addition of n-hexane. The resulting precipitate was filtered, dissolved in methanol, and injected on a ChiralPak IA® column (Fig. 8E). Spiking experiments with the synthetic racemate of sterubin revealed an increase in the peak intensity of the *S*-enantiomer (Fig 8F), showing that the plant contained sterubin in an enantiomerically pure form as its (*S*)-enantiomer. No racemization had occurred during the extraction procedure, while extraction under reflux conditions as described in the literature[132] can lead to racemization.

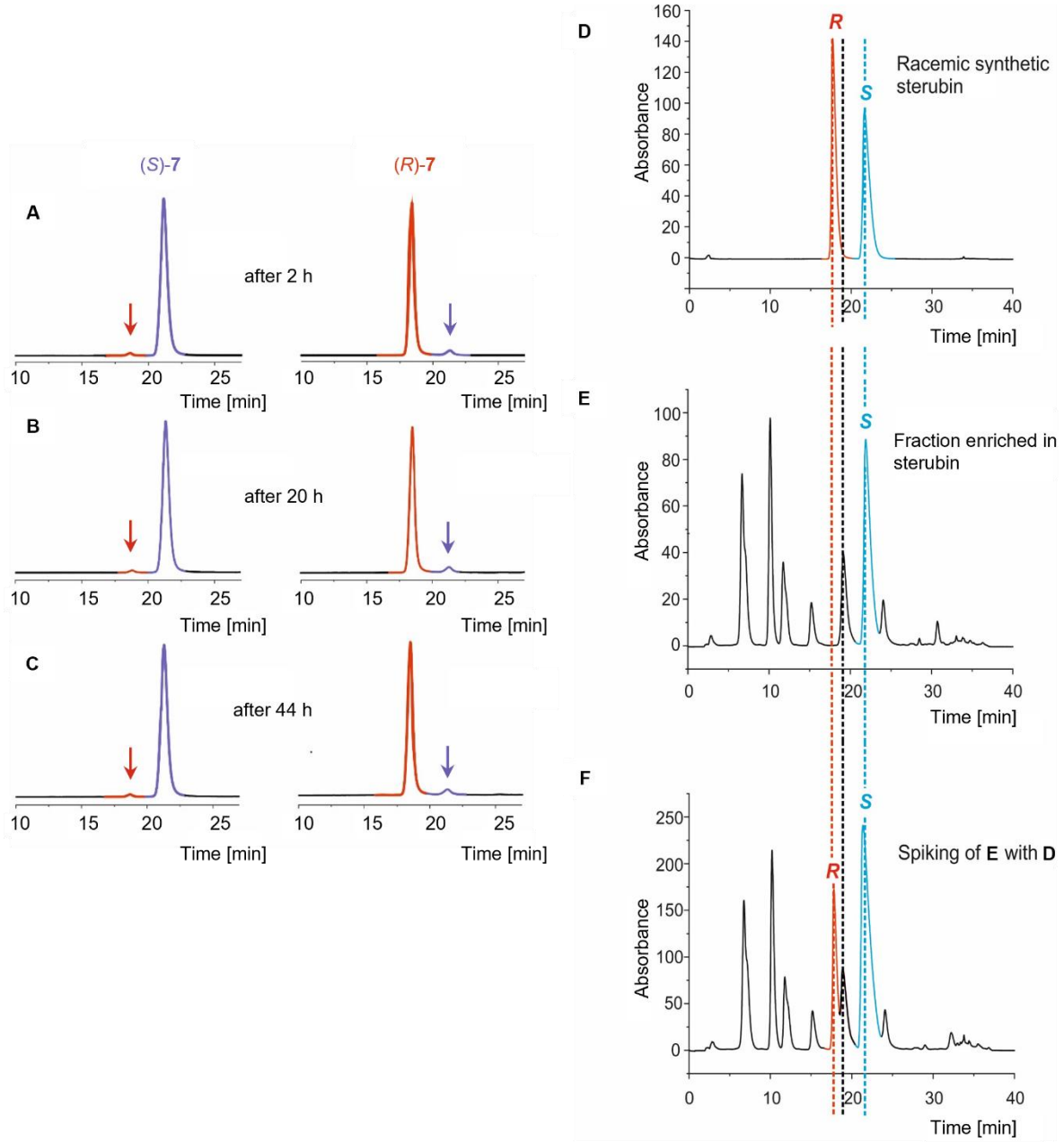

Figure 8: Stability studies on the (*R*)- and (*S*)-enantiomers of sterubin (A-C) and chromatograms of synthetic racemic sterubin (D), *E. californicum* extract containing sterubin (E), and coelution of racemic sterubin with the sterubin containing *E. californicum* extract on a ChiralPak IA® column. (*R*)- and (*S*)-sterubin were configurationally stable over the entire 44 h. The arrows indicate the expected sites of the respective minor enantiomer. Chromatogram F shows an increased peak intensity of the (*S*)-enantiomer evidencing that sterubin is produced in an enantiopure *S*-form in *E. californicum*.

3.3 Biology

3.3.1 Neuroprotection in HT22 cells

It is widely known that enantiomers of chiral compounds can have significant impact on their biological activity.[139] Therefore, the pure enantiomers were tested for their activity in the oxytosis assay. Like described before, an extracellular excess of glutamate leads to an oxidative stress cascade resulting in cell death.[60] The pure enantiomers of sterubin as well as the synthetic racemic mixture were investigated in the oxytosis assay to identify possible differences in activity between the stereoisomers. The flavonol quercetin served as a positive control at a high concentration (25 µM) (Fig. 9). Unexpectedly, no difference in activity was observed between the racemic mixture and any of the pure enantiomers. All of them provided significant neuroprotection at concentrations from 2.5 µM to 10 µM, which even exceeded that of the positive control quercetin at a concentration of 5 µM. The lack of a difference in bioactivity between the pure enantiomers (and between them and the racemic mixture) raised the question whether the pure enantiomers might possibly undergo racemization upon contact with cells or even upon exposure to the culture medium, in contrast to their proven configurational stability in methanol (see above).

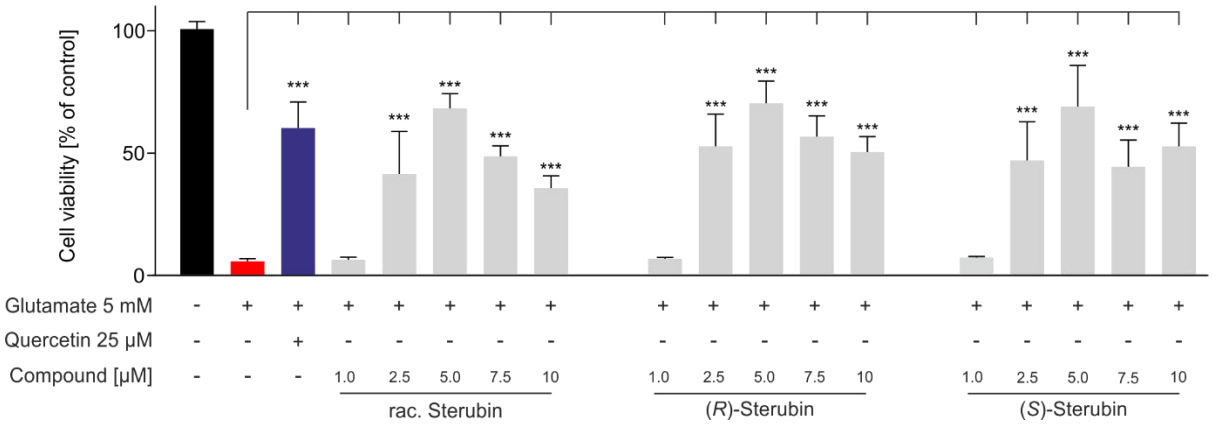

Figure 9: HT22 cells were treated with 5 mM glutamate (red) to induce oxytosis. Quercetin (blue) served as a positive control, racemic sterubin, (*S*)-sterubin, and (*R*)-sterubin showed the same neuroprotective efficacy. Data are presented as means ± SEM of three independent experiments and results refer to untreated control cells (black). Statistical analysis was performed using One-Way ANOVA followed by Dunnett's multiple comparison posttest using GraphPad Prism 5 referring to cells treated with 5 mM glutamate. Level of significance: *** $p < 0.001$.

3.3.2 Cellular Uptake and Racemization

Previous studies by Vrba et al.[140] and Gunesch et al.[126] observed the formation of dehydrogenated products of hybrid compounds combining the flavonoid taxifolin and polyphenolic acids in macrophages (RAW264.7) or microglia cells (BV-2). If this is also the case for sterubin, this would cause a loss of the stereogenic center at C-2 and explain the same activities found for (*R*)- and (*S*)-sterubin. Another explanation would be racemization upon contact with cells or in cell culture medium. Therefore, cellular uptake experiments in microglial BV-2 cells and stability measurements in cell culture medium were performed. BV-2 cells were treated with 50 µM (*R*)-sterubin and incubated for 2 h, 4 h or lysed immediately. Lysates were analyzed by HPLC/UV and also on a chiral-phase column. While no conversion of sterubin to dehydrosterubin could be detected (Fig. 10A), HPLC on a chiral stationary phase revealed rapid racemization in the cell culture medium even without the presence of cells (Fig. 10B).

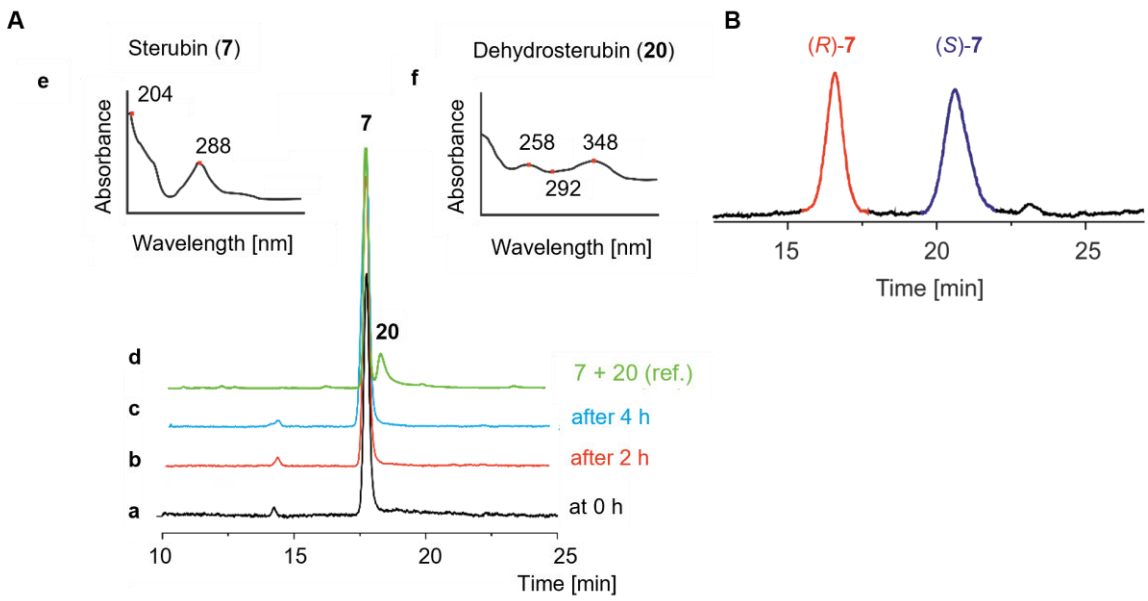

Figure 10: (A) The chemical stability of (*R*)-Sterubin in BV-2 cells was assigned by HPLC/UV: (a) at 0 h (black), (b) after 2 h (red), and (c) after 4 h (blue) of incubation. A reference chromatogram of sterubin together with dehydrosterubin (d) was recorded (green) as well as UV spectra of sterubin (e) and dehydrosterubin (f). (*R*)-Sterubin was chemically stable over the whole time and did not convert to dehydrosterubin (**20**). (B) Chromatogram of (*R*)-Sterubin immediately after dissolving enantiomerically pure compound in DMSO and further dilution in cell culture medium.

3.3.3 Neuroprotection *in vivo*

Natural products and derivatives, most notably the polyphenolic flavonoids, have been investigated *in vitro* and *in vivo* as multifunctional agents against neurodegeneration and AD.[122, 141] Surprisingly, sterubin showed a higher activity against oxidative stress and neuroinflammation than several other flavonoids *in vitro*.[113] To determine if sterubin also has neuroprotective effects *in vivo*, experiments were performed using a interventional mouse model of AD.[142-143] AD-like neurotoxicity and memory impairments were induced by intracerebroventricular (ICV) injection of the preaggregated amyloid β (Aβ) fragment $A\beta_{25-35}$ (9 nmol) on the first day of the study. The ICV injection leads to cell loss in the frontoparietal cortex and the hippocampal formation. Control mice received distilled water (V1) ICV. Racemic sterubin was dissolved in a mixture of 60% DMSO and 40% saline (0.9% NaCl in milliQ water) and the solutions were injected intraperitoneally (IP) once per day for the following 7 d at doses between 0.3 and 3 mg/kg. Injections of vehicle (60% DMSO + 40% saline, V2) were used for the two control groups. Short-term spatial memory was evaluated in the Y-maze test (YMT) on day 8 and long-term memory was evaluated on days 9 (training) and 10 (measurement of step-through latency) in the step-through passive-avoidance assay (STPA). Sterubin significantly improved the $A\beta_{25-35}$-induced alternation deficit in the YMT at doses greater than 1 mg/kg (Fig. 11A), further substantiating the neuroprotective effects observed *in vitro*.[113] In agreement with the results obtained in the YMT (Figure 7A), the $A\beta_{25-35}$-induced deficit in long-term memory was also compensated at a dose of 1 mg/kg and higher (Fig. 11B). Sterubin exceeded the activity of previously studied polyphenols such as silibinin[144], taxifolin[145] and taxifolin derivatives[126] used in the same mouse model of AD with respect to the dose needed to compensate for the $A\beta_{25-35}$ induced effects.

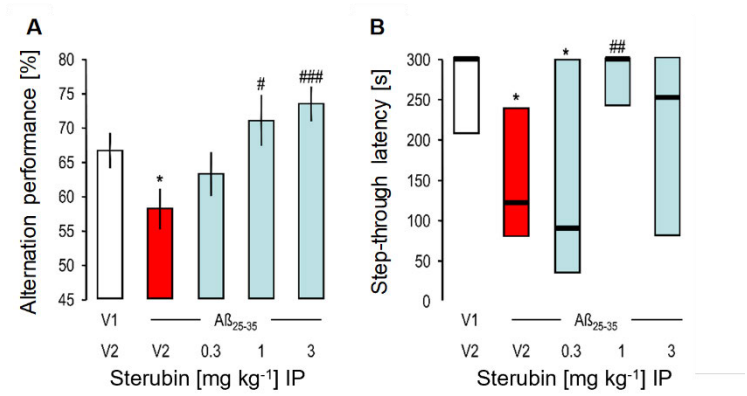

Figure 11: Effect of sterubin on Aß$_{25\text{-}35}$-induced learning impairments in mice. Sterubin was administered IP: (A) spontaneous alternation performance in YMT and (B) step-through latency in the STPA. Animals obtained distilled water (V1) or Aß25-35 (9 nmol ICV) on day 1 and received sterubin (0.3-3 mg/kg IP), or DMSO 60% in saline (V2), o.d. between day 1 and 7. They were examined in the YMT on day 8 and passive avoidance training was performed on day 9, with retention being tested after 24 h. Data show mean ± SEM in (A) and median and interquartile range in (B). n = 12-18 per groups. ANOVA: $F(4,57) = 3.85$, $p < 0.01$ in (A). Kruskal-Wallis ANOVA: $H = 11.6$, $p < 0.05$ in (B). * $p < 0.05$ vs. (V+V)-treated group; # $p < 0.05$, ## $p < 0.01$, ### $p < 0.001$ vs. (V+Aß25-35)-treated group; Dunnett's test in (A), Dunn's test in (B).

3.4 Conclusion

Racemic sterubin was successfully synthesized and resolution by HPLC on a chiral phase column into its pure enantiomers was achieved. Additionally, dehydrosterubin was synthesized as reference compound. Configurational stability of the enantiomers was observed in methanol; however, fast racemization took place in the cell culture medium. These findings explain why no difference in the neuroprotective activity in HT22 cells was found between racemic sterubin and its pure enantiomers. More importantly, the in vivo experiments revealed the high potency of sterubin as a neuroprotective agent against Aβ$_{25\text{-}35}$-induced AD-like memory loss in mice. The effects were observed in both short-term and long-term memory assays. These findings suggest crossing of the BBB and sufficient metabolic stability of sterubin. It can be concluded that sterubin exhibits strong neuroprotective properties during the 7-day treatment of the mice, leading to improved memory in the behavioural tests after the treatment was stopped. Hence, these findings strongly support that sterubin holds significant potential as a disease-modifying neuroprotectant in AD.

4. Synthesis and Biological Evaluation of Flavonoid - Cinnamic Acid Amide Hybrids with Distinct Activity in Phenotypic Screening Assays for Neurodegeneration

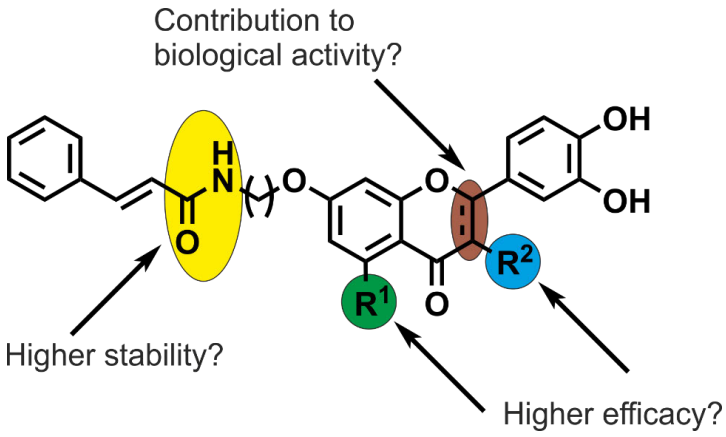

Author contributions:

J. Hofmann under supervision of Prof. Dr. Michael Decker designed and synthesized the compounds and performed the biological experiments.

R. Walther assisted with the planning and the execution of the analytics for stability and cellular up experiments.

Dr. Marcus Gutmann performed fluorescence microcopy experiments.

4.1 Introduction

Due to the complexity of neurodegeneration and AD, multi-target directed ligands have drawn the attention of research.[141] Respectiv efforts of our group focus in this regard on hybrid compounds consistent of two natural products: an aromatic acid combined with a flavonolignan or flavanoid. Compounds of the first generation contained esterified silibinin with different polyphenolic acids and were studied towards their neuroprotective and antioxidant properties (Fig. 12).[125] The esterification was done at the 7-OH group of silibinin, because this position is suspected to have a pro-oxidant character.[146] Interestingly, the 7-*O*-esters of silibinin have shown overall lower antioxidant capacities in the physicochemical, cell free FRAP-assay, however, some of these compounds, especially the derivatives with ferulic or cinnamic acid, have shown overaddtive neuroprotective effects in the oxytosis assay in HT22 cells. Additionally, an overadditve effect was observed against inflammation, ATP-depletion and on PC12 cell differantiation, respectively.[125] Outclassing the respective single components of the hybrids as well as their 1:1 mixture, the hybridization concept was proven to be very successful. Nevertheless, these compounds are only moderatly stable towards hydrolysis.[125, 147] Their high molecular weight and a restricted solubility represent additional drawbacks.[147]

Therefore, the compounds of second generation combined the smaler but structural familiar taxifolin with ferulic or cinnamic acid in analogy to the silibinin compouds (Fig. 12).[126] These compounds also had a significant overaddtive effect in a varierty of phenotypic screening assays in HT22 and BV-2 cells. And even *in vivo* these compouds have shown a remarkable neuroprotective effect in an $A\beta_{25\text{-}35}$-induced memory impaired mouse model. Modification of these compounds with an alkine tag as chemical probe for target identification in activity-based protein profiling revealed specific intracellular targets.[148] Additionally, microscopy studies revealed their localization in mitochondria.

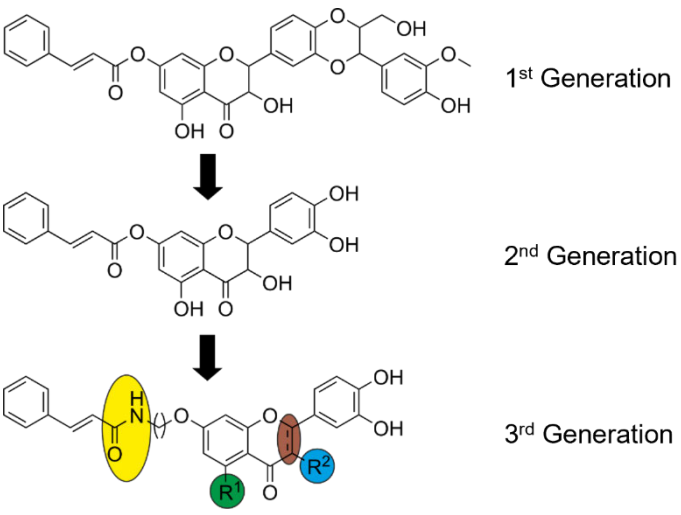

Figure 12: Compound development of flavonoid-cinnamic acid amides based on the structure of compounds of the 1st and 2nd Generation. Yellow: Amide-linker; green and blue: hydroxylation pattern; brown: dehydro-site.

Based on the encouraging results of the previous studies, a set of six flavonoid-cinnamic acid amide derivates was synthesized, containing three pairs of a flavanone and the respective flavone (Fig. 13). The flavonoid part of these hybrids was exchanged by several flavanoids, which are known to be more active in phenotypic screening assays related to neurodegeneration than taxifolin as single compound. The amide linker was supposed to improve the stability towards hydrolysis and the flavanones were compared with the flavones to investigate the influence of the double bond at the C-ring on biological activity, as it is known, that conversion to dehydrocompounds is taking place within assay conditions.[126, 140, 147]

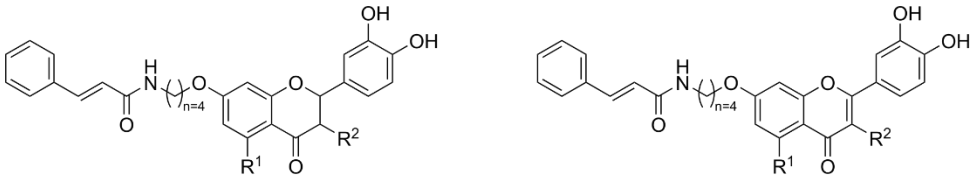

Taxifolin-CA	R^1 = OH	R^2 = OH	Quercetin-CA	R^1 = OH	R^2 = OH
Eriodictyol-CA	R^1 = OH	R^2 = H	Luteolin-CA	R^1 = OH	R^2 = H
Fustin-CA	R^1 = H	R^2 = OH	Fisetin-CA	R^1 = H	R^2 = OH

Figure 13: Overview target compounds. CA = cinnamic acid amide.

4.2 Chemistry

The synthesis of the desired target compounds was achieved in total synthesis or semi synthetically. Taxifolin, quercetin and fisetin were purchased from commercial suppliers and had not to be synthesized, whereas eriodictyol, luteolin and fustin were synthesized in analogy to sterubin and dehydrosterubin (hydroxygenkwanin) like described above. MOM-protected acetophenones were combined by condensation reaction under basic conditions to the respective chalcone. In case of fustin, the double bond of the respective chalcone was oxidized with H_2O_2 under basic conditions to an epoxide, which is the precursor of the hydroxy group at C-3, of fustin. To obtain fustin and eriodictyol, heating of the respective chalcones in 10 % HCl in MeOH cleaved the MOM-groups and simultaneously formed the flavonoids. All flavonoids were fully protected with acetyl groups with acetic acid anhydride in the presence of catalytic amounts of iodine. For luteolin, acetylated eriodictyol was dehydrogenated with *N*-bromosuccinimide (NBS) in the presence of catalytic amounts of azobisisobutyronitrile (AIBN).

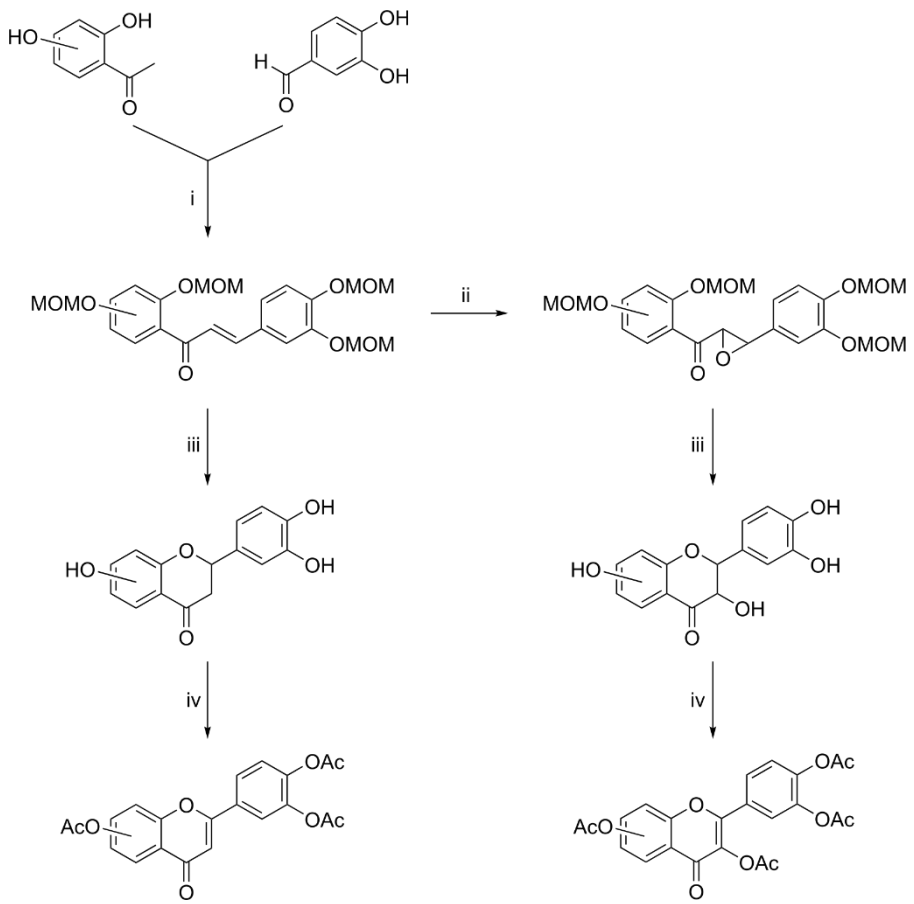

Figure 14: General synthesis of flavonoids. Reagents: i) 1. NaH/K_2CO_3, DMF/acetone, MOM-Cl, 2. KOH, EtOH; ii) H_2O_2, NaOH, MeOH; iii) 10% HCl in MeOH; iv) 1. Ac_2O, I_2, 2. NBS, BPO, $CHCl_3$.

The per-*O*-acetylated flavonoids were selectively deprotected at position 7 by a literature procedure using imidazole.[149-150] Cinnamic acid was transformed to its acyl chloride with oxalyl chloride, and an amine linker with terminal bromide was introduced to from an amide. For the connection of flavonoid and cinnamic acid amide, the bromide was transformed into an iodide via Finkelstein reaction and final hybridization was achieved via Williamson ether synthesis, directly followed by deprotection of the acetyl groups with 6M HCl in acetonitrile.

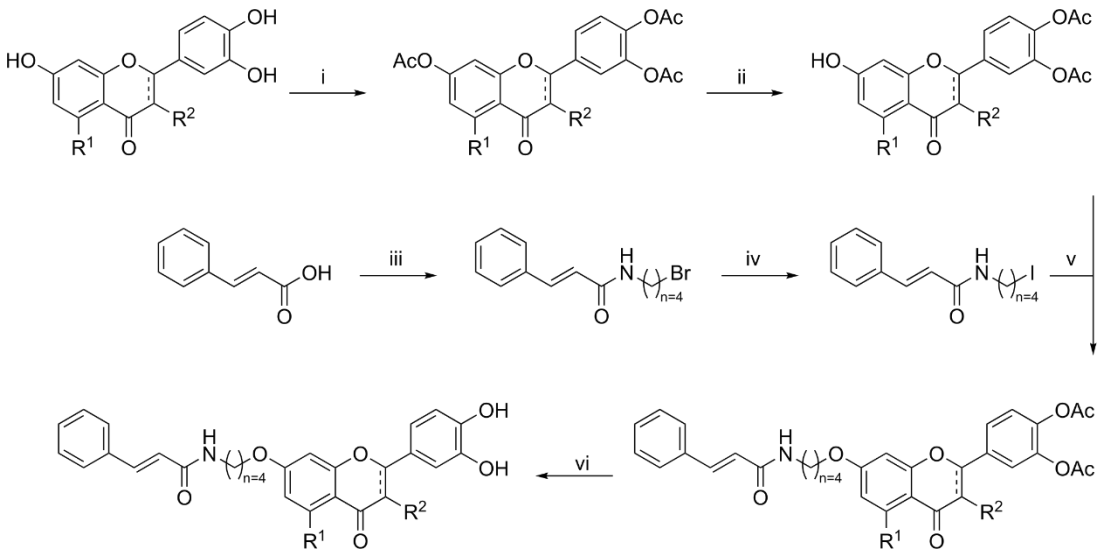

Figure 15: General synthesis of flavonoid-cinnamic acid amides. Reagents: i) 1. Ac_2O, I_2; ii) imidazole, CH_2Cl_2; iii) 1. oxalyl chloride, 2. NEt_3, $H_2N(CH_2)_4Br$; iv) NaI, acetone; v) K_2CO_3, DMF vi) 6 M HCl in MeOH.

4.3 Biology

The compounds hold two so-called “pan assay interference (PAIN) motifs”, the catechol, and the Michael-System of cinnamic acid. PAINS are compounds, which can interfere with the assay read out e.g., by fluorescence or unspecific binding to proteins, leading to false positive results.[151] Even if the threat of PAINS is mostly relevant for high throughput screens and *in vitro* assays with isolated molecular targets, it has to be taken into consideration and the applied assays have to be critically examined. Therefore, the compounds were tested in a variety of assays and importantly in cell-based assays (HT22 cells), which reflect a more complex system in comparison to e.g. an isolated enzyme, and have proven to be more robust against PAINS, in particular against aggregators.[152] Additionally, the compounds do not interfere with the assay read out.

4.3.1 Neuroprotection in HT22 cells – Oxytosis

Oxytosis describes a programmed cell death due to oxidative stress. It is a general pathway and the initial screening assay within the phenotypic screening approach from Maher and Schubert et al.[15] An overview of the oxytosis and the closely related ferroptosis pathway is given in Figure 16.

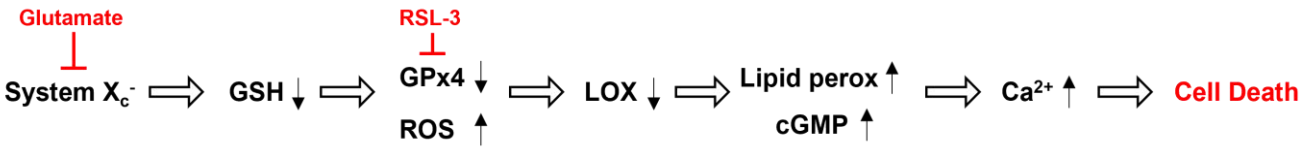

Figure 16: Overview Oxytosis/Ferroptosis pathway**.**

All compounds showed protection against the glutamate induced cell death and the quercetin derivative was the most active compound at a concentration of 1.56 µM (Fig. 17). Interestingly, the quercetin-CA was at one concentration level lower active than the taxifolin derivate. The eriodictyol derivative showed greater protection than the luteolin derivative (3.12 µM vs. 6.25 µM) and the fustin derivative showed comparable results to the fisetin derivative. Overall, there was no clear trend within the results of the oxytosis assays if there is a significant difference between the flavanones and the flavones.

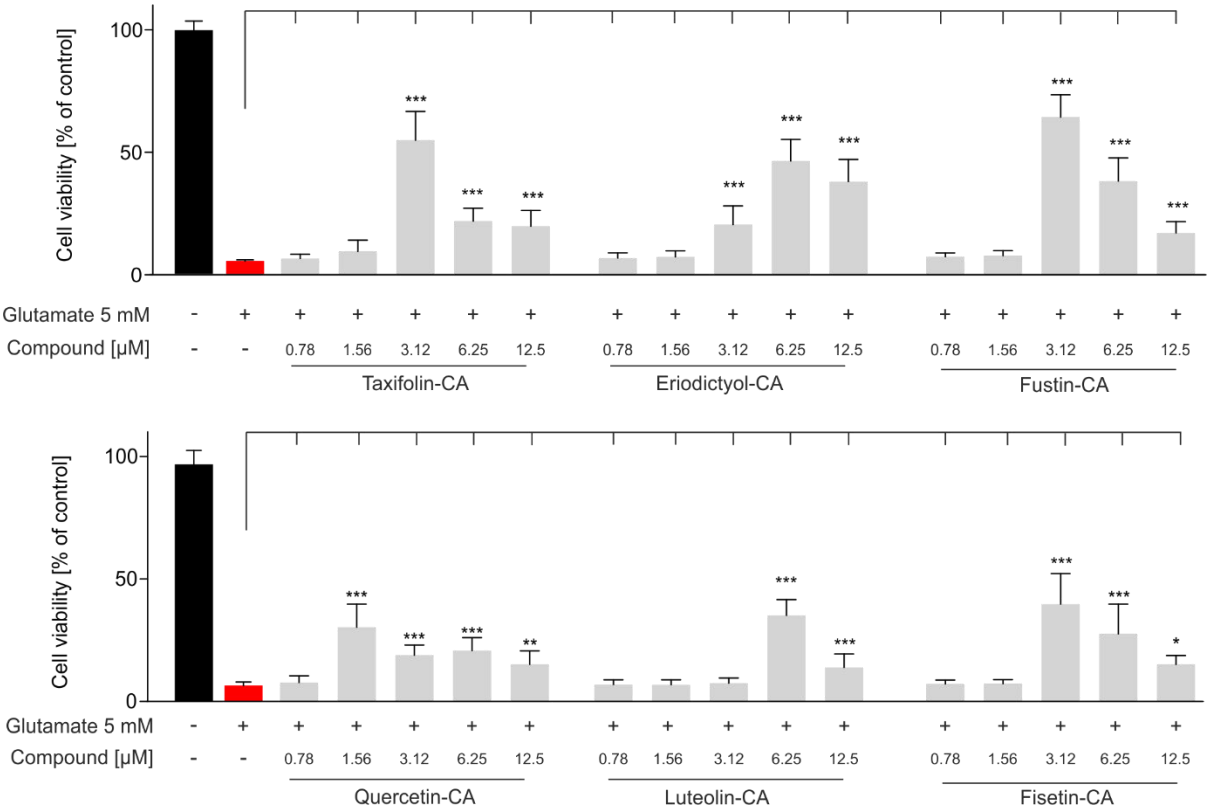

Figure 17: Oxytosis assay in murine hippocampal HT22 cells. Cells were treated with 5 mM glutamate alone (red) or in the presence of the indicated compound (grey). Data are presented as means ± SEM of three independent experiments and results refer to untreated control cells (black). Statistical analysis was performed using One-Way ANOVA followed by Dunnett's multiple comparison posttest using GraphPad Prism 5 referring to cells treated with 5 mM glutamate. Level of significance: * $p < 0.05$; ** $p < 0.01$; *** $p < 0.001$.

4.3.2 Quantification of Reactive Oxygen Species (ROS)

There is an increase in ROS within 6-8 h after glutamate treatment downstream the X_c^- cystine/glutamate antiporter.[59-60] Notably to say, that ROS themself do not kill the cells directly, but activate a number of further cascades, leading to apoptosis or necrosis.[67] There are even compounds that act downstream of ROS and are neuroprotective in presence of elevated ROS levels.[153] For a better understanding of the mode of action of the hybrid compounds and to get more information at which site of the oxytosis/ferroptosis pathway the compounds may act, ROS accumulation was investigated using the reduced fluoresceine derivate CM-H_2DCFDA, a versatile oxidative stress indicator and a fluorogenic probe, which evolves its fluorescence after oxidation by ROS.[154] The most active compound pair of the oxytosis assay, the taxifolin and the quercetin derivative, were investigated regarding their influence on ROS accumulation. The quercetin derivative could prevent glutamate induced ROS accumulation at 1.56 µM, whereas taxifolin-CA did not (Fig. 18 A and C). These results were consistent with

the activities found in the oxytosis assay and indicated, that the compounds could even decrease the basal level of ROS. Thus, the influence of the two compounds on HT22 cells without glutamate treatment was investigated (Fig. 18B). Both compounds decreased the basal level of oxidative stress in HT22 cells, the quercetin derivative decreased basal ROS already at 3.12 µM significantly, whereas the taxifolin derivative showed statistically significant activity only at 12.5 µM.

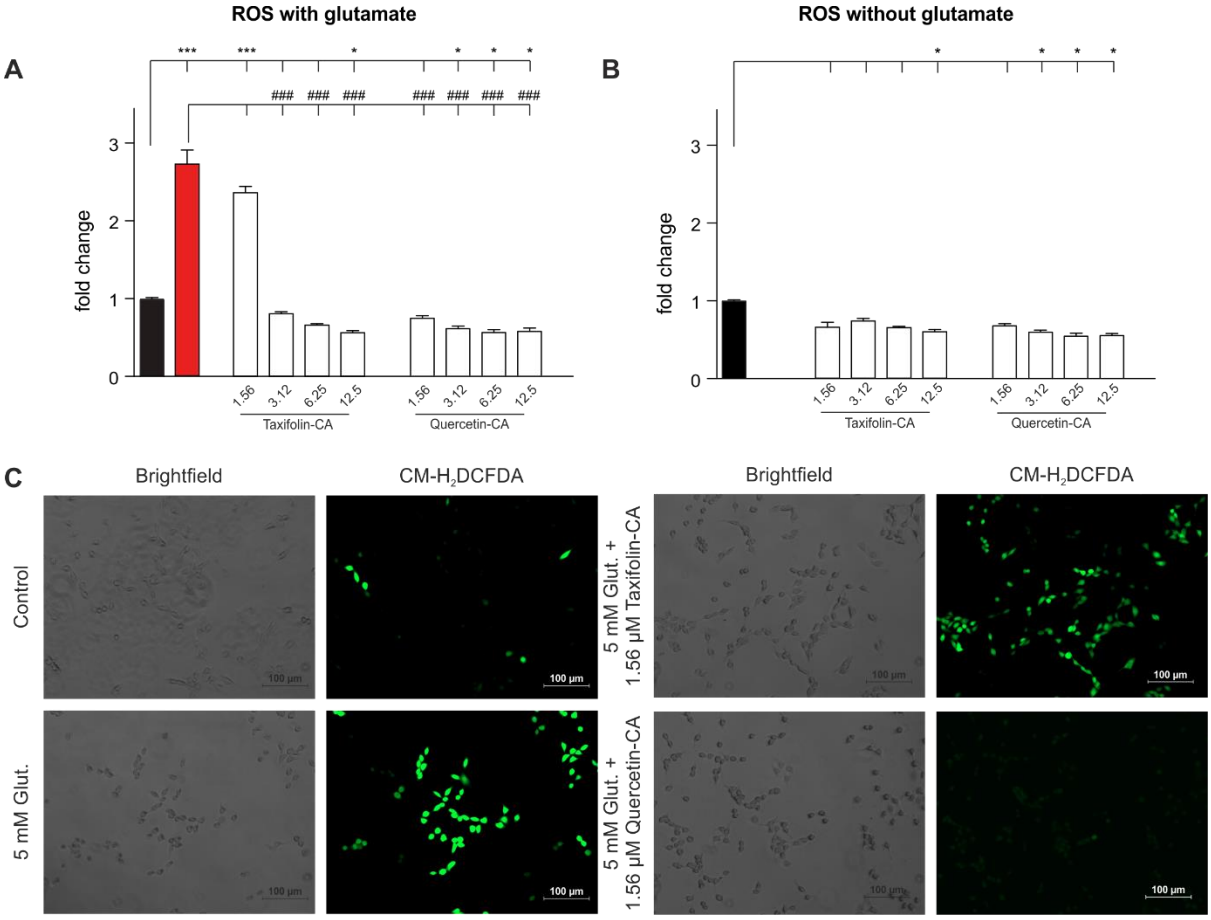

Figure 18: Qualitative and quantitative analysis of reactive oxygen species (ROS) with CM-H_2DCFDA in HT22 cells. The cells were treated with (red) or without glutamate (black) for 6 h in the presence or absence of taxifolin-CA and quercetin-CA (white). (A) Dose dependent effect of taxifolin-CA and quercetin-CA on glutamate induced ROS-levels, (B) dose dependent effect of taxifolin-CA and quercetin-CA on basal ROS levels, (C) visualization of glutamate induced ROS via fluorescence microscopy at compound concentration 1.56 µM. Statistical analysis was performed using One-Way ANOVA followed by Dunnett's multiple comparison posttest using GraphPad Prism 5 referring to untreated control cells (*) or cells treated with 5 mM glutamate (#). Level of significance: */# $p < 0.05$; **/## $p < 0.01$; ***/### $p < 0.001$.

4.3.3 Neuroprotection in HT22 cells – Ferroptosis

Ferroptosis is closely related to oxytosis. The small molecule RSL-3 induces cell death by inhibition of GPx4, which acts rather in the middle of the oxytosis/ferroptosis pathway.[70] All compounds were neuroprotective against ferroptosis (Fig. 19). Taxifolin-CA and quercetin-CA were again the most active compounds and quercetin-CA was also at one concentration level lower active than the taxifolin derivate. Fustin-CA and fisetin-CA showed comparable results, both were active at 6.25 µM. Interestingly the eriodictyol and luteolin derivative changed their activity profile. In the oxytosis assay, luteolin-CA showed neuroprotection at 6.25 µM and eriodictyol-CA at 3.12 µM. In the ferroptosis assay, the lowest active concentration of luteolin-CA was 3.12 µM.

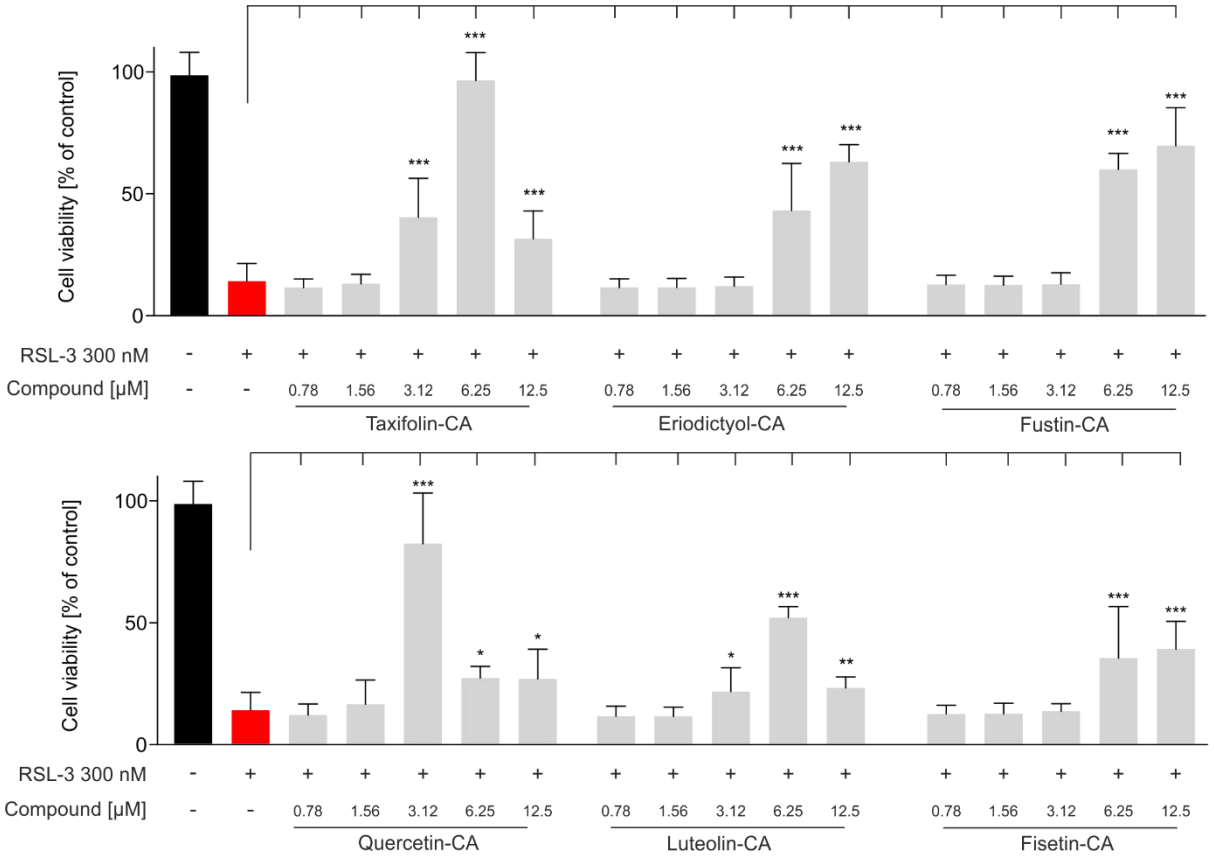

Figure 19: Ferroptosis assay in murine hippocampal HT22 cells. Cells were treated with 300 nM RSL-3 alone (red) or in the presence of the indicated compound (grey). Data are presented as means ± SEM of three independent experiments and results refer to untreated control cells (black). Statistical analysis was performed using One-Way ANOVA followed by Dunnett's multiple comparison posttest using GraphPad Prism 5 referring to cells treated with 300 nM RSL-3. Level of significance: * $p < 0.05$; ** $p < 0.01$; *** $p < 0.001$.

4.3.4 Neuroprotection in HT22 cells – Protection against energy loss

Like described above, breakdown of energy production and the decrease of ATP levels in the brain is associated with neuronal damage and neurodegeneration.[155] This is reflected in mouse hippocampal HT22 cells by inhibition of the enzyme glyceraldehyde 3-phosphate dehydrogenase (GAPDH) with IAA.[85] Like seen in the oxytosis and ferroptosis assay as well as in the ROS accumulation assay, the cinnamic acid amide flavonoids rescued the cells from death (Fig. 20). Furthermore, taxifolin-CA and quercetin-CA were the most active compounds and like in the other assays, quercetin-CA was more active than taxifolin-CA (3.12 µM vs. 6.25 µM).

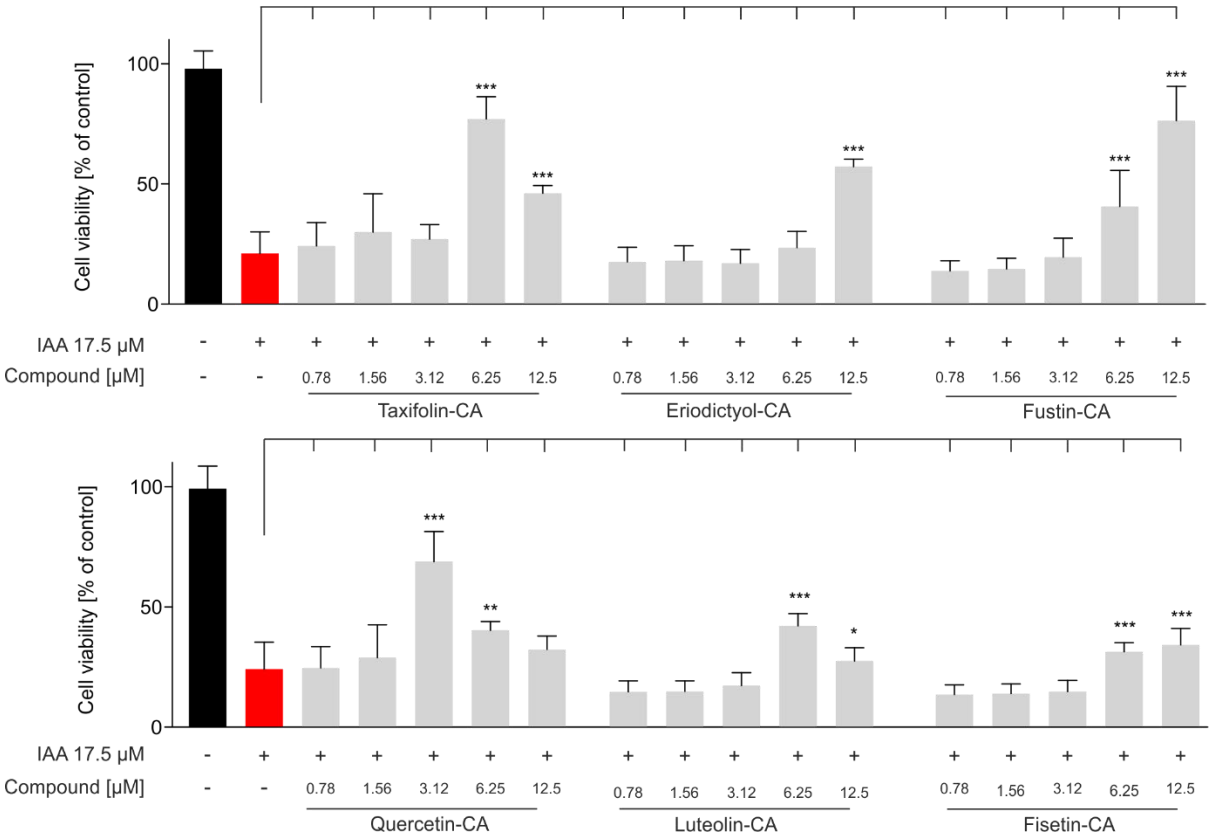

Figure 20: ATP-depletion was induced with 17.5 µM IAA in the absence (red) or presence of the indicated compound (grey). Data are presented as means ± SEM of three independent experiments and results refer to untreated control cells (black). Statistical analysis was performed using One-Way ANOVA followed by Dunnett's multiple comparison posttest using GraphPad Prism 5 referring to cells treated with 17.5 µM IAA. Level of significance: * $p < 0.05$; ** $p < 0.01$; *** $p < 0.001$.

4.3.5 Cytotoxicity in HT22 cells

The dehydro-derivative of silibinin-CA from compounds of the first generation have shown higher toxicity compared to the parent compound.[147] Therefore, toxicity studies using the widely applied colorimetric 3-(4,5-dimethylthiazol-2-yl)-2,5-diphenyl tetrazolium bromide (MTT) assay were examined (Fig. 21). Cells were treated for 24 h with the respective compounds, before the cell viability was determined. All compounds showed significant toxic effects, starting from 3.12 µM. The dehydro derivates showed overall higher cytotoxic effects i.e., a smaller therapeutic window.

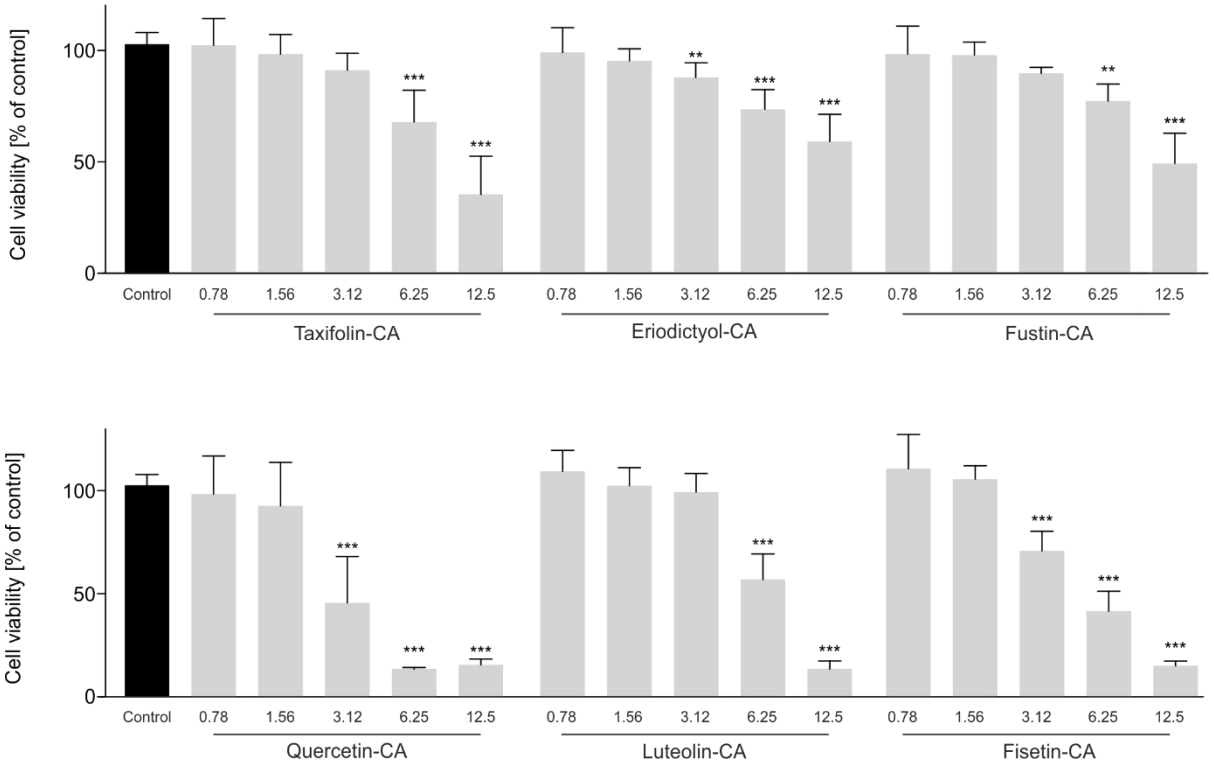

Figure 21: HT22 cells were treated with different concentrations of flavonoid-CA and cell viability was determined with a colorimetric 3-(4,5-dimethylthiazol-2-yl)-2,5-diphenyl tetrazolium bromide (MTT) assay. Data is presented as means ± SEM of three independent experiments and results refer to untreated control cells (black). Statistical analysis was performed using One-Way ANOVA followed by Dunnett's multiple comparison posttest using GraphPad Prism 5 referring to cells treated with 5 mM glutamate. Level of significance: *** $p < 0.001$, ** $p < 0.01$.

4.3.6 Stability in cell culture medium and cellular uptake

It is known that the taxifolin hybrids of the second generation as well as comparable derivatives from literature and also the silibinin compounds from the first generation can be oxidized to the respective dehydro derivative in the presence of BV-2 microglia, RAW264.7 macrophages or even in assay medium.[125-126, 140, 147] Therefore, cellular uptake experiments were conducted to get information about the intracellular behavior of taxifolin-CA and quantification of the intracellular taxifolin-CA concentration was done by calibration curve. Standard as well as a blank chromatogram was measured beforehand (Fig. 22A). Prior to cellular uptake experiments, the stability of taxifolin-CA was assessed in assay medium. No specific degradation product was found, however, the compound concentration decreased over time to 54.6 % of the initial concentration after 4 h (Tab. 1).

Table 1: Stability of taxifolin-CA in cell culture medium. The compound was dissolved in DMSO, diluted in cell culture medium, and incubated for the indicated time period prior to LC/MS analysis.

Time [h]	Amount [%]	SEM
0	100.0	0.0
0.5	88.8	6.1
1	82.1	8.7
2	70.5	6.9
4	54.6	3.0

The maximal intracellular concentration of taxifolin-CA was reached after 0.5 h at a concentration of 3.4 µM. Besides the chromatographic peak of taxifolin-CA at retention time 21.9 min (red) with m/z 506.1, three prominent peaks have risen at 22.7 min (blue), 24.2 min (orange) and 25.4 min (green) (Fig. 22B). Mass spectroscopic analysis revealed the molecular ions $[M+H]^+$ with m/z 520.15 for the blue peak, *m/z* 504.05 for the orange peak, and m/z 518.15 for the green peak. The m/z 504.05 and the retention time of 24.2 min (orange) refer to the quercetin-CA derivative. Compared to literature data[126, 140], the conversion rate of the taxifolin hybrid to the quercetin hybrid is much lower. The masses *m/z* 520.15 and *m/z* 518.15 may refer to the methylated taxifolin or quercetin hybrid, respectively. Similar results were obtained in HT22 cells (Fig. 22C).

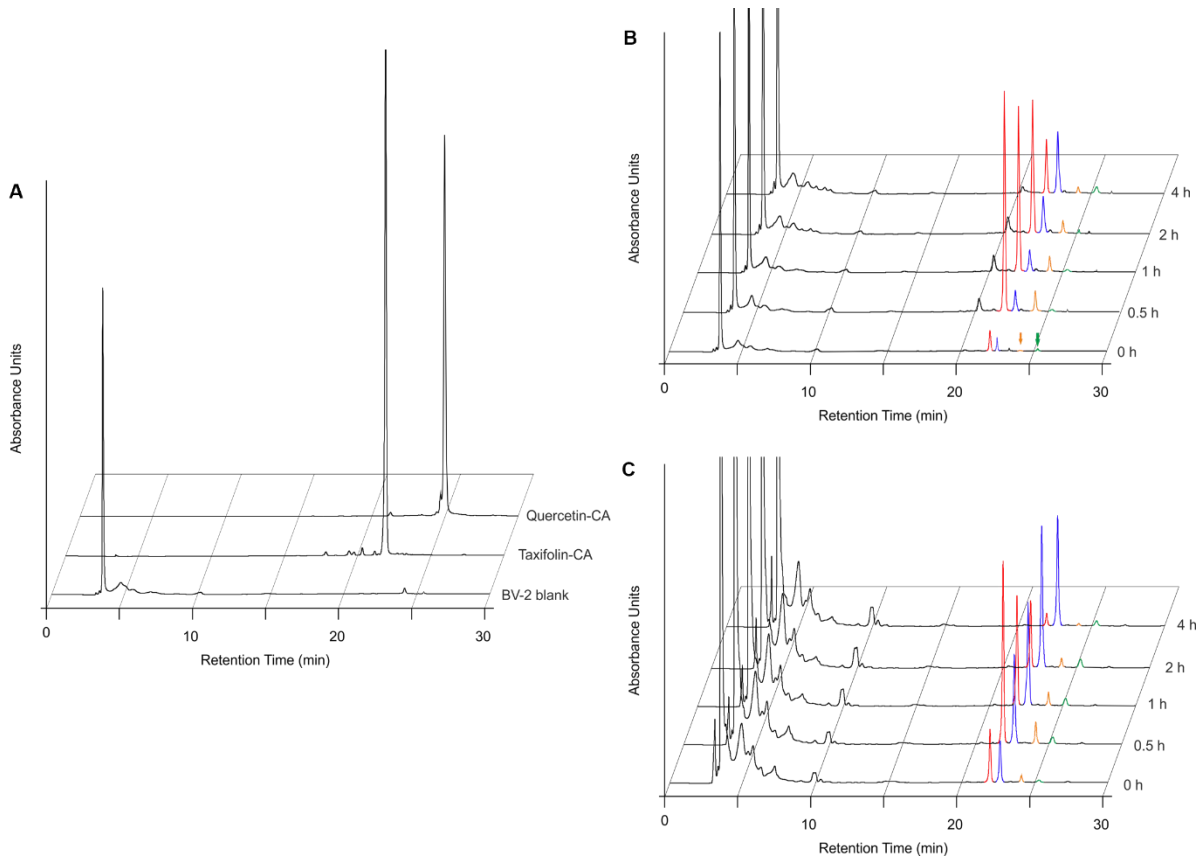

Figure 22: (A) HPLC chromatogram of 50 µM quercetin-CA, 50 µM taxifolin-CA and blank chromatogram of BV-2 cell lysate. Chromatogram overlay of cellular uptake experiments of taxifolin-CA. BV-2 (B) or HT22 (C) cells were treated for the indicated time with 50 µM taxifolin-CA. Taxifolin-CA (red) was converted into quercetin-CA (orange) and both compounds show a conversion to a compound, one methyl group heavier (m/z +15.0) than the parent compound (blue, taxifolin-CA + methyl; green, quercetin-CA + methyl). UV-spectra were recorded at 314 nm.

4.4 Conclusion

This chapter reports the synthesis of the third generation of natural products hybrids containing a flavonoid and a cinnamic acid amide moiety and their activity in neurodegeneration related phenotypic screening assays. All compounds have shown good neuroprotection in a variety of assays. Even if there was no clear trend regarding the influence of the double bond at the C-ring within all compounds, it was demonstrated, that in case of taxifolin-CA and quercetin-CA the active concentration was reduced by introducing the double bond and that small changes at the flavonoid core structure can go along with different behavior in various biological assays. Taxifolin-CA showed longer intracellular residence time compared to compounds of the second generation and was stable towards hydrolysis as expected. Further studies for a deeper molecular characterization of the mode of action of these compounds are ongoing and *in vivo* studies are planned to correlate the longer residence time in cells to a respective *in vivo* outcome.

5. Azobioisosteres of Curcumin with Pronounced Activity Against Amyloid Aggregation, Intracellular Oxidative Stress and Neuroinflammation

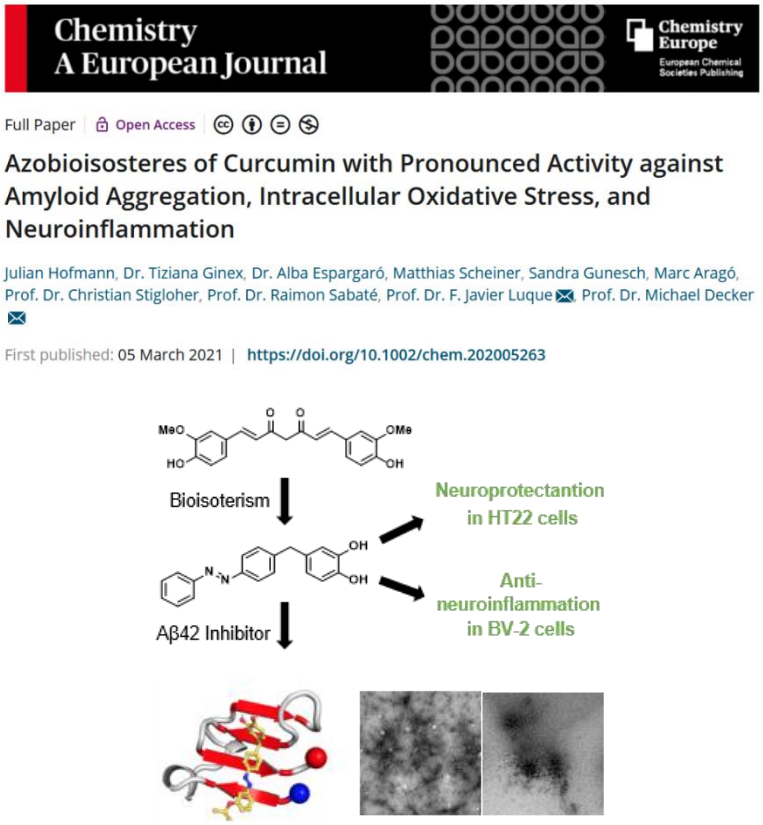

The content of this chapter was previously published and adapted with the permission of Wiley-VCH GmbH.

Hofmann, J.; Ginex, T.; Espargaró, A.; Scheiner, M.; Gunesch, S.; Aragó, M.; Stigloher, C.; Sabaté, R.; Luque, J.; Decker, M. Azobioisosteres of Curcumin with Pronounced Activity against Amyloid Aggregation, Intracellular Oxidative Stress, and Neuroinflammation. *Chem. Eur. J.* **2021**, *27* (19), 6015–6027.

Author contributions:

J. Hofmann under supervision of Prof. Dr. M. Decker synthesized the compounds and performed the assays in HT22 cells, and under supervision of Prof. Dr. C. Stigloher the TEM experiments.

Dr. T. Ginex, M. Aragó, and Prof. Dr. F. Javier performed computational analysis.

Dr. A. Espargaró and Prof. Dr. R. Sabaté performed aggregation experiments in bacterial cells.

M. Scheiner under supervision of Prof. Dr. M. Decker performed the DPPH-assay.

S. Gunesch under supervision of Prof. Dr. M. Decker performed the anti-inflammation assay.

5.1 Introduction

Since aggregation of Aβ peptides is believed to be the initial event of AD, the identification of potential inhibitors of amyloid aggregation has attracted much interest.[156-157] The natural product curcumin is the major curcuminoid of *Curcuma longa* which is used in traditional Chinese medicine.[158] Besides other polyphenolic natural products like taxifolin (**1**) and apigenin (**23**) (Fig. 23), curcumin has shown positive effects on counteracting oxidative stress and inflammation as well as preventing amyloid-β aggregation.[159-161]

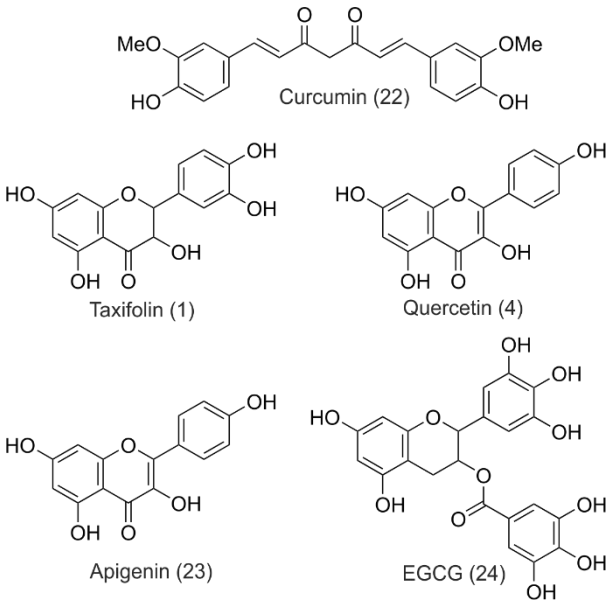

Figure 23: Chemical structure of curcumin (**22**) , taxifolin (**1**), quercetin (**4**), apigenin (**23**) and epigallocatechin-gallate (EGCG) (**24**).

Structure-activity relationship studies have shown that methylation of the free hydroxy groups of curcumin leads to loss of its activity.[162] Nevertheless, the therapeutic potential of curcumin is limited by poor pharmacokinetics, high rate of metabolism and low stability in aqueous environment.[163] Additionally, curcumin is considered as a pan-assay interference compound (PAIN),[163] which can possibly interfere with the assay readout or bind unspecifically to proteins leading to false positive results.[151]

A common strategy to improve the pharmacological and/or pharmacokinetic profile of bioactive molecules is bioisosterism. This applies changes in the molecular structure of a lead compound to improve their physicochemical properties, while preserving the relevant pharmacophoric features of the lead structure.[164]

Recent studies on taxifolin revealed its anti-aggregative ability on Aβ and defined the catechol as pharmacophore.[165-166] This was further confirmed by computational studies suggesting an Aza-Michael reaction between K16 and/or K28 residues of preformed amyloid fibrils with the oxidized catechol of taxifolin.[167]

This project focuses on a new class of compounds, conceived by hybridizing relevant structural elements present in curcumin and taxifolin following the rationale summarized in (Fig. 24).

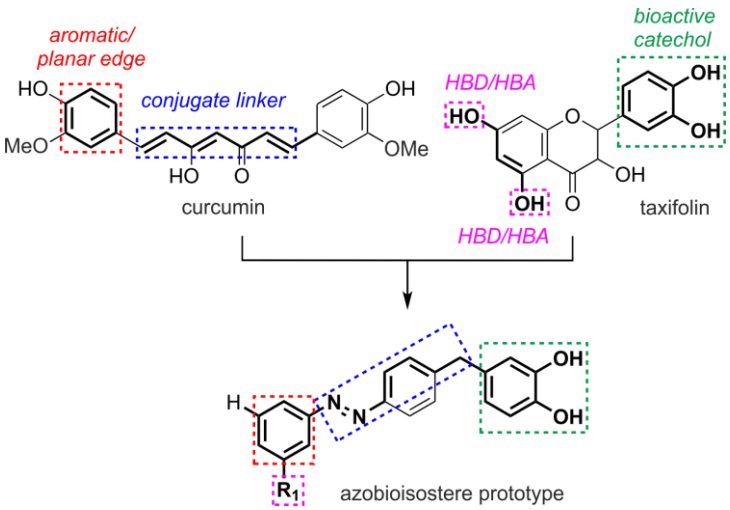

Figure 24: Rationalization of the azobioisostere prototype from the $A\beta_{42}$ inhibitors, curcumin and taxifolin. HBD = hydrogen bond donor; HBA = hydrogen bond acceptor.

5.2 Chemistry

Start of the synthesis was Friedel-Crafts acylation of 4-nitrobenzoic acid chloride (**22**) with dimethoxy benzene (**23**) to yield the corresponding acetophenone **24**. Ether cleavage of the methoxy groups to obtain the pharmacophoric catechol was achieved in a mixture of concentrated hydrobromic and acetic acids, followed by hydrogenation of the keto group by H_2 on Pd/C to obtain compound **26a** as first building block. The second part of the target compounds was introduced in a Baeyer-Mills reaction. Beforehand, partial oxidation of respective anilines with oxone to their nitroso derivatives was performed. Compound **29g** was synthesized in analogy to compounds **29 a-f**, but without cleavage of the methoxy groups of **24**. This compound was important to explore the role of the catechol moiety in the respective assays by comparison with the activity of the target compounds **29 a-f**.

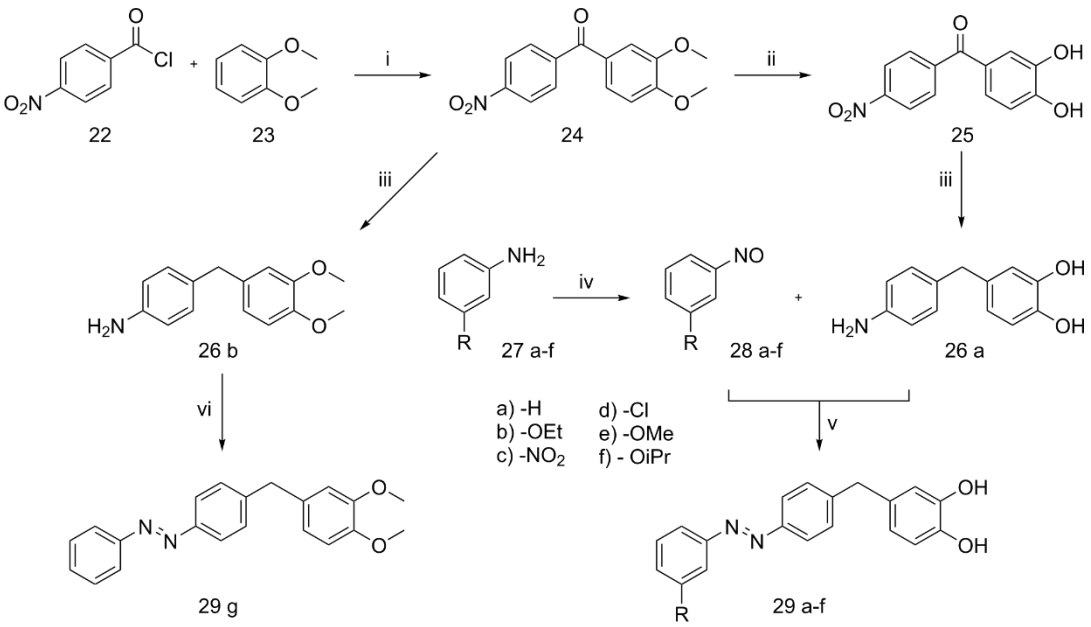

Figure 25: Synthesis of target compounds **29 a-f** and comparison compound **29 g**. Reagents and conditions: i) $FeCl_3$, 60 °C, 16 h (41%); ii) 48% HBr, AcOH, reflux, 3.5 h (85%); iii) H_2, Pd/C, MeOH, 10 bars, r.t., 16 h (45%-56%); iv) oxone®, CH_2Cl_2/H_2O, r.t., 3.5 h; v) AcOH, r.t., 16 h (16%-64%); vi) nitroso benzene, AcOH, r.t., 16 h (25%).

5.2 Biology

5.2.1 *In Vitro* inhibition of Aβ42 and tau aggregation

Aggregation of Aβ and NFTs containing aggregates of hyperphosphorylated tau protein are associated with AD and compounds with anti-aggregative properties are considered as disease modifying, even if Aβ and tau may not be the single cause of AD and neurodegeneration.[30-31, 168-169] A common method for the detection of aggregated proteins is the use of thioflavin dyes.[170-171] However, the detection of amyloid fibrils by fluorescent dyes can be biased by compounds with absorptive and fluorescent properties like the molecules investigated in this study.[172] Hence, the inhibitory effect of these compounds was firstly examined by transmission electron microscopy, which provides a dye-independent and therefore unsusceptible to PAINS compounds approach to assess the anti-aggregative effect of the compounds. The results clearly confirmed an inhibitory effect on fibril formation of Aβ42 at 10 µM for curcumin and the compounds **29 a-f** (Fig. 26 and Appendix II, Supporting Information). Compound **29g** did not show a significant reduction of the Aβ fibrils, indicating the importance of the free catechol group. Based on the TEM pictures, the bioisosteres seemed to have a stronger anti-aggregative activity. Further evaluation and a quantitative analysis of the anti-aggregative capacity against Aβ and tau of the target compounds was investigated applying a screening method in *E. coli* overexpressing the respective protein (Aβ42, human tau).[161, 173]

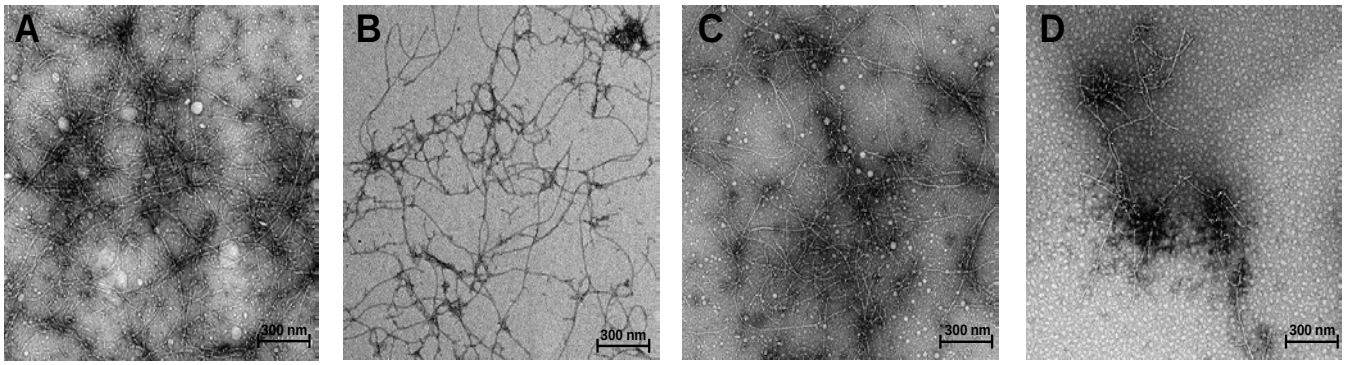

Figure 26: TEM analysis of the inhibitory effect on Aβ42. The Aβ monomer (100 µM) was incubated at 37°C in PBS for 24 h with or without 10 µM of the respective compound. A) control; B) curcumin ; C) **29g**; D) **29f**. Scale bar 300 nm.

The proteins form inclusion bodies (IB), which are consequently stained by thioflavin-S (Th-S) to assess the amount of aggregated protein. Similar anti-aggregative activity for Aβ42 and tau were found. The compounds reduced the aggregation of both proteins very effectively between 65-80% at 10 µM (Tab. 2). Compounds **29a** and **29f** display an average (Aβ42 and tau) inhibition of 75.8 and 75.7% against these proteins. Compound **29c**, and at less extent

29b, showed, however, a higher inhibitory potency against aggregation of Aβ42. Interestingly, compound **29g**, which has a protected catechol moiety, displays practically no activity (< 10%) in the bacterial system. The parent compounds curcumin and taxifolin served as controls and as shown in Table 2, a similar anti-aggregation activity was observed for Aβ42 and tau, whereas taxifolin displays practically no activity (< 5%), curcumin was found to have a moderate inhibitory effect (~ 36%). The activity of the target compounds greatly exceeds the potency of curcumin and taxifolin, revealing the suitability of the bioisosteric design.

Table 2: *In vitro* anti-amyloid activity of taxifolin, curcumin and 8a-g. *E. coli* is overexpressing the respective protein, which forms IBs and can be quantified by Th-S staining. Compounds were tested at 10 µM.

	Aβ42		***tau***	
Compound	**Inhibition %**	**SEM**	**Inhibition %**	**SEM**
Control	0.0	2.0	0.0	2.1
taxifolin	4.9	4.0	1.1	4.4
curcumin	37.8	2.7	35.2	3.2
29a	80.4	2.1	71.0	2.1
29b	78.2	3.4	65.1	2.4
29c	81.3	1.6	58.0	3.9
29d	63.1	4.2	66.6	2.9
29e	67.5	2.9	73.6	3.6
29f	73.3	4.3	78.3	4.1
29g	9.6	3.9	5.7	3.8

The experimental results of the Aβ42 aggregation inhibition were further confirmed by molecular simulations combining classical molecular dynamics (MD) and replica-exchange molecular dynamics (REMD). For more details see Appendix II.

5.2.2 Neurotoxicity and neuroprotection in HT22 cells

Cytotoxicity and neuroprotective properties against oxytosis were examined using the murine hippocampal neuronal cell line HT22. Compounds **29 a-f** showed very strong protection against the intracellular oxidative stress at concentrations between 2.5 and 7.5 µM (Fig. 27). The target compounds even exceeded the positive control quercetin. Curcumin as well as **29g** did not show distinct neuroprotection. Only at 10 µM weak protection with a cell survival of 21% was observed.

5.2.3 DPPH radical scavenging assay

The DPPH radical scavenging assay was performed to elucidate and exclude unspecific protection against oxidative stress by radical scavenging. This assay measures the direct antioxidant capacity in a cell free system by the use of the stable radical 2,2-diphenyl-1-picrylhydrazyl (DPPH), which is decolorized upon reduction.[174] The known antioxidant ascorbic acid (vitamin C) served as positive control with an IC_{50} value of 8.4 µM. The parent compound curcumin showed an IC_{50} value of 10.5 µM. The target compounds were active in a similar range, from 5 µM to 10 µM (Tab. 3). Compound **29g** did not show any activity at all, as there is no functionality to react with the free DPPH radical.

Table 3: Free radical scavenging capacity determined by DPPH assay

Compound	EC_{50} [µM]	SEM
ascorbic acid	8.4	0.5
curcumin	10.5	0.2
29a	9.1	0.3
29b	7.7	0.4
29c	5.4	0.5
29d	5.6	0.1
29e	9.6	0.4
29f	5.4	0.1
29g	not active	

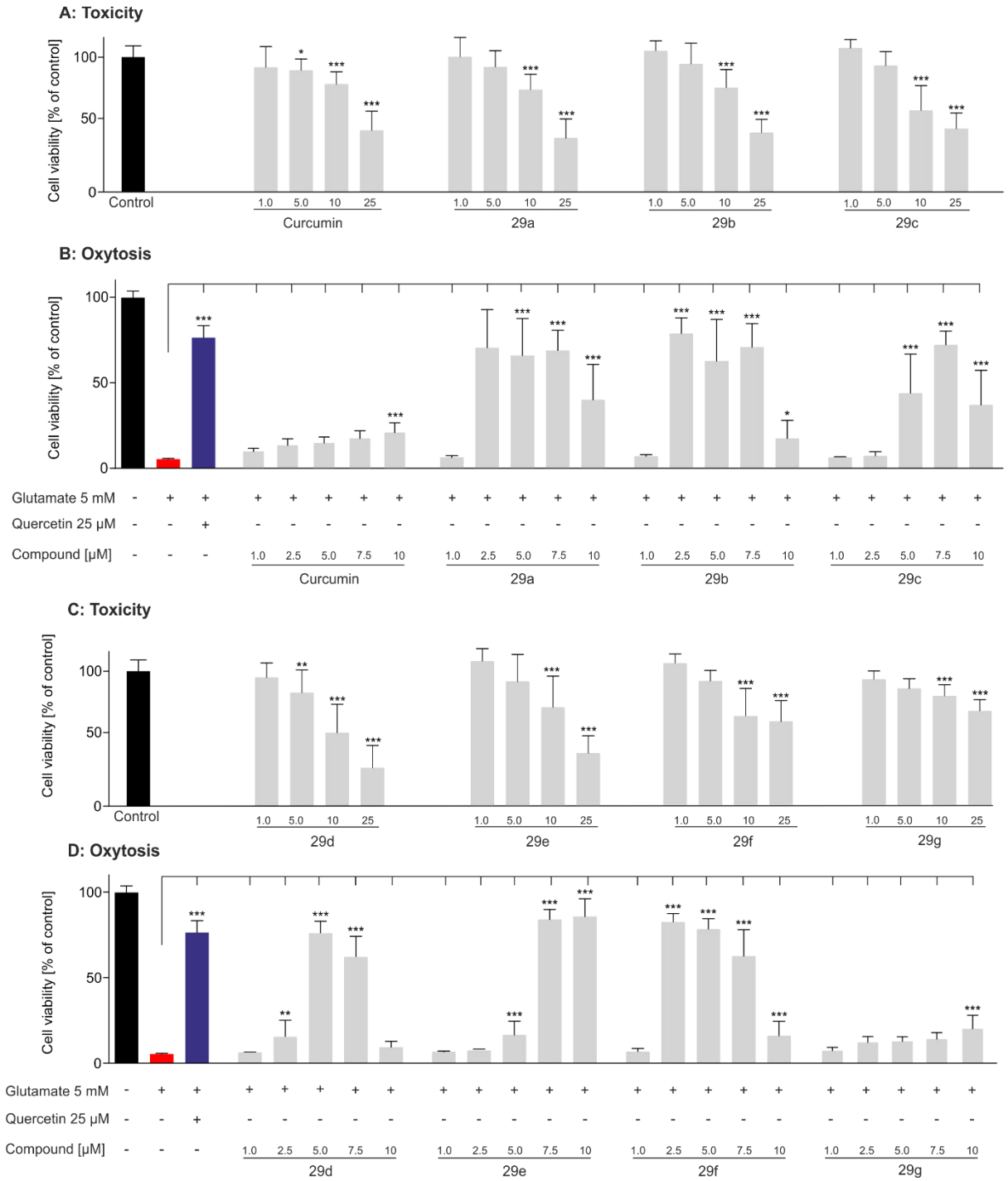

Figure 27: Neuroprotection and neurotoxicity were determined in HT22 cells. 5 mM glutamate (red) induced cell death, 25 µM quercetin (blue) served as positive control for cell survival: (A) Neurotoxicity of curcumin and 29 a-c; (B) neuroprotection of curcumin and 29 a-c; (C) neurotoxicity of 29 d-g; (D) neuroprotection of 29 d-g. Data is presented as means ± SEM of three independent experiments and results refer to untreated control cells (black). Statistical analysis was performed using One-Way ANOVA followed by Dunnett's multiple comparison posttest using GraphPad Prism 5 referring to cells treated with 5 mM glutamate. Level of significance: *** $p < 0.001$, ** $p < 0.01$, *$p < 0.05$.

5.2.4 Anti-inflammatory effect on BV-2 cells

Besides oxidative stress, amyloid and tau plaques, neuroinflammation represents a key hallmark of AD.[97] In this regard, BV-2 cells, stimulated with bacterial LPS were used to evaluate a possible anti-inflammatory effect of the target compounds. Cells were treated with bacterial lipopolysaccharide (LPS) to induce inflammation and the production of NO was quantified in the Griess assay. All compounds reduced NO production dose-dependently with the strongest anti-inflammatory effect at 10 µM (Fig 28). Like the results for neuroprotectivity in HT22 cells, the target compounds exceeded the activity of curcumin. Compound **29c** was the most active compound with a decrease of inflammation down to 17% at a concentration of 10 µM compared to the LPS control. The other compounds tested reduced NO production in a similar manner from 31% to 42% at 10 µM (compound **29f** is shown as representative).

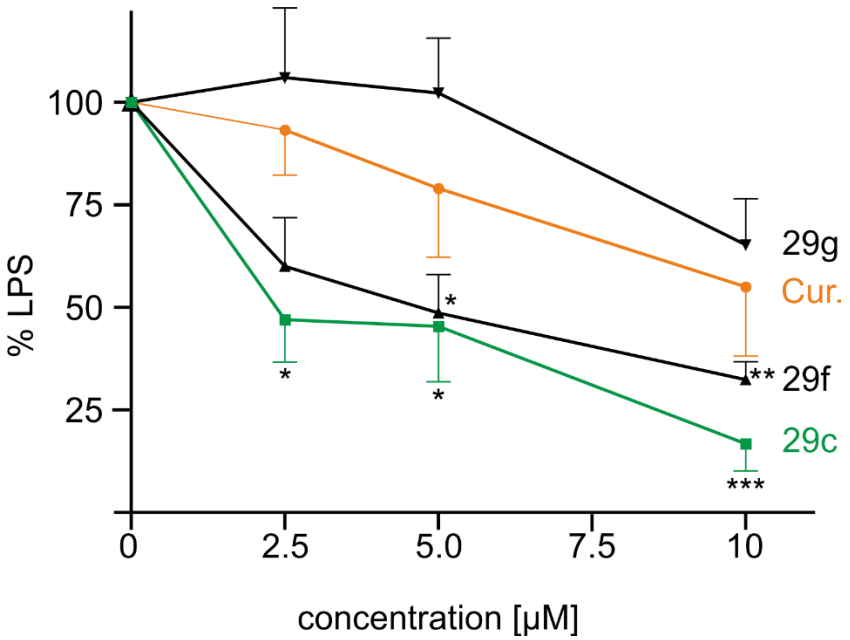

Figure 28: Effect of compounds **29c**, **f**, **g**, and curcumin on the production of NO as inflammation marker. BV-2 cells were treated with 50 ng/mL LPS alone or with the respective compound. NO was determined by the Griess assay in the supernatant. Data is presented as means ± SEM of three independent experiments and results refer to LPS treated cells. Statistical analysis was performed using One-Way ANOVA followed by Dunnett's multiple comparison posttest using GraphPad Prism 5. Level of significance: *** $p < 0.001$, ** $p < 0.01$, *$p < 0.05$.

5.5 Conclusion

A series of azobioisosteres of curcumin, carrying the pharmacophoric catechol moiety of taxifolin, have been synthesized. Their pharmacological profile was assessed in two phenotypic screening assays and additionally, their effect on protein aggregation of Aβ42 and tau was investigated. The synthetic bioisosteric compounds showed higher aggregation inhibition of Aβ42 relative to the parent compound curcumin. This could be observed in a bacterial *in vitro* assay with Th-S staining as well as in dye-independent in TEM experiments. Additionally, the compounds showed higher protection against glutamate induced intracellular oxidative stress in HT22 cells than curcumin. Moreover, the compounds revealed pronounced anti-inflammatory properties in BV-2 cells. The observed effects seem to be due to a specific mechanism, as the activity of the compounds in the DPPH radical scavenging assay did not show substantial differences.

6. Discussion and Outlook

With an aging society and an increased life expectancy, the annual number of patients with AD and other forms of dementia is expected to double in 2050.[175] There is still no medication to alter or slow down the disease progression and the single target approach mainly focusing on the peptide Aβ did not deliver a promising treatment.[30]

The natural product sterubin has long been known to be a constituent of *E. californicum*[137], a plant used for medicinal purposes by native people in Mendocino County, California, for the treatment of e.g. fever.[176] Sterubin was rediscovered in the context of Alzheimer´s disease and neurodegeneration as very potent neuroprotective compound.[113] Consistent with the reported use of *E. californicum* by indigenous people, sterubin has shown very strong anti-inflammatory effects. Furthermore, sterubin was active against oxytosis, ferroptosis and energy loss. Sterubin is an activator of the cytoprotective[177] and anti-inflammatory[178] transcription factor nuclear factor (erythroid-derived 2)-related factor 2 (Nrf2). Activation of Nrf2 leads to suppression of cytokines and the upregulation of gens related to counteract oxidative stress. Therefore, sterubin holds a special interest in the context of neurodegeneration as a potential disease modifying agent and the *in vivo* studies conducted in this work strongly support this hypothesis.

The second aim of this work was the development of the 3rd generation of flavonoid-aromatic acid hybrid compounds. Previous work[125-126, 147-148] have shown the beneficial effect of the combination of taxifolin or silibinin with different phenolic acids and cinnamic acid. These compounds have shown their potential against inflammation, oxidative stress, and ATP-depletion in neurodegeneration associated phenotypic screening assays and also beneficial effects in an $A\beta_{25-35}$-induced memory-impaired mouse model. While the compounds of the 1st generation could already be improved regarding their molecular weight, compounds of the 2nd generation still contained a hydrolysis labile ester connection between the flavonoid and the phenolic acid. Therefore, the compounds of the 3rd generation contained a more stable amid connection.

The former hybrids exceeded the activity of the single components and as there are single flavonoids known to have stronger neuroprotective properties than taxifolin, e.g., fisetin[179] and eriodictyol[113], there was the question if the activity of flavonoids could be increased by hybridization with cinnamic acid.

Chemical conversion of the taxifolin hybrid of generation 2 to the respective quercetin compound was observed, leading to the question, which of the compounds is the active form and how do they contribute to the biological activity.

To answer these questions a set of six flavonoid-cinnamic acid amide derivates was synthesized, containing three pairs of a flavanone and the corresponding flavone. Overall, no clear trend within the activity related to the oxidation state of the C-ring was observed. However, in case of the taxifolin- and quercetin-hybrid quercetin-CA was always at one concentration level lower active than the taxifolin derivative, showing that small changes within the flavonoid structure can have significant impact on the biological activity.

Especially the compounds of the 1st generation were instable towards hydrolysis and also conversion to the dehydro compounds took place in cell culture medium. Also, the 2nd generation compounds showed high rate of conversion to the respective dehydro derivative. The amide compounds of the 3rd generation were stable towards hydrolysis under assay conditions. Nonetheless, there was a time dependent concentration decrease to ~55% of the starting concentration within 4 hours. This may be explained by unspecific binding to fetal bovine serum (FBS).[180] The conversion of the taxifolin compound to the quercetin analogue was also observed for this kind of compounds, but in a much slower rate compared to literature data.[126, 140] This might be a hint for specific enzyme catalyzed transformation of the respective compound rather than an unspecific oxidation by e.g., ROS. The additionally found metabolites within the cellular uptake experiments strongly support the hypothesis that these compounds get methylated. The methylation reaction could be catalyzed by the well-known enzyme catechol-*O*-methyltransferase (COMT). This enzyme catalyzes the transfer of a methyl group of S-adenosyl methionine to catechol structures like in the neurotransmitter dopamine or catechol containing drugs.[181] The flavonoids quercetin and luteolin are substrates of COMT suggesting that the hybrid compounds may also get methylated by COMT.[182-184] Methylation of the catechol group of flavonoids leads to a decrease of biological acitvity[113, 185] and the same observations were made within the studies of the curcumin bioisosteres. Hence, future studies should aim for protection of the catechol by an intracellularly cleaved protection group for a potential increase in efficacy of these compounds. Suitable protection groups for this purpose might be boronic acids/esters. This strategy is discussed in tumor biology to reduce side effects of chemotherapeutics.[186-187] High levels of ROS in tumor tissue cleave the boronic group and lead to release of the active drug. The same concept might be viable for the protection of the catechol to protect the compounds from methylation.

Another drawback of the flavonoid hybrid compounds is their poor solubility. Even if solubility was not determined, at concentrations >50 µM precipitation could be observed. A common strategy to improve solubility is the insertion of more polar groups. This can be realized by e.g., the exchange of the linker group to a polyethylene glycol (PEG) chain.[188] Another possibility to improve solubility and also metabolic stability is the conjugation with phosphodiester glycans like impressively demonstrated by Romanucci et al.[189] Similar to glycosylation is the formulation with cyclodextrins (CD) like described for the anthocyanin

delphinidin.[190]

The flavonoid hybrid compounds are active in the oxytosis and the ferroptosis assay, meaning they act downstream the X_c^- antiporter and downstream GPx4 as well as GSH loss. They decrease ROS within glutamate treated HT22 cells and also basal ROS levels in untreated cells to a comparable level. This indicates that the compounds activate anti-oxidative intracellular pathways, which prevent general ROS formation like the Nrf2 pathway. Further studies e.g., on the effect on mitochondrial function, Nrf2 signaling or PC12 cell differentiation might bring deeper insights into the molecular mode of action of these compounds.

The natural product curcumin is controversially discussed whether it is “solid gold” for the treatment of several diseases or just a PAINS compound.[163] Nevertheless, curcumin has shown some potential to prevent Aβ aggregation.[161-162, 191-192] Curcumin itself has only little till no activity in the phenotypic screening assays, but the curcumin derivative J147 shows outstanding therapeutic activities.[193] The bioisosteres of curcumin synthesized in this work carried the pharmacophoric catechol of flavonoids and the data presented underlined the importance of the free catechol, because methylation of the free catechol led to dramatic loss of activity in all of the performed assays. The compounds have shown strong cellular protection against intracellular oxidative stress in the oxytosis assay, but only moderate radical scavenging activity. This suggests that the neuroprotection in HT22 cells is based on a target-specific mode of action. It must be considered that azobenzenes are commonly suspected to cause long-term toxicity due to instability towards bacterial azoreductases, which might cleave the azobenzenes into toxic anilines. But there are several examples of food colorants and drugs, which support the safe use of molecules containing azobenzene moieties[194] and at least in *E. coli*, the compounds synthesized were not cytotoxic indicating stability towards azoreductases. The compounds have shown greater activity than the parent natural products, proofing the successful accomplishment of the bioisosterism and since azobenzene compounds can undergo *cis-/trans*-photoisomerization upon irradiation with appropriate wavelengths, the compounds can potentially be used as molecular tool for the characterization of a respective biological system.

With the establishment of the large “omics” approaches like proteomics, transcriptomics, and metabolomics[78, 148, 195-196], new potential molecular targets and signaling pathways are characterized and there is deeper understanding of the intertwined network of AD and neurodegeneration. The molecular mode of action of the compounds presented in this work and their potential as disease modifying agents can be further explored with the increasing knowledge about the cause of the disease in the future.

7. Summary

Alzheimer´s disease (AD) is a neurodegenerative disease and the most common form of dementia with still no preventive or curative treatment. Besides several risk factors, age is one of the major risks for AD and with an aging society, there is an urgent need for disease modifying agents. The strategy to address only one target within the intertwined network of AD failed so far.

Natural products especially the phytochemical flavonoids, which are poly-phenolic natural products, have shown great potential as disease modifying agents against neurodegenerative disorders like Alzheimer´s disease (AD) with activities even *in vivo*. Flavonoids are produced by many plants and the native Californian plant *Eriodictyon californicum* is particularly rich in flavonoids. One of the major flavonoids of *E. californicum* is sterubin, a very potent agent against oxidative stress and inflammation, two hallmarks and drivers of AD and neurodegeneration. Herein, racemic sterubin was synthesized and separated into its pure (*R*)- and (*S*)-enantiomer by chiral HPLC. The pure enantiomers showed comparable neuroprotection *in vitro* with no significant differences. The stereoisomers were configurationally stable in methanol, but fast racemization was observed in culture medium. Moreover, the activity of sterubin was investigated *in vivo*, in an AD mouse model. Sterubin showed a significant positive impact on short- and long-term memory at low dosages.

A promising concept for the increase of activity of single flavonoids is hybridization with aromatic acids like cinnamic or ferulic acids. Hybridization of the natural products taxifolin and silibinin with cinnamic acid led to an overadditive effect of these compounds in phenotypic screening assays related to neurodegeneration and AD. Because there are more potent agents as taxifolin or silibinin, the hybrids were further developed, and different flavonoid cinnamic acid hybrids were synthesized. The connection between flavonoids and cinnamic acid was achieved by an amide instead of a labile ester to improve the stability towards hydrolysis to gain better “druggability” of the compounds. To investigate the oxidation state of the C-ring of the flavonoid part, the dehydro analogues of the respective hybrids were also synthesized. The compounds show neuroprotection against oxytosis, ferroptosis and ATP-depletion in the murine hippocampal cell line HT22. While no overall trend within the flavanones compared to the flavones could be assigned, the taxifolin and the quercetin derivative were the most active compounds in course of all assays. The quercetin derivate even shows greater activity than the taxifolin derivate in every assay. As desired no hydrolysis product was found in cellular uptake experiments after 4h, whereas different metabolites were found.

The last part of this work focused on synthetic bioisoteres of the natural product curcumin. Due to the drawbacks of curcumin and flavonoids arising from poor pharmacokinetics, rapid metabolism and sometimes instability in aqueous medium, we have examined the biological activity of azobenzene compounds designed as bioisoteres of curcumin, carrying the pharmacophoric catechol group of flavonoids. These bioisosteres exceeded their parent compounds in counteracting intracellular oxidative stress, neuroinflammation and amyloid-beta aggregation. By incorporating an azobenzene moiety and the isosteric behaviour to the natural parent compounds, these compounds may act as molecular tools for further investigation towards the molecular mode of action of natural products.

8. Zusammenfassung

Die Alzheimersche Krankheit ist eine neurodegenerative Erkrankung und die häufigste Form der Demenz, für die es noch keine präventive oder kurative Behandlung gibt. Neben mehreren Risikofaktoren ist das Alter eines der Hauptrisiken für die Krankheit und in einer alternden Gesellschaft besteht ein dringender Bedarf an Mitteln zum Stoppen oder Heilen der Krankheit. Die Strategie, nur ein Ziel innerhalb des verflochtenen Netzwerks der Pathogenese von AD zu adressieren, ist bisher gescheitert.

Naturstoffe, insbesondere die sekundären Pflanzenmetabolite Flavonoide, bei denen es sich um polyphenolische Naturstoffe handelt, haben ein großes Potenzial zum Eindämmen von neurodegenerativen Erkrankungen. Zahlreiche Studien, *in vitro* und auch *in vivo*, legen eine Wirksamkeit dieser Stoffe nahe. Flavonoide werden von vielen Pflanzen produziert und die kalifornische Pflanze *Eriodictyon californicum* ist besonders reich an Flavonoiden. Eines der wichtigsten Flavonoide von *E. californicum* ist Sterubin, ein sehr potenter Wirkstoff gegen oxidativen Stress und Entzündungen, zwei Treiber der Alzheimerschen Erkrankung und Neurodegeneration. In dieser Arbeit wurde racemisches Sterubin synthetisiert und durch chirale HPLC in das reine (*R*)- beziehungsweise (*S*)-Enantiomer getrennt. Die reinen Enantiomere zeigten *in vitro* eine vergleichbare neuroprotektive Aktivität ohne signifikante Unterschiede. Die Stereoisomere waren in Methanol konfigurativ stabil, in Zellkulturmedium wurde jedoch schnelle Racemisierung beobachtet. Darüber hinaus wurde die Aktivität von Sterubin *in vivo* in einem Alzheimer-Mausmodell untersucht. Sterubin zeigte bei niedrigen Dosierungen einen signifikanten positiven Einfluss auf das Kurz- und Langzeitgedächtnis.

Ein vielversprechendes Konzept zur Aktivitätssteigerung einzelner Flavonoide ist die Hybridisierung mit aromatischen Säuren wie Zimt- oder Ferulasäure. Die Hybridisierung der Naturstoffe Taxifolin und Silibinin mit Zimtsäure führte zu einer überadditiven Wirkung dieser Verbindungen in phänotypischen Screening-Assays im Zusammenhang mit Neurodegeneration und Alzheimer. Da es potentere Moleküle als Taxifolin oder Silibinin gibt, wurden die Hybride weiterentwickelt und verschiedene Flavonoid-Zimtsäure-Hybride synthetisiert. Die Verbindung zwischen dem Flavonoid und der Zimtsäure wurde durch ein Amid anstelle eines labilen Esters geknüpft, um die Stabilität gegenüber Hydrolyse zu verbessern. Um die Oxidationsstufe des C-Rings des Flavonoidteils zu untersuchen, wurden auch die Dehydro-Analoga der jeweiligen Hybride synthetisiert. Die Verbindungen zeigten Neuroprotektion gegen Oxytose, Ferroptose und dem Verlust von ATP in der murinen Hippocampus-Zelllinie HT22. Während kein allgemeiner Trend zur besseren Wirksamkeit der Flavanone gegenüber den Flavonen festzustellen war, waren das Taxifolin und das Querzetin-Derivat die aktivsten Verbindungen in allen Assays. Das Querzetin-Derivat zeigt in jedem

Assay sogar eine höhere Aktivität als das Taxifolin-Derivat. Wie erwartet wurde in zellulären Aufnahmeexperimenten nach 4 h kein Hydrolyseprodukt gefunden, wohingegen verschiedene Metabolite gefunden wurden.

Der letzte Teil dieser Arbeit beschäftigte sich mit synthetischen Bioisosteren des Naturstoffs Curcumin. Aufgrund der Nachteile von Curcumin und Flavonoiden, die aus einer schlechten Pharmakokinetik, einem schnellen Metabolismus und manchmal einer Instabilität in wässrigem Medium resultieren, wurde die biologische Aktivität von Azobenzolverbindungen untersucht, die als Bioisostere von Curcumin konzipiert sind und die pharmakophore Catecholgruppe der Flavonoide tragen. Diese Bioisostere übertrafen ihre Stammverbindungen in der Protektion gegen intrazellulären oxidativen Stress, Neuroinflammation und der anti-aggregativen Eigenschaften gegen Amyloid-Beta. Durch den Einbau einer Azobenzoleinheit und das isostere Verhalten zu den natürlichen Stammverbindungen könnten diese Verbindungen als molekulare Werkzeuge für die weitere Untersuchung der molekularen Wirkungsweise von Naturstoffen dienen.

8. Experimental Section

8.1 Chemistry

General

All reagents were used without further purification and bought from common commercial suppliers. Thin-layer chromatography was performed on silica gel 60 (alumina foils with fluorescent indicator 254 nm). UV light (254 and 366 nm) was used for detection. For column chromatography, silica gel 60 (particle size 0.040−0.063 mm) was used. Nuclear magnetic resonance (NMR) spectra were recorded with a Bruker AV-400 NMR instrument (Bruker, Karlsruhe, Germany) in $CDCl_3$ or DMSO-d_6, and chemical shifts are expressed in ppm relative to $CDCl_3$ (7.26 ppm for ^1H and 77.16 ppm for ^{13}C) or DMSO-d_6 (2.50 ppm for ^1H and 39.52 ppm for ^{13}C). Purity of the synthesis products was determined by HPLC (Shimadzu Products), containing a DGU-20A3R degassing unit, a LC20AB liquid chromatograph, and an SPD-20A UV/vis detector. UV detection was measured at 254 nm. Mass spectra were obtained by a LCMS 2020 (Shimadzu Products) running in positive ionization mode. As a stationary phase, a Synergi 4U fusion-RP (150 mm × 4.6 mm) column was used, and as a mobile phase, a gradient of methanol/water with 0.1 % (v/v) formic acid. Parameters: A = water, B = methanol, V(B)/(V(A) + V(B)) = from 5 % to 90 % over 10 min, V(B)/(V(A)+V(B)) = 90 % for 5 min, V(B)/(V(A) + V(B)) = from 90 % to 5 % over 3 min. The method was performed with a flow rate of 1.0 mL/min. Compounds were only used for biological evaluation if the purity was ≥95 %. Melting points/decomposition (dec.) were determined using an OptiMelt automated melting point system (Scientific Instruments GmbH, Gilching, Germany).

3,4-bis(methoxymethoxy)benzaldehyde

K_2CO_3 (10.7 g, 77.9 mmol) was added to a solution of 3,4-trihydroxylbenzaldehyde (2.00 g, 12.9 mmol) in dry acetone (50 mL) at 0–5 °C. Chloromethyl methyl ether (2.94 mL, 38.9 mmol) was slowly added over a period of 15 min to keep the temperature under 5°C. The reaction mixture was stirred at room temperature overnight (16 h), quenched by the addition of cold distilled water (100 mL) and extracted with ethyl acetate (200 mL). The combined organic layer was washed with distilled water (200 mL) and brine (100 mL) and dried over Na_2SO_4. The solvent was removed under reduced pressure and the crude product was purified by silica gel column chromatography using a mixture of cyclohexane/ethyl acetate (4/1). The product was obtained as a white solid in 96 % yield (2.82 g, 12.5 mmol). ^{1}H NMR: (400 MHz, $CDCl_3$): δ = 9.87 (s, 1H, C*HO*), 7.68 (d, ^4J = 2.0 Hz, 1H, Ph), 7.51 (dd, ^3J = 8.3, ^4J = 2.0 Hz, 1H, Ph), 7.28 (d, ^3J = 8.3 Hz, 1H, Ph), 5.33 (s, 2H, CH_2OCH$_3$), 5.30 (s, 2H, CH$_2$OCH_3), 3.53 (s, 3H, CH$_2$OCH_3), 3.52 (s, 3H, CH$_2$OCH_3). – ^{13}C NMR (100 MHz, $CDCl_3$): δ = 190.9 (C_q, *C*HO), 152.7 (C_q, Ph-*C*), 147.5 (C_q, Ph-C), 131.2 (+ ,Ph-*C*), 126.4 (+, Ph-*C*), 116.0 (+, Ph-*C*), 115.5 (+, Ph-*C*), 95.5 (-, *C*H$_2$OCH$_3$), 95.1 (-, *C*H$_2$OCH$_3$), 56.6 (+, CH$_2$O*C*H$_3$), 56.5 (+, CH$_2$O*C*H$_3$). – ESI-MS $[C_{11}H_{14}O_5+H]^+$: *m/z* calcd 227.09; found 227.1. MP 68.9 °C. The analytical data were consistent with those reported in the literature.[185]

1-(2,4,6-tris(methoxymethoxy)phenyl)ethan-1-one

To a mixture of NaH (0.989 g, 24.7 mmol) and 4 Å molecular sieve (3 g) in dry DMF (50 mL), a dried solution of 1-(2,4,6-trihydroxyphenyl)ethan-1-one monohydrate (1.00 g, 5.49 mmol) in dry DMF (15 mL) was added dropwise at 4 °C under an argon atmosphere and the reaction mixture was stirred for 45 min at room temperature. Chloromethyl methyl ether (1.88 mL, 24.7 mmol) was slowly added over a period of 15 min keeping the temperature under 5 °C. The reaction mixture was stirred overnight (16 h) at room temperature, then water (75 mL) was added, and the mixture was extracted with ethyl acetate (350 mL). The combined organic layers were dried over Na_2SO_4, and the solvent was removed under reduced pressure. The crude product was purified by silica gel chromatography using a mixture of cyclohexane and ethyl acetate (4/1) as the eluent. The product was obtained as a colorless oil in 84 % yield (1.38 g, 4.61 mmol). ^{1}H-NMR: (400 MHz, $CDCl_3$): δ = 6.51 (s, 2H, 2 Ar-H), 5.14 (s, 2H, CH_2OCH$_3$), 5.13 (s, 4H, CH_2OCH$_3$), 3.47 (s, 3H, CH$_2$OCH_3), 3.46 (s, 6H, CH$_2$OCH_3), 2.49 (s, 3H, CH_3) ppm; ^{13}C NMR (100 MHz, $CDCl_3$): δ = 201.6 (C_q, *C*=O), 159.6 (C_q, Ar-C), 155.4 (C_q, 2 Ar-C), 117.1 (C_q, Ar-C), 97.3 (+, 2 x Ar-C), 94.9 (-, 2 *C*H$_2$OCH$_3$), 94.6 (-, *C*H$_2$OCH$_3$), 56.5 (+, 2 CH$_2$O*C*H$_3$), 56.4 (+, CH$_2$O*C*H$_3$), 32.7 ppm (+, *C*H$_3$); ESI-MS: *m/z* calcd for $[C_{14}H_{20}O_7+H]^+$:

301.12, found 301.10. The analytical data are consistent with those reported in the literature.[197]

1-(2,4-bis(methoxymethoxy)phenyl)ethan-1-one

NaH (0.788 g, 19.7 mmol, 3.00 equiv.) was suspended in dry DMF (20 mL) under argon atmosphere at cooled to 4 °C. A solution of 1-(2,4-dihydroxyphenyl)ethan-1-one (1.0 g, 6.57 mmol, 1.00 equiv.) in dry DMF was added dropwise and stirred for 45 minutes at room temperature. The solution was cooled again to 4 °C and MOM-Cl (1.58 g, 19.7 mmol, 1.5 mL, 3 equiv.) was added dropwise. The reaction was stirred overnight. After that time, water was added, and the mixture was extracted with ethyl acetate. The combined organic layers were dried with Na_2SO_4, and the solvent was removed under reduced pressure. The crude product was purified via silica gel chromatography using a mixture of cyclohexane/ethyl acetate (4/1). The product was obtained as colorless oil in 66 % yield (1.17 g). ^{1}H NMR: (400 MHz, $CDCl_3$): δ = 7.78 (d, ^3J = 8.8, 1H, Ph), 6.82 (d, ^4J = 2.2 Hz, 1H, Ph), 6.72 (dd, ^3J = 8.8 Hz, ^4J = 2.3 Hz, 1H, Ph), 5.27 (s, 2H, OC*H*$_2$OCH$_3$), 5.20 (s, 2H, OC*H*$_2$OCH$_3$), 3.52 (s, 3H, OCH$_2$OC*H*$_3$), 3.48 (s, 3H, OCH$_2$OC*H*$_3$), 2.61 (s, 3H, C*H*$_3$). – ^{13}C NMR (100 MHz, $CDCl_3$): δ = 197.9 (C_q, *C*=O), 161.9 (C_q, Ar-C), 158.4 (C_q, Ar-C), 132.4 (C_q, Ar-C), 122.7 (+, Ar-C), 109.0 (+, Ar-C), 102.9 (+, Ar-C), 94.6 (-, 2 *C*H$_2$OCH$_3$), 94.3 (-, 2 *C*H$_2$OCH$_3$), 56.6 (+, 2 CH$_2$O*C*H$_3$), 56.4 (+, CH$_2$O*C*H$_3$), 32.9 (+, *C*H$_3$) ppm – ESI-MS $[C_{12}H_{16}O_5+H]^+$: *m/z* calcd 241.10; found 241.19. The analytical data are consistent with those reported in the literature.[198]

(E)-1-(2,4-bis(methoxymethoxy)phenyl)-3-(3,4-bis(methoxymethoxy)phenyl)prop-2-en-1-one

A saturated KOH-solution in EtOH (15 mL) was added to an ice-cold solution of 1-(2,4-bis(methoxymethoxy)phenyl)ethan-1-one (1.2 g, 4.96 mmol) dissolved in EtOH (20 mL) and stirred for 15 min. A solution of 3,4-bis(methoxymethyl)benzaldehyde (1.12 g, 4.96 mmol) in EtOH (15 mL) was added dropwise and allowed to stir over night at room temperature. The reaction as quenched with water (20 mL) and extracted with ethyl acetate (200 mL). The combined organic layer was dried over Na_2SO_4, and the solvent was removed under reduces pressure. The crude product was purified by silica gel chromatography using a mixture of cyclohexane/ethyl acetate (3/1). The product was obtained as yellow oil in 80 % yield (1.76 g, 3.92 mmol). ^{1}H NMR (400 MHz, $CDCl_3$): δ = 7.67 (d, ^3J = 8.6 Hz, 1H, Ar-H), 7.58 (d, ^3J = 15.7 Hz, 1H, *H*C=C*H*), 7.45 (d, ^4J = 1.9 Hz, 1H, Ar-H), 7.36 (d, ^3J = 15.9 Hz, 1H, *H*C=C*H*), 7.19 (dd, ^{3}J = 8.6 Hz, ^4J = 1.9 Hz, 1H, Ar-H), 7.16 (d, ^3J = 8.4 Hz, 1H, Ar-H), 6.85 (d, ^4J = 2.3 Hz, 1H,

Ar-H), 6.77 (dd, ^3J = 8.5 Hz, ^{4}J = 2.2 Hz, 1H, Ar-H), 5.27 (s, 2H, -OC*H*$_2$OCH$_3$), 5.25 (s, 2H, -OC*H*$_2$OCH$_3$), 5.25 (s, 2H, -OC*H*$_2$OCH$_3$), 5.21 (s, 2H, -OC*H*$_2$OCH$_3$), 3.52 (s, 3H, -OCH$_2$OC*H*$_3$), 3.51 (s, 3H, -OCH$_2$OC*H*$_3$), 3.50 (s, 3H, -OCH$_2$OC*H*$_3$), 3.49 (s, 3H, -OCH$_2$OC*H*$_3$) ppm. – ^{13}C NMR (100 MHz, CDCl$_3$): δ = 191.2 (C$_q$, *C*=O), 161.3 (C$_q$, Ar-C), 157.6 (C$_q$, Ar-C), 149.2 (C$_q$, Ar-C), 147.6 (C$_q$, Ar-C), 142.4 (+, HC=*C*H), 132.2 (C$_q$, Ar-C), 129.9 (C$_q$, Ar-C), 126.0 (+, H*C*=CH), 124.1 (+, Ar-C), 123.9 (+, Ar-C), 116.3 (+, Ar-C), 115.7 (+, Ar-C), 109.3 (+, Ar-C), 103.5 (+, Ar-C), 95.6 (-,*C*H$_2$OCH$_3$), 95.3 (-,*C*H$_2$OCH$_3$), 95.0 (-,*C*H$_2$OCH$_3$), 94.4 (-,*C*H$_2$OCH$_3$), 56.6 (+,CH$_2$O*C*H$_3$), 56.4 (+,CH$_2$O*C*H$_3$), 56.4 (+,CH$_2$O*C*H$_3$), 56.3 (+,CH$_2$O*C*H$_3$) ppm – ESI-MS: *m/z* calcd for [C$_{23}$H$_{28}$O$_9$+H]$^+$: 449.18; found 449.20. The analytical data were consistent with those reported in the literature.[198]

(2,4-bis(methoxymethoxy)phenyl)(3-(3,4-bis(methoxymethyl)phenyl)oxiran-2-yl)methanone

H$_2$O$_2$ (30 % w/v) was added to a solution of (E)-1-(2,4-bis(methoxymethoxy)phenyl)-3-(3,4-bis(methoxymethoxy)phenyl)prop-2-en-1-one (100 mg, 0.223 mmol) in methanol (5 ml) with 2 N NaOH (0.5 mL) and stirred at room temperature overnight. The mixture was concentrated under reduced pressure and the residue was extracted with ethyl acetate (50 mL). The combined organic layers were washed with water (50 mL) and brine (50 mL) and dried over Na$_2$SO$_4$. The solvent was removed under reduced pressure and the product was obtained as pale-yellow solid in 80 % yield (82 mg, 0.178 mmol). ^{1}H NMR (400 MHz, CDCl$_3$): δ = 7.83 (d, ^3J = 8.7 Hz, 1H, Ar-H), 7.16 (d, ^3J = 8.4 Hz, 1H, Ar-H), 7.13 (d, ^4J = 1.9 Hz, 1H, Ar-H), 6.99 (dd, ^{3}J = 8.4 Hz, ^4J = 2.1 Hz, 1H, Ar-H), 6.78 (d, ^4J = 2.2 Hz, 1H, Ar-H), 6.76 (dd, ^3J = 8.4 Hz, ^4J = 2.2 Hz, 1H, Ar-H), 5.23 (s, 2H, -OC*H*$_2$OCH$_3$), 5.22 (d, ^2J = 6.9 Hz, 1H, -OC*H*$_2$OCH$_3$), 5.20 (s, 2H, -OC*H*$_2$OCH$_3$), 4.98 (d, ^2J = 6.9 Hz, 1H, -OC*H*$_2$OCH$_3$), 4.88 (d, ^2J = 5.56 Hz, 1H, -OC*H*$_2$OCH$_3$), 4.30 (d, ^3J = 1.9 Hz, 1H, H$_{\alpha/\beta}$), 3.92 (d, ^3J = 1.9 Hz, 1H, H$_{\alpha/\beta}$), 3.53 (s, 3H, -OCH$_2$OC*H*$_3$), 3.51 (s, 3H, -OCH$_2$OC*H*$_3$), 3.50 (s, 3H, -OCH$_2$OC*H*$_3$), 3.47 (s, 3H, -OCH$_2$OC*H*$_3$) ppm. – ^{13}C NMR (100 MHz, CDCl$_3$): δ = 193.0 (C$_q$, C=O), 162.8 (C$_q$, Ar-C), 159.2 (C$_q$, Ar-C), 147.7 (C$_q$, 2 x Ar-C), 132.5 (C$_q$, Ar-C), 131.0 (C$_q$, Ar-C), 120.6 (+, Ar-C), 120.3 (+, Ar-C), 116.9 (+, Ar-C), 114.2 (+, Ar-C), 109.5 (+, Ar-C), 102.5 (+, Ar-C), 95.6 (-, *C*H$_2$OCH$_3$), 95.5 (-, *C*H$_2$OCH$_3$), 94.6 (-, *C*H$_2$OCH$_3$), 94.5 (-,*C*H$_2$OCH$_3$), 64.8 (C$_q$, C$_{\alpha/\beta}$), 59.5 (C$_q$, C$_{\alpha/\beta}$), 56.5 (+, CH$_2$O*C*H$_3$), 56.4 (+, CH$_2$O*C*H$_3$), 56.4 (+, CH$_2$O*C*H$_3$), 56.3 (+, CH$_2$O*C*H$_3$) ppm – ESI-MS: *m/z* calcd for [C$_{23}$H$_{28}$O$_{10}$+K]$^+$: 503.13; found 503.20. – MP 138.5 °C. The analytical data are consistent with those reported in the literature.[198]

(E)-3-(3,4-bis(methoxymethoxy)phenyl)-1-(2,4,6-tris(methoxymethyl)phenyl)prop-2-en-1-one

A saturated KOH-solution in EtOH (15 mL) was added to an ice-cold solution of 1-(2,4,6-tris(methoxymethoxy)phenyl)ethan-1-one (1.38 g, 4.60 mmol) dissolved in EtOH (20 mL) and stirred for 15 min. A solution of 3,4-bis(methoxy methoxy)benzaldehyde (1.04 g, 4.60 mmol) in EtOH (15 mL) was added dropwise and allowed to stir over night at room temperature. The reaction was quenched with water (20 mL) and extracted with ethyl acetate (200 mL). The combined organic layer was dried over Na_2SO_4, and the solvent was removed under reduces pressure. The crude product was purified by silica gel chromatography using a mixture of cyclohexane/ethyl acetate (2/1). The product was obtained as yellow oil in 84 % yield (1.96 g, 3.86 mmol). ^{1}H NMR (400 MHz, $CDCl_3$): δ = 7.35 (d, ^4J = 1.2 Hz, 1H, Ar-H), 7.28 (d, ^3J = 16.0 Hz, 1H, *H*C=C*H*), 7.14 (d, ^4J = 1.2 Hz, 1H, Ar-H), 6.87 (d, ^3J = 16.0 Hz, 1H, *H*C=C*H*), 6.56 (s, 2H, Ar-H), 5.25 (s, 2H, -OCH_2OCH$_3$), 5.23 (s, 2H, -OCH_2OCH$_3$), 5.18 (s, 2H, -OCH_2OCH$_3$), 5.11 (s, 4H, -OCH_2OCH$_3$), 3.51 (s, 3H, -OCH$_2$OCH_3), 3.51 (s, 6H, -OCH$_2$OCH_3), 3.39 (s, 6H, -OCH$_2$OCH_3) ppm. – ^{13}C NMR (100 MHz, $CDCl_3$): *δ* = 194.4 (C_q, C=O), 159.7 (C_q, Ar-C), 155.9 (C_q, 2 x Ar-C), 149.4 (C_q, Ar-C), 147.6 (C_q, Ar-C), 144.9 (+, HC=*C*H), 129.4 (C_q, Ar-C), 128.0 (+, H*C*=CH), 123.8 (C_q, Ar-C), 116.3 (+, Ar-C), 116.0 (+, Ar-C), 115.0 (+, Ar-C), 97.3 (+, 2 x Ar-C), 95.6 (-, *C*H$_2$OCH$_3$), 95.3 (-, *C*H$_2$OCH$_3$), 94.8 (-, *C*H$_2$OCH$_3$), 94.7 (-, 2 x *C*H$_2$OCH$_3$), 56.5 (+,CH$_2$O*C*H$_3$), 56.4 (+, 3 x CH$_2$O*C*H$_3$), 56.3 (+, CH$_2$O*C*H$_3$) ppm – ESI-MS: *m/z* calcd for $[C_{25}H_{32}O_{11}+H]^+$: 509.20; found 509.40.[197]

Eriodictyol (2-(3,4-dihydroxyphenyl)-5,7-dihydroxychroman-4-one)

A solution of chalcone (1.20 g, 2.36 mmol) in 10 % methanolic HCl (100 mL) was stirred for 60 min at reflux. The solvent was removed under reduced pressure and the crude product was purified by silica gel chromatography using an eluent of dichloromethane/methanol (10/1). The product was obtained as white solid in 57 % yield (680 mg, 2.36 mmol). ^{1}H NMR: (400 MHz, DMSO-d$_6$): δ = 12.13 (s, 1H, O*H*), 9.04 (s, 2H, O*H*), 6.87 (s, 1H, Ar-*H*), 6.74 (s, 2H, Ar-*H*), 5.88 – 5.87 (m, 2H, Ar-*H*), 5.37 (dd, ^3J = 12.6, ,^4J = 3.1 Hz, 1H, C*H*), 3.17 (dd, ^2J = 17.1 Hz, ^3J = 12.9 Hz, 1H, C*H*) 2.68 (dd, ^2J = 17.1 Hz, ^3J = 3.1 Hz, 1H, CH) – ^{13}C NMR (100 MHz, DMSO-d$_6$): δ = 196.3 (C_q, *C*=O), 166.6 (C_q, Ph-*C*), 163.4 (C_q, Ph-*C*), 162.8 (C_q, Ph-*C*), 145.7 (C_q, Ph-*C*), 145.2 (C_q, Ph-*C*), 129.4 (C_q, Ph-*C*), 117.9 (+, Ph-*C*), 115.3 (+, Ph-*C*), 114.3 (+, Ph-*C*), 101.7 (C_q, Ph-*C*), 95.7 (+, Ph-*C*), 94.9 (+, Ph-*C*), 78.4 (+, *C*H), 45.6 (-, *C*H$_2$). – ESI-MS: $[C_{15}H_{12}O_6+H]^+$: *m/z* calcd 289.07; found 289.10 – MP 246 °C dec. Analytical data are consistent with those reported in the literature.[132, 199]

Fustin (2-(3,4-dihydroxyphenyl)-3,7-dihydroxychroman-4-one)

A solution of chalcone (567 mg, 1.22 mmol) in 10 % methanolic HCl (50 mL) was stirred for 45 min at reflux. The solvent was removed under reduced pressure and the crude product was purified by silica gel chromatography using an eluent of dichloromethane/methanol (20/1). The product was obtained as light brown solid in 57 % yield (200 mg, 0.694 mmol). ^{1}H NMR: (400 MHz, DMSO-d_6): δ = 10.59 (s, 1H, O*H*), 8.98 (s, 1H, O*H*), 8.94 (s, 1H, O*H*), 7.63 (d, ^3J = 8.7 Hz, 1H, Ar-*H*), 6.88 (d, ^4J = 1.8 Hz, 1H, Ar-*H*), 6.76 (dd, ^{3}J = 8.2, ^{4}J = 1.8 Hz, 1H, Ar-*H*), 6.73 (d, ^{3}J = 8.0 Hz, 1H, Ar-*H*), 6.53 (dd, ^3J = 8.7, ^4J = 2.2 Hz, 1H Ar-*H*), 6.30 (d, ^4J = 2.1 Hz, 1H Ar-*H*), 5.47 (s, 1H, O*H*), 4.97 (d, ^3J = 11.3 Hz, 1H), 4.40 (dd, ^3J = 11.3, 5.2 Hz, 1H). – ^{13}C NMR (100 MHz, DMSO-d_6): δ = 192.5 (C_q, *C*=O), 164.7 (C_q, Ph-*C*), 162.7 (C_q,Ph-*C*), 145.6 (C_q, Ph-*C*), 144.8 (C_q, Ph-*C*), 128.6 (C_q, Ph-*C*), 128.3 (+, Ph-*C*), 119.4 (+, Ph-*C*), 115.3 (+, Ph-*C*), 115.0 (+, Ph-*C*), 112.1 (C_q, Ph-*C*), 110.5 (+, Ph-*C*), 102.3 (+, Ph-*C*), 83.5 (+, *C*H), 72.5 (+, *C*H). – ESI-MS: $[C_{15}H_{12}O_6+H]^+$: *m/z* calcd 289.07; found 289.11 – MP 205 °C dec. The analytical data are consistent with those reported in the literature.[200]

General Procedure for acetyl protection of flavonoids

To a suspension of the respective flavonoid (1 equiv.) in acetic anhydride (10 equiv.), iodine (0.07 equiv.) was added, and the reaction mixture was stirred 2 h at room temperature. For protected flavanones, ethyl acetate was added, and the mixture was washed with saturated $Na_2S_2O_3$-solution (aq.) and saturated $NaHCO_3$-solution (aq.). The organic layer was dried over Na_2SO_4, and the solvent was removed under reduced pressure. The crude products were recrystallized in a mixture of cyclohexane and ethyl acetate (1/1) and the products were obtained as white solid.

For protected quercetin and fisetin, the precipitant was filtered off and washed with cyclohexane, saturated $Na_2S_2O_3$-solution (aq.) and saturated $NaHCO_3$-solution (aq.). The residues were dissolved in dichloromethane and washed with saturated $NaHCO_3$-solution (aq.) and brine. The organic layer was dried over Na_2SO_4, and the solvent was removed under reduced pressure. The products were obtained as white solid.

Penta-*O*-acetyl taxifolin (2-(3,4-diacetoxyphenyl)-4-oxochromane-3,5,7-triyl triacetate)

Yield: 77 % – ^{1}H NMR: (400 MHz, $CDCl_3$): δ = 7.37 (dd, ^3J = 8.4, ^4J = 2.1 Hz, 1H, Ph), 7.28 (d, ^4J = 2.1 Hz, 1H, Ph), 7.25 (d, ^3J = 8.4, 1H, Ph), 6.77 (d, ^4J = 2.3, 1H), 6.59 (d, ^4J = 2.2, 1H), 5.64 (d, ^3J = 12.3 Hz, 1H), 5.41 (d, ^3J = 12.3 Hz, 1H), 2.36 (s, 3H, OAc), 2.28 (s, 6H, OAc), 2.20 (s, 3H, OAc), 2.03 (s, 3H, OAc). – ^{13}C NMR (100 MHz, $CDCl_3$): δ = 184.8 (C_q, *C*=O), 169.2 (C_q, CH_3*C*OO), 169.1 (C_q, CH_3*C*OO), 168.0 (C_q, CH_3*C*OO), 168.0 (C_q, CH_3*C*OO), 167.9

(C_q, CH_3*C*OO), 162.4 (C_q, Ph), 156.4 (C_q, Ph), 151.4 (C_q, Ph), 143.0 (C_q, Ph), 142.2 (C_q, Ph), 133.5 (C_q, Ph-*C*), 125.3 (+, Ph-*C*), 123.8 (+, Ph-*C*), 122.8 +, Ph-*C*), 111.4 (+, Ph-*C*), 110.6 (C_q, Ph-*C*), 109.0 (+, Ph-*C*), 80.3 (+, *C*H), 73.1 (+, *C*H), 22.1 (+, *C*H_3COO), 20.9 (+, *C*H_3COO), 20.6 (+, *C*H_3COO), 20.6 (+, *C*H_3COO), 20.2 (+, *C*H_3COO). – ESI-MS $[C_{25}H_{22}O_{12}+Na]^+$: *m/z* calcd 537.12; found 537.10. – MP 145 °C. Analytical data are consistent with those reported in the literature.[201]

Penta-*O*-acetyl quercetin (2-(3,4-diacetoxyphenyl)-4-oxo-4H-chromene-3,5,7-triyl triacetate)

Yield: 75 % – ^{1}H NMR: (400 MHz, $CDCl_3$): δ = 7.71 (dd, ^3J = 8.4, ^4J = 2.1 Hz, 1H, Ph), 7.69 (d, ^4J = 2.1 Hz, 1H, Ph), 7.35 (d, ^3J = 8.5, 1H, Ph), 7.33 (d, ^{4}J = 2.2 Hz, 1H, Ph), 6.87 (d, ^4J = 2.2, 1H, Ph), 2.43 (s, 3H, C*H*$_3$COO), 2.33 (s, 6H, C*H*$_3$COO), 2.32 (s, 6H, C*H*$_3$COO). – ^{13}C NMR (100 MHz, $CDCl_3$): δ = 170.2 (C_q, *C*=O), 169.3 (C_q, CH_3*C*OO), 168.0 (C_q, CH_3*C*OO), 167.9 (C_q, CH_3*C*OO), 167.9 (C_q, CH_3*C*OO), 167.8 (C_q, CH_3*C*OO), 157.0 (C_q, Ph-*C*), 154.4 (C_q, 2 x Ph-*C*), 153.9 (C_q, Ph-*C*), 150.5 (C_q, Ph-*C*), 144.5 (C_q, Ph-*C*), 142.3 (C_q, Ph-*C*), 134.2 (C_q, Ph-*C*), 127.8 (+, Ph-*C*), 124.0 (+, Ph-*C*), 123.9 (+, Ph-*C*), 114.9 (+, Ph-*C*), 114.0 (+, Ph-*C*), 109.1 (+, Ph-*C*), 21.3 (+, *C*H_3COO), 21.2 (+, *C*H_3COO), 20.7 (+, 2 x *C*H_3COO), 20.6 (+, *C*H_3COO). – ESI-MS $[C_{25}H_{21}O_{12}+H]^+$: *m/z* calcd 513.10; found 513.20 – MP 191 °C. Analytical data are consistent with those reported in the literature.[149]

Tetra-*O*-acetyl eriodictyol (4-(5,7-diacetoxy-4-oxochroman-2-yl)-1,2-phenylene diacetate)

Yield: 83 % – ^{1}H NMR: (400 MHz, $CDCl_3$): δ = 7.35 – 7.29 (m, 2H, Ar-H), 7.25 (d, ^{3}J = 8.8 Hz, 1H, Ar-H), 6.79 (d, ^4J = 2.2, 1H), 6.55 (d, ^4J = 2.2 Hz, 1H), 5.48 (dd, ^3J = 13.6, ^{4}J = 2.8 Hz, 1H), 3.00 (dd, ^2J = 16.7 Hz, ^{3}J = 13.6 Hz, 1H), 2.80 (dd, ^2J = 16.7, ^{3}J = 13.6 Hz, 1H), 2.38 (s, 3H, OAc), 2.31 (s, 3H, OAc), 2.30 (s, 3H, OAc), 2.30 (s, 3H, OAc). – ^{13}C NMR (100 MHz, $CDCl_3$): δ = 188.7 (C_q, *C*=O), 169.4 (C_q, CH_3*C*OO), 168.2 (C_q, CH_3*C*OO), 168.1 (C_q, CH_3*C*OO), 168.0 (C_q, CH_3*C*OO), 163.0 (C_q, Ph-*C*), 156.1 (C_q, Ph-*C*), 151.4 (C_q, CH_3*C*OO) 142.5 (C_q, 2 x Ph), 137.0 (C_q, Ph-*C*), 124.3 (+, Ph-*C*), 124.0 (+, Ph-*C*), 121.5 (+, Ph-*C*), 111.9 (C_q, Ph-*C*), 110.0 (+, Ph-*C*), 109.2 (+, Ph-*C*), 78.6 (+, *C*H), 60.5 (-, *C*H_2), 21.3 (+, *C*H_3COO), 21.1 (+, *C*H_3COO), 20.8 (+, *C*H_3COO) 20.7 (+, *C*H_3COO). – ESI-MS $[C_{23}H_{21}O_{10}+H]^+$: *m/z* calcd 457.11; found 457.15. – MP 133 °C. Analytical data are consistent with those reported in the literature.[202]

Tetra-*O*-acetyl luteolin (4-(5,7-diacetoxy-4-oxo-4H-chromen-2-yl)-1,2-phenylene diacetate)

Dibenzoyl peroxide (12 mg, 0.05 mmol) was added to a solution of tetra-*O*-eriodictyol (233 mg, 0.511 mmol) and *N*-bromosuccinimide (109 mg, 0.613 mmol) in chloroform (2.5 mL) and heated to reflux for 2 h. Chloroform was added (25 mL) and the mixture was washed with water (50 mL) and brine (25 mL). The organic layer was dried over Na_2SO_4, and the solvent was removed under reduced pressure. The crude product was purified by silica gel column chromatography using an eluent of cyclohexane and ethyl acetate (2/1 → pure ethyl acetate). The product was obtained as white solid in 60 % yield (139 mg, 0.306 mmol). ^{1}H NMR: (400 MHz, $CDCl_3$): δ = 7.72 (dd, ^3J = 8.5, ^4J = 2.3 Hz, 1H, Ph), 7.69 (d, ^4J = 2.1 Hz, 1H, Ph), 7.35 (d, ^3J = 8.5, 1H, Ph), 7.33 (d, ^{4}J = 2.2 Hz, 1H, Ph), 6.85 (d, ^4J = 2.2, 1H, Ph), 6.60 (s, 1H, C=C*H*), 2.43 (s, 3H, C*H*$_3$COO), 2.33 (s, 6H, C*H*$_3$COO), 2.31 (s, 3H, C*H*$_3$COO). – ^{13}C NMR (100 MHz, $CDCl_3$): δ = 176.2 (C_q, *C*=O), 169.4 (C_q, CH_3*C*OO), 168.0 (C_q, 2 x CH_3*C*OO), 167.8 (C_q, CH_3*C*OO), 160.8 (C_q, Ph-*C*), 157.6 (C_q, Ph-*C*), 154.1 (C_q, Ph-*C*), 150.3 (C_q, Ph-*C*), 144.9 (C_q, Ph-*C*), 142.7 (C_q, Ph-*C*), 129.7 (C_q, Ph-*C*), 124.6 (+, Ph-*C*), 124.4 (+, Ph-*C*), 121.7 (+, Ph-*C*), 115.0 (C_q, Ph-*C*), 113.9 (+, Ph-*C*), 109.1 (+, Ph-*C*), 109.0 (+, C=*C*H), 21.3 (+, *C*H$_3$COO), 21.1 (+, *C*H$_3$COO), 20.8 (+, *C*H$_3$COO), 20.7 (+, *C*H$_3$COO). – ESI-MS $[C_{23}H_{19}O_{10}+H]^+$: *m/z* calcd 455.10; found 455.15 – MP 213 °C. Analytical data are consistent with those reported in the literature.[203-204]

Tetra-*O*-acetyl fustin (4-(3,7-diacetoxy-4-oxochroman-2-yl)-1,2-phenylene diacetate)

Yield: 67 % – ^{1}H NMR: (400 MHz, $CDCl_3$): δ = 7.94 (d, ^{3}J = 8.6 Hz, 1H, Ar-H), 7.41 (dd, ^3J = 8.4, ^4J = 2.1 Hz, 1H, Ar-H), 7.32 (d, ^4J = 2.1 Hz, 1H, Ar-H), 7.27 (d, ^3J = 8.7, 1H, Ar-H), 6.87 (dd, ^{3}J = 8.6, ^4J = 2.1, 1H), 6.84 (d, ^4J = 2.1, 1H), 5.72 (d, ^3J = 12.2 Hz, 1H), 5.44 (d, ^3J = 12.2 Hz, 1H), 2.31 (s, 3H, OAc), 2.30 (s, 6H, OAc), 2.07 (s, 3H, OAc). – ^{13}C NMR (100 MHz, $CDCl_3$): δ = 187.1 (C_q, *C*=O), 169.3 (C_q, CH_3*C*OO), 168.4 (C_q, CH_3*C*OO), 168.1 (C_q, CH_3*C*OO), 168.0 (C_q, CH_3*C*OO), 161.7 (C_q, Ph-*C*), 157.1 (C_q, Ph-*C*), 142.9 (C_q, Ph), 142.2 (C_q, Ph), 133.9 (C_q, Ph-*C*), 129.1 (+, Ph-*C*), 125.4 (+, Ph-*C*), 123.9 (+, Ph-*C*), 122.9 (+, Ph-*C*), 117.6 (C_q, Ph-*C*), 116.7 (+, Ph-*C*), 111.2 (+, Ph-*C*), 81.0 (+, *C*H), 73.7 (+, *C*H), 21.2 (+, *C*H$_3$COO), 20.8 (+, *C*H$_3$COO), 20.6 (+, *C*H$_3$COO) 20.4 (+, *C*H$_3$COO). – ESI-MS $[C_{23}H_{21}O_{10}+H]^+$: *m/z* calcd 457.11; found 457.10. – MP 138 °C.

Tetra-*O*-acetyl fisetin (4-(3,7-diacetoxy-4-oxo-4H-chromen-2-yl)-1,2-phenylene diacetate)

Yield: 84 % – ^{1}H NMR: (400 MHz, $CDCl_3$): δ = 8.25 (d, ^{3}J = 8.8 Hz, 1H, Ph), 7.77-7.74 (m, 2H, Ph), 7.40 (d, ^{4}J = 2.1, 1H, Ph), 7.36 (d, ^{3}J = 8.3 Hz, 1H, Ph), 7.18 (dd, ^{3}J = 8.9 Hz, ^{4}J = 1.74 Hz, 1H, Ph), 2.36 (s, 3H, C*H*$_3$COO), 2.35 (s, 3H, C*H*$_3$COO), 2.33 (s, 6H, C*H*$_3$COO). – ^{13}C NMR (100 MHz, $CDCl_3$): δ = 171.6 (C_q, *C*=O), 168.5 (C_q, CH_3*C*OO), 168.1 (C_q, CH_3*C*OO), 167.9 (C_q, CH_3*C*OO), 167.9 (C_q, CH_3*C*OO), 156.0 (C_q, Ph-*C*), 155.0 (C_q, Ph-*C*), 154.9 (C_q, Ph-*C*), 144.5 (C_q, Ph-*C*), 142.3 (C_q, Ph-*C*), 134.0 (C_q, Ph-*C*), 128.2 (C_q, Ph-*C*), 127.6 (+, Ph-*C*), 126.6 (C_q, Ph-*C*), 124.1 (+, Ph-*C*), 124.0 (+, Ph-*C*), 121.4 (+, Ph-*C*), 119.8 (+, Ph-*C*), 111.1 (+, Ph-*C*), 21.3 (+, *C*H$_3$COO), 20.8 (+, 2 x *C*H$_3$COO), 20.6 (+, *C*H$_3$COO). – ESI-MS $[C_{23}H_{18}O_{10}+Na]^+$: *m/z* calcd 455.10; found 455.15 – MP 197 °C.

General procedure for deprotection of the position 7

The selective deprotection was done like previously described.[11] A solution of imidazole (2.00 equiv.) in dichloromethane was added dropwise to an -15 °C cold solution of the respective peracetylted flavonoid in dichloromethane. The reaction mixture was warmed to room temperature and stirred for 2 hours. Dichloromethane was added and the solution was washed with 5 % HCl and brine. The organic layer was dried over Na_2SO_4, and the solvent was removed under reduced pressure. The crude product was purified by silica gel chromatography using an eluent of dichloromethane/methanol (40/1). The products were obtained as colourless foam.

7-*OH*-Taxifolin (4-(3,5-diacetoxy-7-hydroxy-4-oxochroman-2-yl)-1,2-phenylene diacetate)

Yield: 40 % – ^{1}H NMR: (400 MHz, $CDCl_3$): δ = 7.31 (dd, ^{3}J = 8.4, ^{4}J =2.1 Hz, 1H, Ph), 7.25 (d, ^{4}J = 2.1 Hz, 1H), 7.23 (d, ^{3}J = 8.3 Hz, 1H, Ph), 6.19 (d, ^{4}J = 2.3, 1H, Ph), 6.11 (d, ^{4}J = 2.3, 1H, Ph) 5.58 (d, ^{3}J = 12.1 Hz, 1H), 5.30 (d, ^{3}J = 12.2 Hz, 1H), 2.37 (s, 3H, *CH*$_3$COO), 2.31 (s, 3H, *CH*$_3$COO), 2.30 (s, 3H, *CH*$_3$COO), 2.00 (s, 3H, *CH*$_3$COO). – ^{13}C NMR (100 MHz, $CDCl_3$): δ = 185.8 (C_q, *C*=O), 170.7 (C_q, CH_3*C*OO), 169.6 (C_q, CH_3*C*OO), 168.7 (C_q, CH_3*C*OO), 168.6 (C_q, CH_3*C*OO), 164.0 (C_q, Ph-*C*), 163.2 (C_q, Ph-*C*), 152.0 (C_q, Ph-*C*), 142.8 (C_q, Ph-*C*), 142.1 (C_q, Ph-*C*), 134.2 (C_q, Ph-*C*), 125.7 (+, Ph-*C*), 123.9 (+, Ph-*C*), 122.9 (+, Ph-*C*), 111.4 (C_q, Ph-*C*), 106.5 (+, Ph-*C*), 102.0 (+, Ph-*C*), 80.2 (+, *C*H), 73.1 (+, *C*H), 21.2 (+, *C*H$_3$COO), 20.7 (+, 2 x *C*H$_3$COO), 20.5 (+, *C*H$_3$COO). – ESI-MS $[C_{23}H_{20}O_{11}+H]^+$: *m/z* calcd 473.11; found 473.05. MP 134 °C. Analytical data are consistent with those reported in the literature.[205]

7-*OH*-Quercetin (4-(3,5-diacetoxy-7-hydroxy-4-oxo-4H-chromen-2-yl)-1,2-phenylene diacetate)

Yield: 48 % – ^{1}H NMR: (400 MHz, $CDCl_3$): δ = 7.66-7.64 (m, 2H, Ph), 7.29 (d, ^{3}J = 9.1 Hz, 1H, Ph), 6.63 (d, ^{4}J = 2.3 Hz, 1H, Ph), 6.50 (d, ^{4}J = 2.3 Hz, 1H, Ph), 2.38 (s, 3H, CH_3COO), 2.32 (s, 3H, CH_3COO), 2.31 (s, 6H, CH_3COO). – ^{13}C NMR (100 MHz, $CDCl_3$): δ = 170.7 (C_q, *C*=O), 170.2 (C_q, CH_3*C*OO), 168.8 (C_q, CH_3*C*OO), 168.2 (C_q, CH_3*C*OO), 168.1 (C_q, CH_3*C*OO), 162.1 (C_q, Ph-*C*), 158.0 (C_q, Ph-*C*), 153.6 (C_q, Ph-*C*), 150.7 (C_q, Ph-*C*), 144.4 (C_q, Ph-*C*), 142.2 (C_q, Ph-*C*), 133.4 (C_q, Ph-*C*), 128.0 (C_q, Ph-*C*), 126.6 (+, Ph-*C*), 124.0 (+, Ph-*C*), 123.8 (+, Ph-*C*), 110.3 (C_q, Ph-*C*), 109.7 (+, Ph-*C*), 101.3 (+, Ph-*C*), 21.2 (+, *C*H_3COO), 20.8 (+, 2 x *C*H_3COO), 20.7 (+, *C*H_3COO). – ESI-MS $[C_{23}H_{18}O_{11}+H]^+$: *m/z* calcd 471.08; found 471.10. MP 180 °C. Analytical data are consistent with those reported in the literature.[149]

7-*OH*-Eriodictyol (4-(5-acetoxy-7-hydroxy-4-oxochroman-2-yl)-1,2-phenylene diacetate)

Yield: 45 % – ^{1}H NMR: (400 MHz, $CDCl_3$): δ = 7.32 (d, ^{4}J = 1.6 Hz, 1H, Ar-H), 7.26 (d, ^{3}J = 1.1 Hz, 2H, Ar-H), 6.20 (d, ^{4}J = 2.3, 1H), 6.16 (d, ^{4}J = 2.4 Hz, 1H), 5.35 (dd, ^{3}J = 13.4, ^{4}J = 2.8 Hz, 1H), 2.93 (dd, ^{2}J = 16.7 Hz, ^{3}J = 13.5 Hz, 1H), 2.72 (dd, ^{2}J = 16.7, ^{3}J = 2.9 Hz, 1H), 2.43 (s, 3H, OAc), 2.36 (s, 3H, OAc), 2.36 (s, 3H, OAc). – ^{13}C NMR (100 MHz, $CDCl_3$): δ = 188.7 (C_q, *C*=O), 170.6 (C_q, CH_3*C*OO), 168.7 (C_q, CH_3*C*OO), 168.5 (C_q, CH_3*C*OO), 163.9 (C_q, Ph-*C*), 163.3 (C_q, Ph-*C*), 151.9 (C_q, CH_3*C*OO), 142.3 (C_q, Ph-*C*), 142.2 (C_q, Ph-*C*), 137.4 (C_q, Ph-*C*), 124.7 (+, Ph-*C*), 124.0 (+, Ph-*C*), 121.6 (+, Ph-*C*), 107.5 (C_q, Ph-*C*), 105.8 (+, Ph-*C*), 102.0 (+, Ph-*C*), 78.4 (+, *C*H), 44.7 (-, *C*H_2), 21.3 (+, *C*H_3COO), 20.7 (+, 2 x *C*H_3COO). – ESI-MS $[C_{21}H_{18}O_9+H]^+$: *m/z* calcd 415.10; found 415.15. – MP 128 °C.

7-*OH*-Luteolin (4-(5-acetoxy-7-hydroxy-4-oxo-4H-chromen-2-yl)-1,2-phenylene diacetate)

Yield: 31 % – ^{1}H NMR: (400 MHz, DMSO-d_6): δ = 11.15 (s, 1H, O*H*), 8.00-7.98 (m, 2H, Ar-*H*), 7.48 (d, ^{3}J = 9.2 Hz, 1H, Ar-*H*), 6.95 (d, ^{4}J = 2.3 Hz, 1H, Ar-*H*), 6.77 (s, 1H, C=C*H*), 6.57 (d, ^{4}J = 2.3 Hz, 1H, Ar-*H*), 2.33 (s, 3H, CH_3COO), 2.31 (s, 6H, CH_3COO), 2.29 (s, 3H, CH_3COO). – ^{13}C NMR (100 MHz, DMSO-d_6): δ = 175.1 (C_q, *C*=O), 168.8 (C_q, CH_3*C*OO), 168.2 (C_q, CH_3*C*OO), 167.9 (C_q, CH_3*C*OO), 162.3 (C_q, Ph-*C*), 159.4 (C_q, Ph-*C*), 158.2 (C_q, Ph-*C*), 150.0 (C_q, Ph-*C*), 144.5 (C_q, Ph-*C*), 142.5 (C_q, Ph-*C*), 129.4 (C_q, Ph-*C*), 124.7 (+, Ph-*C*), 124.5 (+, Ph-*C*), 121.7 (+, Ph-*C*), 109.4 (C_q, Ph-*C*), 108.8 (+, Ph-*C*), 107.9 (+, Ph-*C*), 100.9 (+, C=*C*H),

20.9 (+, *C*H_3COO), 20.4 (+, *C*H_3COO), 20.3 (+, *C*H_3COO). – ESI-MS [$C_{23}H_{19}O_{10}$+H]$^+$: *m/z* calcd 413.09; found 413.20 – MP 191 °C. The analytical data are consistent with those reported in the literature.[204]

7-*OH*-Fustin (4-(3-acetoxy-7-hydroxy-4-oxochroman-2-yl)-1,2-phenylene diacetate)

Yield: 44 % – ^{1}H NMR: (400 MHz, $CDCl_3$): δ = 7.80 (d, ^{3}J = 8.6 Hz, 1H, Ar-H), 7.40 (dd, ^{3}*J* = 8.4, ^{4}*J* = 2.1 Hz, 1H, Ar-H), 7.31 (d, ^{4}*J* = 2.1 Hz, 1H, Ar-H), 7.25 (d, ^{3}*J* = 8.6, 1H, Ar-H), 6.53 (dd, ^{3}J = 8.7, ^{4}*J* = 2.3, 1H), 6.41 (d, ^{4}*J* = 2.2, 1H), 5.67 (d, ^{3}*J* = 12.2 Hz, 1H), 5.37 (d, ^{3}*J* = 12.1 Hz, 1H), 2.31 (s, 3H, OAc), 2.30 (s, 3H, OAc), 2.07 (s, 3H, OAc). – ^{13}C NMR (100 MHz, $CDCl_3$): δ = 186.8 (C_q, *C*=O), 169.7 (C_q, CH_3*C*OO), 168.3 (C_q, CH_3*C*OO), 168.3 (C_q, CH_3*C*OO), 163.7 (C_q, 2 x Ph-*C*), 142.8 (C_q, Ph), 142.2 (C_q, Ph), 134.4 (C_q, Ph-*C*), 129.9 (+, Ph-*C*), 125.5 (+, Ph-*C*), 123.9 (+, Ph-*C*), 122.9 (+, Ph-*C*), 113.5 (C_q, Ph-*C*), 111.7 (+, Ph-*C*), 103.5 (+, Ph-*C*), 80.8 (+, *C*H), 73.8 (+, *C*H), 20.8 (+, *C*H_3COO), 20.7 (+, *C*H_3COO), 20.5 (+, *C*H_3COO). – ESI-MS [$C_{21}H_{18}O_9$+H]$^+$: *m/z* calcd 415.11; found 415.15. – MP 143 °C.

7-*OH*-Fisetin (4-(3-acetoxy-7-hydroxy-4-oxo-4H-chromen-2-yl)-1,2-phenylene diacetate)

Yield: 30 % – ^{1}H NMR: (400 MHz, $CDCl_3$): δ = 8.26 (d, ^{3}J = 8.7, 1H, Ph), 7.72 (d, ^{4}J = 2.1 Hz, 1H, Ph), 7.69 (dd, ^{3}J = 8.5, ^{4}*J* = 2.2 Hz, 1H, Ph), 7.40 (d, ^{3}J = 2.1 Hz, 1H, Ph), 7.17 (dd, ^{3}J = 8.7, ^{4}J = 2.1 Hz, 1H, Ph), 7.13 (d, ^{3}J = 8.5 Hz, 1H, Ph), 2.41 (s, 3H, *CH*$_3$COO), 2.37 (s, 3H, *CH*$_3$COO), 2.36 (s, 3H, *CH*$_3$COO). – ^{13}C NMR (100 MHz, $CDCl_3$): δ = 170.2 (C_q, *C*=O), 168.2 (C_q, CH_3*C*OO), 168.0 (C_q, CH_3*C*OO), 167.9 (C_q, CH_3*C*OO), 156.9 (C_q, Ph-*C*), 153.1 (C_q, Ph-*C*), 152.4 (C_q, Ph-*C*), 144.1 (C_q, Ph-*C*), 142.1 (C_q, Ph-*C*), 132.8 (C_q, Ph-*C*), 127.8 (C_q, Ph-*C*), 127.4 (+, Ph-*C*), 126.5 (C_q, Ph-*C*), 126.9 (+, Ph-*C*), 124.9 (+, Ph-*C*), 124.0 (+, Ph-*C*), 116.1 (+, Ph-*C*), 103.1 (+, Ph-*C*), 20.8 (+, *C*H_3COO), 20.7 (+, *C*H_3COO), 20.6 (+, *C*H_3COO). – ESI-MS [$C_{21}H_{16}O_9$+H]$^+$: *m/z* calcd 413.36; found 413.30 – MP 213 °C.

N-(4-Bromobutyl)cinnamamide

To an ice-cold solution of cinnamic acid (174 mg, 1.17 mmol) and DMF (10 µL) in dry dichloromethane (10 mL) oxychloride (149 µL, 1.29 mmol) was added. The solution was stirred 1 h at room temperature before 4-bromobutan-1-amonie hydrobromide (300 mg, 1.29 mmol) was added. A solution of NEt_3 (734 µL, 5.27 mmol.) in dry dichloromethane (5 mL) was added and the reaction mixture was stirred 1 h. Water (30 mL) was added, and the mixture was extracted with dichloromethane (90 mL). The combined organic layers were

washed with 5 % HCl-solution (150 mL), saturated $NaHCO_3$-solution (100 mL) and brine (50 mL) and dried over Na_2SO_4. The solvent was removed under reduced pressure and the product was obtained as pale-yellow solid in 80 % yield (287 mg).

^{1}H NMR: (400 MHz, $CDCl_3$): δ = 7.62 (d, $^3J_{trans}$ = 15.6 Hz, 1H), 7.48 (m, 2H, Ph), 7.35 (m, 3H, Ph), 6.41 (d, $^3J_{trans}$ = 15.6 Hz, 1H), 5.90 (s, 1H, N*H*), 3.43 (m, 4H, CH_2), 1.99 – 1.88 (m, 2H, CH_2), 1.79 – 1.70 (m, 2H, CH_2). – ^{13}C NMR (100 MHz, $CDCl_3$): δ = 166.2 (C_q, C=*C*ONH), 141.2 (+, HC=CH), 134.9 (C_q, Ph), 129.8 (+, Ph-*C*), 128.9 (+, 2 x Ph-*C*), 127.8 (+, 2 x Ph-*C*), 120.7 (+, HC=CH), 38.9 (CH_2) , 33.4 (CH_2), 30.1 (CH_2), 28.4 (CH_2). – ESI-MS $[C_{13}H_{16}BrNO+H]^+$: *m/z* calcd 282.05; found 282.10. – MP 101 °C.

N-(4-Iodobutyl)cinnamamide

A suspension of NaI (800 mg, 5.33 mol) and N-(4-bromobutyl)cinnamamide (287 mg, 1.07 mmol) in dry acetone (10 mL) was heated to reflux for 1.5 h. The solution was diluted with water (20 mL) and extracted with ethyl acetate (80 mL). The organic layer was washed with water (50 mL) and brine (50 mL) and dried over Na_2SO_4. The solvent was removed under reduced pressure and the crude product was used directly without further purification.

General procedure for ether synthesis and deprotection

N-(4-iodobutyl)cinnamamide (1.2 equiv.) and K_2CO_3 (1 equiv.) were added to a solution of the respective 7-*OH*-flavonoid in dry DMF under argon atmosphere and stirred overnight (16 h) at room temperature. Dichloromethane was added and the organic layer was washed with 5 % $HCl_{(aq.)}$ and brine. The organic layer was dried over Na_2SO_4, and the solvent was removed under reduced pressure. The crude product was dissolved in acetonitrile and the same amount of concentrated $HCl_{(aq.)}$ was added. The reaction mixture was stirred 15 minutes at 70°C. Ethyl acetate was added, and the organic layer was washed with 5 % $HCl_{(aq.)}$ and brine. The organic layer was dried over Na_2SO_4, and the solvent was removed under reduced pressure. The crude product was purified using an Interchim Puri Flash 430 purification system equipped with a 12 g C18 50 µm spherical RP column as stationary phase. A mixture of A = water, B = methanol was used a mobile phase, V(B)/(V(A) + V(B)) = from 10 % to 70 % over 15 min, V(B)/(V(A)+V(B)) = 70 % for 35 min. The method was performed with a flow rate of 30.0 mL/min.

Taxifolin-cinnamic acid amide (N-(4-((2-(3,4-dihydroxyphenyl)-3,5-dihydroxy-4-oxochroman-7-yl)oxy)butyl)cinnamamide)

The product was obtained as white solid in 15 % yield (40 mg).

^{1}H NMR: (400 MHz, DMSO-d_6): δ = 11.46 (s, 1H, O*H*), 9.08 (s, 2H, O*H*), 8.12 (t, ^3J = 5.7 Hz, 1H, N*H*), 7.54 (d, ^{3}J = 7.27 Hz, 2H, Ar-*H*), 7.42-7.34 (m, 4H, 3 x Ar-*H, H*C=CH), 6.89 (s, 1H, Ar-*H*), 6.75 (s, 2H, Ar-*H*), 6.61 (d, $^3J_{trans}$ = 15.8 Hz, 1H, HC=C*H*), 6.10 (d, ^4J = 2.2 Hz, 1H, Ar-*H*), 6.07 (d, ^4J = 2.2 Hz, 1H), 5.78 (s, 1H, *OH*), 5.02 (d, ^3J = 11.2 Hz, 1H, OC*H*), 4.54 (d, ^3J = 11.3 Hz, 1H, C*H*), 4.05 (t, ^3J = 6.3 Hz, 2H, OCH_2), 3.22 (q, ^3J = 6.6 Hz, 2H, NC*H*), 1.72 (m, 2H, CH_2), 1.58 (m, 2H, CH_2) ppm. – ^{13}C NMR (100 MHz, DMSO-d_6): δ 198.2 (C_q, *C*=O), 166.9 (C_q, Ar-*C*), 164.8 (N*C*=O), 162.9 (C_q, Ar-*C*), 162.4 (C_q, Ar-*C*), 145.7 (C_q, Ar-*C*), 144.9 (C_q, Ar-*C*), 138.4 (+, H*C*=CH), 134.9 (C_q, Ar-*C*), 129.3 (+, Ar-*C*), 128.9 (+, 2 x Ar-*C*), 127.8 (C_q, Ar-*C*), 127.4 (+, 2 x Ar-*C*), 122.2 (+, H*C*=CH), 119.3 (+, Ar-*C*), 115.3 (+, Ar-*C*), 115.0 (+, Ar-*C*), 101.3 (C_q, Ar-*C*), 95.2 (+, Ar-*C*), 94.1 (+, Ar-*C*), 83.1 (+, *C*H), 71.6 (+, *C*H), 68.0 (-, O*C*H_2), 38.2 (-, N*C*H_2), 25.9 (-, *C*H_2), 25.6 (-, *C*H_2) ppm. – ESI-MS $[C_{28}H_{27}NO_8+H]^+$: *m/z* calcd 506.18; found 506.15. – MP 153 °C dec.

Quercetin-cinnamic acid amide (N-(4-((2-(3,4-dihydroxyphenyl)-3,5-dihydroxy-4-oxo-4H-chromen-7-yl)oxy)butyl)cinnamamide)

The product was obtained as yellow solid in yield 10 % (15 mg).

^{1}H NMR: (400 MHz, DMSO-d_6): δ = 12.46 (s, 1H, O*H*), 9.44 (s, 2H, O*H*), 8.15 (t, ^3J = 5.8 Hz, 1H, N*H*), 7.73 (d, ^{4}J = 1.85 Hz, 1H, Ar-*H*), 7.58-7.53 (m, 3H, 3 x Ar-*H*), 7.45-7.34 (m, 4H, 3 x Ar-*H, H*C=CH), 6.89 (d, 1H, ^{3}J = 8.4 Hz, Ar-*H*), 6.70 (dd, 1H, ^{3}J = 8.05, ^{4}J = 2.2 Hz, Ar-*H*), 6.62 (d, $^3J_{trans}$ = 15.8 Hz, 1H, HC=C*H*), 6.33 (d, ^4J = 2.2 Hz, 1H, Ar-*H*), 4.12 (t, ^3J = 5.1 Hz, 2H, OCH_2), 3.26 (q, ^3J = 6.5 Hz, 2H, NC*H*), 1.73 (m, 2H, CH_2), 1.62 (m, 2H, CH_2) ppm. – ^{13}C NMR (100 MHz, DMSO-d_6): δ 175.9 (C_q, *C*=O), 164.9 (N*C*=O), 164.2 (C_q, Ar-*C*), 160.3 (C_q, Ar-*C*), 156.0 (C_q, Ar-*C*), 147.8 (C_q, Ar-*C*), 147.2 (C_q, Ar-*C*), 145.0 (C_q, Ar-*C*), 138.4 (+, H*C*=CH), 136.0 (C_q, Ar-*C*), 134.9 (C_q, Ar-*C*), 129.3 (+, Ar-*C*), 128.9 (+, 2 x Ar-*C*), 127.4 (+, 2 x Ar-*C*), 122.3 (+, H*C*=CH), 121.84 (C_q, Ar-*C)*, 119.9 (+, Ar-*C*), 115.5 (+, Ar-*C*), 115.2 (+, Ar-*C*), 103.9 (C_q, Ar-*C*), 97.4 (+, Ar-*C*), 92.2 (+, Ar-*C*), 68.1 (-, O*C*H_2), 38.2 (-, N*C*H_2), 26.0 (-, *C*H_2), 25.7 (-, *C*H_2) ppm. – ESI-MS $[C_{28}H_{25}NO_8+H]^+$: *m/z* calcd 504.16; found 504.15. – MP 205 °C dec.

Eriodictyol-cinnamic acid amide (N-(4-((2-(3,4-dihydroxyphenyl)-5-hydroxy-4-oxochroman-7-yl)oxy)butyl)cinnamamide)

The product was obtained as white solid in 55 % yield (31 mg).

^{1}H NMR: (400 MHz, DMSO-d_6): δ = 12.10 (s, 1H, O*H*), 9.04 (s, 2H, O*H*), 8.13 (t, ^3J = 5.7 Hz, 1H, N*H*), 7.58 – 7.51 (m, 2H, Ar-*H*), 7.45 – 7.34 (m, 4H, Ar-*H*), 6.89 (d, ^4J = 1.3 Hz, 1H, Ar-*H*), 6.75 (d, ^4J = 1.2 Hz, 2H, Ar-*H*), 6.62 (d, $^3J_{trans}$ = 15.8 Hz, 1H, HC=C*H*), 6.08 (d, ^4J = 2.3 Hz, 1H, Ar-*H*), 6.07 (d, ^4J = 2.3 Hz, 1H, Ar-*H*), 5.41 (dd, $^3J_{trans}$ = 12.5, $^3J_{cis}$ = 3.0 Hz, 1H, OC*H*), 4.05 (t, ^3J = 6.4 Hz, 2H, OCH_2), 3.27 – 3.17 (m, 3H, CH_2, C*H*), 2.71 (dd, ^2J = 17.2, $^3J_{cis}$ = 3.1 Hz, 1H, C*H*), 1.73 (m, 2H, CH_2), 1.58 (m, 2H, CH_2). ppm. – ^{13}C NMR (100 MHz, DMSO-d_6): δ 196.28(C_q, *C*=O), 166.7 (C_q, Ar-*C*), 164.8 (N*C*=O), 163.1 (C_q, Ar-*C*), 162.8 (C_q, Ar-*C*), 145.8 (C_q, Ar-*C*), 145.2 (C_q, Ar-*C*), 138.5 (+, H*C*=CH), 134.9 (C_q, Ar-*C*), 129.4 (+, Ar-*C*), 129.3 (C_q, Ar-*C*), 128.9 (+, 2 x Ar-*C*), 127.4 (+, 2 x Ar-*C*), 122.3 (+, H*C*=CH), 117.9 (+, Ar-*C*), 115.3 (+, Ar-*C*), 114.3 (+, Ar-*C*), 102.5 (C_q, Ar-*C*), 94.9 (+, Ar-*C*), 94.1 (+, Ar-*C*), 78.6 (+, *C*H), 67.9 (-, O*C*H_2), 42.1 (-, CH_2), 38.2 (-, N*C*H_2), 25.9 (-, *C*H_2), 25.6 (-, *C*H_2) ppm. – ESI-MS $[C_{28}H_{27}NO_7+H]^+$: *m/z* calcd 490.18; found 490.20. – MP 164 °C dec.

Luteolin-cinnamic acid amide (N-(4-((2-(3,4-dihydroxyphenyl)-5-hydroxy-4-oxo-4H-chromen-7-yl)oxy)butyl)cinnamamide)

The product was obtained as yellow solid in 15 % yield (11 mg).

^{1}H NMR: (400 MHz, DMSO-d_6): δ = 12.96 (s, 1H, O*H*), 8.15 (t, ^3J = 5.7 Hz, 1H, N*H*), 7.55 (m, 2H), 7.46 – 7.33 (m, 6H), 6.89 (d, ^3J = 8.1 Hz, 1H, Ar-*H*), 6.74 – 6.69 (m, 2H, C=C*H*, Ar-*H*), 6.63 (d, $^3J_{trans}$ = 15.8, 1H), 6.36 (d, ^4J = 2.2 Hz, 1H, Ar-*H*), 4.13 (t, ^3J = 6.6 Hz, 2H, OCH_2), 3.33 – 3.22 (q, ^3J = 6.5 Hz, 2H, NC*H*), 1.78 (m, 2H, CH_2), 1.64 (m, 2H, CH_2) ppm. – ^{13}C NMR (100 MHz, DMSO-d_6): δ 181.7 (C_q, *C*=O), 164.8 (N*C*=O), 164.4 (C_q, Ar-*C*), 164.2 (C_q, Ar-*C*), 161.1 (C_q, Ar-*C*), 157.2 (C_q, Ar-*C*), 146.9 (C_q, Ar-*C*), 145.8 (C_q, Ar-*C*), 138.4 (+, H*C*=CH), 134.9 (C_q, Ar-*C*), 129.3 (+, Ar-*C*), 128.9 (+, 2 x Ar-*C*), 127.4 (+, 2 x Ar-*C*), 122.2 (+, H*C*=CH), 121.3 (C_q, Ar-*H*), 119.9 (+, Ar-*C*), 115.9 (+, Ar-*C*), 113.4 (+, Ar-*C*), 104.5 (C_q, Ar-*C*), 102.9 (+, Ar-*C*), 98.3 (+, Ar-*C*), 92.9 (+, Ar-*C*), 68.1 (-, O*C*H_2), 38.2 (-, N*C*H_2), 25.9 (-, *C*H_2), 25.6 (-, *C*H_2) ppm. – ESI-MS $[C_{28}H_{25}NO_7+H]^+$: *m/z* calcd 488.17; found 488.20. – MP 209 °C.

Fustin-cinnamic acid amide (N-(4-((2-(3,4-dihydroxyphenyl)-3-hydroxy-4-oxochroman-7-yl)oxy)butyl)cinnamamide)

The product was obtained as off-white solid in 11 % yield (5 mg).

^{1}H NMR: (400 MHz, DMSO-d_6): δ = 8.13 (s, 1H, t, ^3J = 5.6 Hz, 1H, N*H*), 7.69 (d, ^3J = 8.8 Hz, 1H, Ar-*H*), 7.58 – 7.51 (m, 2H, Ar-*H*), 7.44 – 7.34 (m, 4H, 3 x Ar-*H*, C=C*H*), 6.89 (d, ^4J = 2.0 Hz, 1H, Ar-*H*), 6.76 (dd, ^3J = 8.16 , ^4J = 1.9 Hz, 1H, Ar-*H*), 6.73 (d, *J* = 8.16 Hz, 1H, Ar-*H*), 6.67 (dd, ^3J = 8.8, ^4J = 2.3 Hz, 1H, Ar-*H*), 6.61 (d, $^3J_{trans}$ = 15.9 Hz, 1H, C=C*H*), 6.56 (d, ^4J = 2.3 Hz, 1H, Ar-*H*), 5.01 (d, ^3J = 11.4 Hz, 1H, C*H*), 4.45 (d, ^3J = 11.4 Hz, 1H, C*H*), 4.08 (t, ^3J = 6.6 Hz, 2H, OCH_2), 3.24 (m, 2H, NCH_2), 1.76-1.72 (m, 2H, CH_2), 1.64 – 1.55 (m, 2H, CH_2) ppm. – ^{13}C NMR (100 MHz, DMSO-d_6): δ 192.6 (C_q, *C*=O), 165.0 (C_q, Ar-*C*), 164.8 (C_q, N*C*=O), 162.8 (C_q, Ar-*C*), 145.8 (C_q, Ar-*C*), 144.9 (C_q, Ar-*C*), 138.4 (+, H*C*=CH), 134.9 (C_q, Ar-*C*), 129.3 (+ Ar-*C*), 128.8 (+, 2 x Ar-*C*), 128.2 (+, Ar-*C*), 127.4 (+, 2 x Ar-*C*), 125.5 (C_q, Ar-*C*), 122.3 (+, H*C*=CH), 119.5 (+, Ar-*C*), 115.3 (+, Ar-*C*), 115.0 (+, Ar-*C*), 114.4 (C_q, Ar-*C*), 110.4 (+, Ar-*C*), 101.2 (+, Ar-*C*), 83.6 (+, *C*H), 72.5 (+, *C*H), 67.8 (-, O*C*H_2), 38.2 (-, N*C*H_2), 25.9 (-, *C*H_2), 25.7 (-, *C*H_2) ppm. – ESI-MS $[C_{28}H_{27}NO_7+H]^+$: *m/z* calcd 490.18; found 490.15. – MP 169 °C.

Fisetin-cinnamic acid amide (N-(4-((2-(3,4-dihydroxyphenyl)-3-hydroxy-4-oxo-4H-chromen-7-yl)oxy)butyl)cinnamamide)

The product was obtained as yellow solid in 12 % yield (12 mg).

^{1}H NMR: (400 MHz, DMSO-d_6): δ = 9.23 (s, 2H, O*H*), 8.15 (t, ^3J = 5.2 Hz, 1H, N*H*), 7.91 (d, 1H, ^{3}J = 8.5 Hz, Ar-*H*), 7.70 (d, ^{4}J = 2.2 Hz, 1H, Ar-*H*), 7.62 (dd, 1H, ^{3}J = 8.6, ^{4}J = 2.2 Hz, 7.56 – 7.53 (m, 3H, 3 x Ar-*H,*), 7.45 – 7.35 (m, 4H, Ar-*H*, *H*C=CH), 7.07 (d, 1H, ^{3}J = 8.7 Hz, Ar-*H*), 6.87 (d, 1H, ^{4}J = 2.2 Hz, Ar-*H*), 6.63 (d, $^3J_{trans}$ = 15.8 Hz, 1H, HC=C*H*), 4.08 (t, ^3J = 6.3 Hz, 2H, OCH_2), 3.27 (q, ^3J = 6.5 Hz, 2H, NC*H*), 1.80 (m, 2H, CH_2), 1.65 (m, 2H, CH_2) ppm. – ^{13}C NMR (100 MHz, DMSO-d_6): δ 171.9 (C_q, *C*=O), 164.8 (N*C*=O), 162.7 (C_q, Ar-*C*), 156.4 (C_q, Ar-*C*), 156.2 (C_q, Ar-*C*), 148.1 (C_q, Ar-*C*), 146.5 (C_q, Ar-*C*), 145.4 (C_q, Ar-*C*), 138.4 (+, H*C*=CH), 134.9 (C_q, Ar-*C*), 129.3 (+, Ar-*C*), 128.8 (+, 2 x Ar-*C*), 127.4 (+, 2 x Ar-*C*), 126.4 (+, Ar-*C*), 122.3 (+, H*C*=CH), 121.8 (C_q, Ar-*C)*, 119.3 (+, Ar-*C*), 115.5 (+, Ar-*C*), 114.5 (+, Ar-*C*), 113.8 (C_q, Ar-*C*), 112.9 (+, Ar-*C*), 101.7 (+, Ar-*C*), 67.9 (-, O*C*H_2), 38.3 (-, N*C*H_2), 26.1 (-, *C*H_2), 25.8 (-, *C*H_2) ppm. – ESI-MS $[C_{28}H_{25}NO_7+H]^+$: *m/z* calcd 488.16; found 488.15– MP 218 °C.

HPLC-chromatograms for Purity Control of the Target Compounds

Purity of the synthesis products was determined by HPLC (Shimadzu Products), containing a DGU-20A3R degassing unit, a LC20AB liquid chromatograph, and an SPD-20A UV/vis detector. UV detection was measured at 254 nm. Mass spectra were obtained by a LCMS 2020 (Shimadzu Products) running in positive ionisation mode. As a stationary phase, a Synergi 4U fusion-RP (150 mm × 4.6 mm) column was used, and as a mobile phase, a gradient of methanol/water with 0.1 % (v/v) formic acid. Parameters: A = water, B = methanol, V(B)/(V(A) + V(B)) = from 5 % to 90 % over 10 min, V(B)/(V(A)+V(B)) = 90 % for 5 min, V(B)/(V(A) + V(B)) = from 90 % to 5 % over 3 min. The method was performed with a flow rate of 1.0 mL/min.

Taxifolin-CA

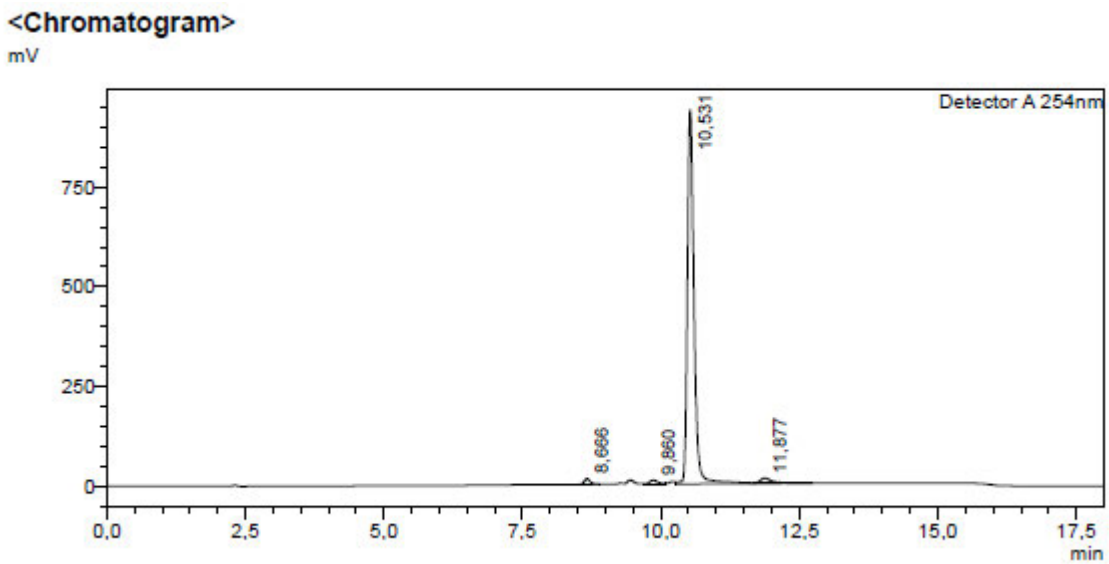

Detector A 254nm

Peak#	Ret. Time	Area	Height	Conc.	Unit	Mark	Area%
1	8,666	101221	14176	1,228			1,228
2	9,860	100893	10184	1,224		V	1,224
3	10,531	7886979	937389	95,659		SV	95,659
4	11,877	155804	12038	1,890		T	1,890
Total		8244897	973787				100,000

Quercetin-CA

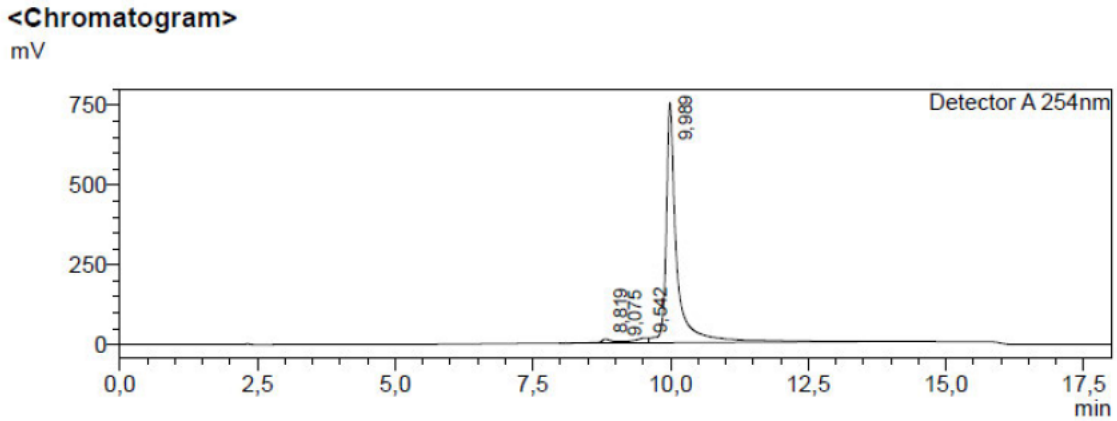

Peak#	Ret. Time	Area	Area%
1	8,819	180404	1,683
2	9,075	33998	0,317
3	9,542	267992	2,501
4	9,989	10234304	95,499
Total		10716698	100,000

Eriodictyol-CA

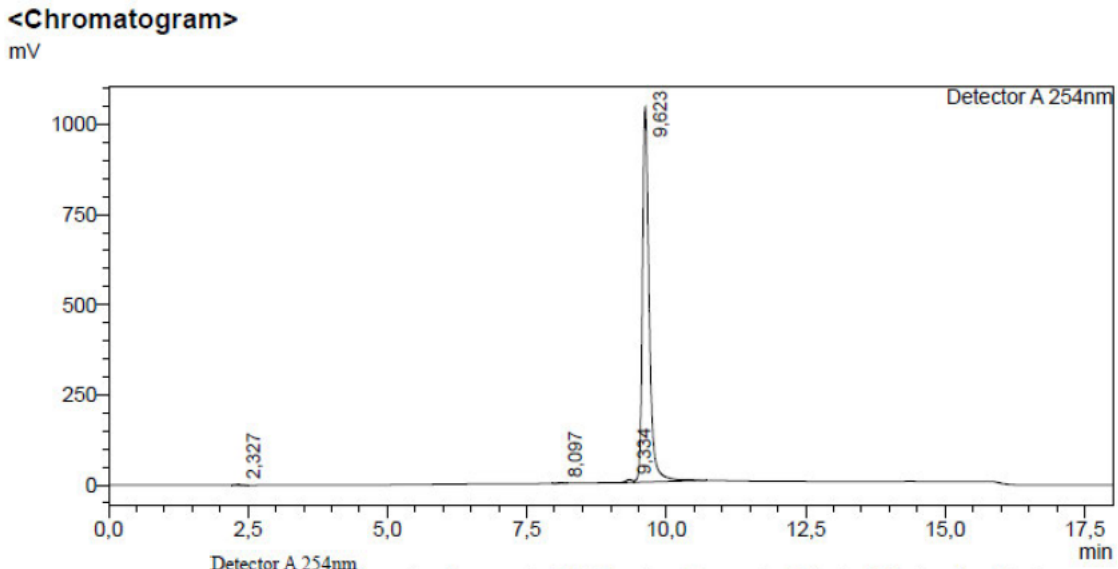

Detector A 254nm

Peak#	Ret. Time	Area	Height	Conc.	Unit	Mark	Area%
1	2.327	11882	2302	0.134			0.134
2	8.097	11511	1658	0.130			0.130
3	9.334	68853	8298	0.777			0.777
4	9.623	8773834	1038367	98.960		SV	98.960
Total		8866080	1050624				100.000

Luteolin-CA

<Chromatogram>

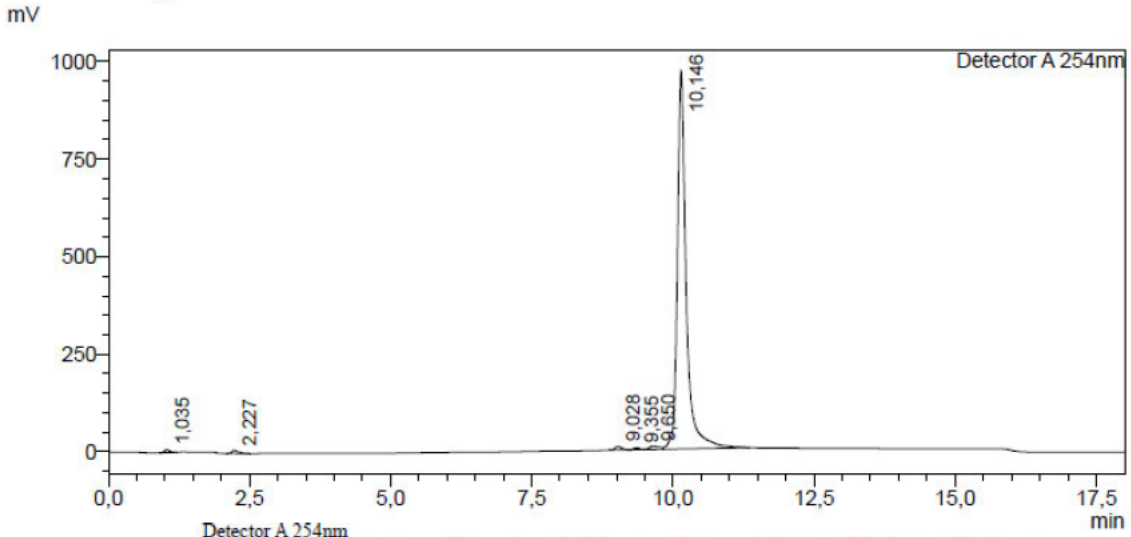

Detector A 254nm

Peak#	Ret. Time	Area	Height	Conc.	Unit	Mark	Area%
1	1,035	48393	7591	0,446			0,446
2	2,227	65456	8382	0,604			0,604
3	9,028	75236	8887	0,694			0,694
4	9,355	36748	5011	0,339		V	0,339
5	9,650	105867	8285	0,976		V	0,976
6	10,146	10511534	967713	96,941		V	96,941
Total		10843234	1005869				100,000

Fustin-CA

<Chromatogram>

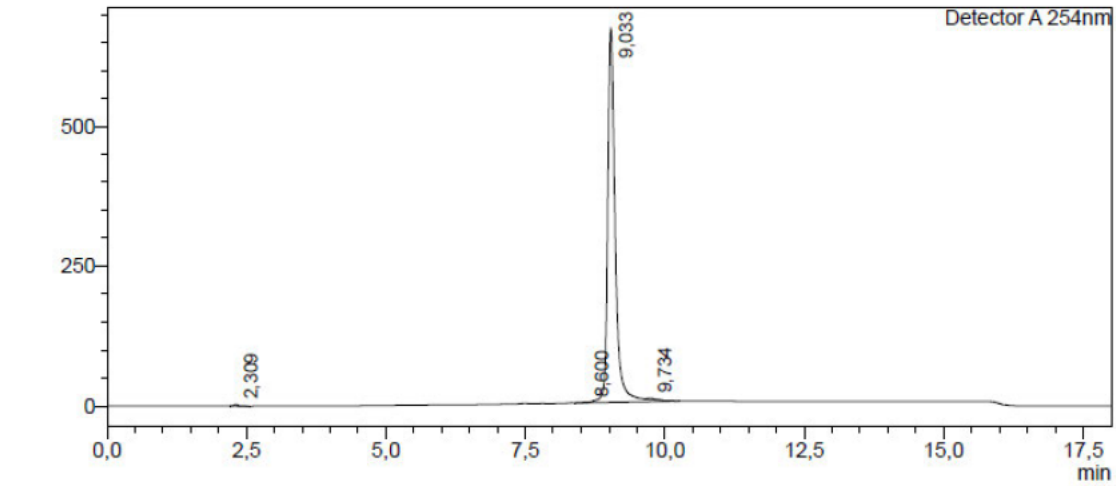

Detector A 254nm

Peak#	Ret. Time	Area	Height	Conc.	Unit	Mark	Area%
1	2,309	13316	2841	0,211			0,211
2	8,600	15040	1377	0,238		V	0,238
3	9,033	6272620	667297	99,304		SV	99,304
4	9,734	15613	2109	0,247		T	0,247
Total		6316589	673624				100,000

Fisetin-CA

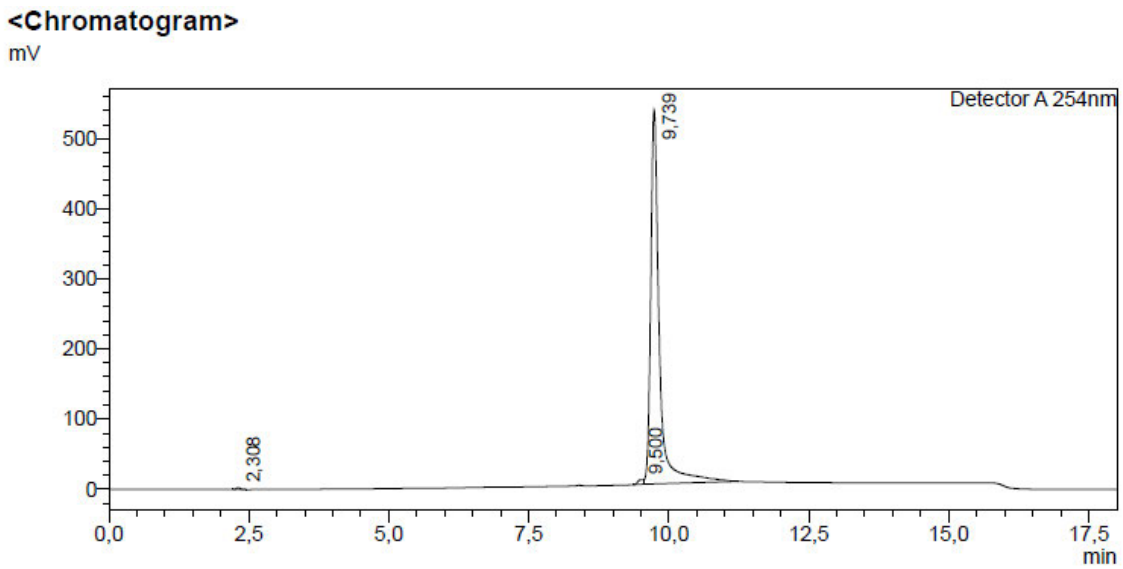

Detector A 254nm

Peak#	Ret. Time	Area	Height	Conc.	Unit	Mark	Area%
1	2.308	11051	2439	0.191			0.191
2	9.500	42481	6784	0.735			0.735
3	9.739	5724520	533597	99.074		V	99.074
Total		5778052	542820				100.000

8.2 Biology

Cell Culture general procedures

HT22 cells were grown in Dulbecco's Modified Eagle Medium (DMEM, Sigma Aldrich, Munich Germany) supplemented with 10 % (v/v) fetal calf serum (FCS) and 1 % (v/v) penicillin-streptomycin. BV-2 cells were grown in low glucose DMEM (Invitrogen, Carlsbad, CA, USA) supplemented with 10 % FCS and 1 % (v/v) penicillin-streptomycin. Cells were subcultured every two days and incubated at 37°C with 5 % CO_2 in a humidified incubator.

Compounds were dissolved in dimethyl sulfoxide (DMSO, Sigma Aldrich, Munich, Germany) as stock solutions and diluted further into culture medium.

For determination of cell viability, a colorimetric 3-(4,5-dimethylthiazol-2-yl)-2,5- diphenyl tetrazolium bromide (MTT, Sigma Aldrich, Munich, Germany) assay was used. MTT solution (4 mg/mL in PBS) was diluted 1:10 with medium and added to the wells after removal of the old medium. Cells were incubated for 3 hours and then lysis buffer (10 % SDS) was applied. The next day, absorbance at 560 nm was determined with a multiwell plate photometer (Tecan, SpectraMax 250).

Oxytosis in HT22 cells

HT22 cells were seeded into sterile 96-well plates at a density of 5 x 10^3 per well and incubated overnight. The medium was exchanged, and cells were treated with 5 mM glutamate (monosodium-*L*-glutamate, Sigma Aldrich, Munich, Germany) alone or together with 1.56, 3.12, 6.25 or 12.5 µM of the respective compound. After 24 hours cell viability was determined using a colorimetric MTT assay as described above. Results are presented as percentage of untreated control cells. Data is expressed as means ± SEM of three independent experiments. Analysis was accomplished using GraphPad Prism 5 Software applying Oneway ANOVA followed by Dunnett's multiple comparison posttest. Levels of significance: * $p < 0.05$; ** $p < 0.01$; *** $p < 0.001$.

Reactive oxygen species (ROS) measurement

HT22 cells were seeded into sterile black walled 96-well plates at a density of 5 x 10^3 per well and incubated overnight. The medium was exchanged, and cells were treated with 5 mM glutamate (monosodium-*L*-glutamate, Sigma Aldrich, Munich, Germany) alone or together with 1.56, 3.12, 6.25 or 12.5 µM of the respective compound for 6 hours. The medium was removed and 100 µL phenol red-free Hank's balanced salt solution (Sigma Aldrich, Munich, Germany) containing 1 µM CM-H_2DCFDA (Thermo Fisher Scientific, Darmstadt, Germany) was added. After 20 min incubation, fluorescence (λ excitation = 495 nm, λ emission = 525 nM) was determined using a Tecan Infinite M Plus microplate reader or subjected to fluorescence microscopy using a Zeiss Axiovert Observer fluorescence microscope. Fluorescence was normalized to control cells not exposed to glutamate. Images were processed with the ZEN 3.4 (blue edition) software. Data is expressed as means ± SEM of three independent experiments. Analysis was accomplished using GraphPad Prism 5 Software applying Oneway ANOVA followed by Dunnett's multiple comparison posttest. Levels of significance: */# $p < 0.05$; **/## $p < 0.01$; ***/### $p < 0.001$.

Ferroptosis in HT22 cells

HT22 cells were seeded into sterile 96-well plates at a density of 3 x 10^3 per well and incubated overnight. The medium was exchanged, and cells were treated with 300 nM RSL-3 (Sigma Aldrich, Munich, Germany) alone or together with 1.56, 3.12, 6.25 or 12.5 µM of the respective compound. After 24 hours cell viability was determined using a colorimetric MTT assay as described above. Results are presented as percentage of untreated control cells. Data is expressed as means ± SEM of three independent experiments. Analysis was accomplished

using GraphPad Prism 5 Software applying Oneway ANOVA followed by Dunnett's multiple comparison posttest. Levels of significance: * $p < 0.05$; ** $p < 0.01$; *** $p < 0.001$.

ATP depletion in HT22 cells

HT22 cells were seeded into sterile 96-well plates at a density of 3×10^3 per well and incubated overnight. The medium was exchanged, and cells were treated with 17.5 µM iodoacetic acid (IAA) (Sigma Aldrich, Munich, Germany) alone or together with 1.56, 3.12, 6.25 or 12.5 µM of the respective compound. After 24 hours cell viability was determined using a colorimetric MTT assay as described above. Results are presented as percentage of untreated control cells. Data is expressed as means ± SEM of three independent experiments. Analysis was accomplished using GraphPad Prism 5 Software applying Oneway ANOVA followed by Dunnett's multiple comparison posttest. Levels of significance: * $p < 0.05$; ** $p < 0.01$; *** $p < 0.001$.

Cellular uptake experiments and stability in cell culture medium

BV-2 cells or HT22 cells were grown in sterile 100 mm dishes at a density of 8×10^6 cells overnight. The next day, 50 µM taxifolin-CA diluted in cell culture medium (4 mL) was added. Cells were incubated for the indicated time periods, after which the supernatant was removed, and cells were washed twice with PBS. Further PBS (1 mL) was added, cells were scraped and transferred to Eppendorf tubes. The samples were centrifuged (10000 x g for 5 minutes) and resuspended in 200 µL of MeOH. The cells were frozen in liquid nitrogen and thawed at 37 °C (10 times). Cell debris was pelleted by centrifugation (10000 x g for 10 minutes) and the supernatant was collected for HPLC analysis using the HPLC system described above equipped with a Synergi 4U fusion-RP (250 mm × 10 mm) column as a stationary phase. As a mobile phase, a gradient of methanol/water with 0.1 % (v/v) formic acid. Parameters: A = water, B = methanol, V(B)/(V(A) + V(B)) = from 5 % to 80 % over 20 min, V(B)/(V(A)+V(B)) = 80 % for 10 min, V(B)/(V(A) + V(B)) = from 80 % to 5 % over 5 min. The method was performed with a flow rate of 1.0 mL/min and the injection volume was 50 µL.
For stability experiments, taxifolin-CA was diluted in Dulbecco's Modified Eagle Medium (DMEM, Sigma Aldrich, Munich Germany) supplemented with 10 % (v/v) fetal calf serum (FCS) and 1 % (v/v) penicillin-streptomycin to a final concentration of 50 µM and incubated for the indicated time period at 37 °C in an Eppendorf Thermo Mixer F1.5. The solution was mixed 1/1 with ice-cold methanol and precipitant was removed by centrifugation (10000 x g for 10

minutes). The supernatant was subjected to HPLC-UV/MS analysis and quantification was done by calibration curve.

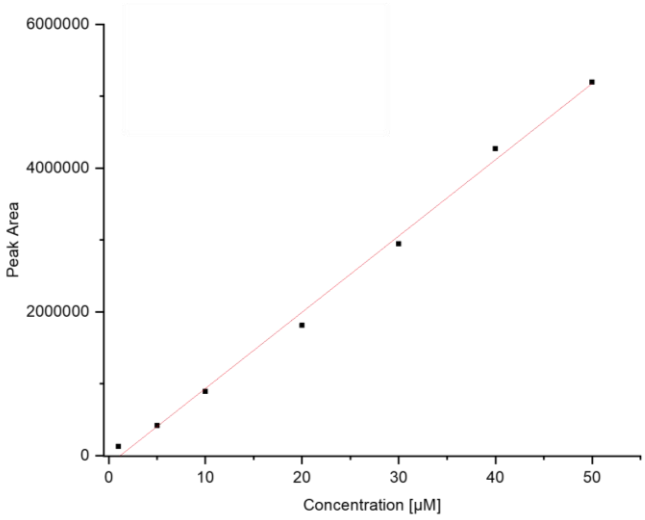

Figure 29: Calibration curve of taxifolin-CA. Injections were done in triplicates. Y axis fraction = -124431.28, slope = 106014.18, R^2 = 0.9959.

9. Abbreviations

12/15 LOX	12/15 lipid oxygenase
AD	Alzheimer´s disease
ANOVA	analysis of variance
APP	amyloid precursor protein
ATP	adenosin triphosphate
Aβ	β-amyloid
B.C.	before christ
BBB	blood brain barrier
BPO	benzoyl peroxide
CA	cinnamic acid
CD	clyco dextrine
cGMP	cyclic guanosine monophosphate
COMT	catechol-O-methyltransferase
DMF	dimethyl formamide
DMSO	dimethyl sulfoxide
DPPH	2,2-diphenyl-1-picrylhydrazyl
E. californicum	*Eriodictyon californicum*
E. coli	Escherichia coli
ECD	electron capture detector
EGCG	epigallocatechin-3-gallate
EtOH	ethanol
FCS	fetal bovine serum
FRAP	ferric ion reducing antioxidant parameter
GAPDH	glyceraldehyde 3-phosphate dehydrogenase
GPx4	glutathione peroxidase 4
GSH	glutathione
HBA	hydrogen bond acceptor
HBD	hydrogen bond donor
HBr	hydrobromic acide
HCl	hydrochloric acid
HPLC	high-pressure liquid chromatography
IAA	iodoacetic acid
IB	inclusion bodies
icv	intracerebroventricular

IL-6	interleukin 6
ip	intraperitoneal
KOH	potassium hydroxide
LPS	lipopolysaccharide
MCI	mild cognitive impairment
MeCN	acetonitrile
MeOH	methanol
MOM	methoxymethyl
MS	mass spectrometry
NaH	sodium hydride
NaOAc	sodium acetate
NaOH	sodium hydroxide
NBS	*N*-bromosuccinimide
NFT	neurofibrillary tangles
nm	nanometer
NMR	nuclear magnetic resonance
NO	nitrogen monoxide
Nrf2	nuclear factor (erythroid-derived 2)-related factor 2
PAINS	pan assay interference compounds
PD	Parkinson´s disease
PDA	photodiode-array
PEG	polyethylene glycol
r.t.	room temperature
rac.	racemic
ROS	reactive oxygen species
SAR	structure-activity relationship
SEM	standard error of mean
SP	senile plaques
STPA	step-through passive-avoidance assay
TFA	trifluoroacetic acid
Th-S	thioflavin-S
TLC	thin layer chromatography
TNF-α	tumor necrosis factor-alpha
UV	ultraviolet
v	vehicle
YMT	Y-maze test

10. References

1. Gauthier S., Rosa-Neto P., Morais JA, & Webster C., World Alzheimer Report 2021. *London, England: Alzheimer's Disease International.* **2021**.

2. 2020 Alzheimer's disease facts and figures. *Alzheimers. Dement.* **2020,** *16* (3), 391-460.

3. Alzheimer, A., Über eine Eigenartige Erkrankung der Hirnrinde. *Allg. Z. Psychiat.* **1907,** *64*, 146-148.

4. Villemagne, V. L.; Burnham, S.; Bourgeat, P.; Brown, B.; Ellis, K. A.; Salvado, O.; Szoeke, C.; Macaulay, S. L.; Martins, R.; Maruff, P.; Ames, D.; Rowe, C. C.; Masters, C. L., Amyloid β deposition, neurodegeneration, and cognitive decline in sporadic Alzheimer's disease: a prospective cohort study. *Lancet Neurol.* **2013,** *12* (4), 357-367.

5. Reiman, E. M.; Quiroz, Y. T.; Fleisher, A. S.; Chen, K.; Velez-Pardo, C.; Jimenez-Del-Rio, M.; Fagan, A. M.; Shah, A. R.; Alvarez, S.; Arbelaez, A.; Giraldo, M.; Acosta-Baena, N.; Sperling, R. A.; Dickerson, B.; Stern, C. E.; Tirado, V.; Munoz, C.; Reiman, R. A.; Huentelman, M. J.; Alexander, G. E.; Langbaum, J. B. S.; Kosik, K. S.; Tariot, P. N.; Lopera, F., Brain imaging and fluid biomarker analysis in young adults at genetic risk for autosomal dominant Alzheimer's disease in the presenilin 1 E280A kindred: a case-control study. *Lancet Neurol.* **2012,** *11* (12), 1048-1056.

6. Jack, C. R., Jr; Lowe, V. J.; Weigand, S. D.; Wiste, H. J.; Senjem, M. L.; Knopman, D. S.; Shiung, M. M.; Gunter, J. L.; Boeve, B. F.; Kemp, B. J.; Weiner, M.; Petersen, R. C.; Initiative, t. A. s. D. N., Serial PIB and MRI in normal, mild cognitive impairment and Alzheimer's disease: implications for sequence of pathological events in Alzheimer's disease. *Brain* **2009,** *132* (5), 1355-1365.

7. Bateman, R. J.; Xiong, C.; Benzinger, T. L. S.; Fagan, A. M.; Goate, A.; Fox, N. C.; Marcus, D. S.; Cairns, N. J.; Xie, X.; Blazey, T. M.; Holtzman, D. M.; Santacruz, A.; Buckles, V.; Oliver, A.; Moulder, K.; Aisen, P. S.; Ghetti, B.; Klunk, W. E.; McDade, E.; Martins, R. N.; Masters, C. L.; Mayeux, R.; Ringman, J. M.; Rossor, M. N.; Schofield, P. R.; Sperling, R. A.; Salloway, S.; Morris, J. C., Clinical and Biomarker Changes in Dominantly Inherited Alzheimer's Disease. *N. Engl. J. Med.* **2012,** *367* (9), 795-804.

8. Gordon, B. A.; Blazey, T. M.; Su, Y.; Hari-Raj, A.; Dincer, A.; Flores, S.; Christensen, J.; McDade, E.; Wang, G.; Xiong, C.; Cairns, N. J.; Hassenstab, J.; Marcus, D. S.; Fagan, A. M.; Jack, C. R.; Hornbeck, R. C.; Paumier, K. L.; Ances, B. M.; Berman, S. B.; Brickman, A. M.; Cash, D. M.; Chhatwal, J. P.; Correia, S.; Förster, S.; Fox, N. C.; Graff-Radford, N. R.; la Fougère, C.; Levin, J.; Masters, C. L.; Rossor, M. N.; Salloway, S.; Saykin, A. J.; Schofield, P. R.; Thompson, P. M.; Weiner, M. M.; Holtzman, D. M.; Raichle, M. E.; Morris, J. C.; Bateman, R. J.; Benzinger, T. L. S., Spatial patterns of neuroimaging biomarker change in individuals from families with autosomal dominant Alzheimer's disease: a longitudinal study. *Lancet Neurol.* **2018,** *17* (3), 241-250.

9. Braak, H.; Thal, D. R.; Ghebremedhin, E.; Del Tredici, K., Stages of the Pathologic Process in Alzheimer Disease: Age Categories From 1 to 100 Years. *J. Neuropathol. Exp. Neurol.* **2011,** *70* (11), 960-969.

10. Sperling, R.; Aisen, P.; Beckett, L.; Bennett, D.; Craft, S.; Fagan, A.; Iwatsubo, T.; Jack Jr, C. R.; Kaye, J.; Montine, T., Towards defining the preclinical stages of Alzheimer's disease: recommendations from the National Institute on Aging–Alzheimer's Association workgroups on diagnostic guidelines for Alzheimer's disease. *Alzheimers. Dement.* **2011,** *7* (3), 280-292.

11. Marilyn S. Albert; Steven T. DeKosky; Dennis Dickson; Bruno Dubois; Howard H. Feldman; Nick C. Fox; Anthony Gamst; David M. Holtzman; William J. Jagust; Ronald C. Petersen; Peter J. Snyder; Maria C. Carrillo; Bill Thies, and; Creighton H. Phelps, The Diagnosis of Mild Cognitive Impairment due to Alzheimer's Disease: Recommendations from the National Institute on Aging-Alzheimer's Association Workgroups on Diagnostic Guidelines for Alzheimer's Disease. *FOCUS* **2013,** *11* (1), 96-106.

12. McKhann, G. M.; Knopman, D. S.; Chertkow, H.; Hyman, B. T.; Jack Jr., C. R.; Kawas, C. H.; Klunk, W. E.; Koroshetz, W. J.; Manly, J. J.; Mayeux, R.; Mohs, R. C.; Morris, J. C.; Rossor, M. N.; Scheltens, P.; Carrillo, M. C.; Thies, B.; Weintraub, S.; Phelps, C. H., The diagnosis of dementia due to Alzheimer's disease: Recommendations from the National Institute on Aging-Alzheimer's Association workgroups on diagnostic guidelines for Alzheimer's disease. *Alzheimers. Dement.* **2011,** *7* (3), 263-269.

13. Jack Jr., C. R.; Albert, M. S.; Knopman, D. S.; McKhann, G. M.; Sperling, R. A.; Carrillo, M. C.; Thies, B.; Phelps, C. H., Introduction to the recommendations from the National Institute on Aging-Alzheimer's Association workgroups on diagnostic guidelines for Alzheimer's disease. *Alzheimers. Dement.* **2011,** *7* (3), 257-262.

14. Przedborski, S.; Vila, M.; Jackson-Lewis, V., Series Introduction: Neurodegeneration: What is it and where are we? *J. Clin. Invest.* **2003,** *111* (1), 3-10.

15. Prior, M.; Chiruta, C.; Currais, A.; Goldberg, J.; Ramsey, J.; Dargusch, R.; Maher, P. A.; Schubert, D., Back to the Future with Phenotypic Screening. *ACS Chem. Neurosci.* **2014,** *5* (7), 503-513.

16. Bishop, N. A.; Lu, T.; Yankner, B. A., Neural mechanisms of ageing and cognitive decline. *Nature* **2010,** *464* (7288), 529-535.

17. Bloom, G. S., Amyloid-β and tau: the trigger and bullet in Alzheimer disease pathogenesis. *JAMA Neurol.* **2014,** *71* (4), 505-508.

18. Hebert, L. E.; Bienias, J. L.; Aggarwal, N. T.; Wilson, R. S.; Bennett, D. A.; Shah, R. C.; Evans, D. A., Change in risk of Alzheimer disease over time. *Neurology* **2010,** *75* (9), 786-791.

19. Hebert, L. E.; Weuve, J.; Scherr, P. A.; Evans, D. A., Alzheimer disease in the United States (2010–2050) estimated using the 2010 census. *Neurology* **2013,** *80* (19), 1778-1783.

20. Mattson, M. P., Addendum: Pathways towards and away from Alzheimer's disease. *Nature* **2004,** *431* (7004), 107-107.

21. Sun, X.; Chen, W.-D.; Wang, Y.-D., β-Amyloid: The Key Peptide in the Pathogenesis of Alzheimer's Disease. *Front. Pharmacol.* **2015,** *6* (221).

22. Thinakaran, G.; Koo, E. H., Amyloid Precursor Protein Trafficking, Processing, and Function. *J. Biol. Chem.* **2008,** *283* (44), 29615-29619.

23. J. Baranello, R.; L. Bharani, K.; Padmaraju, V.; Chopra, N.; K. Lahiri, D.; H. Greig, N.; A. Pappolla, M.; Sambamurti, K., Amyloid-Beta Protein Clearance and Degradation (ABCD) Pathways and their Role in Alzheimer´s Disease. *Curr. Alzheimer Res.* **2015,** *12* (1), 32-46.

24. Cline, E. N.; Bicca, M. A.; Viola, K. L.; Klein, W. L., The Amyloid-β Oligomer Hypothesis: Beginning of the Third Decade. *J. Alzheimer's Dis.* **2018,** *64*, S567-S610.

25. Beyreuther, K.; Dyrks, T.; Hilbich, C.; Mönning, U.; König, G.; Multhaup, G.; Pollwein, P.; Masters, C., Amyloid precursor protein (APP) and beta A4 amyloid in Alzheimer's disease and Down syndrome. *Prog. Clin. Biol. Res.* **1992,** *379*, 159-182.

26. Hardy, J.; Allsop, D., Amyloid deposition as the central event in the aetiology of Alzheimer's disease. *Trends Pharmacol. Sci.* **1991,** *12*, 383-388.

27. Hardy, J. A.; Higgins, G. A., Alzheimer's disease: the amyloid cascade hypothesis. *Science* **1992,** *256* (5054), 184-186.

28. Selkoe, D. J., The molecular pathology of Alzheimer's disease. *Neuron* **1991,** *6* (4), 487-498.

29. Selkoe, D. J.; Hardy, J., The amyloid hypothesis of Alzheimer's disease at 25 years. *EMBO Mol. Med.* **2016,** *8* (6), 595-608.

30. Frautschy, S. A.; Cole, G. M., Why Pleiotropic Interventions are Needed for Alzheimer's Disease. *Mol. Neurobiol.* **2010,** *41* (2), 392-409.

31. Pimplikar, S. W., Reassessing the amyloid cascade hypothesis of Alzheimer's disease. *Int. J. Biochem. Cell Biol.* **2009,** *41* (6), 1261-1268.

32. Aisen, P. S.; Gauthier, S.; Ferris, S. H.; Saumier, D.; Haine, D.; Garceau, D.; Duong, A.; Suhy, J.; Oh, J.; Lau, W. C.; Sampalis, J., Tramiprosate in mild-to-moderate Alzheimer's disease - a randomized, double-blind, placebo-controlled, multi-centre study (the Alphase Study). *Arch. Med. Sci.* **2011,** *7* (1), 102-111.

33. Green, R. C.; Schneider, L. S.; Amato, D. A.; Beelen, A. P.; Wilcock, G.; Swabb, E. A.; Zavitz, K. H.; Tarenflurbil Phase 3 Study, G., Effect of tarenflurbil on cognitive decline and activities of daily living in patients with mild Alzheimer disease: a randomized controlled trial. *JAMA* **2009,** *302* (23), 2557-2564.

34. Doody, R. S.; Raman, R.; Farlow, M.; Iwatsubo, T.; Vellas, B.; Joffe, S.; Kieburtz, K.; He, F.; Sun, X.; Thomas, R. G.; Aisen, P. S.; Siemers, E.; Sethuraman, G.; Mohs, R., A Phase 3 Trial of Semagacestat for Treatment of Alzheimer's Disease. *N. Engl. J. Med.* **2013,** *369* (4), 341-350.

35. Salloway, S.; Sperling, R.; Fox, N. C.; Blennow, K.; Klunk, W.; Raskind, M.; Sabbagh, M.; Honig, L. S.; Porsteinsson, A. P.; Ferris, S.; Reichert, M.; Ketter, N.; Nejadnik, B.;

Guenzler, V.; Miloslavsky, M.; Wang, D.; Lu, Y.; Lull, J.; Tudor, I. C.; Liu, E.; Grundman, M.; Yuen, E.; Black, R.; Brashear, H. R.; Bapineuzumab; Clinical Trial, I., Two phase 3 trials of bapineuzumab in mild-to-moderate Alzheimer's disease. *N. Engl. J. Med.* **2014,** *370* (4), 322-333.

36. Phase 3 Trials of Solanezumab and Bapineuzumab for Alzheimer's Disease. *N. Engl. J. Med.* **2014,** *370* (15), 1459-1460.

37. Lalli, G.; Schott, J. M.; Hardy, J.; De Strooper, B., Aducanumab: a new phase in therapeutic development for Alzheimer's disease? *EMBO Mol. Med.* **2021,** *13* (8), e14781.

38. Walsh, S.; Merrick, R.; Milne, R.; Brayne, C., Aducanumab for Alzheimer's disease? *BMJ* **2021,** *374*, n1682.

39. Gao, Y.; Tan, L.; Yu, J.-T.; Tan, L., Tau in Alzheimer's Disease: Mechanisms and Therapeutic Strategies. *Curr. Alzheimer Res.* **2018,** *15* (3), 283-300.

40. Binder, L. I.; Frankfurter, A.; Rebhun, L. I., The distribution of tau in the mammalian central nervous system. *J. Cell Biol.* **1985,** *101* (4), 1371-1378.

41. Dawson, H. N.; Ferreira, A.; Eyster, M. V.; Ghoshal, N.; Binder, L. I.; Vitek, M. P., Inhibition of neuronal maturation in primary hippocampal neurons from τ deficient mice. *J. Cell Sci.* **2001,** *114* (6), 1179-1187.

42. Lee, G.; Newman, S. T.; Gard, D. L.; Band, H.; Panchamoorthy, G., Tau interacts with src-family non-receptor tyrosine kinases. *J. Cell Sci.* **1998,** *111* (21), 3167-3177.

43. Iqbal, K.; Liu, F.; Gong, C. X.; Grundke-Iqbal, I., Tau in Alzheimer Disease and Related Tauopathies. *Curr. Alzheimer Res.* **2010,** *7* (8), 656-664.

44. Cohen, T. J.; Guo, J. L.; Hurtado, D. E.; Kwong, L. K.; Mills, I. P.; Trojanowski, J. Q.; Lee, V. M. Y., The acetylation of tau inhibits its function and promotes pathological tau aggregation. *Nat. Commun.* **2011,** *2* (1), 252.

45. Min, S.-W.; Cho, S.-H.; Zhou, Y.; Schroeder, S.; Haroutunian, V.; Seeley, W. W.; Huang, E. J.; Shen, Y.; Masliah, E.; Mukherjee, C.; Meyers, D.; Cole, P. A.; Ott, M.; Gan, L., Acetylation of Tau Inhibits Its Degradation and Contributes to Tauopathy. *Neuron* **2010,** *67* (6), 953-966.

46. Karran, E.; De Strooper, B., The amyloid cascade hypothesis: are we poised for success or failure? *J. Neurochem.* **2016,** *139* (S2), 237-252.

47. Nisbet, R. M.; Polanco, J.-C.; Ittner, L. M.; Götz, J., Tau aggregation and its interplay with amyloid-β. *Acta Neuropathol.* **2015,** *129* (2), 207-220.

48. Spires-Jones, T. L.; Attems, J.; Thal, D. R., Interactions of pathological proteins in neurodegenerative diseases. *Acta Neuropathol.* **2017,** *134* (2), 187-205.

49. Guerrero-Muñoz, M. J.; Gerson, J.; Castillo-Carranza, D. L., Tau Oligomers: The Toxic Player at Synapses in Alzheimer's Disease. *Front. Cell. Neurosci.* **2015,** *9* (464).

50. Ittner, L. M.; Götz, J., Amyloid-β and tau — a toxic pas de deux in Alzheimer's disease. *Nat. Rev. Neurosci.* **2011,** *12* (2), 67-72.

51. Lage, O. M.; Ramos, M. C.; Calisto, R.; Almeida, E.; Vasconcelos, V.; Vicente, F., Current Screening Methodologies in Drug Discovery for Selected Human Diseases. *Marine Drugs* **2018,** *16* (8), 279.

52. Currais, A.; Chiruta, C.; Goujon-Svrzic, M.; Costa, G.; Santos, T.; Batista, M. T.; Paiva, J.; Céu Madureira, M. d.; Maher, P., Screening and identification of neuroprotective compounds relevant to Alzheimer′s disease from medicinal plants of S. Tomé e Príncipe. *J. Ethnopharmacol.* **2014,** *155* (1), 830-840.

53. Sagara, Y.; Vanhnasy, J.; Maher, P., Induction of PC12 cell differentiation by flavonoids is dependent upon extracellular signal-regulated kinase activation. *J. Neurochem.* **2004,** *90* (5), 1144-1155.

54. Sopher, B. L.; Fukuchi, K.-i.; Smith, A. C.; Leppig, K. A.; Furlong, C. E.; Martin, G. M., Cytotoxicity mediated by conditional expression of a carboxyl-terminal derivative of the β-amyloid precursor protein. *Brain Res. Mol.* **1994,** *26* (1), 207-217.

55. Tönnies, E.; Trushina, E., Oxidative Stress, Synaptic Dysfunction, and Alzheimer's Disease. *J. Alzheimer's Dis.* **2017,** *57*, 1105-1121.

56. Huang, W. J.; Zhang, X.; Chen, W. W., Role of oxidative stress in Alzheimer's disease. *Biomed Rep* **2016,** *4* (5), 519-522.

57. Tan, S.; Wood, M.; Maher, P., Oxidative Stress Induces a Form of Programmed Cell Death with Characteristics of Both Apoptosis and Necrosis in Neuronal Cells. *J. Neurochem.* **1998,** *71* (1), 95-105.

58. Kerr, J. F. R.; Wyllie, A. H.; Currie, A. R., Apoptosis: A Basic Biological Phenomenon with Wideranging Implications in Tissue Kinetics. *Br. J. Cancer* **1972,** *26* (4), 239-257.

59. Murphy, T. H.; Miyamoto, M.; Sastre, A.; Schnaar, R. L.; Coyle, J. T., Glutamate toxicity in a neuronal cell line involves inhibition of cystine transport leading to oxidative stress. *Neuron* **1989,** *2* (6), 1547-1558.

60. Tan, S.; Schubert, D.; Maher, P., Oxytosis: A Novel Form of Programmed Cell Death. *Curr. Top. Med. Chem.* **2001,** *1* (6), 497-506.

61. Dixon, Scott J.; Lemberg, Kathryn M.; Lamprecht, Michael R.; Skouta, R.; Zaitsev, Eleina M.; Gleason, Caroline E.; Patel, Darpan N.; Bauer, Andras J.; Cantley, Alexandra M.; Yang, Wan S.; Morrison, B.; Stockwell, Brent R., Ferroptosis: An Iron-Dependent Form of Nonapoptotic Cell Death. *Cell* **2012,** *149* (5), 1060-1072.

62. Lewerenz, J.; Ates, G.; Methner, A.; Conrad, M.; Maher, P., Oxytosis/Ferroptosis—(Re-) Emerging Roles for Oxidative Stress-Dependent Non-apoptotic Cell Death in Diseases of the Central Nervous System. *Front. Neurosci.* **2018,** *12* (214).

63. Davis, J. B.; Maher, P., Protein kinase C activation inhibits glutamate-induced cytotoxicity in a neuronal cell line. *Brain Res.* **1994,** *652* (1), 169-173.

64. Gout, P. W.; Buckley, A. R.; Simms, C. R.; Bruchovsky, N., Sulfasalazine, a potent suppressor of lymphoma growth by inhibition of the xc− cystine transporter: a new action for an old drug. *Leukemia* **2001,** *15* (10), 1633-1640.

65. Schafer, F. Q.; Buettner, G. R., Redox environment of the cell as viewed through the redox state of the glutathione disulfide/glutathione couple. *Free Radic. Biol. Med.* **2001,** *30* (11), 1191-1212.

66. Tan, S.; Sagara, Y.; Liu, Y.; Maher, P.; Schubert, D., The regulation of reactive oxygen species production during programmed cell death. *J. Cell Biol.* **1998,** *141* (6), 1423-1432.

67. Maher, P.; Currais, A.; Schubert, D., Using the Oxytosis/Ferroptosis Pathway to Understand and Treat Age-Associated Neurodegenerative Diseases. *Cell Chem. Biol.* **2020,** *27* (12), 1456-1471.

68. Seiler, A.; Schneider, M.; Förster, H.; Roth, S.; Wirth, E. K.; Culmsee, C.; Plesnila, N.; Kremmer, E.; Rådmark, O.; Wurst, W.; Bornkamm, G. W.; Schweizer, U.; Conrad, M., Glutathione Peroxidase 4 Senses and Translates Oxidative Stress into 12/15-Lipoxygenase Dependent- and AIF-Mediated Cell Death. *Cell Metab.* **2008,** *8* (3), 237-248.

69. Imai, H.; Nakagawa, Y., Biological significance of phospholipid hydroperoxide glutathione peroxidase (PHGPx, GPx4) in mammalian cells. *Free Radic. Biol. Med.* **2003,** *34* (2), 145-169.

70. Yang, Wan S.; SriRamaratnam, R.; Welsch, Matthew E.; Shimada, K.; Skouta, R.; Viswanathan, Vasanthi S.; Cheah, Jaime H.; Clemons, Paul A.; Shamji, Alykhan F.; Clish, Clary B.; Brown, Lewis M.; Girotti, Albert W.; Cornish, Virginia W.; Schreiber, Stuart L.; Stockwell, Brent R., Regulation of Ferroptotic Cancer Cell Death by GPX4. *Cell* **2014,** *156* (1), 317-331.

71. Li, Y.; Maher, P.; Schubert, D., A Role for 12-lipoxygenase in Nerve Cell Death Caused by Glutathione Depletion. *Neuron* **1997,** *19* (2), 453-463.

72. Feng, H.; Stockwell, B. R., Unsolved mysteries: How does lipid peroxidation cause ferroptosis? *PLoS Biol.* **2018,** *16* (5), e2006203.

73. Lei, P.; Bai, T.; Sun, Y., Mechanisms of Ferroptosis and Relations With Regulated Cell Death: A Review. *Front. Physiol.* **2019,** *10* (139).

74. Stoyanovsky, D. A.; Tyurina, Y. Y.; Shrivastava, I.; Bahar, I.; Tyurin, V. A.; Protchenko, O.; Jadhav, S.; Bolevich, S. B.; Kozlov, A. V.; Vladimirov, Y. A.; Shvedova, A. A.; Philpott, C. C.; Bayir, H.; Kagan, V. E., Iron catalysis of lipid peroxidation in ferroptosis: Regulated enzymatic or random free radical reaction? *Free Radic. Biol. Med.* **2019,** *133*, 153-161.

75. Murphy, T. H.; Malouf, A. T.; Sastre, A.; Schnaar, R. L.; Coyle, J. T., Calcium-dependent glutamate cytotoxicity in a neuronal cell line. *Brain Res.* **1988,** *444* (2), 325-332.

76. Jelinek, A.; Heyder, L.; Daude, M.; Plessner, M.; Krippner, S.; Grosse, R.; Diederich, W. E.; Culmsee, C., Mitochondrial rescue prevents glutathione peroxidase-dependent ferroptosis. *Free Radic. Biol. Med.* **2018,** *117*, 45-57.

77. Landshamer, S.; Hoehn, M.; Barth, N.; Duvezin-Caubet, S.; Schwake, G.; Tobaben, S.; Kazhdan, I.; Becattini, B.; Zahler, S.; Vollmar, A.; Pellecchia, M.; Reichert, A.; Plesnila, N.; Wagner, E.; Culmsee, C., Bid-induced release of AIF from mitochondria causes immediate neuronal cell death. *Cell Death Differ.* **2008,** *15* (10), 1553-1563.

78. Huang, L.; McClatchy, D. B.; Maher, P.; Liang, Z.; Diedrich, J. K.; Soriano-Castell, D.; Goldberg, J.; Shokhirev, M.; Yates, J. R.; Schubert, D.; Currais, A., Intracellular amyloid toxicity induces oxytosis/ferroptosis regulated cell death. *Cell Death Dis.* **2020,** *11* (10), 828.

79. Hou, Y.; Dan, X.; Babbar, M.; Wei, Y.; Hasselbalch, S. G.; Croteau, D. L.; Bohr, V. A., Ageing as a risk factor for neurodegenerative disease. *Nat. Rev. Neurol.* **2019,** *15* (10), 565-581.

80. López-Otín, C.; Blasco, M. A.; Partridge, L.; Serrano, M.; Kroemer, G., The Hallmarks of Aging. *Cell* **2013,** *153* (6), 1194-1217.

81. Devi, L.; Prabhu, B. M.; Galati, D. F.; Avadhani, N. G.; Anandatheerthavarada, H. K., Accumulation of Amyloid Precursor Protein in the Mitochondrial Import Channels of Human Alzheimer's Disease Brain Is Associated with Mitochondrial Dysfunction. *J. Neurosci.* **2006,** *26* (35), 9057-9068.

82. Pérez-Gracia, E.; Torrejón-Escribano, B.; Ferrer, I., Dystrophic neurites of senile plaques in Alzheimer's disease are deficient in cytochrome c oxidase. *Acta Neuropathol.* **2008,** *116* (3), 261-268.

83. Reichmann, H.; Fhirke, S.; Hebenstreit, G.; Schrubar, H.; Riederer, P., Analyses of energy metabolism and mitochondrial genome in post-mortem brain from patients with Alzheimer's disease. *J. Neurol.* **1993,** *240* (6), 377-380.

84. Warren, R. E.; Frier, B. M., Hypoglycaemia and cognitive function. *Diabetes Obes. Metab.* **2005,** *7* (5), 493-503.

85. Maher, P.; Salgado, K. F.; Zivin, J. A.; Lapchak, P. A., A novel approach to screening for new neuroprotective compounds for the treatment of stroke. *Brain Res.* **2007,** *1173*, 117-125.

86. Heneka, M. T.; Carson, M. J.; Khoury, J. E.; Landreth, G. E.; Brosseron, F.; Feinstein, D. L.; Jacobs, A. H.; Wyss-Coray, T.; Vitorica, J.; Ransohoff, R. M.; Herrup, K.; Frautschy, S. A.; Finsen, B.; Brown, G. C.; Verkhratsky, A.; Yamanaka, K.; Koistinaho, J.; Latz, E.; Halle, A.; Petzold, G. C.; Town, T.; Morgan, D.; Shinohara, M. L.; Perry, V. H.; Holmes, C.; Bazan, N. G.; Brooks, D. J.; Hunot, S.; Joseph, B.; Deigendesch, N.; Garaschuk, O.; Boddeke, E.; Dinarello, C. A.; Breitner, J. C.; Cole, G. M.; Golenbock, D. T.; Kummer, M. P., Neuroinflammation in Alzheimer's disease. *Lancet Neurol.* **2015,** *14* (4), 388-405.

87. Kettenmann, H.; Hanisch, U.-K.; Noda, M.; Verkhratsky, A., Physiology of Microglia. *Physiol. Rev.* **2011,** *91* (2), 461-553.

88. Ji, K.; Akgul, G.; Wollmuth, L. P.; Tsirka, S. E., Microglia Actively Regulate the Number of Functional Synapses. *PloS One* **2013,** *8* (2), e56293.

89. Parkhurst, Christopher N.; Yang, G.; Ninan, I.; Savas, Jeffrey N.; Yates, John R.; Lafaille, Juan J.; Hempstead, Barbara L.; Littman, Dan R.; Gan, W.-B., Microglia Promote Learning-Dependent Synapse Formation through Brain-Derived Neurotrophic Factor. *Cell* **2013,** *155* (7), 1596-1609.

90. Streit, W. J.; Mrak, R. E.; Griffin, W. S. T., Microglia and neuroinflammation: a pathological perspective. *J. Neuroinflammation* **2004,** *1* (1), 14.

91. Lyman, M.; Lloyd, D. G.; Ji, X.; Vizcaychipi, M. P.; Ma, D., Neuroinflammation: The role and consequences. *Neurosci. Res.* **2014,** *79*, 1-12.

92. Stewart, C. R.; Stuart, L. M.; Wilkinson, K.; van Gils, J. M.; Deng, J.; Halle, A.; Rayner, K. J.; Boyer, L.; Zhong, R.; Frazier, W. A.; Lacy-Hulbert, A.; Khoury, J. E.; Golenbock, D. T.; Moore, K. J., CD36 ligands promote sterile inflammation through assembly of a Toll-like receptor 4 and 6 heterodimer. *Nat. Immunol.* **2010,** *11* (2), 155-161.

93. El Khoury , J. B.; Moore , K. J.; Means , T. K.; Leung , J.; Terada , K.; Toft , M.; Freeman , M. W.; Luster , A. D., CD36 Mediates the Innate Host Response to β-Amyloid. *J. Exp. Med.* **2003,** *197* (12), 1657-1666.

94. Fillit, H.; Ding, W.; Buee, L.; Kalman, J.; Altstiel, L.; Lawlor, B.; Wolf-Klein, G., Elevated circulating tumor necrosis factor levels in Alzheimer's disease. *Neurosci. Lett.* **1991,** *129* (2), 318-320.

95. Strauss, S.; Bauer, J.; Ganter, U.; Jonas, U.; Berger, M.; Volk, B., Detection of interleukin-6 and alpha 2-macroglobulin immunoreactivity in cortex and hippocampus of Alzheimer's disease patients. *Lab. Invest.* **1992,** *66* (2), 223-230.

96. Hansen, D. V.; Hanson, J. E.; Sheng, M., Microglia in Alzheimer’s disease. *J. Cell Biol.* **2017,** *217* (2), 459-472.

97. Wyss-Coray, T.; Rogers, J., Inflammation in Alzheimer Disease—A Brief Review of the Basic Science and Clinical Literature. *Cold Spring Harb. Perspect. Med.* **2012,** *2* (1).

98. Dias, D. A.; Urban, S.; Roessner, U., A Historical Overview of Natural Products in Drug Discovery. *Metabolites* **2012,** *2* (2), 303-336.

99. Sarker, S. D.; Nahar, L., An Introduction to Natural Products Isolation. In *Natural Products Isolation*, Sarker, S. D.; Nahar, L., Eds. Humana Press: Totowa, NJ, 2012; pp 1-25.

100. Newman, D. J.; Cragg, G. M., Natural Products as Sources of New Drugs from 1981 to 2014. *J. Nat. Prod.* **2016,** *79* (3), 629-661.

101. Yun, B.-W.; Yan, Z.; Amir, R.; Hong, S.; Jin, Y.-W.; Lee, E.-K.; Loake, G. J., Plant natural products: history, limitations and the potential of cambial meristematic cells. *Biotechnol. Genet. Eng. Rev.* **2012,** *28* (1), 47-60.

102. Bakoyiannis, I.; Daskalopoulou, A.; Pergialiotis, V.; Perrea, D., Phytochemicals and cognitive health: Are flavonoids doing the trick? *Biomed. Pharmacother.* **2019,** *109*, 1488-1497.

103. Ververidis, F.; Trantas, E.; Douglas, C.; Vollmer, G.; Kretzschmar, G.; Panopoulos, N., Biotechnology of flavonoids and other phenylpropanoid-derived natural products. Part I: Chemical diversity, impacts on plant biology and human health. *Biotechnol. J.* **2007,** *2* (10), 1214-1234.

104. Wagner, H.; Farkas, L., Synthesis of Flavonoids. In *The Flavonoids*, Harborne, J. B.; Mabry, T. J.; Mabry, H., Eds. Springer US: Boston, MA, 1975; pp 127-213.

105. Beking, K.; Vieira, A., Flavonoid intake and disability-adjusted life years due to Alzheimer's and related dementias: a population-based study involving twenty-three developed countries. *Public Health Nutr.* **2010,** *13* (9), 1403-1409.

106. Commenges, D.; Scotet, V.; Renaud, S.; Jacqmin-Gadda, H.; Barberger-Gateau, P.; Dartigues, J. F., Intake of flavonoids and risk of dementia. *Eur. J. Epidemiol.* **2000,** *16* (4), 357-363.

107. Gao, X.; Cassidy, A.; Schwarzschild, M. A.; Rimm, E. B.; Ascherio, A., Habitual intake of dietary flavonoids and risk of Parkinson disease. *Neurology* **2012,** *78* (15), 1138-1145.

108. Li, Y. L.; Guo, H.; Zhao, Y. Q.; Li, A. F.; Ren, Y. Q.; Zhang, J. W., Quercetin protects neuronal cells from oxidative stress and cognitive degradation induced by amyloid β-peptide treatment. *Mol. Med. Rep.* **2017,** *16* (2), 1573-1577.

109. Frandsen, J.; Narayanasamy, P., Flavonoid Enhances the Glyoxalase Pathway in Cerebellar Neurons to Retain Cellular Functions. *Sci. Rep.* **2017,** *7* (1), 5126.

110. Lee, M.; McGeer, E. G.; McGeer, P. L., Quercetin, not caffeine, is a major neuroprotective component in coffee. *Neurobiol. Aging* **2016,** *46*, 113-123.

111. Tanaka, M.; Saito, S.; Inoue, T.; Satoh-Asahara, N.; Ihara, M., Novel Therapeutic Potentials of Taxifolin for Amyloid-β-associated Neurodegenerative Diseases and Other Diseases: Recent Advances and Future Perspectives. *Int. J. Mol. Sci.* **2019,** *20* (9), 2139.

112. Maher, P., How fisetin reduces the impact of age and disease on CNS function. *Front. Biosci. (Schol. Ed.)* **2015,** *7*, 58-82.

113. Fischer, W.; Currais, A.; Liang, Z.; Pinto, A.; Maher, P., Old age-associated phenotypic screening for Alzheimer's disease drug candidates identifies sterubin as a potent neuroprotective compound from Yerba santa. *Redox Biol.* **2019,** *21*, 101089.

114. Di Paolo, M.; Papi, L.; Gori, F.; Turillazzi, E., Natural Products in Neurodegenerative Diseases: A Great Promise but an Ethical Challenge. *Int. J. Mol. Sci.* **2019,** *20* (20), 5170.

115. Shoji, Y.; Nakashima, H., Nutraceutics and Delivery Systems. *J. Drug Target* **2004,** *12* (6), 385-391.

116. Kivipelto, M.; Mangialasche, F.; Ngandu, T., Lifestyle interventions to prevent cognitive impairment, dementia and Alzheimer disease. *Nat. Rev. Neurol.* **2018,** *14* (11), 653-666.

117. Bakoyiannis, I.; Gkioka, E.; Pergialiotis, V.; Mastroleon, I.; Prodromidou, A.; Vlachos, G. D.; Perrea, D., Fetal alcohol spectrum disorders and cognitive functions of young children. *Rev. Neurosci.* **2014,** *25* (5), 631-639.

118. Abbott, N. J.; Patabendige, A. A. K.; Dolman, D. E. M.; Yusof, S. R.; Begley, D. J., Structure and function of the blood–brain barrier. *Neurobiol. Dis.* **2010,** *37* (1), 13-25.

119. Andres-Lacueva, C.; Shukitt-Hale, B.; Galli, R. L.; Jauregui, O.; Lamuela-Raventos, R. M.; Joseph, J. A., Anthocyanins in aged blueberry-fed rats are found centrally and may enhance memory. *Nutr. Neurosci.* **2005,** *8* (2), 111-120.

120. Peng, H. W.; Cheng, F. C.; Huang, Y. T.; Chen, C. F.; Tsai, T. H., Determination of naringenin and its glucuronide conjugate in rat plasma and brain tissue by high-performance liquid chromatography. *J. Chromatogr. B Biomed. Appl.* **1998,** *714* (2), 369-374.

121. Abd El Mohsen, M. M.; Kuhnle, G.; Rechner, A. R.; Schroeter, H.; Rose, S.; Jenner, P.; Rice-Evans, C. A., Uptake and metabolism of epicatechin and its access to the brain after oral ingestion. *Free Radic. Biol. Med.* **2002,** *33* (12), 1693-1702.

122. Maher, P., The Potential of Flavonoids for the Treatment of Neurodegenerative Diseases. *Int. J. Mol. Sci.* **2019,** *20* (12).

123. Xie, H.; Wang, J.-R.; Yau, L.-F.; Liu, Y.; Liu, L.; Han, Q.-B.; Zhao, Z.; Jiang, Z.-H., Quantitative Analysis of the Flavonoid Glycosides and Terpene Trilactones in the Extract of Ginkgo biloba and Evaluation of Their Inhibitory Activity towards Fibril Formation of β-Amyloid Peptide. *Molecules* **2014,** *19* (4), 4466-4478.

124. Tan, M.-S.; Yu, J.-T.; Tan, C.-C.; Wang, H.-F.; Meng, X.-F.; Wang, C.; Jiang, T.; Zhu, X.-C.; Tan, L., Efficacy and Adverse Effects of Ginkgo Biloba for Cognitive Impairment and Dementia: A Systematic Review and Meta-Analysis. *J. Alzheimer's Dis.* **2015,** *43*, 589-603.

125. Schramm, S.; Huang, G.; Gunesch, S.; Lang, F.; Roa, J.; Högger, P.; Sabaté, R.; Maher, P.; Decker, M., Regioselective synthesis of 7-O-esters of the flavonolignan silibinin and SARs lead to compounds with overadditive neuroprotective effects. *Eur. J. Med. Chem.* **2018,** *146*, 93-107.

126. Gunesch, S.; Kiermeier, C.; Hoffmann, M.; Fischer, W.; Pinto, A. F. M.; Maurice, T.; Maher, P.; Decker, M., 7-O-Esters of taxifolin with pronounced and overadditive effects in neuroprotection, anti-neuroinflammation, and amelioration of short-term memory impairment in vivo. *Redox Biol.* **2019**, 101378.

127. Bui Thanh, T.; Nguyen Thanh, H., Natural product for the treatment of Alzheimer's disease. In *J. Basic Clin. Physiol. Pharmacol.*, 2017; Vol. 28, pp 413-423.

128. Pohl, F.; Kong Thoo Lin, P., The potential use of plant natural products and plant extracts with antioxidant properties for the prevention/treatment of neurodegenerative diseases: in vitro, in vivo and clinical trials. *Molecules* **2018,** *23* (12), 3283.

129. Chesnut, V. K., *Plants used by the Indians of Mendocino County, California*. Mendocino County Historical Society Incorporated: 1974; Vol. 7.

130. Walker, J.; Reichelt, K. V.; Obst, K.; Widder, S.; Hans, J.; Krammer, G. E.; Ley, J. P.; Somoza, V., Identification of an anti-inflammatory potential of Eriodictyon angustifolium compounds in human gingival fibroblasts. *Food Func.* **2016,** *7* (7), 3046-3055.

131. Pluskal, T.; Weng, J.-K., Natural product modulators of human sensations and mood: molecular mechanisms and therapeutic potential. *Chem. Soc. Rev.* **2018,** *47* (5), 1592-1637.

132. Ley, J. P.; Krammer, G.; Reinders, G.; Gatfield, I. L.; Bertram, H.-J., Evaluation of Bitter Masking Flavanones from Herba Santa (Eriodictyon californicum (H. & A.) Torr., Hydrophyllaceae). *J. Agric. Food. Chem.* **2005,** *53* (15), 6061-6066.

133. Singh, N.; Vrontakis, M.; Parkinson, F.; Chelikani, P., Functional bitter taste receptors are expressed in brain cells. *Biochem. Biophys. Res. Com.* **2011,** *406* (1), 146-151.

134. Hillis, W. E., Biosynthesis of Flavonoids. *Nature* **1960,** *186* (4725), 635-635.

135. Bringmann, G.; Messer, K.; Wohlfarth, M.; Kraus, J.; Dumbuya, K.; Rückert, M., HPLC−CD On-Line Coupling in Combination with HPLC−NMR and HPLC−MS/MS for the Determination of the Full Absolute Stereostructure of New Metabolites in Plant Extracts. *Anal. Chem.* **1999,** *71* (14), 2678-2686.

136. Gaffield, W., Circular dichroism, optical rotatory dispersion and absolute configuration of flavanones, 3-hydroxyflavanones and their glycosides: Determination of aglycone chirality in flavanone glycosides. *Tetrahedron* **1970,** *26* (17), 4093-4108.

137. Johnson, N. D., Flavonoid aglycones from Eriodictyon californicum resin and their implications for herbivory and UV screening. *Biochem. Syst. Ecol.* **1983,** *11* (3), 211-215.

138. Krause, M.; Galensa, R., Analysis of enantiomeric flavanones in plant extracts by high-performance liquid chromatography on a cellulose triacetate based chiral stationary phase. *Chromatographia* **1991,** *32* (1), 69-72.

139. Waldeck, B., Biological significance of the enantiomeric purity of drugs. *Chirality* **1993,** *5* (5), 350-355.

140. Vrba, J.; Gažák, R.; Kuzma, M.; Papoušková, B.; Vacek, J.; Weiszenstein, M.; Křen, V.; Ulrichová, J., A Novel Semisynthetic Flavonoid 7-O-Galloyltaxifolin Upregulates Heme Oxygenase-1 in RAW264.7 Cells via MAPK/Nrf2 Pathway. *J. Med. Chem.* **2013,** *56* (3), 856-866.

141. Patil, P.; Thakur, A.; Sharma, A.; Flora, S. J. S., Natural products and their derivatives as multifunctional ligands against Alzheimer's disease. *Drug Dev. Res.* **2020,** *81* (2), 165-183.

142. Maurice, T.; Lockhart, B. P.; Privat, A., Amnesia induced in mice by centrally administered β-amyloid peptides involves cholinergic dysfunction. *Brain Res.* **1996,** *706* (2), 181-193.

143. Lahmy, V.; Meunier, J.; Malmström, S.; Naert, G.; Givalois, L.; Kim, S. H.; Villard, V.; Vamvakides, A.; Maurice, T., Blockade of Tau Hyperphosphorylation and Aβ1–42 Generation by the Aminotetrahydrofuran Derivative ANAVEX2-73, a Mixed Muscarinic and σ1 Receptor Agonist, in a Nontransgenic Mouse Model of Alzheimer's Disease. *Neuropsychopharmacology* **2013,** *38* (9), 1706-1723.

144. Lu, P.; Mamiya, T.; Lu, L.; Mouri, A.; Zou, L.; Nagai, T.; Hiramatsu, M.; Ikejima, T.; Nabeshima, T., Silibinin prevents amyloid β peptide-induced memory impairment and oxidative stress in mice. *Br. J. Pharmacol.* **2009,** *157* (7), 1270-1277.

145. Saito, S.; Yamamoto, Y.; Maki, T.; Hattori, Y.; Ito, H.; Mizuno, K.; Harada-Shiba, M.; Kalaria, R. N.; Fukushima, M.; Takahashi, R.; Ihara, M., Taxifolin inhibits amyloid-β oligomer formation and fully restores vascular integrity and memory in cerebral amyloid angiopathy. *Acta Neuropathol. Commun.* **2017,** *5* (1), 26.

146. Gažák, R.; Sedmera, P.; Vrbacký, M.; Vostálová, J.; Drahota, Z.; Marhol, P.; Walterová, D.; Křen, V., Molecular mechanisms of silybin and 2,3-dehydrosilybin antiradical activity—role of individual hydroxyl groups. *Free Radic. Biol. Med.* **2009,** *46* (6), 745-758.

147. Schramm, S.; Gunesch, S.; Lang, F.; Saedtler, M.; Meinel, L.; Högger, P.; Decker, M., Investigations into neuroprotectivity, stability, and water solubility of 7-O-cinnamoylsilibinin, its hemisuccinate and dehydro derivatives. *Arch. Pharm. Chem. Life Sci.* **2018,** *351* (11), 1800206.

148. Gunesch, S.; Soriano-Castell, D.; Lamer, S.; Schlosser, A.; Maher, P.; Decker, M., Development and Application of a Chemical Probe Based on a Neuroprotective Flavonoid Hybrid for Target Identification Using Activity-Based Protein Profiling. *ACS Chem. Neurosci.* **2020,** *11* (22), 3823-3837.

149. Mattarei, A.; Biasutto, L.; Rastrelli, F.; Garbisa, S.; Marotta, E.; Zoratti, M.; Paradisi, C., Article Regioselective O-Derivatization of Quercetin via Ester Intermediates. An Improved Synthesis of Rhamnetin and Development of a New Mitochondriotropic Derivative. *Molecules* **2010,** *15* (7), 4722-4736.

150. Li, M.; Han, X.; Yu, B., Facile Synthesis of Flavonoid 7-O-Glycosides. *J. Org. Chem.* **2003,** *68* (17), 6842-6845.

151. Baell, J. B.; Holloway, G. A., New Substructure Filters for Removal of Pan Assay Interference Compounds (PAINS) from Screening Libraries and for Their Exclusion in Bioassays. *J. Med. Chem.* **2010,** *53* (7), 2719-2740.

152. Owen, S. C.; Doak, A. K.; Wassam, P.; Shoichet, M. S.; Shoichet, B. K., Colloidal Aggregation Affects the Efficacy of Anticancer Drugs in Cell Culture. *ACS Chem. Biol.* **2012,** *7* (8), 1429-1435.

153. Maher, P.; Schubert, D., Signaling by reactive oxygen species in the nervous system. *Cell. Mol. Life Sci.* **2000,** *57*.

154. Oparka, M.; Walczak, J.; Malinska, D.; van Oppen, L. M. P. E.; Szczepanowska, J.; Koopman, W. J. H.; Wieckowski, M. R., Quantifying ROS levels using CM-H2DCFDA and HyPer. *Methods* **2016,** *109*, 3-11.

155. Saxena, U., Bioenergetics failure in neurodegenerative diseases: back to the future. *Expert Opin. Ther. Targets* **2012,** *16* (4), 351-354.

156. Giorgetti, S.; Greco, C.; Tortora, P.; Aprile, F. A., Targeting Amyloid Aggregation: An Overview of Strategies and Mechanisms. *Int. J. Mol. Sci.* **2018,** *19* (9).

157. Panza, F.; Lozupone, M.; Logroscino, G.; Imbimbo, B. P., A critical appraisal of amyloid-β-targeting therapies for Alzheimer disease. *Nat. Rev. Neurol.* **2019,** *15* (2), 73-88.

158. Priyadarsini, K. I., The Chemistry of Curcumin: From Extraction to Therapeutic Agent. *Molecules* **2014,** *19* (12), 20091-20112.

159. Fang, L.; Gou, S.; Liu, X.; Cao, F.; Cheng, L., Design, synthesis and anti-Alzheimer properties of dimethylaminomethyl-substituted curcumin derivatives. *Bioorg. Med. Chem. Lett.* **2014,** *24* (1), 40-43.

160. Venigalla, M.; Sonego, S.; Gyengesi, E.; Sharman, M. J.; Münch, G., Novel promising therapeutics against chronic neuroinflammation and neurodegeneration in Alzheimer's disease. *Neurochem. Int.* **2016,** *95*, 63-74.

161. Espargaró, A.; Ginex, T.; Vadell, M. d. M.; Busquets, M. A.; Estelrich, J.; Muñoz-Torrero, D.; Luque, F. J.; Sabate, R., Combined in Vitro Cell-Based/in Silico Screening of Naturally Occurring Flavonoids and Phenolic Compounds as Potential Anti-Alzheimer Drugs. *J. Nat. Prod.* **2017,** *80* (2), 278-289.

162. Reinke, A. A.; Gestwicki, J. E., Structure–activity Relationships of Amyloid Beta-aggregation Inhibitors Based on Curcumin: Influence of Linker Length and Flexibility. *Chem. Biol. Drug Des.* **2007,** *70* (3), 206-215.

163. Nelson, K. M.; Dahlin, J. L.; Bisson, J.; Graham, J.; Pauli, G. F.; Walters, M. A., The Essential Medicinal Chemistry of Curcumin. *J. Med. Chem.* **2017,** *60* (5), 1620-1637.

164. Lima, L. M.; Barreiro, E. J., Bioisosterism: a useful strategy for molecular modification and drug design. *Curr. Med. Chem.* **2005,** *12* (1), 23-49.

165. Sato, M.; Murakami, K.; Uno, M.; Ikubo, H.; Nakagawa, Y.; Katayama, S.; Akagi, K.-i.; Irie, K., Structure–activity relationship for (+)-taxifolin isolated from silymarin as an inhibitor of amyloid β aggregation. *Biosci. Biotech. Biochem.* **2013,** *77* (5), 1100-1103.

166. Sato, M.; Murakami, K.; Uno, M.; Nakagawa, Y.; Katayama, S.; Akagi, K.-i.; Masuda, Y.; Takegoshi, K.; Irie, K., Site-specific inhibitory mechanism for amyloid β42 aggregation by catechol-type flavonoids targeting the Lys residues. *J. Biol. Chem.* **2013,** *288* (32), 23212-23224.

167. Ginex, T.; Trius, M.; Luque, F. J., Computational Study of the Aza-Michael Addition of the Flavonoid (+)-Taxifolin in the Inhibition of β-Amyloid Fibril Aggregation. *Chem. Eur. J.* **2018**.

168. Chiti, F.; Dobson, C. M., Protein Misfolding, Amyloid Formation, and Human Disease: A Summary of Progress Over the Last Decade. *Annu. Rev. Biochem.* **2017,** *86* (1), 27-68.

169. Invernizzi, G.; Papaleo, E.; Sabate, R.; Ventura, S., Protein aggregation: Mechanisms and functional consequences. *Int. J. Biochem. Cell Biol.* **2012,** *44* (9), 1541-1554.

170. Bolder, S. G.; Sagis, L. M. C.; Venema, P.; van der Linden, E., Thioflavin T and Birefringence Assays to Determine the Conversion of Proteins into Fibrils. *Langmuir* **2007,** *23* (8), 4144-4147.

171. Hawe, A.; Sutter, M.; Jiskoot, W., Extrinsic fluorescent dyes as tools for protein characterization. *Pharm. Res.* **2008,** *25* (7), 1487-1499.

172. Hudson, S. A.; Ecroyd, H.; Kee, T. W.; Carver, J. A., The thioflavin T fluorescence assay for amyloid fibril detection can be biased by the presence of exogenous compounds. *FEBS J.* **2009,** *276* (20), 5960-5972.

173. Espargaró, A.; Medina, A.; Di Pietro, O.; Muñoz-Torrero, D.; Sabate, R., Ultra rapid in vivo screening for anti-Alzheimer anti-amyloid drugs. *Sci. Rep.* **2016,** *6* (1), 23349.

174. Blois, M. S., Antioxidant determinations by the use of a stable free radical. *Nature* **1958,** *181* (4617), 1199-1200.

175. Hebert, L. E.; Beckett, L. A.; Scherr, P. A.; Evans, D. A., Annual Incidence of Alzheimer Disease in the United States Projected to the Years 2000 Through 2050. *Alzheimer Dis. Assoc. Disord.* **2001,** *15* (4), 169-173.

176. Chesnut, V. K., *Plants used by the Indians of Mendocino County, California*. US Government Printing Office: 1902.

177. Hayes, J. D.; Dinkova-Kostova, A. T., The Nrf2 regulatory network provides an interface between redox and intermediary metabolism. *Trends Biochem. Sci* **2014,** *39* (4), 199-218.

178. Ahmed, S. M. U.; Luo, L.; Namani, A.; Wang, X. J.; Tang, X., Nrf2 signaling pathway: Pivotal roles in inflammation. *Biochim. Biophys. Acta Mol. Basis Dis.* **2017,** *1863* (2), 585-597.

179. Maher, P., Modulation of multiple pathways involved in the maintenance of neuronal function during aging by fisetin. *Genes Nutr.* **2009,** *4* (4), 297.

180. Huntley, T. E.; Neitzel, J. K.; Elson, M. K., Binding properties of purified adult and fetal bovine serum albumin. *Biochim. Biophys. Acta Mol. Prot. Struc.* **1977,** *490* (1), 112-119.

181. Richard M. Weinshilboum; Diane M. Otterness, a.; Szumlanski, C. L., METHYLATION PHARMACOGENETICS: Catechol O-Methyltransferase, Thiopurine Methyltransferase, and Histamine N-Methyltransferase. *Annu. Rev. Pharmacool. Toxicol.* **1999,** *39* (1), 19-52.

182. Zhu, B. T.; Ezell, E. L.; Liehr, J. G., Catechol-O-methyltransferase-catalyzed rapid O-methylation of mutagenic flavonoids. Metabolic inactivation as a possible reason for their lack of carcinogenicity in vivo. *J. Biol. Chem.* **1994,** *269* (1), 292-299.

183. Chen, Z.; Chen, M.; Pan, H.; Sun, S.; Li, L.; Zeng, S.; Jiang, H., Role of catechol-O-methyltransferase in the disposition of luteolin in rats. *Drug Metab. Dispos.* **2011,** *39* (4), 667-674.

184. Cao, Y.; Chen, Z.-J.; Jiang, H.-D.; Chen, J.-Z., Computational Studies of the Regioselectivities of COMT-Catalyzed Meta-/Para-O Methylations of Luteolin and Quercetin. *J. Phys. Chem. B* **2014,** *118* (2), 470-481.

185. Roschek, B.; Fink, R. C.; McMichael, M. D.; Li, D.; Alberte, R. S., Elderberry flavonoids bind to and prevent H1N1 infection in vitro. *Phytochemistry* **2009,** *70* (10), 1255-1261.

186. Peng, X.; Gandhi, V., ROS-activated anticancer prodrugs: a new strategy for tumor-specific damage. *Ther. Deliv.* **2012,** *3* (7), 823-833.

187. Ganta, S.; Devalapally, H.; Shahiwala, A.; Amiji, M., A review of stimuli-responsive nanocarriers for drug and gene delivery. *J. Controlled Release* **2008,** *126* (3), 187-204.

188. Özdemir, C.; Güner, A., Solubility profiles of poly(ethylene glycol)/solvent systems, I: Qualitative comparison of solubility parameter approaches. *Eur. Polym. J.* **2007,** *43* (7), 3068-3093.

189. Romanucci, V.; Agarwal, C.; Agarwal, R.; Pannecouque, C.; Iuliano, M.; De Tommaso, G.; Caruso, T.; Di Fabio, G.; Zarrelli, A., Silibinin phosphodiester glyco-conjugates: Synthesis, redox behaviour and biological investigations. *Bioorg. Chem.* **2018,** *77*, 349-359.

190. Sauer, R.-S.; Krummenacher, I.; Bankoglu, E. E.; Yang, S.; Oehler, B.; Schöppler, F.; Mohammadi, M.; Güntzel, P.; Ben-Kraiem, A.; Holzgrabe, U., Stabilization of delphinidin in complex with sulfobutylether-β-cyclodextrin allows for antinociception in inflammatory pain. *Redox. Signal.* **2021,** *34* (16), 1260-1279.

191. Ono, K.; Hasegawa, K.; Naiki, H.; Yamada, M., Curcumin has potent anti-amyloidogenic effects for Alzheimer's β-amyloid fibrils in vitro. *J. Neurosci. Res.* **2004,** *75* (6), 742-750.

192. Kim, D. S. H. L.; Park, S.-Y.; Kim, J.-Y., Curcuminoids from Curcuma longa L. (Zingiberaceae) that protect PC12 rat pheochromocytoma and normal human umbilical vein endothelial cells from βA(1–42) insult. *Neurosci. Lett.* **2001,** *303* (1), 57-61.

193. Prior, M.; Dargusch, R.; Ehren, J. L.; Chiruta, C.; Schubert, D., The neurotrophic compound J147 reverses cognitive impairment in aged Alzheimer's disease mice. *Alzheimer's Res. Ther.* **2013,** *5* (3), 25.

194. Broichhagen, J.; Frank, J. A.; Trauner, D., A Roadmap to Success in Photopharmacology. *Acc. Chem. Res.* **2015,** *48* (7), 1947-1960.

195. Vailati-Riboni, M.; Palombo, V.; Loor, J. J., What Are Omics Sciences? In *Periparturient Diseases of Dairy Cows: A Systems Biology Approach*, Ametaj, B. N., Ed. Springer International Publishing: Cham, 2017; pp 1-7.

196. Wingo, A. P.; Liu, Y.; Gerasimov, E. S.; Gockley, J.; Logsdon, B. A.; Duong, D. M.; Dammer, E. B.; Robins, C.; Beach, T. G.; Reiman, E. M.; Epstein, M. P.; De Jager, P. L.; Lah, J. J.; Bennett, D. A.; Seyfried, N. T.; Levey, A. I.; Wingo, T. S., Integrating human brain proteomes with genome-wide association data implicates new proteins in Alzheimer's disease pathogenesis. *Nat. Genet.* **2021,** *53* (2), 143-146.

197. Pandurangan, N.; Bose, C.; Banerji, A., Synthesis and antioxygenic activities of seabuckthorn flavone-3-ols and analogs. *Bioorg. Med. Chem. Lett.* **2011,** *21* (18), 5328-5330.

198. Taichiro, O.; Hajime, B., A New Synthesis of Polyhydroxydihydroflavonols. *Bull. Chem. Soc. Jpn.* **1966,** *39* (3), 507-511.

199. Geissman, T., The isolation of eriodictyol and homoeriodictyol. An improved procedure. *J. Am. Chem. Soc.* **1940,** *62* (11), 3258-3259.

200. Hu, C.; Zhou, Z.; Xiang, Y.; Song, X.; Wang, H.; Tao, K.; Ye, X., Design, synthesis and anti-inflammatory activity of dihydroflavonol derivatives. *Med. Chem. Res.* **2018,** *27* (1), 194-205.

201. Kiehlmann, E.; Szczepina, M. G., Epimerization, transacylation and bromination of dihydroquercetin acetates; synthesis of 8-bromodihydroquercetin. *Cent. Eur. J. Chem.* **2011,** *9* (3), 492-498.

202. Rubio, S.; Quintana, J.; López, M.; Eiroa, J. L.; Triana, J.; Estévez, F., Phenylbenzopyrones structure-activity studies identify betuletol derivatives as potential antitumoral agents. *Eur. J. Pharmacol.* **2006,** *548* (1), 9-20.

203. Hoang, T. K.-D.; Huynh, T. K.-C.; Nguyen, T.-D., Synthesis, characterization, anti-inflammatory and anti-proliferative activity against MCF-7 cells of O-alkyl and O-acyl flavonoid derivatives. *Bioorg. Chem.* **2015,** *63*, 45-52.

204. Li, Y.-Q.; Yang, F.; Wang, L.; Cao, Z.; Han, T.-J.; Duan, Z.-A.; Li, Z.; Zhao, W.-J., Phosphoramidate protides of five flavones and their antiproliferative activity against HepG2 and L-O2 cell lines. *Eur. J. Med. Chem.* **2016,** *112*, 196-208.

205. Kiehlmann, E., Preparation and Partial Deacetylation of Dihydroquercetin Acetates. *Org. Prep. Proced. Int.* **1999,** *31* (1), 87-97.

Appendix

Appendix I:

- **Hofmann J.**; Fayez, S.; Scheiner, M.; Hoffmann, M.; Oerter, S.; Appelt-Menzel, A.; Maher, P.; Maurice, T.; Bringmann, G.; Decker, M. Sterubin: Enantioresolution and Configurational Stability, Enantiomeric Purity in Nature, and Neuroprotective Activity in Vitro and in Vivo. *Chem. Eur. J.* **2020**, *26* (32), 7299–7308.
- Supporting Information

Appendix II:

- **Hofmann, J.**; Ginex, T.; Espargaró, A.; Scheiner, M.; Gunesch, S.; Aragó, M.; Stigloher, C.; Sabaté, R.; Luque, J.; Decker, M. Azobioisosteres of Curcumin with Pronounced Activity against Amyloid Aggregation, Intracellular Oxidative Stress, and Neuroinflammation. *Chem. Eur. J.* **2021**, *27* (19), 6015–6027.
- Supporting Information

Appendix III:

- Curriculum Vitae

Appendix I:

Hofmann J.*; Fayez, S.*; Scheiner, M.; Hoffmann, M.; Oerter, S.; Appelt-Menzel, A.; Maher, P.; Maurice, T.; Bringmann, G.; Decker, M. Sterubin: Enantioresolution and Configurational Stability, Enantiomeric Purity in Nature, and Neuroprotective Activity in Vitro and in Vivo. *Chem. Eur. J.* **2020**, *26* (32), 7299–7308.

* These authors contributed equally

Full Paper
doi.org/10.1002/chem.202001264
Chemistry Europe
European Chemical Societies Publishing

Natural Products

Sterubin: Enantioresolution and Configurational Stability, Enantiomeric Purity in Nature, and Neuroprotective Activity in Vitro and in Vivo

Julian Hofmann[+],[a] Shaimaa Fayez[+],[b, c] Matthias Scheiner,[a] Matthias Hoffmann,[a, d] Sabrina Oerter,[e] Antje Appelt-Menzel,[e, f] Pamela Maher,[g] Tangui Maurice,[d] Gerhard Bringmann,*[b] and Michael Decker*[a]

Abstract: Alzheimer's disease (AD) is a neurological disorder with still no preventive or curative treatment. Flavonoids are phytochemicals with potential therapeutic value. Previous studies described the flavanone sterubin isolated from the Californian plant *Eriodictyon californicum* as a potent neuroprotectant in several in vitro assays. Herein, the resolution of synthetic racemic sterubin (**1**) into its two enantiomers, (*R*)-**1** and (*S*)-**1**, is described, which has been performed on a chiral chromatographic phase, and their stereochemical assignment online by HPLC-ECD coupling. (*R*)-**1** and (*S*)-**1** showed comparable neuroprotection in vitro with no significant differences. While the pure stereoisomers were configurationally stable in methanol, fast racemization was observed in the presence of culture medium. We also established the occurrence of extracted sterubin as its pure (*S*)-enantiomer. Moreover, the activity of sterubin (**1**) was investigated for the first time in vivo, in an AD mouse model. Sterubin (**1**) showed a significant positive impact on short- and long-term memory at low dosages.

Introduction

Alzheimer's disease (AD) is an age-associated neurodegenerative disorder and the most common form of dementia (60–80%) among people aged between 65 and 85 years.[1] Pathological hallmarks of the disease include the deposition of amyloid-β (Aβ) containing plaques and tau (τ) containing neurofibrillary tangles.[2] This protein accumulation is accompanied by the loss of neurotrophic factors, ATP depletion, oxidative stress, and neuroinflammation,[3] which lead to neurodegeneration with subsequent cognitive problems and loss of memory.[4]

Over the past few decades, numerous plant-derived natural products have been investigated for their activities against neurodegenerative in vitro hallmarks, including the reduction of oxidative stress, Aβ aggregation, and neuroinflammation.[5] Among these compounds, flavonoids and related polyphenols are powerful antioxidants with potential therapeutic effects.[6] Nevertheless, putative metabolic instability and a potential lack of blood–brain barrier (BBB) penetration are considered as

[a] J. Hofmann,[+] M. Scheiner, Dr. M. Hoffmann, Prof. Dr. M. Decker
Pharmaceutical and Medicinal Chemistry
Institute of Pharmacy and Food Chemistry
University of Würzburg
Am Hubland, 97074 Würzburg (Germany)
E-mail: michael.decker@uni-wuerzburg.de

[b] Dr. S. Fayez,[+] Prof. Dr. G. Bringmann
Institute of Organic Chemistry
University of Würzburg
Am Hubland, 97074 Würzburg (Germany)
E-mail: bringman@chemie.uni-wuerzburg.de

[c] Dr. S. Fayez[+]
Department of Pharmacognosy, Faculty of Pharmacy
Ain-Shams University
Organization of African Unity Street 1, 11566 Cairo (Egypt)

[d] Dr. M. Hoffmann, Dr. T. Maurice
MMDN, University of Montpellier
INSERM, EPHE, UMR-S1198
34095 Montpellier (France)

[e] Dr. S. Oerter, Dr. A. Appelt-Menzel
Department for Tissue Engineering and Regenerative Medicine
University Hospital Würzburg
Röntgenring 11, 97070 Würzburg (Germany)

[f] Dr. A. Appelt-Menzel
Translational Center Regenerative Therapies (TLC-RT)
Fraunhofer Institute for Silicate Research ISC
Röntgenring 11, 97070 Würzburg (Germany)

[g] Dr. P. Maher
The Salk Institute for Biological Studies
10010 North Torrey Pines Rd., CA 92037 La Jolla (USA)

[+] These authors contributed equally.

Supporting information and the ORCID identification number(s) for the author(s) of this article can be found under: https://doi.org/10.1002/chem.202001264.

drawbacks regarding "druggability".[7] Recent studies by Schramm et al.[8] and Gunesch et al.[9] have shown a remarkable increase in potency of both flavonoids and flavonolignan derivatives, in vitro and in vivo, by esterification of the hydroxy group at C-7 with phenolic acids. The resulting esters, however, suffer from poor water solubility and high molecular weight.[10]

Recently, Fischer et al.[11] have investigated the extract of *Eriodictyon californicum* (known as yerba santa) from a new pharmacological and medicinal perspective. This plant has long been used for medicinal purposes by native inhabitants of California, where the plant is indigenous.[12] The leaves contain different flavonoids (Figure 1), which are known for their anti-inflammatory and anti-microbial activities against Gram-positive bacteria, and are also used as ingredients in food and pharmaceuticals as bitter-masking agents.[13] Fischer et al. tested extracts of *E. californicum* in a set of age-associated phenotypic screening assays related to AD. They assigned sterubin (7-methoxy-3′,4′,5-trihydroxyflavanone, **1**) as the most active compound in the extract of *E. californicum*, showing a remarkably higher in vitro activity than the co-existing flavonoids eriodictyol (**2**) or homoeriodictyol (**3**).[11] The only very minor structural difference between **1** and **2** demonstrates the "steep" structure–activity relationships of flavonoids. Nothing, however, has so far been reported on the activity of **1** in vivo. Moreover, the chirality of sterubin (**1**), as a result of the stereocenter at C-2, was not taken into consideration, making it unclear which enantiomer was responsible for the activity. Previous reports had shown that flavonoids mainly exist as their respective (*S*)-enantiomers in the plants and that they tend to racemize during the isolation workup procedure.[14] Herein, we report on the synthesis of sterubin (**1**), the chiral resolution of its synthetic racemate, the chiroptical analysis and stereochemical assignment of the (*R*)- and (*S*)-enantiomers, (*R*)-**1** and (*S*)-**1**, online, by HPLC coupled to electronic circular dichroism (ECD), and on the configurational stability of the two stereoisomers. Furthermore, we determined the enantiomeric purity of sterubin in the plant *E. californicum*. Moreover, we describe the in vitro activity of the isolated enantiomers against intracellular oxidative stress using the murine hippocampal neuronal cell line HT22. And, for the first time, we have conducted in vivo investigations on sterubin (**1**) in an AD mouse model with $A\beta_{25-35}$-induced memory impairment[15] and normal mice.

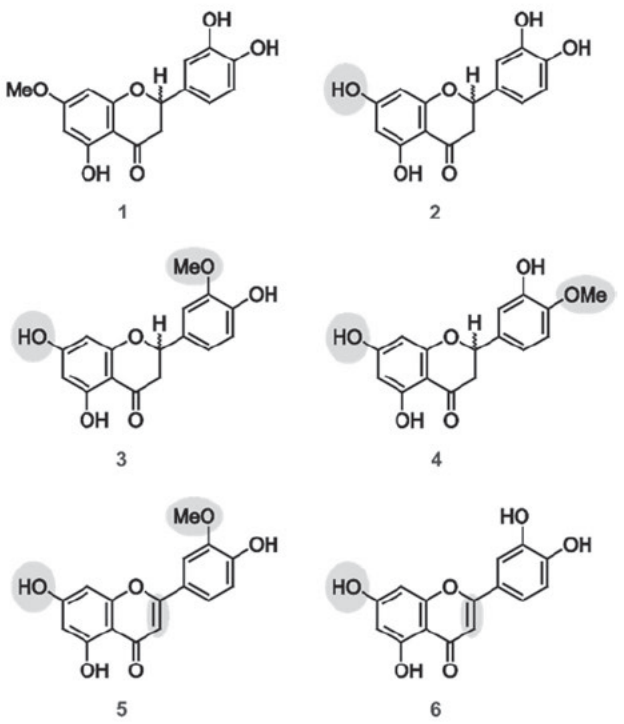

Figure 1. Flavonoids of *Eriodictyon californicum* (yerba santa): sterubin (**1**), eriodictyol (**2**), homoeriodictyol (**3**), hesperetin (**4**), chrysoeriol (**5**), and luteolin (**6**). The structural differences of **2**–**6** as compared to **1** are underlaid in grey.

Results and Discussion

Synthesis of sterubin (1)

The synthesis of **1** was performed by analogy to methods for the preparation of similar racemic flavonoids described in the literature.[16] A key step was the condensation of the known[17] acetophenone **7** with the likewise known[18] aldehyde **8** to form the respective chalcone **9** (Scheme 1). Cleavage of the MOM groups and concomitant ring closure was achieved by heating **9** in 10% HCl in MeOH, followed by treatment with sodium acetate to give racemic sterubin (**1**).

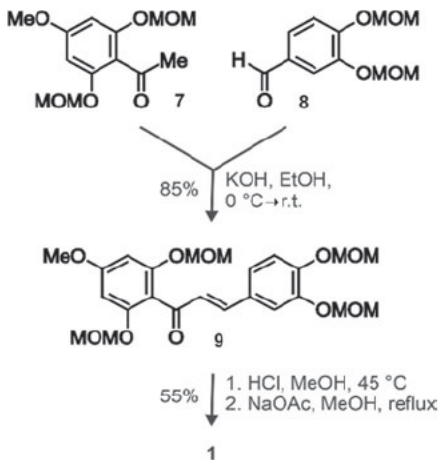

Scheme 1. Key steps in the synthesis of racemic sterubin (**1**). MOM = methoxymethyl.

Resolution of the sterubin enantiomers, (*R*)-1 and (*S*)-1

The synthetic racemate of **1** was successfully resolved on a ChiralPak IA® column (10×25 mm, 5 μm) using gradient elution with initial condition from 32% B to 60% B in 29 min and a flow rate of 6 mL min^{-1}, where B is 90% acetonitrile in water with 0.05% TFA as a buffer (Figure 2A). Maximum absorption and peak detection was achieved using a PDA detector at $\lambda =$ 290 nm.

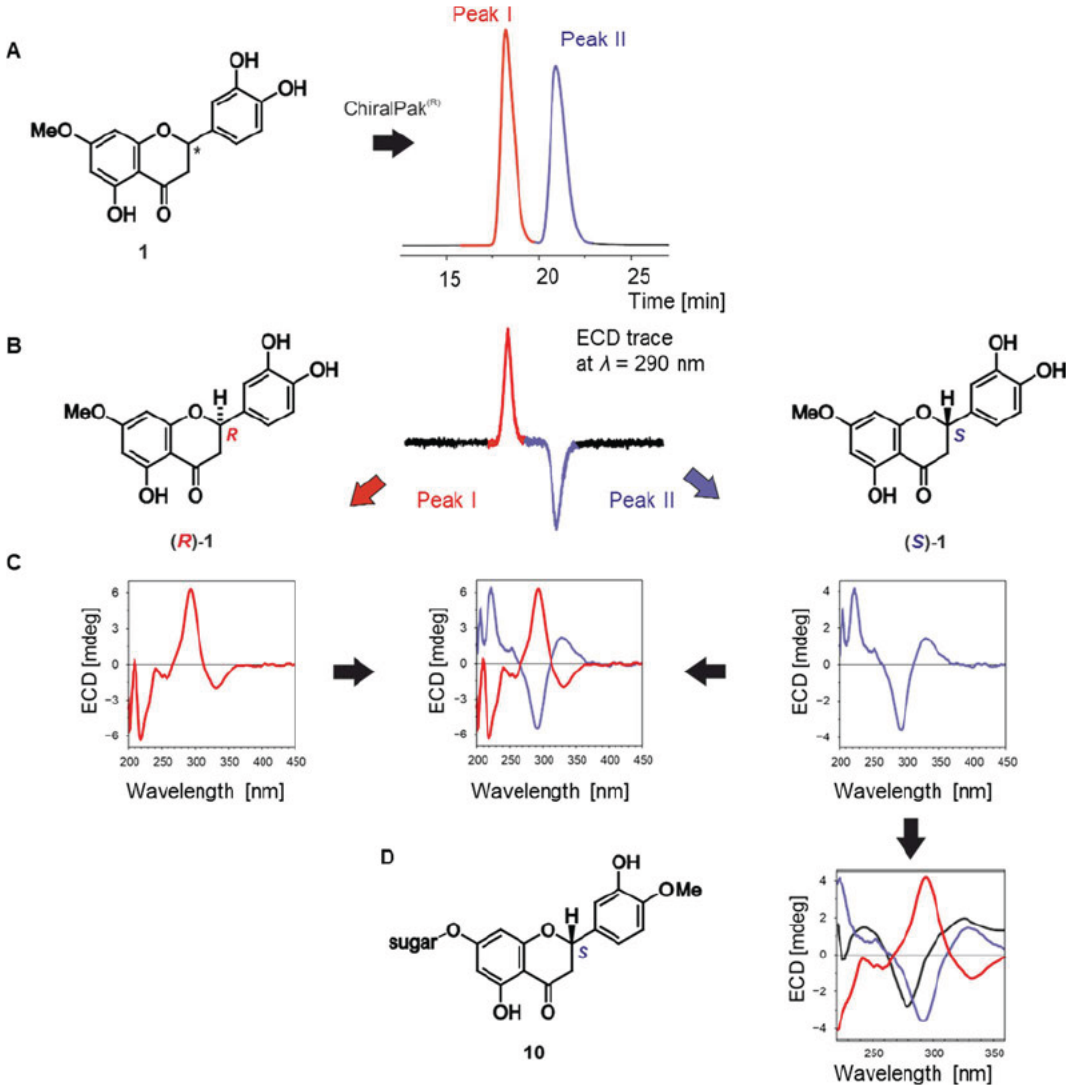

Figure 2. (A) Enantiomeric resolution of racemic sterubin (**1**) on a ChiralPak IA® column; (B) ECD trace (recorded at $\lambda = 290$ nm); (C) online LC-ECD spectra of the two sterubin enantiomers; (D) configurational assignment of the two enantiomers by comparison of their online ECD curves with the offline spectrum reported for the closely related, and configurationally known flavanone glycoside hesperidin (**10**). Sugar = rutinose.

Configurational assignment of the sterubin enantiomers, (*R*)-1 and (*S*)-1, by HPLC-ECD coupling

The absolute configuration of the two resolved peaks was assigned online, by HPLC-ECD coupling.[19] By measurement at a single wavelength, 290 nm, the chiroptically opposite behavior of the two peaks was clearly seen (Figure 2B), further supporting the assumption that the compounds were indeed enantiomers. This was corroborated by the full online ECD spectra showing a first, negative couplet at 330 nm (Peak I) and a second, positive one at 290 nm (Peak II) for the fast enantiomer and an opposite curve for the slower peak (Figure 2C). The assignment of the rapidly eluting peak as corresponding to the *R*-enantiomer of sterubin, (*R*)-**1**, and the slower one as its (*S*)-configured isomer, (*S*)-**1**, was achieved by comparison of the ECD spectra of the two enantiomers with that of the known, closely related, *S*-configured flavanone glycoside hesperidin (**10**) (Figure 2D).[20] The ECD curve of the second peak (Peak II) showed a good match with the spectrum of **10**, hence the slower enantiomer was *S*-configured. For the first peak, by contrast (Peak I), virtually opposite spectra were detected, so the faster eluting enantiomer was (*R*)-**1**.

Assignment of the absolute configuration and enantiomeric purity of sterubin (1) in *Eriodictyon californicum*

Most naturally occurring flavonoids have so far been isolated as the respective (*S*)-enantiomers.[14] To investigate the absolute configuration and the enantiomeric purity of sterubin (**1**) in *E. californicum*, dried leaves of the plant were extracted by mild maceration in ethyl acetate assisted by ultrasonication for 30 min at room temperature. Sterubin (**1**) and related flavanones were enriched by precipitation from the ethyl acetate crude extract after addition of *n*-hexane. The resulting precipitate was filtered, dissolved in methanol, and injected on a ChiralPak IA® column (Figure 3B). Spiking experiments with the

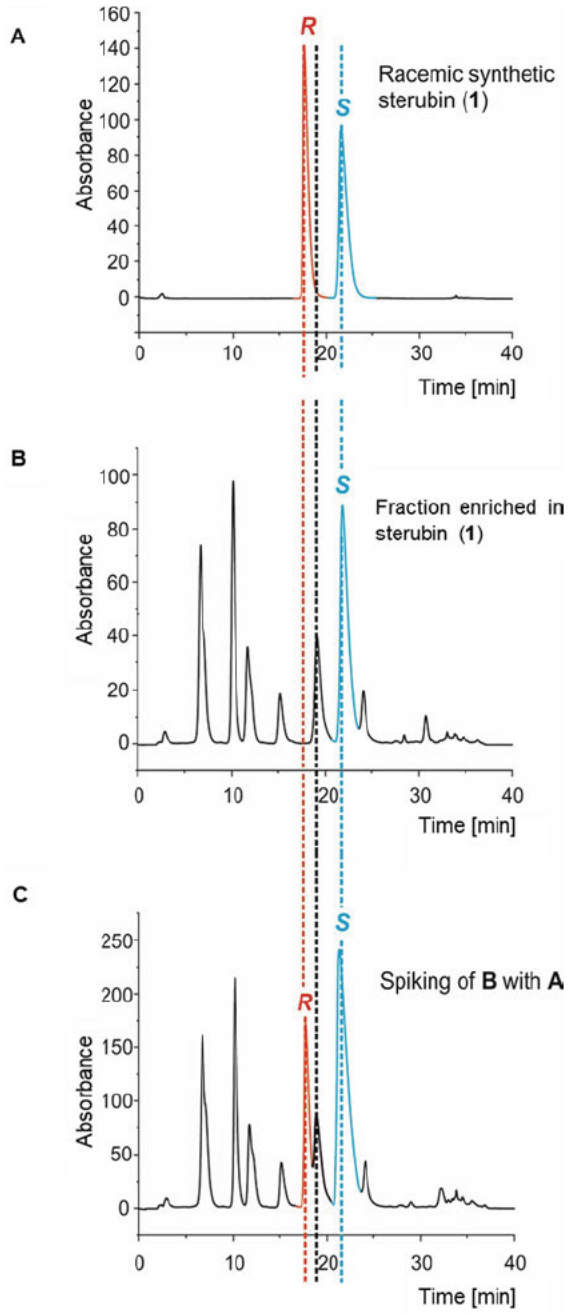

Figure 3. Chromatograms on a ChiralPak IA® column: (A) synthetic racemic sterubin (**1**); (B) the extract enriched with **1**; (C) coelution of **1** with the extract enriched with racemic **1** showing an increase in the peak intensity of the (*S*)-enantiomer and evidencing that in *E. californicum*, sterubin (**1**) is produced in an enantiopure *S*-form, (*S*)-**1**.

synthetic racemate of **1** (Figure 3 A) revealed an increase in the peak intensity of the *S*-enantiomer (Figure 3 C), showing that the plant contained sterubin (**1**) in an enantiomerically pure form, as its (*S*)-enantiomer, (*S*)-**1**. No racemization had occurred during the extraction procedure described, while extraction under reflux conditions as described in the literature[13a] obviously can lead to racemization.

Configurational stability of the sterubin enantiomers (*R*)-1 and (*S*)-1

For an investigation of the configurational stability of sterubin, its pure enantiomers, (*R*)-**1** and (*S*)-**1**, were kept dissolved in methanol at room temperature and the solution was monitored for the formation of the other respective enantiomer by HPLC on a ChiralPak IA® column after 2, 20, and 44 h. Under the applied conditions, the two enantiomers proved to be configurationally fully stable over 2 d and no racemization was observed as seen in Figure 4.

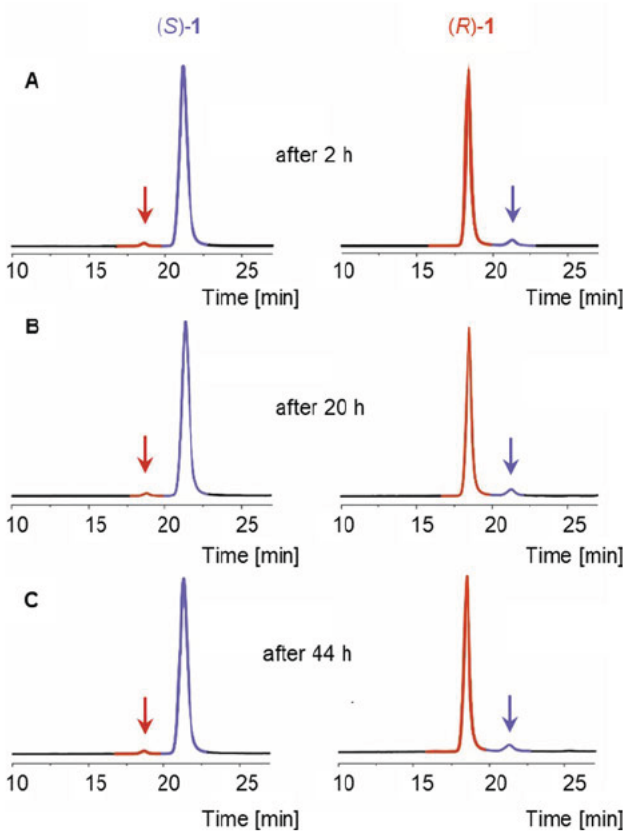

Figure 4. Stability studies on the (*R*)- and (*S*)-enantiomers of sterubin, (*R*)-**1** and (*S*)-**1**, in methanol: (A) after 2 h; (B) after 20 h; (C) after 44 h on a ChiralPak IA® column. The enantiomers were configurationally stable over the entire time. The arrows indicate the expected sites of the respective minor enantiomer.

Oxytosis assay

HT22 cells are a murine hippocampal nerve cell line. They are sensitive to oxidative glutamate toxicity (oxytosis) due to a lack of ionotropic glutamate receptors.[9–10,21] Addition of high concentrations of extracellular glutamate inhibits the transport of cystine, the oxidized form of cysteine, via the cystine/glutamate antiporter, which results in glutathione (GSH) depletion. The consecutive accumulation of ROS and calcium leads to intracellular oxidative stress followed by cell death.[22] As GSH depletion is similarly observed during aging of the brain and is even accelerated in AD, the oxytosis assay gives information

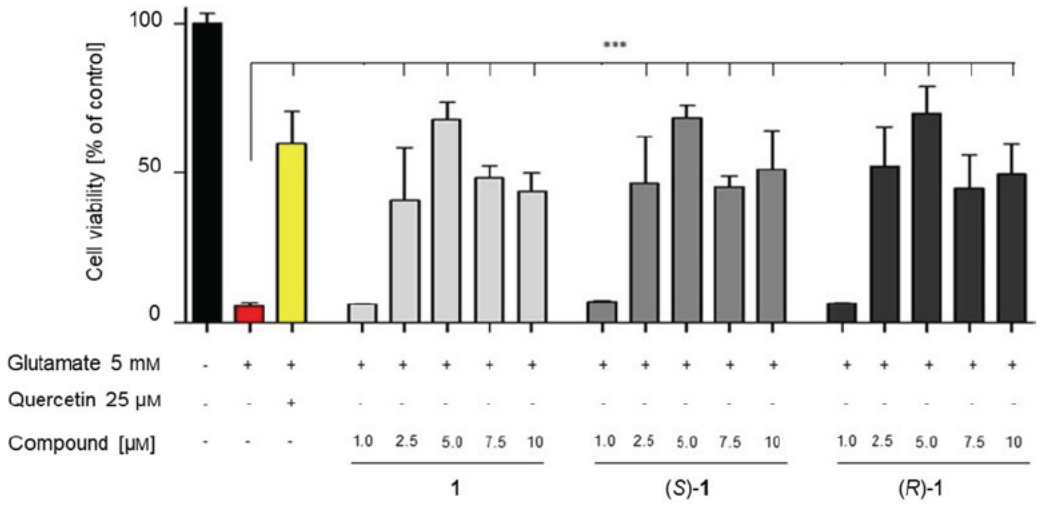

Figure 5. Oxytosis assay: Treatment of HT22 cells with 5 mM glutamate (red) induced cytotoxicity. Quercetin (yellow) served as a positive control, **1**, (*S*)-**1**, and (*R*)-**1** all showed the same neuroprotective efficacy. Data are presented as means ± SEM of three independent experiments and results refer to untreated control cells (black). Statistical analysis was performed using One-Way ANOVA followed by Dunnett's multiple comparison posttest using GraphPad Prism 5 referring to cells treated with 5 mM glutamate. Level of significance: *** $p < 0.001$.

about the neuroprotective properties of **1** against oxidative stress in cells.[23] Flavonoids generally have only moderate antioxidant properties[24] and, as reported by Fischer et al., sterubin (**1**) is one of the more potent flavonoids against oxidative stress and neuroinflammation in vitro.[11] The pure enantiomers of sterubin, (*R*)-**1** and (*S*)-**1**, as well as the synthetic racemic mixture, were investigated in the oxytosis assay to identify possible differences in activity between the stereoisomers. The flavonol quercetin at a high concentration (25 µM) served as a positive control (Figure 5). Unexpectedly, no difference in activity was observed between the racemic mixture and any of the pure enantiomers. All of them provided significant neuroprotection at concentrations from 2.5 µM to 10 µM, which even exceeded that of the positive control quercetin at a concentration of 5 µM. The lack of a difference in bioactivity between the pure enantiomers (and between them and the racemic mixture) raised the question whether the pure enantiomers might possibly undergo racemization upon contact with cells or even upon exposure to the culture medium, in contrast to their proven configurational stability in methanol (see above).

Cellular uptake and racemization

Vrba et al.[25] and Gunesch et al.[9] observed the formation of dehydrogenated products of esters combining the flavonoid taxifolin and polyphenolic acids in RAW264.7 macrophages or BV-2 microglia. In the case of sterubin (**1**), this would cause a loss of the stereogenic center at C-2, which would explain why the same activities were found for **1**, (*S*)-**1**, and (*R*)-**1**. Another explanation could be racemization in the cell culture medium. Therefore, we investigated cellular uptake experiments in microglial BV-2 cells and performed stability measurements in cell culture medium. BV-2 cells were treated with 50 µM of the respective compounds and incubated for 2 h or 4 h or lysed immediately, respectively. Lysates were analyzed by HPLC on a chiral-phase column and LC-UV. Reference chromatograms with sterubin (**1**) and dehydrosterubin (**12**) were recorded beforehand. As seen in Figure 6, sterubin (**1**) is chemically stable in the BV-2 cells. While no conversion of sterubin (**1**) to dehydrosterubin (**12**) was found (Scheme 2), HPLC on a chiral stationary phase revealed rapid racemization in the cell culture medium even without the presence of cells (cf. Supporting Information).

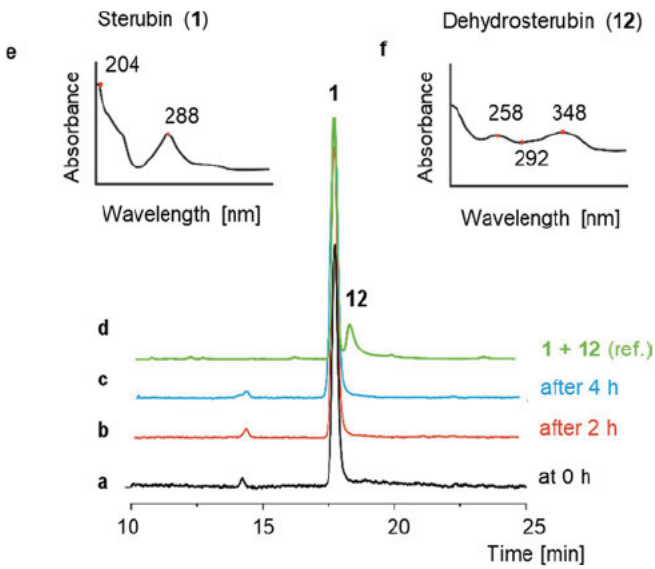

Figure 6. The chemical stability of (*R*)-**1** in BV-2 cells assigned by HPLC/UV: (a) at 0 h (black), (b) after 2 h (red), and (c) after 4 h (blue) of incubation, (d) reference chromatogram of **1** and dehydrosterubin (**12**) (green); (e) UV spectra of **1**; (f) UV spectra of **12**. (*R*)-**1** was chemically stable over the whole time.

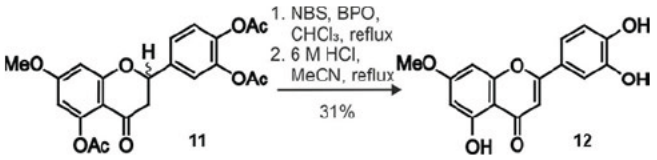

Scheme 2. Final steps in the synthesis of dehydrosterubin (**12**).

Synthesis of dehydrosterubin

Dehydrosterubin (**12**), also named hydroxygenkwanin, as a reference compound was synthesized by analogy to a procedure described by Aft.[26] For this purpose, the triacetate **11**[16] of sterubin (**1**) was dehydrogenated with *N*-bromosuccinimide (NBS) in the presence of catalytic amounts of benzoyl peroxide (BPO) to give the respective dehydro compound. Deprotection was accomplished in 6 M $HCl_{(aq.)}$ in acetonitrile, resulting in dehydrosterubin (**12**).

Neuroprotection in vivo

Recently, a number of polyphenols, including synthetic compounds as well as natural products, have been identified as potent neuroprotective agents in vitro.[9,11,25] Surprisingly, sterubin (**1**) showed a higher activity against oxidative stress and neuroinflammation than several other flavonoids.[11] To determine if sterubin (**1**) also has neuroprotective effects in vivo, experiments were performed using a mouse model of AD described previously.[15,27] Beforehand, in vitro cytotoxicity experiments with human induced pluripotent stem cell derived blood brain barrier endothelial cells were performed (cf. Supporting Information) to exclude toxicity. The results demonstrate, that **1** did not have any major toxic effects. For the in vivo studies described in this work, AD-like neurotoxicity and memory impairments were induced by intracerebroventricular (ICV) injection of the amyloid β (Aβ) fragment $A\beta_{25-35}$ (9 nmol) on the first day of the study. Control mice received distilled water (V1) ICV. Racemic sterubin (**1**) was dissolved in a mixture of 60% DMSO and 40% saline (0.9% NaCl in milliQ water) and the solutions were injected intraperitoneally (IP) once per day (o.d.) for the following 7 d at doses between 0.3 and 3 mg kg^{-1} of **1**. Injections of vehicle (60% DMSO + 40% saline, V2) were used for the two control groups. Sterubin did not affect the mouse body weight gain during the period of treatment (cf. Supporting Information). Short-term spatial memory was evaluated in the Y-maze test (YMT) on day 8 and long-term memory was evaluated on days 9 (training) and 10 (measurement of step-through latency) in the step-through passive-avoidance assay (STPA). On day 11, the mice were sacrificed, and the brains were frozen at −80 °C. Sterubin (**1**) significantly improved the $A\beta_{25-35}$-induced alternation deficit in the YMT at doses greater than 1 mg kg^{-1} (Figure 7A), further substantiating the neuroprotective effects observed in vitro.[11] In agreement with the results obtained in the YMT (Figure 7A), the $A\beta_{25-35}$-induced deficit in long-term memory was also compensated at a dose of sterubin (**1**) of 1 mg kg^{-1} or higher (Figure 7B). Sterubin (**1**) exceeded the activity of previously studied polyphenols such as silibinin and taxifolin used in the same mouse model of AD with respect to the dose needed to compensate for the $A\beta_{25-35}$ induced effects.[9,28]

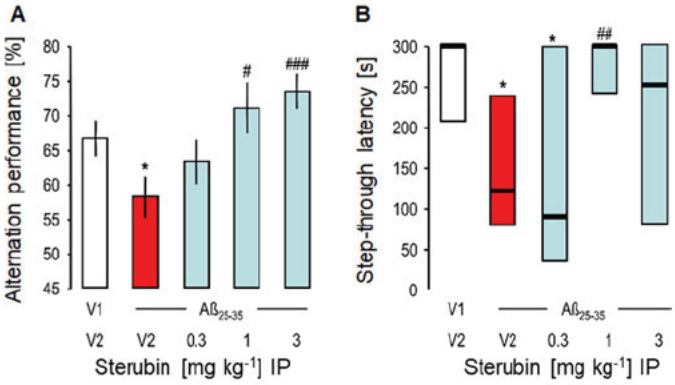

Figure 7. Effect of sterubin (**1**), administered IP, on $A\beta_{25-35}$-induced learning impairments in mice: (A) spontaneous alternation performance in YMT and (B) step-through latency in the STPA. Animals obtained distilled water (V1) or $A\beta_{25-35}$ (9 nmol ICV) on day 1 and received sterubin (0.3–3 mg kg^{-1} IP), or DMSO 60% in saline (V2), o.d. between day 1 and 7. They were examined in the YMT on day 8 and passive avoidance training was performed on day 9, with retention being tested after 24 h. Data show mean ± SEM in (A) and median and interquartile range in (B). $n = 12–18$ per groups. ANOVA: $F_{(4,57)} = 3.85$, $p < 0.01$ in (A). Kruskal-Wallis ANOVA: $H = 11.6$, $p < 0.05$ in (B). * $p < 0.05$ vs. (V + V)-treated group; # $p < 0.05$, ## $p < 0.01$, ### $p < 0.001$ vs. (V + $A\beta_{25-35}$)-treated group; Dunnett's test in (A), Dunn's test in (B).

Effects on memory in normal mice

We also asked if sterubin could improve memory in normal mice as was previously shown for the flavonol fisetin using the object recognition test.[29] In this test, mice are presented with two identical objects during the training period, which they explore for a fixed time period. To test for memory, mice are presented one day later with two different objects, one of which was presented previously during the training and is thus familiar to the mice, and the other that is novel. The better a mouse remembers the familiar object, the more time it will spend exploring the novel object. To test the effects of sterubin in this memory task, it was administered orally to the mice before the start of the training period. Rolipram, a phosphodiesterase inhibitor that potentiates memory in this assay,[30] requires intraperitoneal injection and was used as a positive control. As shown in Figure 8, three doses of sterubin were tested in the object recognition task and 10 mg kg^{-1} showed a strong but not quite significant effect.

Conclusions

By HPLC on a chiral phase column, resolution of synthetically prepared racemic sterubin (**1**) into its pure enantiomers, (*R*)-**1** and (*S*)-**1**, was achieved for the first time. Although in methanol configurational stability was observed, racemization took place in the cell culture medium. These findings explain why no difference in the neuroprotective activity in HT22 cells was found between racemic sterubin (**1**) and its pure enantiomers.

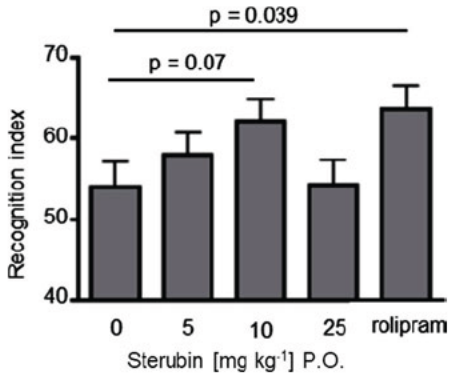

Figure 8. Effect of sterubin (**1**) on memory in normal mice. Sterubin moderately enhances long-term memory in mice. The effect of different oral doses of sterubin on object recognition over a 10 min test period. Rolipram, injected intraperitoneally at 0.1 mg kg^{-1}, served as a positive control. Data represent the mean ± SEM of 11 mice/treatment group. Data were analyzed by one-way ANOVA followed by post-hoc comparisons with Fisher's test.

Importantly, in vivo experiments revealed the high potency of sterubin as a neuroprotective agent against Aβ_{25-35}-induced AD-like memory loss in mice. The effects were observed in both short-term and long-term memory assays. Lesser effects on cognition were seen in normal mice suggesting that the cognitive improvements were not simply symptomatic in nature. It can be concluded that sterubin (**1**) exhibits strong neuroprotective properties during the 7-day treatment, leading to improved memory in the behavioral tests after the treatment was stopped. Hence, these findings strongly support that sterubin (**1**) holds significant potential as a disease-modifying neuroprotectant in AD.

Experimental Section

General: All reagents were bought from Sigma Aldrich, Munich, Germany, unless otherwise noted, and were used without further purification. Thin-layer chromatography was performed using Merck Silica Gel 60 F_{254} plates. For column chromatography, Silica Gel 60 (particle size 0.040–0.063 mm) (Sigma Aldrich, Munich, Germany) was used. Nuclear magnetic resonance (NMR) spectra were recorded with a Bruker AV-400 NMR instrument (Bruker, Karlsruhe, Germany) in $CDCl_3$ or [D_6]DMSO. Chemical shifts are expressed in ppm relative to $CDCl_3$ (7.26 ppm for ^{1}H and 77.16 ppm for ^{13}C) or [D_6]DMSO (2.50 ppm for ^{1}H and 39.52 ppm for ^{13}C). The purity of the synthetic products was determined by HPLC (Shimadzu, Duisburg, Germany), containing a DGU-20A3R degassing unit, an LC-20AB liquid chromatograph, and an SPD-20A UV/Vis detector. UV detection was done at 254 nm. Mass spectra were obtained by an LCMS-2020 device (Shimadzu, Duisburg, Germany). As a stationary phase, a Synergi 4U fusion-RP column (150 mm *x* 4.6 mm) was used, and, as a mobile phase, a gradient of methanol/water with 0.1% formic acid. Parameters: A = water, B = methanol, V(B)/[(V(A) + V(B)] = from 5% to 90% over 10 min, V(B)/[(V(A) + V(B)] = 90% for 5 min, V(B)/[(V(A) + V(B)] = from 90% to 5% over 3 min. The method was performed with a flow rate of 1.0 mL min^{-1}. Compounds were used for biological evaluation only if the purity was 95% or higher.

For the preparation of acetophenone **7** and aldehyde **8**, see the Supporting Information.

Chalcone 9: A mixture of acetophenone **7** (650 mg, 2.16 mmol) in EtOH (10 mL) and a saturated solution of KOH in EtOH (15 mL) was stirred at 4 °C for 15 min. A solution of **8** (490 mg, 2.16 mmol) in EtOH (5 mL) was added dropwise and the mixture was allowed to stir overnight (16 h) at room temperature. The reaction was quenched with water and extracted with ethyl acetate. The combined organic layers were dried over Na_2SO_4 and the solvent was removed under reduced pressure. The crude product was purified by silica gel chromatography using a mixture of cyclohexane and ethyl acetate (3/1). The product was obtained as a yellow solid in 85% yield (1.11 g). The analytical data were consistent with those reported in the literature.[31] ^{1}H NMR (400 MHz, $CDCl_3$): δ 7.35 (s, 1 H, Ar-H), 7.26 (d, ^2J = 16.0 Hz, 1 H, *H*C=CH), 7.13 (s, 2 H, Ar-H), 6.86 (d, ^2J = 16.0 Hz, 1 H, HC=C*H*), 6.43 (s, 2 H, Ar-H), 5.25 (s, 2 H, C*H*$_2$OCH$_3$), 5.22 (s, 2 H, C*H*$_2$OCH$_3$), 5.11 (s, 4 H, C*H*$_2$OCH$_3$), 3.82 (s, 3 H, OC*H*$_3$), 3.51 (s, 3 H, CH$_2$OC*H*$_3$), 3.50 (s, 3 H, CH$_2$OC*H*$_3$), 3.39 ppm (s, 6 H, CH$_2$OC*H*$_3$); ^{13}C NMR (100 MHz, $CDCl_3$): δ 194.4 (C_q, C=O), 162.1 (C_q, Ar-C), 156.0 (2x C_q, Ar-C), 149.4 (C_q, Ar-C), 147.5 (C_q, Ar-C), 144.7 (+, HC=CH), 129.4 (C_q, Ar-C), 128.1 (+, HC=CH), 123.8 (+, Ar-C), 116.3 (+, Ar-C), 116.0 (+, Ar-C), 113.8 (C_q, Ar-C), 95.6 (−, *C*H$_2$OCH$_3$), 95.2 (−, CH$_2$OCH$_3$), 95.1 (2× +, Ar-C), 94.6 (2x, −, CH$_2$OCH$_3$), 56.5 (+, CH$_2$OCH$_3$), 56.4 (+, CH$_2$OCH$_3$), 56.3 (2© +, CH$_2$OCH$_3$), 55.6 ppm (+, OCH$_3$); ESI-MS: *m/z* calcd for $C_{24}H_{30}O_{10}+H^+$: 479.19; found 479.2.

Sterubin (1): A solution of chalcone **9** (1.10 g, 2.32 mmol) in 10% methanolic HCl was stirred for 30 min at 50 °C. NaOAc (3.80 g, 46.4 mmol) was added and the mixture was heated to reflux for 3 h, cooled, then water was added and the mixture was extracted with ethyl acetate. The combined organic layers were dried over Na_2SO_4 and the solvent was removed under reduced pressure. The crude product was purified by silica gel column chromatography using a mixture of dichloromethane and methanol (40/1) as the eluent. The product was obtained as a white solid in 55% yield (391 mg). The analytical data were consistent with those reported in the literature.[13a] ^{1}H NMR (400 MHz, [D_6]DMSO): δ 12.11 (s, 1 H, O*H*), 9.03 (m, 2 H, O*H*), 6.91–6.86 (m, 1 H, Ar-H), 6.78–6.71 (m, 2 H, Ar-H), 6.10 6.06 (m, 2 H, Ar-H), 5.42 (dd, ^3J = 12.6, 3.0 Hz, 1 H), 3.79 (s, 3 H, OC*H*$_3$), 3.24 (dd, ^2J = 17.2, ^3J = 12.6 Hz, 1 H), 2.72 (dd, ^2J = 17.2, ^3J = 3.1 Hz, 1 H); ^{13}C NMR (100 MHz, [D_6]DMSO): δ 196.9 (C_q, *C*=O), 167.4 (C_q, Ar-C), 163.1 (C_q, Ar-C), 162.8 (C_q, Ar-C), 145.7 (C_q, Ar-C), 145.1 (C_q, Ar-C), 129.2 (C_q, Ar-C), 117.9 (+, Ar-C), 115.3 (+, Ar-C), 114.3 (+, Ar-C), 102.6 (C_q, Ar-C), 94.5 (+, Ar-C), 93.7 (+, Ar-C), 78.6 (+, Ar-C), 55.8 (+, CH$_3$, OCH$_3$), 42.1 (−, CH$_2$). ESI-MS: *m/z* calcd for $C_{16}H_{15}O_6+H^+$: 303.09; found 303.15.

For the preparation of **11**, see the Supporting Information.

Tri-*O*-acetyldehydrosterubin: To a solution of tri-*O*-acetylsterubin (**11**) (160 mg, 0.374 mmol) and NBS (67 mg, 0.374 mmol) in chloroform (5 mL) benzoyl peroxide (6 mg, 26 µmol) was added and the reaction mixture was heated to reflux for 2 h. Further chloroform was added, and the mixture was washed with water and brine. The organic layer was dried over Na_2SO_4 and the solvent was removed under reduced pressure. The crude product was purified by silica gel chromatography using an eluent of cyclohexane and ethyl acetate (2:1 → pure ethyl acetate) and the product was obtained as a white solid in 63% yield (100 mg). ^{1}H NMR: (400 MHz, $CDCl_3$): δ 7.73 (dd, ^3J = 8.5, ^4J = 2.2 Hz, 1 H, Ar-H), 7.70 (d, ^4J = 2.1 Hz, 1 H, Ar-H), 7.35 (d, ^3J = 8.5 Hz, 1 H, Ar-H), 6.87 (d, ^4J = 2.5 Hz, 1 H, Ar-H), 6.62 (d, ^4J = 2.4 Hz, 1 H, Ar-H), 6.55 (s, 1 H, C=CH), 3.92 (s, 3 H, OC*H*$_3$), 2.44 (s, 3 H, C*H*$_3$COO), 2.35 (s, 3 H, C*H*$_3$COO), 2.33 (s, 3 H, C*H*$_3$COO); ^{13}C NMR (100 MHz, $CDCl_3$): δ 176.3 (C_q, *C*=O), 169.7 (C_q, CH$_3$COO), 168.1 (C_q, CH$_3$COO), 167.9 (C_q, CH$_3$COO), 163.7 (C_q, Ar-C), 160.3 (C_q, *C*=CH), 158.9 (C_q, Ar-C), 150.7 (C_q, Ar-C), 144.7 (C_q, Ar-C), 142.7 (C_q, Ar-C), 130.2 (C_q, Ar-C), 124.5 (+, Ar-C), 124.3 (+, Ar-C),

121.6 (+, Ar-C), 111.3 (C_q, Ar-C), 109.0 (+, C=CH), 108.6 (+, Ar-C), 99.2 (+, Ar-C), 56.1 (+, OCH_3), 21.2 (CH_3COO), 20.8 (CH_3COO), 20.7 (CH_3COO); ESI-MS: *m/z* calcd for $C_{22}H_{18}O_9+H^+$: 427.10; found 427.20.

Dehydrosterubin (12): A solution of tri-*O*-acetyldehydrosterubin (97 mg, 0.227 mmol) in acetonitrile (3 mL) and conc. aqueous HCl (3 mL) was heated to reflux for 1.5 h. Yellow precipitant was formed, which was filtered off, washed with water, and dried under vacuum. The product was obtained as a yellow solid in 50% yield (34 mg). ^{1}H NMR (400 MHz, [D$_6$]DMSO): δ 12.97 (s, 1H, O*H*), 9.96 (s, 1H, O*H*), 9.37 (s, 1H, O*H*), 7.44 (m, 2H, Ar-H), 6.90 (d, ^3J=8.1 Hz, 1H, Ar-H), 6.72 (s, 1H, C=C*H*), 6.71 (d, ^4J=2.5 Hz, 1H, Ar-H), 6.37 (d, ^4J=2.2 Hz, 1H, Ar-H), 3.87 (s, 3H, OC*H*$_3$); ^{13}C NMR (100 MHz, [D$_6$]DMSO): δ 181.7 (C_q, *C=O*), 165.0 (C_q, Ar-C), 164.2 (C_q, Ar-C), 161.1 (C_q, *C*=CH), 157.1 (C_q, Ar-C), 149.8 (C_q, Ar-C), 145.7 (C_q, Ar-C), 121.3 (C_q, Ar-C), 119.0 (+, Ar-C), 115.9 (+, Ar-C), 113.5 (+, Ar-C), 104.6 (C_q, Ar-C), 103.0 (+, C=CH), 97.9 (+, Ar-C), 92.5 (+, Ar-C), 56.0 (+, OCH_3); ESI-MS: *m/z* calcd for $C_{16}H_{12}O_6+H^+$: 301.07; found 301.15.

Plant material: Leaves of *Eriodictyon californicum* Hook. & Arn. (Boraginaceae) were collected by Ms. Kyra Bobine in May, 2019.

Plant extraction: Dried leaves of *E. californicum* (18.6 g) were soaked in ethyl acetate (3×100 mL), ultrasonicated for 30 min, then shaken overnight (≈16 h) at room temperature. The crude extract was filtered, and the filtrate was concentrated in vacuo. The obtained residue (2.0 g) was re-dissolved in 90% aqueous methanol. By addition of *n*-hexane, chlorophyll and non-polar residues were removed and sterubin (**1**) and related flavones were precipitated. After filtration, the precipitate (0.6 g) was dissolved in methanol and directly subjected to HPLC on a ChiralPak-IA column.

Chiral resolution of racemic sterubin: An HPLC-UV guided resolution of the enantiomers of **1** was performed on a Jasco system equipped with a DG-2080 degassing unit, a PU-1580 ternary pump, an MD-2010 plus multiwavelength detector, and an AS-2055 autosampler. Separation of the enantiomers was done on a ChiralPak IA® (10×25 mm, 5 µm, Daicel Chemical Industries) column using a gradient system with initial conditions 32% B (B: 90% MeCN in water + 0.05% TFA) to 60% B in 29 min. The (*R*)- and (*S*)-enantiomers of sterubin, (*R*)-**1** and (*S*)-**1**, had retention times of 17.8 min and 20.2 min, respectively.

Online LC-ECD analysis of the sterubin enantiomers: ECD spectroscopic analysis was performed using a Jasco J-715 spectropolarimeter. Measurements were done at room temperature and the spectra were processed using the SpecDis software.[32]

Oxytosis assay: HT22 cells were grown in Dulbecco's Modified Eagle Medium (DMEM, Sigma Aldrich, Munich, Germany) supplemented with 10% (v/v) fetal calf serum (FCS) and 1% (v/v) penicillin-streptomycin. 5×10^3 HT22 cells per well were seeded into sterile 96-well plates and incubated overnight (≈16 h). Aqueous glutamate solution (5 mM) (monosodium-L-glutamate, Sigma Aldrich, Munich, Germany) together with 2.5, 5.0, 7.5, or 10 µM of the respective compound was added to the cells and incubated for 24 h. Quercetin (25 µM) (Sigma Aldrich, Munich, Germany) together with glutamate (5 mM) served as a positive control. After 24 h incubation cell viability was determined using a colorimetric 3-(4,5-dimethylthiazol-2-yl)-2,5-diphenyltetrazolium bromide (MTT, Sigma Aldrich, Munich, Germany) assay. MTT solution (5 mg mL^{-1} in PBS) was diluted 1:10 with medium and added to the wells after removal of the old medium. Cells were incubated for 3 h and then lysis buffer (10% SDS) was added. The next day, absorbance at 560 nm was determined with a multiwell plate photometer (Tecan, SpectraMax 250). Results are presented as percentage of untreated control cells. All data are expressed as means ± SEM of three independent experiments. Analysis was accomplished using GraphPad Prism 5 Software applying Oneway ANOVA followed by Dunnett's multiple comparison posttest. Levels of significance: * $p<0.05$; ** $p<0.01$; *** $p<0.001$.

Cellular uptake and racemization experiments: 2×10^6 BV2 cells were grown in sterile 100 mm dishes overnight and 4 mL 50 µM (*S*)-**1** or (*R*)-**1** diluted in cell culture medium were added. Cells were incubated for the indicated time periods, after which the supernatant was removed, and cells were washed twice with PBS. Further PBS (1 mL) was added, cells were scraped and transferred to Eppendorf tubes. The samples were centrifuged and resuspended in 200 µL of MeOH. The cells were frozen in liquid nitrogen and thawed at 37 °C (10 times). Cell debris was pelleted by centrifugation and the supernatant was collected for HPLC analysis.

Neuroprotection studies in vivo: The in vivo behavioral experiments were performed as established and published previously.[15,33] Neurotoxicity was induced by ICV injection of oligomerized Aβ_{25-35} peptide, and sterubin (**1**) was evaluated for its neuroprotective properties. Sterubin was dissolved in 60% DMSO and 40% saline (0.9% NaCl in milliQ water) and was injected once per day IP on days 1–7 to give doses of 0.3, 1, and 3 mg kg^{-1}. The oligomerized Aβ_{25-35} peptide was injected ICV on day 1 of the study. The behavior of the mice was evaluated on day 8 (YMT) and days 9 and 10 (STPA). On day 11, the mice were sacrificed, and the brains were collected. Samples were frozen at −80 °C for further biochemical analysis.

Animals: Male Swiss mice 6 weeks old, body weight 30–40 g, obtained from JANVIER (Saint Berthevin, France) were housed in the animal facility of the University of Montpellier (CECEMA, Office of Veterinary Services agreement #B-34-172-23) with access to food and water *ad libitum* (except during behavioral tests). The humidity and temperature were controlled, and the mice were kept at a 12 h light/12 h dark cycle (lights off at 7:00 p.m.). All animal procedures were conducted in strict adherence to the European Union directives of September 22nd, 2010 (2010/63/UE) and to the ARRIVE guidelines. The project was authorized by the French National Ethics Committee (APAFIS #1485-15034). Animals were assigned to different treatment groups randomly.

Preparation of sterubin injections: Sterubin (**1**) was dissolved in 100% DMSO at a concentration of 6 mg mL^{-1} to give a stock solution, which was diluted with saline (0.9% NaCl in milliQ water) and DMSO to the final test concentration and a final percentage of 60% DMSO. 60% DMSO in saline served as the vehicle (V2). After compound injections, the behavior of the mice in their home cage was checked visually. Weight was examined once per day. As demonstrated in Figure S1, a tendency was observed that weight gain was facilitated with an increasing dose of **1**. Nevertheless, the difference in weight gain remained insignificant compared to Aβ+V2 treated mice in Dunnett's multiple comparison test.

Amyloid peptide preparation and ICV injection: All experiments followed previously described protocols.[15,25,32] The Aβ_{25-35} peptide was prepared according to Maurice et al.[15] Mice were anesthetized with 2.5% isoflurane. Then, oligomerized Aβ_{25-35} peptide (9 nmol in 3 µL/mouse) was injected ICV. Bidistilled water was used as a vehicle (V1).

Spontaneous alternation performance in a Y-maze: On day 8 of the study, the spatial working memory of all mice was evaluated in the Y-maze.[15,25,32] The Y-maze is made from grey polyvinylchloride and has three identical arms (length 40 cm, height 13 cm, bottom width 3 cm, top width 10 cm (walls converge at an equal angle).

For evaluation of memory, every mouse was placed into one arm and was allowed to explore the maze for 8 min. All entries into an arm (including the return into the same arm) were counted and the number of alternations (mouse entered all three arms consecutively) was calculated as percentage of total number of arm entries [alternations/ (arm entries−2)×100].

Step-through passive avoidance test: STPA was performed on day 9 and day 10 in a two-compartment box [(width 10 cm, total length 20 cm (10 cm per compartment), height 20 cm] consisting of polyvinylchloride. One of the compartments was white and illuminated with a bulb (60 W, 40 cm above the center of the compartment), the second compartment was black, covered, and had a grid floor. A guillotine door separated the compartments. On day 9 (training), each animal was placed in the white compartment and was left to explore for 5 s. Then, the door was opened, which allowed the mouse to enter the black compartment. After it had entered, the door was closed, and a foot shock was delivered (0.3 mA) for 3 s generated by a scramble shock generator (Lafayette Instruments, Lafayette, USA). The step-through latency (time the mouse spent in the white compartment after the door was opened) and the level of sensitivity (no sign=0, flinching reactions=1, vocalization=2) were recoded. Treatment with sterubin (**1**) did not affect the measured parameters. On the next day (day 10), each mouse was placed in the white compartment and was allowed to explore for 5 s. Then, the door was opened allowing the mouse to step over into the black compartment. The step-through latency was measured for up to 300 s.

Sacrifice and brain collection: All animals were sacrificed on day 11. The brains were collected, hippocampus and cortex were isolated, and the samples were frozen at −80 °C.

Statistical analysis: Weight gain and results from the YMT were analyzed by the software GraphPad Prism 5.0 using one-way ANOVA, followed by Dunnett's *post-hoc* multiple comparison test. STPA had a maximum step-through latency of 300 s. Therefore, a Gaussian distribution could not be assumed. The results were analyzed using a Kruskal-Wallis non-parametric ANOVA, followed by a Dunn's multiple comparison test. $p<0.05$ was considered significant.

Novel-object recognition test: Male C57Bl/6J mice were used and the testing was done by Scripps Research. All mice were acclimated to the colony room for at least 2 weeks prior to testing and were tested at an average age of 8 weeks. Mice were randomly assigned across treatment groups with 11 mice in each group. For each dose tested, a solution of sterubin in corn oil was prepared. The vehicle was corn oil alone. All were administered orally 60 min prior to the training session at a volume of 10 mL kg^{-1} body weight. Rolipram was dissolved in 10% DMSO and administered intraperitoneally at 0.1 mg kg^{-1} 20 min prior to training. The test was performed as described previously.[29] Briefly, on day 1 mice were habituated to a circular open field arena for one hour in cage groups of four. 24 h later, individual mice were placed back in the same arena which now contained two identical objects for a 15 min training trial. On day 3, vehicle-, sterubin- or rolipram-treated mice were individually placed back in the same arena in the presence of both the familiar object (i.e., previously explored) and a novel object. The spatial positions of the objects were counterbalanced between subjects. Each animal's test trial was recorded and the first 10 min of each session were scored. Object recognition was computed using the formula: Time spent with novel object *x* 100)/Total time spent exploring both objects. Data were analyzed by a one-way ANOVA followed by post-hoc comparisons with Fisher's test.

Acknowledgements

Financial support by the Bavaria California Technology Center to P.M. and M.D. under project number 3 [2018-2] is gratefully acknowledged. M.D. and T.M. acknowledge support from Campus France (PHC Procope), and the German Academic Exchange Service (DAAD) with funds of the Federal Ministry of Education and Research (BMBF). S.F. is grateful to DAAD and to the Egyptian Government for a generous scholarship. We thank William Shamburger for technical support as well as Dominik Moreth and Alevtina Cubukova (Fraunhofer ISC, TLC-RT) for experimental help.

Conflict of interest

The authors declare no conflict of interest.

Keywords: Alzheimer's disease · chiral resolution · circular dichroism · Eriodictyon californicum · flavonoids · sterubin

[1] a) S. J. Allen, J. J. Watson, D. K. Shoemark, N. U. Barua, N. K. Patel, *Pharmacol. Ther.* **2013**, *138*, 155–175; b) C. Patterson, *Alzheimer's Disease International (ADI)*, London (UK), **2018**.
[2] a) D. J. Selkoe, *Science* **2002**, *298*, 789–791; b) K. Blennow, M. J. de Leon, H. Zetterberg, *Lancet* **2006**, *368*, 387–403.
[3] M. Prior, C. Chiruta, A. Currais, J. Goldberg, J. Ramsey, R. Dargusch, P. A. Maher, D. Schubert, *ACS Chem. Neurosci.* **2014**, *5*, 503–513.
[4] a) P. Agostinho, R. A. Cunha, C. Oliveira, *Curr. Pharm. Des.* **2010**, *16*, 2766–2778; b) C. Hölscher, *EBioMedicine* **2019**, *39*, 17–18.
[5] T. Bui Thanh, H. Nguyen Thanh, *J. Basic Clin. Physiol. Pharmacol.* **2017**, *28*, 413–423.
[6] a) F. Pohl, P. Kong Thoo Lin, *Molecules* **2018**, *23*, 3283; b) N. Cho, J. H. Choi, H. Yang, E. J. Jeong, K. Y. Lee, Y. C. Kim, S. H. Sung, *Food Chem. Toxicol.* **2012**, *50*, 1940–1945; c) M. Sato, K. Murakami, M. Uno, H. Ikubo, Y. Nakagawa, S. Katayama, K.-i. Akagi, K. Irie, *Biosci. Biotechnol. Biochem.* **2013**, *77*, 1100–1103.
[7] S. Gunesch, S. Schramm, M. Decker, *Future Med. Chem.* **2017**, *9*, 711–713.
[8] S. Schramm, G. Huang, S. Gunesch, F. Lang, J. Roa, P. Högger, R. Sabaté, P. Maher, M. Decker, *Eur. J. Med. Chem.* **2018**, *146*, 93–107.
[9] S. Gunesch, C. Kiermeier, M. Hoffmann, W. Fischer, A. F. M. Pinto, T. Maurice, P. Maher, M. Decker, *Redox Biol.* **2019**, 101378.
[10] S. Schramm, S. Gunesch, F. Lang, M. Saedtler, L. Meinel, P. Högger, M. Decker, *Arch. Pharm. Chem. Life Sci.* **2018**, *351*, 1800206.
[11] W. Fischer, A. Currais, Z. Liang, A. Pinto, P. Maher, *Redox Biol.* **2019**, *21*, 101089.
[12] V. K. Chesnut, *Plants used by the Indians of Mendocino County, California, Vol. 7*, Mendocino County Historical Society, Fort Bragg (CA, USA), **1974**.
[13] a) J. P. Ley, G. Krammer, G. Reinders, I. L. Gatfield, H.-J. Bertram, *J. Agric. Food Chem.* **2005**, *53*, 6061–6066; b) J. Walker, K. V. Reichelt, K. Obst, S. Widder, J. Hans, G. E. Krammer, J. P. Ley, V. Somoza, *Food Func.* **2016**, *7*, 3046–3055.
[14] M. Krause, R. Galensa, *Chromatographia* **1991**, *32*, 69–72.
[15] T. Maurice, B. P. Lockhart, A. Privat, *Brain Res.* **1996**, *706*, 181–193.
[16] H. Wagner, L. Farkas, in *The Flavonoids* (Eds.: J. B. Harborne, T. J. Mabry, H. Mabry), Springer US, Boston, MA, **1975**, 127–213.
[17] E.-M. Jung, Y. R. Lee, *Bull. Korean Chem. Soc.* **2008**, *29*, 1199–1204.
[18] B. Roschek, R. C. Fink, M. D. McMichael, D. Li, R. S. Alberte, *Phytochemistry* **2009**, *70*, 1255–1261.
[19] G. Bringmann, K. Messer, M. Wohlfarth, J. Kraus, K. Dumbuya, M. Rückert, *Anal. Chem.* **1999**, *71*, 2678–2686.
[20] W. Gaffield, *Tetrahedron* **1970**, *26*, 4093–4108.
[21] J. B. Davis, P. Maher, *Brain Res.* **1994**, *652*, 169–173.
[22] a) S. Tan, D. Schubert, P. Maher, *Curr. Top. Med. Chem.* **2001**, *1*, 497–506; b) T. H. Murphy, M. Miyamoto, A. Sastre, R. L. Schnaar, J. T. Coyle, *Neuron*

1989, *2*, 1547–1558; c) S. Tan, M. Wood, P. Maher, *J. Neurochem.* **2002**, *71*, 95–105.
[23] A. Currais, P. Maher, *Antioxid. Redox Signal.* **2013**, *19*, 813–822.
[24] S. A. B. E. Van Acker, D.-j. Van Den Berg, M. N. J. L. Tromp, D. H. Griffioen, W. P. Van Bennekom, W. J. F. Van Der Vijgh, A. Bast, *Free Radical Biol. Med.* **1996**, *20*, 331–342.
[25] J. Vrba, R. Gažák, M. Kuzma, B. Papoušková, J. Vacek, M. Weiszenstein, V. Křen, J. Ulrichová, *J. Med. Chem.* **2013**, *56*, 856–866.
[26] H. Aft, *J. Org. Chem.* **1965**, *30*, 897–901.
[27] V. Lahmy, J. Meunier, S. Malmström, G. Naert, L. Givalois, S. H. Kim, V. Villard, A. Vamvakides, T. Maurice, *Neuropsychopharmacology* **2013**, *38*, 1706–1723.
[28] a) P. Lu, T. Mamiya, L. Lu, A. Mouri, L. Zou, T. Nagai, M. Hiramatsu, T. Ikejima, T. Nabeshima, *Br. J. Pharmacol.* **2009**, *157*, 1270–1277; b) S. Saito, Y. Yamamoto, T. Maki, Y. Hattori, H. Ito, K. Mizuno, M. Harada-Shiba, R. N. Kalaria, M. Fukushima, R. Takahashi, M. Ihara, *Acta Neuropathol. Commun.* **2017**, *5*, 26.
[29] P. Maher, T. Akaishi, K. Abe, *Proc. Natl. Acad. Sci. USA* **2006**, *103*, 16568–16573.
[30] R. Bourtchouladze, R. Lidge, R. Catapano, J. Stanley, S. Gossweiler, D. Romashko, R. Scott, T. Tully, *Proc. Natl. Acad. Sci. USA* **2003**, *100*, 10518–10522.
[31] H. Takahashi, S. Li, Y. Harigaya, M. Onda, *Heterocycles* **1987**, *26*, 3239–3248.
[32] a) T. Bruhn, A. Schaumlöffel, Y. Hemberger, G. Bringmann, *Chirality* **2013**, *25*, 243–249; b) T. Bruhn, A. Schaumlöffel, Y. Hemberger, G. Pescitelli, **2017**, SpecDis, Version 1.71; www.specdis-software.jimdo.com.
[33] a) M. Scheiner, D. Dolles, S. Gunesch, M. Hoffmann, M. Nabissi, O. Marinelli, M. Naldi, M. Bartolini, S. Petralla, E. Poeta, B. Monti, C. Falkeis, M. Vieth, H. Hübner, P. Gmeiner, R. Maitra, T. Maurice, M. Decker, *J. Med. Chem.* **2019**, *62*, 9078–9102; b) M. Hoffmann, C. Stiller, E. Endres, M. Scheiner, S. Gunesch, C. Sotriffer, T. Maurice, M. Decker, *J. Med. Chem.* **2019**, *62*, 9116–9140; c) T. Maurice, M. Strehaiano, N. Siméon, C. Bertrand, A. Chatonnet, *Behav. Brain Res.* **2016**, *296*, 351–360.

Manuscript received: March 13, 2020
Accepted manuscript online: May 2, 2020
Version of record online: May 15, 2020

Chemistry–A European Journal

Supporting Information

Sterubin: Enantioresolution and Configurational Stability, Enantiomeric Purity in Nature, and Neuroprotective Activity in Vitro and in Vivo

Julian Hofmann+,[a] Shaimaa Fayez+,[b, c] Matthias Scheiner,[a] Matthias Hoffmann,[a, d] Sabrina Oerter,[e] Antje Appelt-Menzel,[e, f] Pamela Maher,[g] Tangui Maurice,[d] Gerhard Bringmann,*[b] and Michael Decker*[a]

Table of Contents

*1. Early Steps in the Synthesis of Sterubin (**1**) and Dehydrosterubin (**12**)*

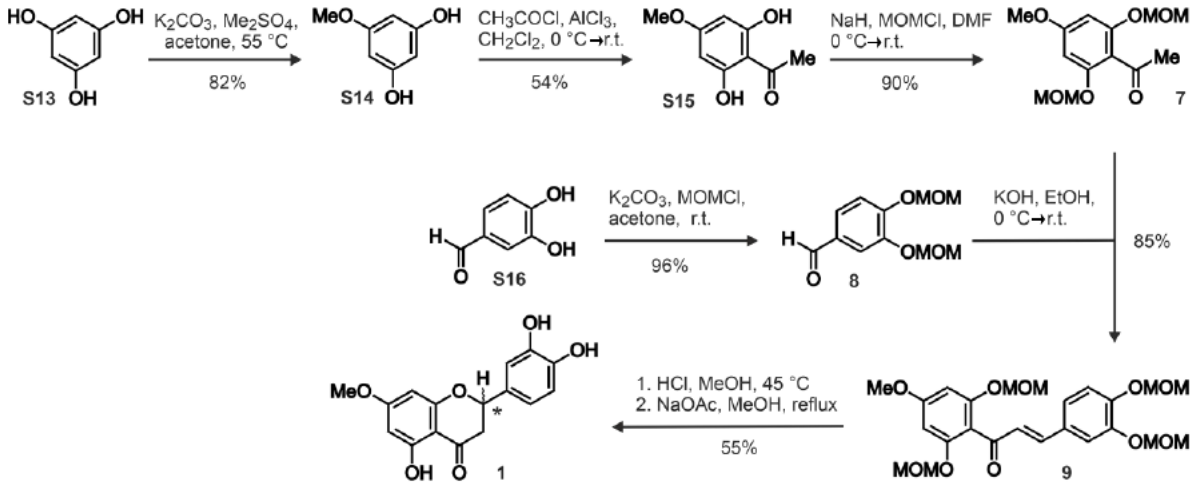

Scheme SI-1. Synthesis of racemic sterubin (**1**). MOM = methoxymethyl.

Phenol S14. To a suspension of K_2CO_3 (4.38 g, 31.7 mmol) and **S13** (4.00 g, 31.7 mmol) in acetone, dimethyl sulfate (1.0 mL,10.6 mmol) was added dropwise and the reaction mixture was stirred at 55 °C overnight (16 h). The solvent was removed under reduced pressure and the residue was transferred to a separatory funnel with ethyl acetate. The organic layer was washed with 1M HCl and brine, and then dried with Na_2SO_4. The solvent was removed under reduced pressure and the crude product was purified by silica gel chromatography using a mixture of cyclohexane and ethyl acetate (3:1) as the eluent. The product was obtained as a pale-orange oil in 82% yield (1.22 g). The analytical data were consistent with those reported in the literature.[1] ^{1}H NMR (400 MHz, DMSO-d_6) δ 9.15 (s, 2H, O*H*), 5.82 (t, ^4J = 2.1 Hz, 1H), 5.78 (d, ^4J = 2.0 Hz, 2H, Ar-H), 3.61 ppm (s, 3H, OCH_3); ^{13}C NMR (100 MHz, DMSO-d_6): δ 161.4 (C_q, Ar-C), 159.3 (2x C_q, Ar-C), 95.9 (+, Ar-C), 93.0 (2x +, Ar-C), 55.0 (+, OCH_3); ESI-MS: *m/z* calcd for $C_7H_8O_3$+H^+: 141.05; found 141.09.

Acetophenone S15. To a mixture of phenol **S14** (472 mg, 3.37 mmol) and aluminum chloride (1.12 g, 8.43 mmol) in dichloromethane, acetyl chloride (250 µL, 3.37 mmol) was added at 4 °C and the mixture was allowed to stir at room temperature overnight. The reaction was quenched by addition of ice. The

resulting mixture was transferred to a separatory funnel and washed with 1M HCl and brine. The organic layer was dried over Na_2SO_4 and the solvent was removed under reduced pressure. The crude product was purified by silica gel chromatography using a mixture of cyclohexane and ethyl acetate (4:1) as the eluent. The product was obtained as a white solid in 54% yield (332 mg, 1.82 mmol). The analytical data were consistent with those reported in the literature.[1] ^{1}H NMR (400 MHz, $CDCl_3$): *δ* 5.92 (s, 2H, Ar-H), 3.79 (s, 3H, OC*H*$_3$), 2.67 ppm (s, 3H, C*H*$_3$); ^{13}C-NMR (100 MHz, $CDCl_3$): *δ* 203.4 (*C*=O), 165.8 (C_q, Ar-C), 105.2 (C_q, Ar-C), 96.5 (C_q, Ar-C), 94.4 (2x +, Ar-C), 90.8 (C_q, Ar-C), 55.7 (O*C*H$_3$), 32.97 ppm (*C*H$_3$); ESI-MS: *m/z* calcd for $C_9H_{10}O_4$+H$^+$: 183.06; found 183.15.

Protected acetophenone 7. To a mixture of NaH (290 mg, 12.1 mmol) in dry DMF (3 mL), a solution of **SI-15** (489 mg, 2.68 mmol) in dry DMF (5 mL) was added dropwise at 4 °C under an argon atmosphere and the reaction mixture was stirred for 45 min at room temperature. Chloromethyl methyl ether (919 µL, 12.1 mmol) was slowly added over a period of 15 min keeping the temperature under 5 °C. The reaction mixture was stirred overnight (16 h) at room temperature, then water was added, and the mixture was extracted with ethyl acetate. The combined organic layers were dried over Na_2SO_4 and the solvent was removed under reduced pressure. The crude product was purified by silica gel chromatography using a mixture of cyclohexane and ethyl acetate (4/1) as the eluent. The product was obtained as a colorless oil in 90% yield (650 mg). The analytical data were consistent with those reported in the literature.[2] ^{1}H-NMR: (400 MHz, $CDCl_3$): *δ* 6.38 (s, 2H, 2 Ar-H), 5.14 (s, 4H, C*H*$_2$OCH$_3$), 3.78 (s, 3H, OC*H*$_3$), 3.46 (s, 6H, CH$_2$OC*H*$_3$), 2.49 ppm (s, 3H, C*H*$_3$); ^{13}C NMR (100 MHz, $CDCl_3$): *δ* 201.5 (C_q, *C*=O), 162.0 (C_q, Ar-C), 155.6 (C_q, 2 Ar-C), 116.0 (C_q, Ar-C), 95.2 (-, 2 *C*H$_2$OCH$_3$), 94.9 (+, 2 Ar-C), 56.4 (+, 2 CH$_2$O*C*H$_3$). 55.6 (+, O*C*H$_3$), 32.7 ppm (+, *C*H$_3$); ESI-MS: *m/z* calcd for $C_{13}H_{18}O_6$+H$^+$: 271.11, found 271.22.

Benzaldehyde 8. To a solution of **S16** (800 mg, 5.79 mmol) in dry DMF (10 mL), K_2CO_3 (7.20 g, 52.1 mmol) was added at 4 °C under argon atmosphere. Chloromethyl methyl ether (1.30 mL, 26.1 mmol) was slowly added over a period of 15 min keeping the temperature under 5 °C. The reaction mixture was stirred at room temperature overnight (16 h), quenched by addition of cold distilled water, and extracted with ethyl acetate. The combined organic layer was washed with distilled water and brine

and dried over Na_2SO_4. The solvent was removed under reduced pressure and the crude product was purified by silica gel column chromatography using a mixture of cyclohexane and ethyl acetate (4:1). The product was obtained as a white solid in 96 % yield (1.25 g, 5.54 mmol). The analytical data were consistent with those reported in the literature.[3] ^{1}H NMR: (400 MHz, $CDCl_3$): δ 9.87 (s, 1H, C*HO*), 7.68 (d, ^4J = 2.0 Hz, 1H, Ar-H), 7.51 (dd, ^3J = 8.3, ^4J = 2.0 Hz, 1H, Ar-H), 7.28 (d, ^3J = 8.3 Hz, 1H, Ar-H), 5.33 (s, 2H, C*H*$_2$OCH$_3$), 5.30 (s, 2H, C*H*$_2$OCH$_3$), 3.53 (s, 3H, CH$_2$OC*H*$_3$), 3.52 ppm (s, 3H, CH$_2$OC*H*$_3$); ^{13}C NMR (100 MHz, $CDCl_3$): δ 190.9 (C_q, *C*HO), 152.7 (C_q, Ar-C), 147.5 (C_q, Ar-C), 131.2 (C_q, Ar-C), 126.4 (+, Ar-C), 116.0 (+, Ar-C), 115.5 (+, Ar-C), 95.5 (-, *C*H$_2$OCH$_3$), 95.1 (-, *C*H$_2$OCH$_3$), 56.6 (+, CH$_2$O*C*H$_3$), 56.5 ppm (+, CH$_2$O*C*H$_3$); ESI-MS: *m/z* calcd for $C_{11}H_{14}O_5$+H$^+$: 227.09; found 227.1.

Tri-*O*-acetylsterubin (11). To a suspension of sterubin (**1**) (194 mg, 0.642 mmol) in Ac_2O (3 mL), iodine (6 mg, 44.9 µmol) was added. The reaction mixture was stirred at room temperature for 2 h. Ethyl acetate was added, and the mixture was washed with a saturated aqueous $Na_2S_2O_3$ solution, a saturated aqueous $NaHCO_3$ solution and brine. The organic layer was dried over Na_2SO_4 and the solvent was removed under reduced pressure. The crude product was purified by silica gel chromatography using an eluent of cyclohexane and ethyl acetate (2:1). The product was obtained as white solid in 70% yield (193 mg). The analytical data were consistent with those reported in the literature.[4] ^{1}H NMR: (400 MHz, $CDCl_3$): δ 7.30-7.16 (m, 3H, Ar-H), 6.36 (d, ^4J = 2.5 Hz, 1H, Ar-H), 6.23 (d, ^4J = 2.5 Hz, 1H, Ar-H), 5.38 (dd, $^3J_{trans}$ = 13.5, $^3J_{cis}$ = 2.9 Hz, 1H), 3.77 (s, 3H, OC*H*$_3$), 2.90 (dd, ^2J = 16.7, $^3J_{trans}$ = 13.4 Hz, 1H), 2.68 (dd, ^2J = 16.7, $^3J_{cis}$ = 2.9 Hz, 1H), 2.32 (s, 3H, C*H*$_3$COO), 2.24 (s, 6H, 2x C*H*$_3$COO); ^{13}C NMR (100 MHz, $CDCl_3$): δ 188.3 (C_q, *C*=O), 169.5 (C_q, CH$_3$*C*OO), 168.2 (C_q, CH$_3$*C*OO), 168.2 (C_q, CH$_3$*C*OO), 165.6 (C_q, Ar-C), 164.0 (C_q, Ar-C), 151.9 (C_q, Ar-C), 142.4 (C_q, Ar-C), 142.4 (C_q, Ar-C), 137.3 (C_q, Ar-C), 124.3 (+, Ar-C), 123.9 (+, Ar-C), 121.4 (+, Ar-C), 108.0 (C_q, Ar-C), 105.0 (+, Ar-C), 99.6 (+, Ar-C), 78.5 (+, O*C*H), 55.9 (+, O*C*H$_3$), 45.1 (-, *C*H$_2$), 21.2 (*C*H$_3$COO), 20.7 (*C*H$_3$COO), 20.7 (*C*H$_3$COO); ESI-MS: *m/z* calcd for $C_{22}H_{20}O_9$+H$^+$: 429.12; found 429.15.

2. Racemization in Cell Culture Medium

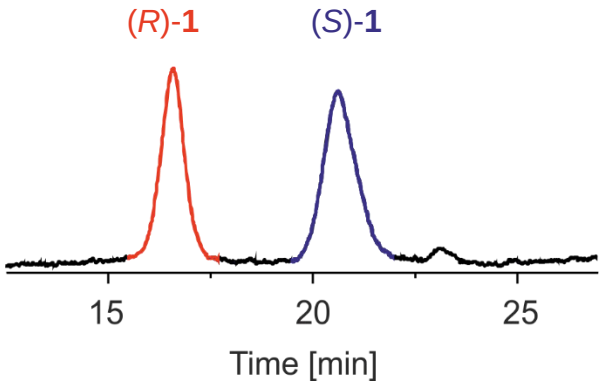

Figure SI-1: Chromatogram of (*R*)-**1** immediately after dissolving the enantiomerically pure compound in DMSO and dilution in cell culture medium.

(*R*)-Sterubin [(R)-**1**)] was dissolved in DMSO and diluted to a final concentration of 50 µM in Dulbecco's Modified Eagle Medium (DMEM, Sigma Aldrich, Munich, Germany) supplemented with 10% (v/v) fetal calf serum (FCS) and 1% (v/v) penicillin-streptomycin. The samples were further diluted 1:1 with methanol and centrifuged at 12,000 rpm for 10 min. The supernatants were analyzed by HPLC on a ChiralPak IA® column (10 x 25 mm, 5 µm, Daicel Chemical Industries) using a gradient system with initial conditions 32% B (B: 90% MeCN in water + 0.05% TFA) to 60% B in 29 min.

*3. Cytotoxicity of **1***

The human induced pluripotent stem cell line IMR90-4 was differentiated to blood-brain barrier endothelial cells (EC) as previously described.[5] Differentiated ECs were plated to three wells per condition on a collagen IV/fibronectin coated 96-well plate (1 x 10^6 cells/cm²) in EC medium (hESFM + B27) additionally containing hbFGF and retinoic acid. On the next day, medium was changed to EC medium. 48 h after seeding, the cells were treated with a dosage of sterubin (**1**) in DMSO (0.5, 5 and 50 mg/L) and placed for 24 h in a 5 % CO_2 incubator at 37 °C. A control of either EC medium (negative control), 1 % SDS (positive control) or a 1:1000 dilution of DMSO (cell blank) in EC medium (highest applied sample concentration) were tested in parallel. Upon completion of the treatment, the wells were washed with PBS and 200 µl CellTiter-Glo® solution (CellTiter-Glo® Luminescent Cell Viability Assay, Promega) was added per well at a 1:2 ratio in EC medium. The plate was transferred into a plate reader, mixed for 2 min following an incubation time of 10 min. After incubation, the luminescence of each sample was measured. The cell viability was calculated using the negative control (100 % viability) as a reference.

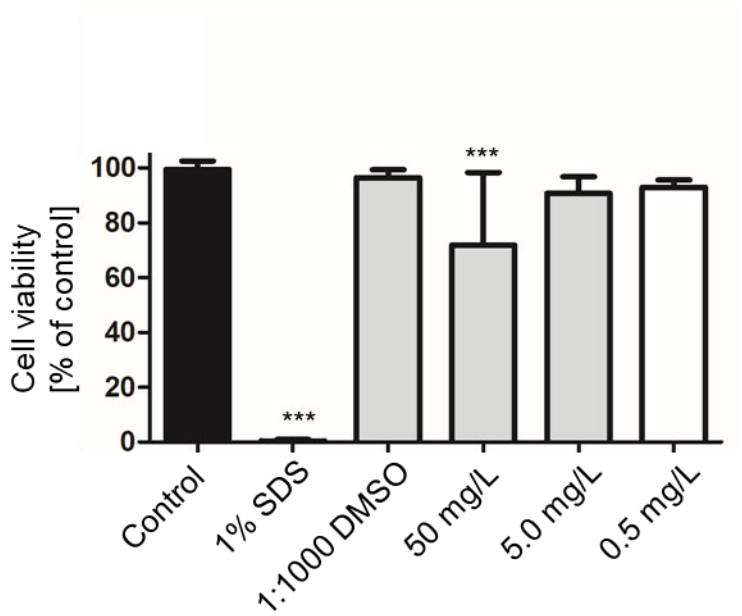

Figure SI-2: Cell viability of hiPSC-derived endothelial cells after Sterubin treatment. After treatment with 50, 5.0 and 0.5 mg/l Sterubin for 24 hours the cell viability of hiPSC-derived BBB ECs was measured via CellTiter-Glo® test. Only significant cell death was measured in the positive control (1% SDS). All Sterubin concentrations showed mostly unaffected cell viability. Results are presented as mean ± SD of three independent experiments and refer to untreated control cells which were set as 100% value. Statistical analysis was performed using One-Way ANOVA followed by Dunnett's multiple comparison posttest using GraphPad Prism 5. Levels of significance: * $p < 0.05$; ** $p < 0.01$; *** $p < 0.001$.

4. Mouse Body Weight

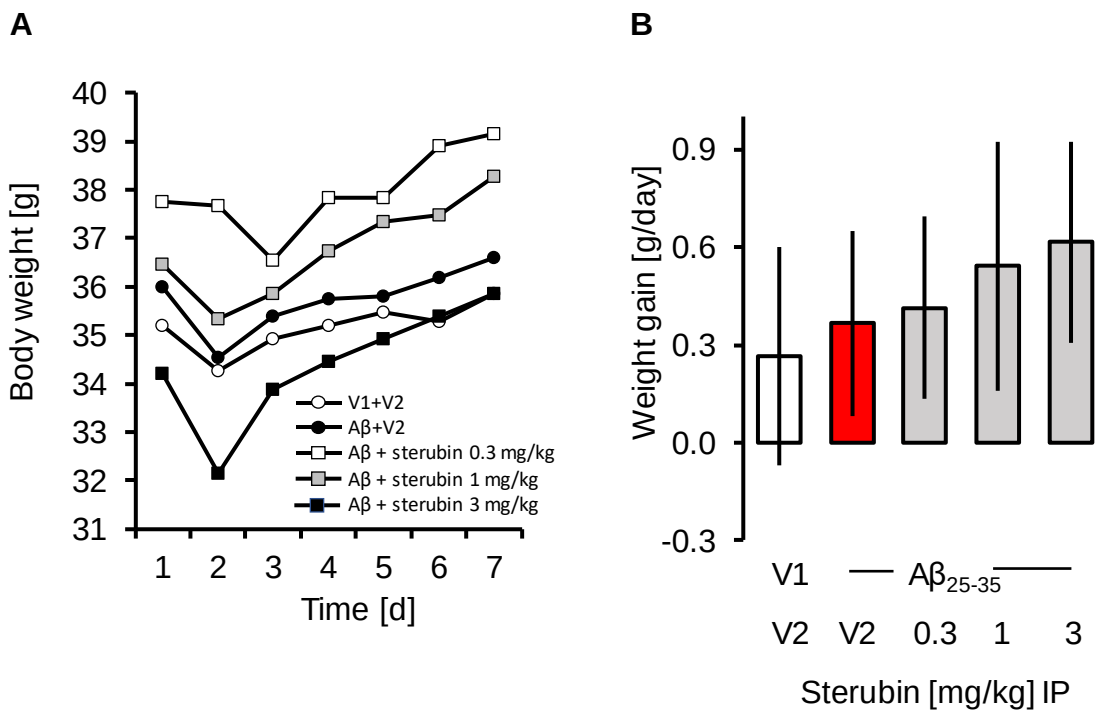

Figure SI-3: (A) Development of body weight. Weight loss was observed on day 2, induced by stress from ICV injection. Animals recovered during the following day. The data show mean; (B) average weight gain from day 2-7. The data show mean ± SEM. ANOVA: $F_{(4,77)} = 2.87$, p = 0.029, n = 12-18. Data were not significantly different from those of the Aβ+V2-treated group, Dunnett's test.

5. Protocol Mouse Treatment

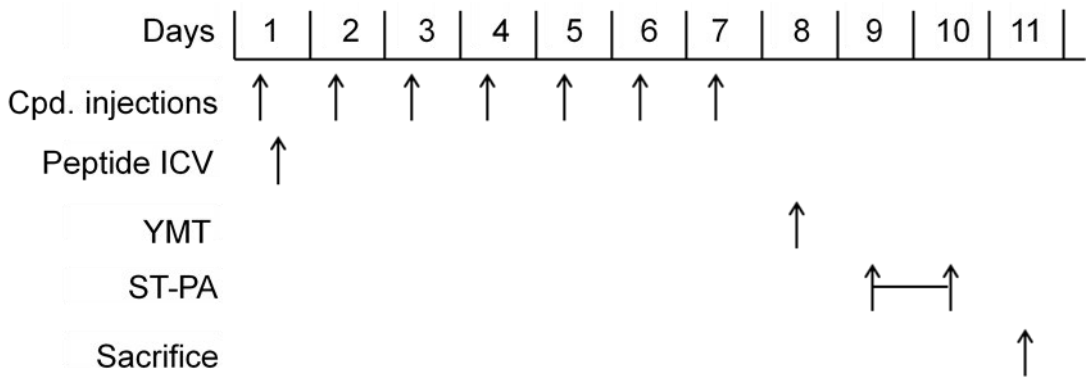

Figure SI-4: Time regime for the in vivo experiments. Abbreviations: Cpd., compound; ICV, intracerebroventricular injection; YMT, Y-maze spontaneous alternation test; ST-PA, step-through passive avoidance test.

6. References

[1] C. A. Hansen, J. W. Frost, *J. Am. Chem. Soc.* **2002**, *124*, 5926-5927.

[2] A. J. Grenning, J. H. Boyce, J. A. Porco, *J. Am. Chem. Soc.* **2014**, *136*, 11799-11804.

[3] B. Roschek Jr, R. C. Fink, M. D. McMichael, D. Li, R. S. Alberte, *Phytochemistry* **2009**, *70*, 1255-1261.

[4] H. Wagner, L. Farkas, *The Flavonoids* , Springer US, Boston, MA, **1975**, 127-213.

[5] a) A. Appelt-Menzel, A. Cubukova, K. Günther, F. Edenhofer, J. Piontek, G. Krause, T. Stüber, H. Walles, W. Neuhaus, M. Metzger, *Stem Cell Rep.* **2017**, *8*, 894-906; b) A. Appelt-Menzel, A. Cubukova, M. Metzger, *Curr. Protoc. Stem Cell Biol.* **2018**, *47*, 62.

Appendix II:

Hofmann, J.; Ginex, T.; Espargaró, A.; Scheiner, M.; Gunesch, S.; Aragó, M.; Stigloher, C.; Sabaté, R.; Luque, J.; Decker, M.
Azobioisosteres of Curcumin with Pronounced Activity against Amyloid Aggregation, Intracellular Oxidative Stress, and Neuroinflammation.
Chem. Eur. J. **2021**, *27* (19), 6015–6027.

Full Paper
doi.org/10.1002/chem.202005263
Chemistry Europe
European Chemical Societies Publishing

Natural Products

Azobioisosteres of Curcumin with Pronounced Activity against Amyloid Aggregation, Intracellular Oxidative Stress, and Neuroinflammation

Julian Hofmann,[a] Tiziana Ginex,[b] Alba Espargaró,[c] Matthias Scheiner,[a] Sandra Gunesch,[a] Marc Aragó,[b] Christian Stigloher,[d] Raimon Sabaté,[c] F. Javier Luque,*[b] and Michael Decker*[a]

Abstract: Many (poly-)phenolic natural products, for example, curcumin and taxifolin, have been studied for their activity against specific hallmarks of neurodegeneration, such as amyloid-β 42 (Aβ42) aggregation and neuroinflammation. Due to their drawbacks, arising from poor pharmacokinetics, rapid metabolism, and even instability in aqueous medium, the biological activity of azobenzene compounds carrying a pharmacophoric catechol group, which have been designed as bioisoteres of curcumin has been examined. Molecular simulations reveal the ability of these compounds to form a hydrophobic cluster with Aβ42, which adopts different folds, affecting the propensity to populate fibril-like conformations. Furthermore, the curcumin bioisosteres exceeded the parent compound in activity against Aβ42 aggregation inhibition, glutamate-induced intracellular oxidative stress in HT22 cells, and neuroinflammation in microglial BV-2 cells. The most active compound prevented apoptosis of HT22 cells at a concentration of 2.5 μM (83% cell survival), whereas curcumin only showed very low protection at 10 μM (21% cell survival).

Introduction

Alzheimer's disease (AD) is the most common form of dementia and causes progressive deterioration in cognitive behavior.[1] One of the main pathogenic hallmarks of AD is the deposition of senile plaques, which consist of aggregates of amyloid-β (Aβ) peptides, generally containing 40 (Aβ40) or 42 (Aβ42) residues.[2] These plaques are linked to neurotoxicity, oxidative stress, and neurodegeneration.[3,4] Neuroinflammation also contributes to neurodegeneration and accelerates the progression of AD.[5] Because the aggregation of Aβ peptides is believed to be the initial event of AD, the identification of potential inhibitors of amyloid aggregation has attracted much interest.[6] Among these compounds, curcumin (Figure 1) is a diarylheptanoid natural product that has shown positive effects on counteracting oxidative stress and inflammation, as well as preventing Aβ aggregation.[7] Structure–activity relationship (SAR) studies have shown that methylation of the free hydroxy groups of curcumin leads to a loss of activity.[8] Nevertheless, the therapeutic potential of curcumin is limited by poor pharmacokinetics, high rate of metabolism, and low stability in an aqueous environment.[9] Additionally, curcumin is considered as a pan-assay interference compound (PAIN),[9] which can possibly interfere with the assay readout or bind nonspecifically to proteins, leading to false positive results.[10]

Other (poly-)phenolic compounds, such as apigenin, quercetin, and taxifolin (Figure 1), have also shown positive effects in counteracting the causative events of neurodegeneration.[7c,11] In particular, flavonoids, a class of polyphenolic natural products, are promising compounds against amyloid aggregation, neuroinflammation, and oxidative stress.[12] Recent studies have shown that chemical hybrids of taxifolin exhibit pronounced neuroprotectivity in vitro and in vivo.[13] Furthermore, through the development of chemical probes for proteomic

[a] J. Hofmann, M. Scheiner, S. Gunesch, Prof. Dr. M. Decker
Pharmaceutical and Medicinal Chemistry, Institute of Pharmacy and Food Chemistry, University of Würzburg, Am Hubland 97074 Würzburg (Germany)
E-mail: michael.decker@uni-wuerzburg.de

[b] Dr. T. Ginex, M. Aragó, Prof. Dr. F. J. Luque
Department of Nutrition Food Science and Gastronomy
Faculty of Pharmacy, Institute of Theoretical and Computational Chemistry and Institute of Biomedicine, Campus Torribera
University of Barcelona, Santa Coloma de Gramenet 08921 (Spain)
E-mail: fjluque@ub.edu

[c] Dr. A. Espargaró, Prof. Dr. R. Sabaté
Pharmacy and Pharmaceutical Technology and Physical-Chemistry
School of Pharmacy Institute of Nanoscience and Nanotechnology (IN2UB), University of Barcelona, 08028, Barcelona (Spain)

[d] Prof. Dr. C. Stigloher
Imaging Core Facility, Biocenter/Theodor-Boveri-Institute
University of Würzburg, Am Hubland, 97074 Würzburg (Germany)

Supporting information and the ORCID identification number(s) for the author(s) of this article can be found under: https://doi.org/10.1002/chem.202005263.

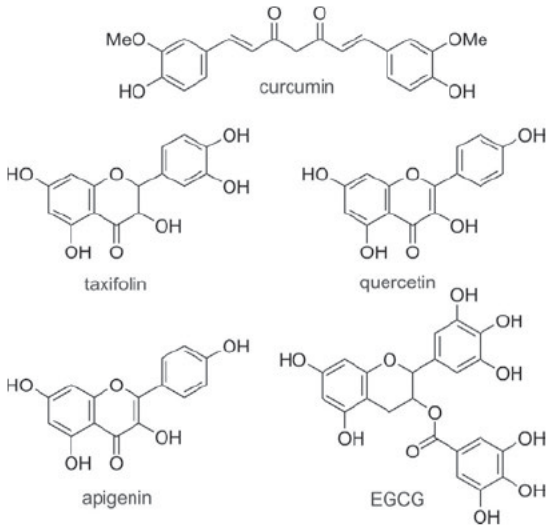

Figure 1. Chemical structures of curcumin, taxifolin, quercetin, apigenin, and epigallocatechin gallate (EGCG).

studies, it was shown that these compounds seemed to specifically address mitochondrial targets.[14] Several studies revealed the importance of the catechol unit of flavonoids for their activity against age-related disease processes, especially in the context of AD.[15] However, flavonoids suffer from similar drawbacks to those of curcumin, such as poor pharmacokinetics and low metabolic stability.[16]

A clear understanding of the precise mechanism of action of Aβ42 aggregation inhibitors is challenging due to the complexity of the conformational space of Aβ42 monomers, the occurrence of distinct oligomeric species in early aggregates, and the timescale of different events implicated in the formation of Aβ42 fibrils. Furthermore, whether a given compound can exert inhibitory activity acting at different stages of Aβ42 aggregation is also unclear.[17] The antiaggregating activity of small organic compounds has been related to specific chemical features, such as the hydroxylation profile, the presence of carboxyl moieties that may form salts bridges with Aβ42, and the molecular planarity conferred by aromatic rings.[18] Thus, it has been proposed that curcumin could intercalate in Aβ42 assemblies and destabilize preformed fibrils;[19] this effect is improved upon through 1) expansion of the aromatic rings; 2) integration of large conjugated structures; 3) the presence of aromatic rings connected by nitrogen-containing bridge; and 4) hydroxyl groups on aromatic, conjugated rings.[19] Apart from that, (poly-)phenolic compounds bearing a catechol unit, such as taxifolin, were observed to undergo autoxidation, and thus, produce a site-specific covalent inhibition of Aβ42 aggregation by acting on K16 and/or K28 residues of preformed amyloid fibrils, according to an aza-Michael addition mechanism.[20] EGCG (Figure 1), another catechol type (poly-)phenolic compound, naturally occurring in green tea, was observed to produce covalent adducts through a Schiff base mechanism.[21] Interestingly, the reduced form of EGCG was proposed to act at early aggregation stages by redirecting toxic Aβ oligomers towards off-pathway nontoxic oligomers.[22]

A common strategy to improve the pharmacological profile of bioactive molecules is bioisosterism. This applies changes in the molecular structure of a lead compound to improve their physicochemical properties, while preserving the relevant pharmacophoric features of the lead structure.[23] If combined with photopharmacology, which represents an emerging strategy that enables the photochemical control of biologically active molecules and biosensors,[24] bioisoteric compounds might offer a fine-tuning of the antiaggregation activity. In particular, our strategy in this study has been to characterize the pharmacological profile of azobenzene bioisosteres of curcumin suitably modified to incorporate the pharmacophoric catechol moiety of flavonoids. These compounds were conceived by hybridizing relevant structural elements present in curcumin and taxifolin by following the rationale summarized in Figure 2. This led to a new class of compounds that successfully incorporated the previously cited Aβ-related pharmacological properties (bioactive catechol ring, aromaticity, and planarity).

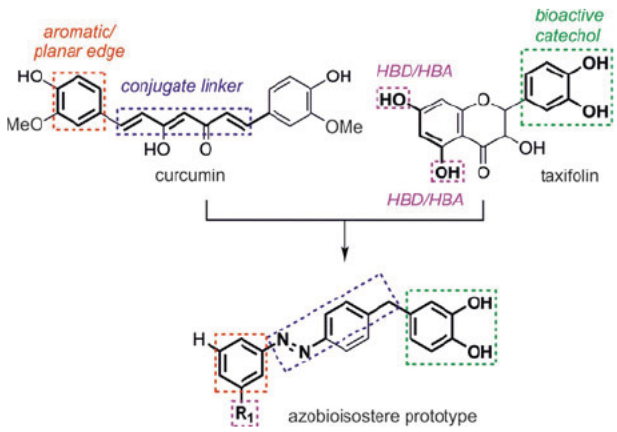

Figure 2. Rationalization for the azobioisostere prototype from the Aβ42 inhibitors curcumin and taxifolin. HBD = hydrogen-bond donor; HBA = hydrogen-bond acceptor.

Herein, we report the design and synthesis of azobenzene-containing bioisosteric analogues of curcumin and investigate their antiaggregation ability against Aβ42 in vitro and in a bacterial model.[25] Furthermore, we evaluate their neuroprotective properties against intracellular oxidative stress in murine hippocampal HT22 cells and their anti-neuroinflammatory potential in microglial BV-2 cells.

Results and Discussion

Synthesis of the target compounds

The synthesis of the target compounds started with the Friedel–Crafts acylation of 4-nitrobenzoyl chloride (**1**) with dimethoxybenzene (**2**) to yield the corresponding acetophenone **3**. Ether cleavage of the methoxy groups was achieved in a mixture of concentrated hydrobromic acid and acetic acid, followed by hydrogenation of the keto group with H_2 on Pd/C, to

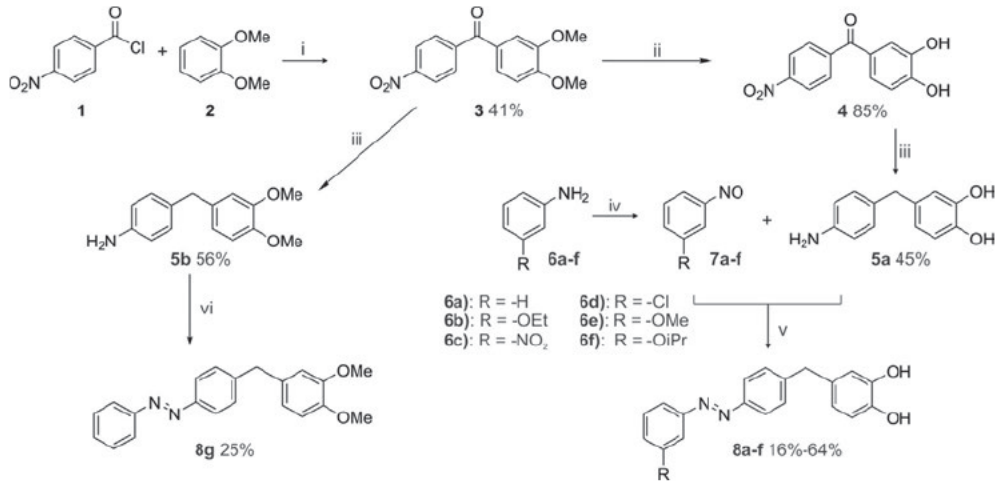

Scheme 1. Synthesis of target compounds **8a–f** and comparison compound **8g**. Reagents and conditions: i) $FeCl_3$, 60 °C, 16 h; ii) 48% HBr, AcOH, reflux, 3.5 h; iii) H_2, Pd/C, MeOH, 10 bar, RT, 16 h; iv) oxone, CH_2Cl_2/H_2O, RT, 3.5 h; v) AcOH, RT, 16 h, vi) nitrosobenzene, AcOH, RT, 16 h.

obtain compound **5a** as the first building block. Partial oxidation of anilines with oxone yielded the respective nitroso derivatives, which were combined with **5a** in a Baeyer–Mills reaction to form the desired target compounds **8a–f** (Scheme 1). Compound **8g**, with both catechol hydroxyl groups methylated, was also synthesized to explore the role of the catechol moiety by comparison (see below) with the activity of target compounds **8a–f**. It was synthesized in analogy to compounds **8a–f**, but without cleavage of the methoxy groups of compound **3**.

In vitro inhibition of Aβ42 and tau aggregation

Because the aggregation of amyloidogenic proteins, such as Aβ42, and deposits of hyperphosphorylated *tau* protein in neurofibrillary tangles are associated with neurodegenerative diseases, such as AD,[26,27] compounds with antiaggregation properties may be a viable option for modifying the disease. To evaluate the antiaggregation activity of the target compounds, a rapid in vitro screening method in bacterial cells was applied.[7c,25] This method is based on *Escherichia coli* overexpressing the respective protein (Aβ42, human *tau*), which forms inclusion bodies (IBs). IBs are consequently stained by thioflavin-S (Th-S) to assess the amount of aggregated protein.

The evaluation of the antiamyloid aggregation activity of the novel compounds displayed good potencies, with an aggregation inhibition between 65 and 80% tested at a concentration of 10 μM (Table 1). In general, similar antiaggregation activity was found against Aβ42 and *tau*. Compounds **8a** and **8f** display an average (Aβ42 and *tau*) inhibition of 75.8 and 75.7%, respectively, against these proteins. Compound **8c**, and to a lesser extent **8b**, showed, however, a higher inhibitory potency against aggregation of Aβ42. Interestingly, compound **8g**, which has a protected catechol moiety, displays practically no activity (< 10%) in the bacterial system.

Because the new compounds were conceived as bioisosteric mimics of curcumin and taxifolin (Figure 1), we also investigated the antiamyloid effect of these natural products against Aβ42 and *tau*. As shown in Table 1, a similar antiaggregation activity was observed for Aβ42 and *tau*, whereas taxifolin displayed practically no activity (< 5%) and curcumin was found to have a moderate inhibitory effect (38%). Remarkably, the activity of the target compounds greatly exceeds the potency of curcumin and taxifolin, revealing the suitability of the bioisosteric design.

Table 1. In vitro antiamyloid activity of taxifolin, curcumin, and **8a–g**. *E. coli* overexpresses the respective protein, which forms IBs and can be quantified by Th-S staining. Compounds were tested at 10 μM.

Compound	Aβ42 inhibition [%]	SEM[a]	*tau* inhibition [%]	SEM[a]
control	0.0	2.0	0.0	2.1
taxifolin	4.9	4.0	1.1	4.4
curcumin	37.8	2.7	35.2	3.2
8a	80.4	2.1	71.0	2.1
8b	78.2	3.4	65.1	2.4
8c	81.3	1.6	58.0	3.9
8d	63.1	4.2	66.6	2.9
8e	67.5	2.9	73.6	3.6
8f	73.3	4.3	78.3	4.1
8g	9.6	3.9	5.7	3.8

[a] SEM = standard error of the mean.

In vitro inhibition of Aβ42 detected by TEM

The detection of amyloid fibrils by fluorescent dyes can be biased by compounds with absorptive and fluorescent properties such as the molecules investigated in this study.[28] Hence, the inhibitory effect of these compounds was further examined by resorting to TEM, which provided a dye-independent approach to assess the antiaggregating effect of the compounds. The results clearly confirmed the inhibitory effect on fibril formation of Aβ42 at 10 μM for curcumin and compounds **8a–f** (cf. Figure 3 and Figure S5 in the Supporting Information).

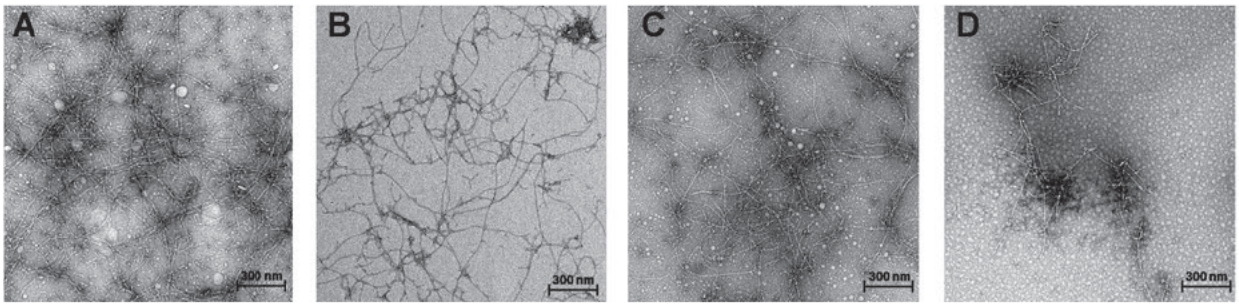

Figure 3. TEM analysis of the inhibitory effect on Aβ42. The Aβ monomer (100 μM) was incubated at 37 °C in phosphate-buffered saline (PBS) for 24 h with or without 10 μM of the respective compound. A) Control; B) curcumin; C) **8 g**; D) **8 f**. Scale bar: 300 nm.

Interaction of the target compounds with Aβ42

In light of these results, molecular simulations that combine docking, classical molecular dynamics (MD) and replica-exchange molecular dynamics (REMD) were carried out to investigate the potential mechanism of action responsible for Aβ42 aggregation inhibition. In particular, our aim was to examine the ability of the catechol-containing target compounds to interfere with both early (oligomerization) and late (fibrillation) stages of Aβ42 aggregation.

Formation of covalent adducts with Aβ42 fibrils

To examine the ability of the target compounds to covalently interfere with Aβ42 aggregation, compounds **8 a–f** were docked in their oxidized (*o*-quinone) form into the 10 conformational states for the solid-state NMR spectroscopy model of Aβ42 (PDB ID: 5KK3)[29] by using Glide.[30] The three top-scoring docking solutions for compound **8 c** were further investigated by means of 100 ns MD simulations with Amber18.[31] The choice of **8 c** was motivated by the presence of the nitro group, which would help to stabilize the binding mode through electrostatic interactions with the protonated amino group of K16 residues along the binding groove. This would enhance the residence time around the reactive site and facilitate the proper arrangement for covalent adduct formation, as described for the aza-Michael addition observed for taxifolin.[32] However, none of the three simulated poses for compound **8 c** were able to maintain a proper orientation around the reactive site delimited by K16 and D22 in the binding groove (cf. distances *d*1 and *d*2 in Figure S1 in the Supporting Information). These results led us to exclude the possibility of a covalent Aβ42 inhibition mechanism for this class of compounds.

Interaction of the target compounds with Aβ42 monomer

As an alternative mechanism, we explored the ability of compound **8 f**, one of the most potent Aβ42 inhibitors found in this study, on the early stage of Aβ42 aggregation by means of REMD simulations. Following previous studies,[22] the Aβ42 monomer ($A\beta42_{mon}$), which crystallized in a nonpolar environment (PDB ID: 1IYT),[33] was selected to model the interaction with compound **8 f**. A total of 30 μs of MD trajectory was collected and the first five replicas, corresponding to the $A\beta42_{mon}$–**8 f** system at 315, 316.7, 318.4, 320.1, and 321.8 K, were analyzed (see the Experimental Section for a more complete discussion of the computational protocol).

Secondary-structure analysis for the first five T-replicas of $A\beta42_{mon}$–**8 f** is reported in Figure 4. The results highlight the large conformational flexibility of $A\beta42_{mon}$, which can adopt a variety of conformations that mediate the interaction with compound **8 f**. In general, turn/coil are the most populated states, followed by β-sheet and α-helix arrangements. A high α-helix content, especially for residues 15–18 and 24–36 of $A\beta42_{mon}$, is observed at the beginning of all simulated replicas, although the α-helical content is lost during the first 50–100 ns of REMD simulation. A transient α-helix to β-sheet conversion of the central (18–24) and C-terminal residues is observed for the first three replicas. Interestingly, a different profile is observed for the fourth replica, in which a stable conformer characterized by an α-helical motif for residues 14–24 and β-sheet fold for residues at the N and C termini is found. This conformation seems to be the most populated one, as noted by the 2D root-mean-square (RMS) analysis (see Figure S2 D in the Supporting Information). Finally, a higher degree of conformational flexibility is observed for the last replica, in which the lack of well-defined secondary structures is generally observed.

Along the trajectories sampled in REMD simulations, compound **8 f** exhibits a tendency to interact with the middle and C-terminal regions of the $A\beta42_{mon}$ sequence (cf. Figure 3), thus affecting its conformational assembly. Interestingly, our data are in agreement with those observed by Zhang et al.,[22a] who performed REMD simulations to study the conformational behavior of the Aβ42–EGCG complex. The present results, however, emphasize the role of hydrophobic interactions formed between **8 f** and the apolar residues of $A\beta42_{mon}$. Generally, the main interactions are formed with residues 12–20 and 32–38 of $A\beta42_{mon}$ ($A\beta42_{mon}$ Cα–**8 f** distances <1.0 nm), although there are differences between the different replicas (see Figure S3 in the Supporting Information).

Collectively, these data are in line with a putative Aβ42 anti-aggregation mechanism, in which the presence of compound **8 f** redirects the conformational landscape of Aβ42 oligomers toward less structured/off-pathway oligomers. No evidence of stable and well-formed β-sheet configuration emerged from our simulations. In fact, the N terminus of $A\beta42_{mon}$ is mainly

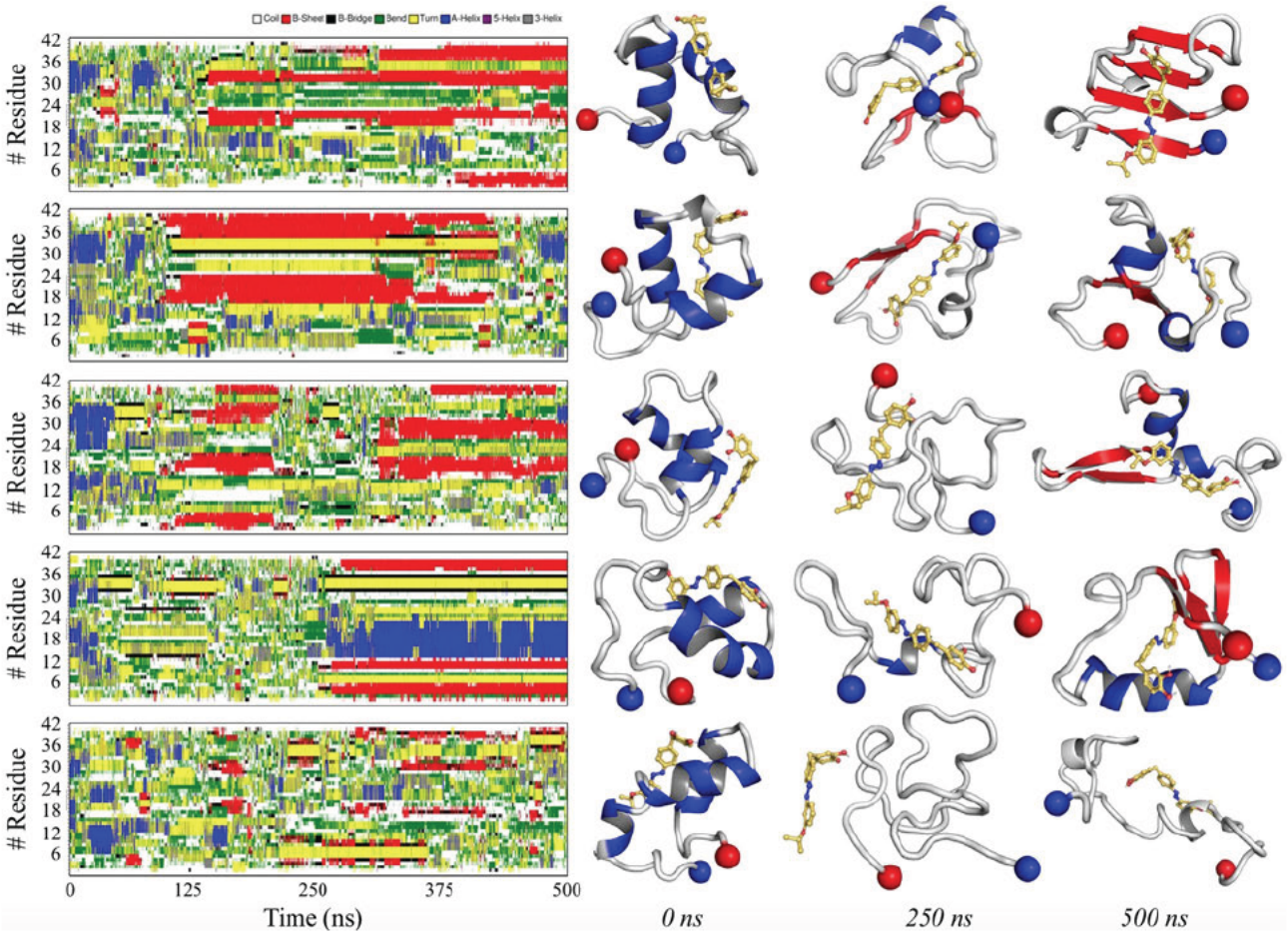

Figure 4. Left: Secondary-structure analysis for the first five T-replicas of $A\beta42_{mon}$–**8f**, according to the DSSP algorithm. Right: Representative geometries for $A\beta42_{mon}$–**8f** at 0, 250, and 500 ns of simulation. The N- and C-terminal edges of $A\beta42_{mon}$ are reported as blue and red spheres, respectively.

unstructured, a transient α-helix propensity is often observed for residues 15–24, and a partial β-sheet-turn-β-sheet propensity is observed for the central and C-terminal region. Compound **8f** is suggested to have a significant impact on this assembly because this compound would stably form contacts with the C-terminal region of the $A\beta42_{mon}$, intercalating the β-sheet-turn-β-sheet region.

Neurotoxicity and neuroprotection in HT22 cells

The effect of the target compounds on neuroprotection and neurotoxicity was examined by using the sensitivity of the murine hippocampal neuronal cell line HT22 to glutamate. High extracellular concentrations of glutamate lead to oxidative glutamate toxicity, so-called oxytosis, a form of programmed cell death.[34] The inhibition of the cystine/glutamate antiporter causes glutathione (GSH) depletion, followed by accumulation of reactive oxygen species (ROS), calcium influx, and finally cell death by oxidative stress.[35] Similar features are observed in the brain during aging and are accelerated in AD.[36] Compounds **8a–f** showed very strong protection against intracellular oxidative stress at concentrations between 2.5 and 7.5 μM (Figure 5). The target compounds even exceeded the flavonol quercetin, which served as a positive control and prevented cell death at 25 μM. Curcumin and **8g** did not show distinct neuroprotection. At only 10 μM, weak protection with 21% cell survival was observed. These data show the importance of the free catechol and are in good agreement with results reported by Maher et al., who showed that chemical alternation of the catechol structure of flavonoids of the plant *Eriodictyon californicum* (also known as *yerba santa*) led to a drastic reduction in activity in different phenotypic screening assays, including the oxytosis assay.[15a]

DPPH radical scavenging assay

To evaluate (and exclude) unspecific protection against oxidative stress by radical scavenging, the direct antioxidant capacity was tested in a cell-free system. The widely applied DPPH radical scavenging assay uses the stable radical 2,2-diphenyl-1-picrylhydrazyl, which is decolorized upon reduction.[37] The known antioxidant ascorbic acid (vitamin C) served as a positive control with an IC_{50} value of 8.4 μM. The parent compound curcumin had an IC_{50} value of 10.5 μM. The target compounds were active over a similar range, from 5 to 10 μM (Table 2). Compound **8g** did not show any activity because there was

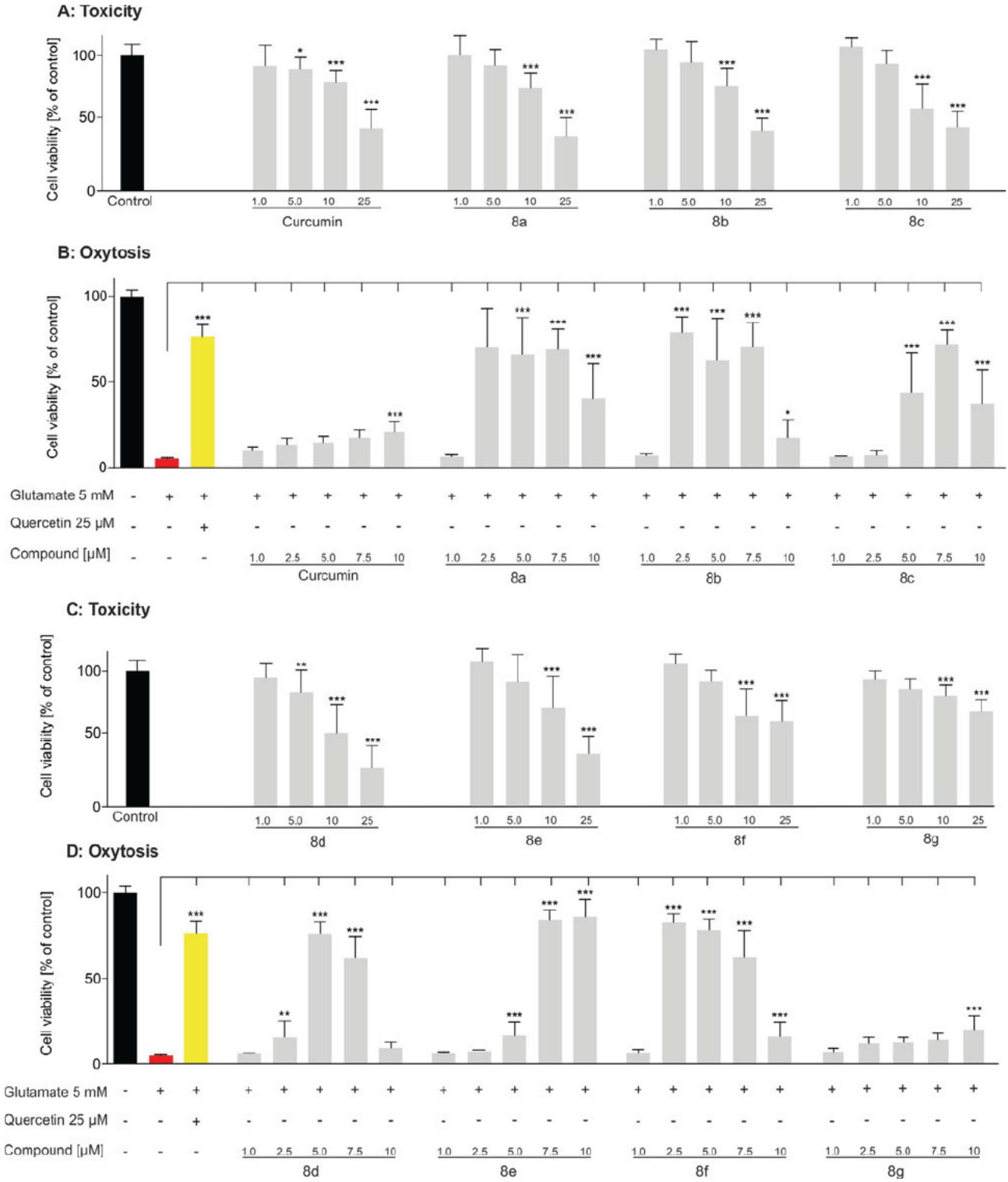

Figure 5. Neuroprotection and neurotoxicity were determined in HT22 cells. 5 mM glutamate (red) induced cell death, 25 µM quercetin (yellow) served as a positive control for cell survival: A) neurotoxicity of curcumin and **8a–c**; B) neuroprotection of curcumin and **8a–c**; C) neurotoxicity of **8d–g**; D) neuroprotection of **8d–g**. Data are presented as means ± SEM of three independent experiments and results refer to untreated control cells (black). Statistical analysis was performed by using one-way analysis of variance (ANOVA) followed by Dunnett's multiple comparison post-test by using GraphPad Prism 5, with reference to cells treated with 5 mM glutamate. Level of significance: ***$p < 0.001$, **$p < 0.01$, *$p < 0.05$.

no functionality to react with the free DPPH radical. Compound **8a** shows strong cellular protection against intracellular oxidative stress, but a weak radical scavenging activity compared with the other target compounds. This suggests that the neuroprotection in HT22 cells is based on a target-specific mode of action. The pronounced differences in the activity of

Table 2. Free radical scavenging capacity determined by the DPPH assay.

Compound	EC_{50} [μM]	SEM
ascorbic acid	8.4	0.5
curcumin	10.5	0.2
8a	9.1	0.3
8b	7.7	0.4
8c	5.4	0.5
8d	5.6	0.1
8e	9.6	0.4
8f	5.4	0.1
8g	not active	

curcumin in the oxytosis assay (10 μM, 21% cell survival) in comparison with the EC_{50} value of 10.5 μM in the DPPH assay strongly indicate a specific intracellular protective mechanism, rather than an unspecific protection due to radical scavenging.

The lack of activity of dimethoxy compound **8g** in the DPPH radical scavenging assay shows the necessity of a catechol (or monohydroxyl) unit for reaction with free radicals.

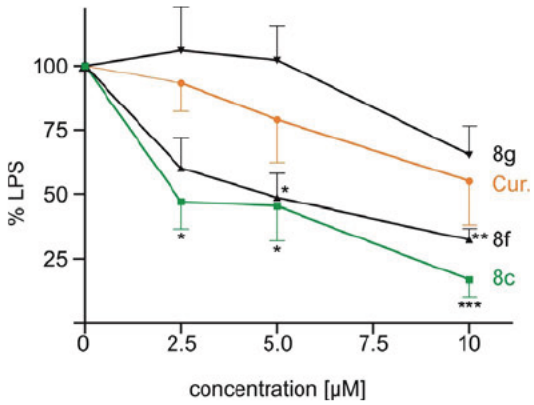

Figure 6. Effect of compounds **8c**, **8f**, **8g**, and curcumin on the production of NO as an inflammation marker. BV-2 cells were treated with 50 ng mL^{-1} LPS alone or with the respective compound. NO was determined by the Griess assay in the supernatant. Data are presented as means ± SEM of three independent experiments and results refer to LPS-treated cells. Statistical analysis was performed by using one-way ANOVA followed by Dunnett's multiple comparison post-test by using GraphPad Prism 5. Level of significance: $***p<0.001$, $**p<0.01$, $*p<0.05$.

Anti-inflammatory effect on BV-2 cells

Apart from amyloid plaques, neuroinflammation represents a key hallmark of AD.[38] Microglia cells act as a major immune defense in the central nervous system.[39] Activation by, for example, bacterial endotoxins to their proinflammatory phenotype results in the production of NO and several other inflammation-promoting factors, such as cytokines, free radicals, and excitatory neurotransmitters.[38] Although active microglia cells are important for brain repair processes and response to immune challenge, chronic activation, such as that in AD, leads to neurodegeneration caused by inflammation and oxidative stress.[39b,40] Therefore, inhibition of the proinflammatory microglia state is important in the context of AD.[41]

Mouse microglial BV-2 cells were used to evaluate a possible anti-inflammatory effect. Cells were treated with bacterial lipopolysaccharide (LPS) to induce inflammation and the production of NO was quantified in the Griess assay. All compounds reduced the NO production dose, with the strongest anti-inflammatory effect at 10 μM (Figure 6). Similar to the results for neuroprotectivity on HT22 cells, the target compounds exceeded the activity of curcumin. Compound **8c** was the most active compound, with a decrease of inflammation down to 17% relative to the LPS control. The other compounds tested reduced NO production in a similar manner to 31–42% (compound **8f** is shown as a representative example; for more detailed information, see the Supporting Information). It is not surprising that compound **8f** was not the most active compound, as in the oxytosis assay or Aβ fibrilization inhibition, since the respective modes of action may well differ from each other. Nevertheless, protection of the catechol with methoxy groups (compound **8g**) led to a dramatic loss of activity, similar to in the other assays applied in this study. No effect on the production of NO was observed at 2.5 and 5 μM. At 10 μM, compound **8g** reduced the amount of NO to 65% in comparison with the control.

Conclusion

In this study, a series of azobioisosteres of curcumin, suitably modified to incorporate the pharmacophoric catechol moiety of flavonoids, have been synthesized and their pharmacological profile against amyloid aggregation, intracellular oxidative stress, and neuroinflammation has been characterized. The synthetic bioisosteric compounds have shown higher aggregation inhibition of Aβ42 relative to the parent compound, curcumin. This could be observed in a bacterial in vitro assay with Th-S staining, as well as dye-independently in TEM experiments. Additionally, the compounds showed strong activity in AD-related cell assays. In particular, there was higher protection against glutamate-induced intracellular oxidative stress in murine hippocampal HT22 cells than that of curcumin. Moreover, the compounds revealed pronounced anti-inflammatory properties in microglial BV-2 cells. The observed effects seemed to underlie a specific mechanism, as the activity of the compounds in the DPPH radical scavenging assay did not show substantial differences.

Until now, drugs targeting Aβ have failed in clinical trials. The reasons for this failure include fluorescence interference during the commonly used thioflavin T assay, poor reproducibility of Aβ experiments in general, and the overall complexity of amyloid aggregation processes in AD with still unknown aspects of toxicity of amyloid species.[42] Therefore, the experimental design of this work includes a dye-based readout for Aβ aggregation that applies to a highly replicable assay, and a dye-independent setup, that is, electron microscopy. In addition to their antiaggregation properties, the compounds presented herein also act against oxidative stress and neuroinflammation.

It must be taken into account that azobenzenes are commonly suspected to cause long-term toxicity due to instability towards bacterial azoreductases, which cleave the azobenzene in anilines, but there are several examples of food colorants

and drugs, which support the safe use of molecules containing azobenzene moieties.[43]

Finally, because azobenzene compounds can undergo *cis–trans* photoisomerization upon irradiation with light of an appropriate wavelength, this paves the way to the photoinduced control of the antiaggregating activity of azobenzene bioisosteres. Currently, the use of the target compounds in a photopharmacological approach is under investigation.

Experimental Section

Computational methods

Docking and MD simulations of complexes with Aβ42 fibrils: The solid-state NMR structure of the Aβ42 fibril (PDB ID 5KK3),[29] corresponding to a double S-shaped Aβ42 fibrillar assembly, was used to model the interaction of compounds **8 a–f** with Aβ42 fibrils, following the same protocol as that adopted in previous studies.[32] Briefly, 20 docking runs, one for each of the two monomers of the 10 NMR models deposited for 5KK3, were performed with Glide.[30] Protonation states for the protein were set at pH 7.4. According to previous pK_a studies,[32] one K16 located in the middle of the fibril assembly was simulated in its neutral form. For each of the six tested compounds, the oxidized *o*-quinone form was generated and used during docking. A total of 2000 poses were generated, and thus, analyzed to identify suitable candidates for further MD studies.

Among the best-ranked poses obtained for compound **8 c**, three docked arrangements were selected and investigated by means of MD simulations. The choice of this compound as a suitable candidate for MD simulation was dictated by the presence of a nitro group, which would be able to stabilize the protein–ligand complex by interacting with K16 residues along the Aβ fibrils. MD simulations were run with Amber18.[31] The Amber ff14SB-ILDN force field[44] was used for the protein and modified parameters (see above) from the general Amber force field (GAFF)[45] were used to parameterize the ligand. Partial charges were derived at the B3LYP/6-31G(d) level, after preliminary geometry optimization, by using the restrained electrostatic potential[46] fitting procedure. Torsional parameters for the C-C-N-N dihedral angle, which defined the conformation of the benzene ring relative to the diazo group, were refined by using 4-({4-[(1*E*)-2-(3-hydroxyphenyl)diazen-1-yl]phenyl}-methyl)cyclohexa-3,5-diene-1,2-dione (see Table S1 in the Supporting Information) as a reference model in quantum mechanical (QM) calculations. To this end, the MM torsional potential energy of C-C-N-N torsion were fitted to the QM-derived potential energy profile obtained from a relaxed scan performed at the M062X/6-31G(d) level in the gas phase with Gaussian 09.[47] The python package *pyevolve*[48] was used to fit the two profiles (see the Supporting Information)

The three **8 c**–Aβ42 fibrils were solvated with TIP3P[49] water molecules by using a truncated octahedron box with a layer of 20 Å and neutralized by adding Na^+ ions.[50] The systems were energy minimized in a three-stage protocol, which involved hydrogen atoms, then water molecules, and finally the whole system, with a maximum number of 20000 minimization cycles for the last stage. Then, the systems were gradually heated from 0 to 300 K in six steps; the first was performed at a constant volume and the rest at constant pressure. To avoid artifactual alterations in the ligand pose due to thermal equilibration, harmonic restraints with a force constant of 10 kcal mol^{-1} Å^{-2} were applied during equilibration to selected ligand–protein contacts. A Cartesian restraint of 2 kcal mol^{-1} Å^{-2} was also applied to the backbone atoms of the first and last Aβ42 monomers to preserve the structural integrity of the fibrils. These restraints were gradually eliminated during the first 50 ns of the MD simulation. The SHAKE algorithm[51] was applied to constrain bonds involving hydrogen atoms. Periodic boundary conditions were used during the MD simulations and a cutoff of 10 Å for the nonbonded interactions and the particle mesh Ewald (PME) method[52] was used for the treatment of electrostatic interactions beyond the cutoff. Langevin dynamics with a collision frequency of 1.0 ps^{-1} were applied for temperature regulation during heating. Finally, 100 ns of the MD production in the NVT ensemble (300 K) were run by using the weak-coupling algorithm[53] (with a time constant of 10.0 ps) for each of the three complexes. The analysis was performed for the set of snapshots saved every 2 fs along the trajectories.

REMD simulation of the interaction between 8 f and the Aβ42 monomer: The solution NMR spectroscopy structure of the Aβ42 peptide (PDB ID: 1IYT)[33] was used to model the interaction between Aβ42 monomer and compound **8 f**, which was simulated in its reduced (catechol) form. The ligand parameters were adopted from the GAFF force field, although both atomic charges (RESP charges derived from B3LYP/6-31G(d) calculations) and torsional (C-C-N-N) parameters were adjusted, and the ff14SB-ILDN force field was used for the protein. Standard protonation states at pH 7.4 were adopted for ionizable residues. The system was embedded in a truncated octahedron box of TIP3P water molecules and counterions (Na^+, Cl^-) were added at a salt concentration of 0.15 M. The final system (18,386 atoms) contained an Aβ42 monomer, one molecule of **8 f** randomly placed around the monomer, 5891 water molecules, 20 Na^+ ions, and 17 Cl^- ions.

REMD simulations were carried out on 60 T-replicas ranging from 315 to 430 K with Gromacs2018.[54] The systems were energy minimized by applying 50000 steps of the steepest descent algorithm followed by 5000 steps of conjugate gradient algorithm. 1 ns of MD simulation in the NVT ensemble by using the velocity-rescaling thermostat (0.1 ps time coupling constant)[55] was run to heat the system to the final temperatures for production. Positional restraints with a force constant of 1000 kJ mol^{-1} mn^{-2} were applied to the Aβ42 backbone atoms to avoid unnatural distortions during heating. Finally, 5 ns of MD simulation in the NPT ensemble by using the Parrinello–Rahman barostat[56] with a 0.5 ps time constant for coupling were run to properly equilibrate density.

500 ns of REMD simulation in the NPT ensemble by using the Parrinello–Rahman barostat[56] under periodic boundary conditions were run for each T-replica, leading to a total of 30 μs of sampled MD trajectory. The LINCS method[57] was applied to constraint bonds involving hydrogen atoms. A cutoff of 1.2 nm was used to treat short-range nonbonded interactions, whereas the PME method was applied to manage long-range electrostatic interactions.[52] A time step of 2 fs was applied to collect trajectories during the simulation. Exchanges between T-replicas were attempted every 100 MD steps, leading to an acceptance ratio of about 45 %.

Demuxed trajectories for the first five replicas were considered for final analysis. Here, time-dependent evolution of the secondary structure of Aβ42 was calculated by using the DSSP algorithm.[58] Finally, *mdmap* and *rms* commands implemented in Gromacs2018 were applied to generate the contact map and 2D-RMS plots, respectively.

General

All reagents were used without further purification and bought from common commercial suppliers. TLC was performed on silica gel 60 (alumina foils with fluorescent indicator 254 nm). UV light (254 and 366 nm) was used for detection. For column chromatography, silica gel 60 (particle size 0.040–0.063 mm) was used. NMR spectra were recorded with a Bruker AV-400 spectrometer (Bruker, Karlsruhe, Germany) in $CDCl_3$ or [D_6]DMSO, and chemical shifts are expressed in ppm relative to $CDCl_3$ ($\delta = 7.26$ ppm for ^{1}H and $\delta = 77.16$ ppm for ^{13}C) or [D_6]DMSO ($\delta = 2.50$ ppm for ^{1}H and $\delta = 39.52$ ppm for ^{13}C). Spectral data reported refer to the thermodynamically more stable *trans* isomer. The purity of the synthesized products was determined by means of HPLC (Shimadzu Products), containing a DGU-20A3R degassing unit, a LC20AB liquid chromatograph, and an SPD-20A UV/Vis detector. UV detection was measured at 254 nm. Mass spectra were obtained by using a LCMS 2020 instrument (Shimadzu Products). As a stationary phase, a Synergi 4U fusion-RP (150 mm × 4.6 mm) column was used and, as a mobile phase, a gradient of methanol/water with 0.1% formic acid was used . Parameters: A = water, B = methanol, $V(B)/[V(A)+V(B)]$ = from 5 to 90% over 10 min, $V(B)/[V(A)+V(B)] = 90\%$ for 5 min, $V(B)/[V(A)+V(B)]$ = from 90 to 5% over 3 min. The method was performed at a flow rate of 1.0 mL min^{-1}. Compounds were only used for biological evaluation if the purity was $\geq 95\%$. Melting points were determined by using an OptiMelt automated melting point system (Scientific Instruments GmbH, Gilching, Germany).

(3,4-Dimethoxyphenyl)(4-nitrophenyl)methanone (3)

4-Nitrobenzoyl chloride (500 mg, 2.69 mmol) was added to a suspension of $FeCl_3$ (436 mg, 2.69 mmol) in veratrole (3 mL) and the reaction mixture was heated to 60 °C for 16 h. Water and methanol were added until the precipitant was dissolved, and the suspension was extracted with dichloromethane. The combined organic layers were washed with water and dried over Na_2SO_4. The solvent was removed under reduced pressure and the crude product was filtered through silica gel by using dichloromethane as the eluent. The solvent was removed under reduced pressure and the residue was kept in the fridge to crystallize the product. The precipitant was washed with ethanol and the product was obtained as a yellow solid (316 mg, 41%). M.p. 148 °C; ^{1}H NMR (400 MHz, $CDCl_3$): $\delta = 8.32$ (d, $^3J = 8.7$ Hz, 2H; Ph), 7.88 (d, $^3J = 8.7$ Hz, 2H; Ph), 7.50 (d, $^4J = 2.0$ Hz, 1H; Ph), 7.30 (dd, $^3J = 8.4$ Hz, $^4J = 2.0$ Hz, 1H), 6.90 (d, $^3J = 8.4$ Hz, 1H; Ph), 3.97 (s, 3H; OCH_3), 3.95 ppm (s, 3H; OCH_3); ^{13}C NMR (100 MHz, $CDCl_3$): $\delta = 193.6$ (C_q), 154.0 (+, Ph-*C*), 149.6 (+, Ph-*C*), 149.6 (+, Ph-*C*), 143.9 (+, Ph-*C*), 130.4 (+, 2×Ph-*C*), 129.1 (+, Ph-*C*), 125.9 (+, Ph-*C*), 123.5 (+, 2×Ph-*C*), 111.8 (+, Ph-*C*), 110.0 (+, Ph-*C*), 56.3 (+, -OCH_3), 56.2 ppm (+, -OCH_3); ESI-MS: *m/z*: 288.28 $[M+H]^+$.

(3,4-Dihydroxyphenyl)(4-nitrophenyl)methanone (4)

Compound **3** (1.00 g, 3.48 mmol) was suspended in acetic acid (10 mL), 48% HBr (20.0 mL) was added, and the reaction mixture was heated to reflux for 3.5 h. After cooling, the precipitant was filtered, washed with water, and dried under vacuum. The product was obtained as a yellowish green solid (733 mg, 85%). M.p. 165 °C; ^{1}H NMR (400 MHz, [D_6]DMSO): $\delta = 10.14$ (s, 1H; OH), 9.56 (s, 1H; OH), 8.34 (d, $^3J = 8.7$ Hz, 2H), 7.86 (d, $^3J = 8.8$ Hz, 2H; Ph), 7.26 (d, $^4J = 2.2$ Hz, 1H; Ph), 7.11 (dd, $^3J = 8.3$, $^4J = 2.1$ Hz, 1H; Ph), 6.87 ppm (d, $^3J = 8.3$ Hz, 1H; Ph); ^{13}C NMR (100 MHz, [D_6]DMSO): 192.9 (C_q), 151.5 (C_q, Ph-*C*), 148.8 (C_q, Ph-*C*), 145.5 (C_q, Ph-*C*), 144.1 (C_q, Ph-*C*), 130.0 (+, 2×Ph-*C*), 127.3 (C_q, Ph-*C*), 124.0 (+, Ph-*C*), 123.4 (+, 2×Ph-*C*), 116.6 (+, Ph-*C*), 115.2 ppm (+, Ph-*C*); ESI-MS: *m/z*: 259.90 $[M+H]^+$.

4-(4-Aminobenzyl)benzene-1,2-diol (5a)

Hydrogenation of **4** (200 mg, 0.772 mmol) was performed at room temperature for 16 h under a hydrogen atmosphere (10 bar) in methanol (10 mL) by using 20 wt% Pd/C. The reaction mixture was filtered through Celite and the solvent was removed under reduced pressure. The crude product was purified by column chromatography on silica gel by using a mixture of dichloromethane/methanol/triethylamine (40:1:0.1) as the eluent. The product was obtained as a light brown solid (76 mg, 45%). M.p. 205 °C; ^{1}H NMR (400 MHz, [D_6]DMSO): $\delta = 8.67$ (s, 1H; OH), 8.55 (s, 1H; OH), 6.81 (d, $^3J = 8.02$ Hz, 2H; Ph), 6.60 (d, $^3J = 7.9$ Hz, 1H; Ph), 6.51 (d, $^4J = 2.1$ Hz, 1H), 6.47 (d, $^3J = 8.3$ Hz, 2H; Ph), 6.41 (dd, $^3J = 8.02$, $^4J = 2.10$ Hz, 1H; Ph), 4.82 (s, 2H; NH_2), 3.55 ppm (s, 2H; CH_2); ^{13}C NMR (100 MHz, [D_6]DMSO) $\delta = 146.4$ (C_q, Ph-*C*), 144.9 (C_q, Ph-*C*), 143.1 (C_q, Ph-*C*), 133.2 (C_q, Ph-*C*), 129.0 (+, 2×Ph-*C*), 128.9 (C_q, Ph-*C*), 119.1 (+, Ph-*C*), 115.9 (+, Ph-*C*), 115.3 (+, Ph-*C*), 113.9 (+, 2×Ph-*C*), 39.8 ppm (−, CH_2); ESI-MS: *m/z*: 216.00 $[M+H]^+$.

4-(3,4-Dimethoxybenzyl)aniline (5b)

Hydrogenation of **3** (400 mg, 1.57 mmol) was performed at room temperature for 16 h under a hydrogen atmosphere (10 bar) in methanol (30 mL) by using 20 wt% Pd/C. The reaction mixture was filtered through Celite and the solvent was removed under reduced pressure. The crude product was purified by column chromatography on silica gel by using a mixture of ethyl acetate/cyclohexane (1:1) as the eluent. The product was obtained as a colorless oil (225 mg, 56%). ^{1}H NMR (400 MHz, $CDCl_3$): $\delta = 7.12$ (d, $^3J = 8.46$, 2H), 6.93 (d, $^4J = 1.9$ Hz, 1H), 6.86 (dd, $^3J = 8.2$, $^4J = 2.0$ Hz, 1H), 6.80 (d, $^3J = 8.2$ Hz, 1H), 6.62 (d, $^3J = 8.46$, 2H), 3.86 (s, 3H; -OCH_3), 3.82 (s, 3H, -OCH_3), 3.49–2.92 ppm (s, 2H); ^{13}C NMR (100 MHz, $CDCl_3$): $\delta = 148.9$ (C_q, Ph-*C*), 148.2 (C_q, Ph-*C*), 145.8 (C_q, Ph-*C*), 137.07 (C_q, Ph-*C*), 134.32 (C_q, Ph-*C*), 127.8 (+, 2×Ph-*C*), 118.7 (+, Ph-*C*), 115.1 (+, 2×Ph-*C*), 110.9 (+, Ph-*C*), 109.7 (+, Ph-*C*), 75.6 (−, CH_2), 55.9 (+, -OCH_3), 55.8 ppm (+, -OCH_3); ESI-MS: *m/z*: 242.95 $[M+H]^+$.

(*E*)-4-[4-(Phenyldiazenyl)benzyl]benzene-1,2-diol (8a)

Compound **5a** (48 mg, 0.22 mmol) and nitrosobenzene (28.7 mg, 0.27 mmol) were stirred in acetic acid (3 mL) at room temperature for 16 h. Ethyl acetate (50 mL) was added, and the organic layer was washed with a 1 M aqueous solution of NaOH (50 mL) and water (50 mL). The solvent was removed under reduced pressure and the crude product was purified by column chromatography on silica gel by using a mixture of ethyl acetate and cyclohexane (1:2→1:1→2:1) as the eluent. The product was obtained as an orange solid (17 mg, 25%). M.p. 121 °C; ^{1}H NMR (400 MHz, $CDCl_3$): $\delta = 7.92$–7.87 (m, 2H; Ph), 7.86–7.80 (m, 2H; Ph), 7.55–7.43 (m, 3H; Ph), 7.34–7.28 (m, 2H; Ph), 6.80 (d, $^3J = 8.00$ Hz, 1H; Ph), 6.70 (d, $^4J = 2.1$ Hz, 1H; Ph), 6.65 (dd, $^3J = 8.1$, $^4J = 2.1$ Hz, 1H), 5.20 (s, 2H; O*H*), 3.93 ppm (s, 2H; CH_2); ^{13}C NMR (100 MHz, $CDCl_3$): $\delta = 152.8$ (C_q, Ph-*C*), 151.2 (C_q, Ph-*C*), 145.0 (C_q, Ph-*C*), 144.0 (C_q, Ph-*C*), 142.4 (C_q, Ph-*C*), 140.7 (C_q, Ph-*C*), 133.3 (+, Ph-*C*), 130.9 (+, Ph-*C*), 129.6 (+, Ph-*C*), 129.1 (+, Ph-*C*), 128.7 (+, Ph-*C*), 127.8 (+, Ph-*C*), 127.1 (+, Ph-*C*), 123.1 (+, Ph-*C*), 122.8 (+, Ph-*C*), 121.2 (+, Ph-*C*), 116.1 (+, Ph-*C*), 115.5 (+, Ph-*C*), 41.23 ppm (−, CH_2); ESI-MS: *m/z*: 304.95 $[M+H]^+$; HPLC purity: 98% (retention time: *cis* = 9.18 min, *trans* = 10.47 min).

General procedure for the partial oxidation of aromatic amines

Amine **6b–f** (1 equiv) was dissolved in dichloromethane (0.3 M) and an aqueous solution of oxone (1 equiv, 0.17 M; commercially available mixture of $2KHSO_5{\cdot}KHSO_4{\cdot}K_2SO_4$) was added. The mixture was stirred for 3.5 h at room temperature. The aqueous layer was extracted with dichloromethane (50 mL); the combined organic layers were washed with a 5% solution of HCl (50 mL), water (25 mL), and brine (25 mL); and dried over Na_2SO_4. The solvent was removed under reduced pressure and the crude product was directly used for the next reaction.

General procedure for the Mills reaction

The crude product of partial oxidation and **5a** were dissolved in acetic acid and stirred at room temperature for 16 h. After that time, the solvent was removed under reduced pressure; ethyl acetate was added; and the organic layer was washed with a saturated aqueous solution of $NaHCO_3$, water, and brine. The solvent was removed under reduced pressure and the crude product was purified by column chromatography on silica gel by using a mixture of ethyl acetate and cyclohexane or cyclohexane and dichloromethane as the eluent.

(*E*)-4-{4-[(3-Ethoxyphenyl)diazenyl]benzyl}benzene-1,2-diol (8b)

The product was purified by column chromatography on silica gel by using a mixture of ethyl acetate and cyclohexane (1:4) as the eluent. The product was obtained as an orange solid (24 mg, 21%). M.p. 126 °C; ^{1}H NMR (400 MHz, $CDCl_3$): δ = 7.83 (d, ^3J = 8.4 Hz, 2H; Ph), 7.51 (d, ^3J = 7.8, 1H; Ph), 7.42 (d, ^3J = 7.95 Hz, 2H; Ph), 7.30 (d, ^3J = 8.4 Hz, 2H; Ph), 7.02 (ddd, ^3J = 8.2, ^4J = 2.6, ^4J = 1.0 Hz, 1H; Ph), 6.80 (d, ^3J = 8.1 Hz, 1H; Ph), 6.70 (d, ^4J = 2.0 Hz, 1H; Ph), 6.66 (dd, ^3J = 8.0, ^4J = 2.1 Hz, 1H; Ph), 5.15 (s, 2H; O*H*), 4.13 (q, ^3J = 7.0 Hz, 2H; OCH_2CH_3), 3.94 (s, 2H; CH_2), 1.45 ppm (t, ^3J = 7.0 Hz, 3H; OCH_2CH_3); ^{13}C NMR (100 MHz, $CDCl_3$): 159.8 (C_q, Ph-*C*), 154.0 (C_q, Ph-*C*), 151.2 (C_q, Ph-*C*), 144.8 (C_q, Ph-*C*), 143.7 (C_q, Ph-*C*), 142.1 (C_q, Ph-*C*), 133.7 (C_q, Ph-*C*), 129.8 (+, Ph-*C*), 129.7 (+, 2×Ph-*C*), 123.1 (+, 2×Ph-*C*), 121.5 (+, Ph-*C*), 118.2 (+, Ph-*C*), 117.0 (+, Ph-*C*), 116.2 (+, Ph-*C*), 115.5 (+, Ph-*C*), 106.5 (+, Ph-*C*), 63.8 (−, OCH_2CH_3), 41.2 (−, CH_2), 14.9 (+, OCH_2CH_3); ESI-MS: *m/z*: 349.00 $[M+H]^+$; HPLC purity: 96% (retention time: *cis* = 9.63 min, *trans* = 10.83 min).

(*E*)-4-{4-[(3-Nitrophenyl)diazenyl]benzyl}benzene-1,2-diol (8c)

The product was purified by column chromatography on silica gel by using a mixture of ethyl acetate and cyclohexane (1:4→1:3) as the eluent. The product was obtained as an orange solid (59 mg, 52%). M.p. 125 °C; ^{1}H NMR (400 MHz, $CDCl_3$): δ = 8.72 (t, ^4J = 2.1 Hz, 1H; Ph), 8.31 (ddd, ^3J = 8.2, ^4J = 2.3, ^4J = 1.0 Hz, 1H; Ph), 8.23 (dt, ^3J = 7.9, ^4J = 1.0 Hz, 1H; Ph), 7.89 (d, ^3J = 8.32, 2H; Ph), 7.69 (t, ^3J = 8.0 Hz, 1H; Ph), 7.35 (d, ^3J = 8.1 Hz, 2H; Ph), 6.81 (d, ^3J = 8.0 Hz, 1H; Ph), 6.72 (^{3}d, *J* = 2.0 Hz, 1H; Ph), 6.67 (dd, ^3J = 8.1, ^4J = 2.0 Hz, 1H), 5.22 (s, 2H; O*H*), 3.96 ppm (s, 2H; CH_2); ^{13}C NMR (100 MHz, $CDCl_3$): δ = 153.2 (C_q, Ph-*C*), 150.8 (C_q, Ph-*C*), 146.2 (C_q, Ph-*C*), 143.8 (C_q, Ph-*C*), 142.1 (C_q, Ph-*C*), 133.5 (C_q, Ph-*C*), 130.0 (+, Ph-*C*), 129.8 (+, 2×Ph-*C*), 129.3 (+, Ph-*C*), 124.8 (+, Ph-*C*), 123.6 (+, 2×Ph-*C*), 121.6 (+, Ph-*C*), 117.1 (+, Ph-*C*), 116.2 (+, Ph-*C*), 115.6 (+, Ph-*C*), 41.3 ppm (−, CH_2); ESI-MS: *m/z*: 350.10 $[M+H]^+$; HPLC purity: 97% (retention time: *cis* = 11.60 min, *trans* = 13.52 min).

(*E*)-4-{4-[(3-Chlorophenyl)diazenyl]benzyl}benzene-1,2-diol (8d)

The crude product was purified by column chromatography on silica gel by using a mixture of ethyl acetate and cyclohexane (1:3) as the eluent. The product was obtained as an orange powder (150 mg, 64%). M.p. 149 °C; ^{1}H NMR (400 MHz, $CDCl_3$): δ = 7.90–7.79 (m, 4H; Ph), 7.44 (d, ^3J = 6.9 Hz, 2H; Ph), 7.32 (d, ^3J = 8.1 Hz, 2H; Ph), 6.81 (d, ^3J = 8.0 Hz, 1H; Ph), 6.71 (d, ^4J = 2.0 Hz, 1H), 6.67 (dd, ^3J = 8.1, ^4J = 2.1 Hz, 1H; Ph), 5.07 (s, 1H; O*H*), 4.99 (s, 1H; O*H*), 3.95 ppm (s, 2H; CH_2); ^{13}C NMR (100 MHz, $CDCl_3$): 148.8 (C_q, Ph-*C*), 145.2 (C_q, Ph-*C*), 141.8 (C_q, Ph-*C*), 130.2 (+, Ph-*C*), 129.7 (+, 2×Ph-*C*), 123.3 (+, Ph-*C*), 121.6 (+, 2×Ph-*C*), 117.1 (+, Ph-*C*), 115.6, 41.2 ppm (−, CH_2); ESI-MS: *m/z*: 335.05 $[M+H]^+$; HPLC purity: 97% (retention time: *cis* = 9.65 min, *trans* = 10.95 min).

(*E*)-4-{4-[(3-Methoxyphenyl)diazenyl]benzyl}benzene-1,2-diol (8e)

The product was purified by column chromatography on silica gel by using a mixture of ethyl acetate and cyclohexane (1:4) as the eluent. The product was obtained as an orange solid (17 mg, 25%). M.p. 122 °C; ^{1}H NMR (400 MHz, $CDCl_3$): δ = 7.84 (d, ^3J = 8.4 Hz, 2H; Ph), 7.47–7.39 (m, 3H; Ph), 7.31 (d, ^3J = 7.95 Hz, 2H; Ph), 7.05–7.01 (m, 1H; Ph), 6.80 (d, ^3J = 8.1, 1H; Ph), 6.71 (d, ^4J = 2.1 Hz, 1H; Ph), 6.66 (dd, ^3J = 8.10 Hz, ^4J = 2.0 Hz, 1H), 5.38 (s, 2H; O*H*), 3.94 (s, 2H; CH_2), 3.90 (s, 3H; OCH_3); ^{13}C NMR (100 MHz, $CDCl_3$): 159.7 (C_q, Ph-*C*), 154.2 (C_q, Ph-*C*), 151.01 (C_q, Ph-*C*), 144.89 (C_q, Ph-*C*), 143.55 (C_q, Ph-*C*), 142.1 (C_q, Ph-*C*), 133.6 (C_q, Ph-*C*), 129.9 (+, Ph-*C*), 129.7 (+, 2×Ph-*C*), 123.2 (+, 2×Ph-*C*), 121.6 (+, Ph-*C*), 117.7 (+, Ph-*C*), 117.1 (+, Ph-*C*), 116.2 (+, Ph-*C*), 115.6 (+, Ph-*C*), 105.8 (+, Ph-*C*), 55.6 (−, OCH_3), 41.2 ppm (−, CH_2); ESI-MS: *m/z*: 335.00 $[M+H]^+$; HPLC purity: 96% (retention time: *cis* = 9.31 min, *trans* = 10.57 min).

(*E*)-4-{4-[(3-Isopropoxyphenyl)diazenyl]benzyl}benzene-1,2-diol (8f)

The product was purified by column chromatography on silica gel by using a mixture of ethyl acetate and cyclohexane (1:4) as the eluent. The product was obtained as an orange solid (37 mg, 16%). M.p. 127 °C; ^{1}H NMR (400 MHz, $CDCl_3$): δ = 7.82 (d, ^3J = 8.1 Hz, 2H; Ph), 7.49 (d, ^3J = 7.8, 1H; Ph), 7.44–7.36 (m, 2H; Ph), 7.30 (d, ^3J = 8.1 Hz, 2H), 7.00 (m, 1H; Ph), 6.80 (d, *J* = 8.0 Hz, 1H; Ph), 6.69 (d, ^4J = 1.9 Hz, 1H; Ph), 6.65 (dd, ^3J = 8.1, ^4J = 2.0 Hz, 1H; Ph), 5.23 (s, 2H; O*H*), 4.66 (p, ^3J = 6.1 Hz, 1H; O*i*Pr-*H*), 3.93 (s, 2H; CH_2), 1.39 (s, 3H; O*i*Pr-CH_3), 1.37 ppm (s, 3H; O*i*Pr-CH_3); ^{13}C NMR (100 MHz, $CDCl_3$): 158.7 (C_q, Ph-*C*), 154.1 (C_q, Ph-*C*), 151.2 (C_q, Ph-*C*), 144.8 (C_q, Ph-*C*), 143.7 (C_q, Ph-*C*), 142.1 (C_q, Ph-*C*), 133.7 (C_q, Ph-*C*), 129.9 (+, Ph-*C*), 129.6 (+, 2×Ph-*C*), 123.1 (+, 2×Ph-*C*), 121.6 (+, Ph-*C*), 119.3 (+, Ph-*C*), 116.6 (+, Ph-*C*), 115.6 (+, Ph-*C*), 108.2 (+, Ph-*C*), 70.3 (+, O*i*Pr-*C*H), 41.2 (−, CH_2), 22.1 (+, 2×O*i*Pr-CH_3); ESI-MS: *m/z*: 363.15 $[M+H]^+$; HPLC purity: 96% (retention time: *cis* = 9.74 min, *trans* = 10.84 min).

(*E*)-1-[4-(3,4-Dimethoxybenzyl)phenyl]-2-phenyldiazene (8g)

The product was purified by column chromatography on silica gel by using a mixture of ethyl acetate and cyclohexane (1:2→1:1→2:1) as the eluent. The product was obtained as an orange oil (17 mg, 25%). ^{1}H NMR (400 MHz, $CDCl_3$): δ = 7.93–7.88 (m, 4H; Ph), 7.60–7.43 (m, 5H; Ph), 6.95–6.81 (m, 3H; Ph), 3.88–3.83, 3.87 (m, 2H; CH_2), (s, 3H; -OMe), 3.85 ppm (s, 3H; -OMe); ^{13}C NMR (100 MHz, $CDCl_3$): 152.8 (C_q, Ph-*C*), 152.2 (C_q, Ph-*C*), 149.2 (C_q, Ph-*C*), 149.1 (C_q, Ph-*C*), 143.2 (C_q, Ph-*C*), 132.4 (C_q, Ph-*C*), 131.2 (+, Ph-*C*),

129.2 (+, 2×Ph-C), 127.6 (+, 2×Ph-C), 123.1 (+, 2×Ph-C), 123.01 (+, 2×Ph-C), 120.2 (+, Ph-C), 111.1 (+, Ph-C), 110.8 (+, Ph-C), 76.5 (−, CH_2), 56.0 (+, OMe); ESI-MS: *m/z*: 331.95 $[M+H]^+$; HPLC purity: 97% (retention time: *cis* = 7.66 min, *trans* = 11.28 min).

Aβ42 aggregation inhibition—TEM analysis

The procedure was adapted from a method reported by Murakami et al.[59] Aβ42, purchased from Amatek, was dissolved in a 0.1% solution of NH_4OH at a concentration of 1 mg mL^{-1}. Each compound was dissolved in ethanol at a concentration of 1 mg mL^{-1}. Samples were diluted to a final concentration of 100 μM Aβ42, and the desired concentration of compound (10 μM/50 μM) in PBS (50 mM sodium phosphate and 100 mM NaCl, pH 7.4). After 24 h incubation at 37 °C, solutions were applied on 200 mesh, fixed with 1.25% glutaraldehyde solution, and negatively stained with 1% uranyl acetate. The aggregates were observed with a JEOL JEM-2100 transmission electron microscope. Images on the transmission electron microscope were acquired with a TemCamF416 camera (Tietz Video and Imaging Processing Systems, Gauting, Germany).

Inhibition assay in *E. coli* cells overexpressing Aβ42 and tau

Cloning and overexpression of Aβ42 peptide: *E. coli* competent cells BL21 (DE3) were transformed with the pET28a vector (Novagen, Inc., Madison, WI, USA) carrying the DNA sequence of Aβ42. Because of the addition of the initiation codon ATG in front of both genes, the overexpressed peptide contained an additional methionine residue at its N terminus. For overnight culture preparation, M9 minimal medium (10 mL) containing 50 μg mL^{-1} kanamycin was inoculated with a colony of BL21 (DE3) bearing the plasmid to be expressed at 37 °C. For expression of the Aβ42 peptide, the required volume of overnight culture to obtain 1:500 dilution was added to fresh M9 minimal medium containing 50 μg mL^{-1} kanamycin and 250 μM Th-S. The bacterial culture was grown at 37 °C and 250 rpm. Once the cell density reached OD600 = 0.6, an aliquot of culture (980 μL) was transferred into 1.5 mL Eppendorf tubes with solutions (10 μL) of each compound to be tested in DMSO and isopropyl 1-thio-β-D-galactopyranoside (IPTG; 10 μL) at 100 mM. The final concentration of drug was fixed at 10 μM. The samples were grown overnight at 37 °C and 1400 rpm by using a Thermomixer (Eppendorf, Hamburg, Germany). As a negative control (maximal amyloid presence), the same amount of DMSO without drug was added to the sample. In parallel, noninduced samples (in the absence of IPTG) were also prepared and used as positive controls (nonamyloid presence). In addition, these samples were used to assess the potential intrinsic toxicity of the compounds and to confirm the correct bacterial growth.

Cloning and overexpression of tau protein: *E. coli* BL21 (DE3) competent cells were transformed with pTARA containing the RNA polymerase gen of T7 phage (T7RP) under the control of the promoter PBAD. *E. coli* BL21 (DE3) with pTARA competent cells were transformed with pRKT42 vector encoding four repeats of tau protein in two inserts. For overnight culture preparation, M9 medium (10 mL) containing 0.5% glucose, 50 μg mL^{-1} ampicillin, and 12.5 μg mL^{-1} chloramphenicol were inoculated with a colony of BL21 (DE3) bearing the plasmids to be expressed at 37 °C. For the expression of *tau* protein, the required volume of overnight culture to obtain 1:500 dilution was added to fresh M9 minimal medium containing 0.5% glucose, 50 μg mL^{-1} ampicillin, 12.5 μg mL^{-1} chloramphenicol, and 250 μM Th-S. The bacterial culture was grown at 37 °C and 250 rpm. Once the cell density reached OD600 = 0.6, an aliquot of culture (980 μL) was transferred into 1.5 mL Eppendorf tubes with solutions (10 μL) of each compound to be tested in DMSO and arabinose (10 μL, 25%). The final concentration of compound was fixed at 10 μM. The samples were grown overnight at 37 °C and 1400 rpm by using a Thermomixer (Eppendorf, Hamburg, Germany). As a negative control (maximal presence of *tau*), the same amount of DMSO without drug was added to the sample. In parallel, noninduced samples (in the absence of arabinose) were also prepared and used as positive controls (absence of *tau*). In addition, these samples were used to assess the potential intrinsic toxicity of the compounds and to confirm the correct bacterial growth.

Th-S steady-state fluorescence: Th-S (T1892) and other chemical reagents were purchased from Sigma (St. Louis, MO). Th-S stock solution (2500 mM) was prepared in double-distilled water purified through a Milli-Q system (Millipore, USA). Th-S fluorescence and absorbance were tracked by using a DTX 800 plate reader multimode detector equipped with multimode analysis software (Beckman-Coulter, USA). Filters of 430/35 and 485/20 nm were used for the excitation and emission wavelengths, respectively. 535/25 nm filters were also used for absorbance determination. To normalize the Th-S fluorescence as a function of the bacterial concentration, OD600 was obtained by using a Shimadzu UV-2401 PC UV/Vis spectrophotometer (Shimadzu, Japan). Notably, fluorescence normalization was carried out by considering the Th-S fluorescence of the bacterial cells expressing the peptide or protein in the absence of drug as 100% and the Th-S fluorescence of the bacterial cells nonexpressing the peptide or protein as 0%.

Cell culture general procedures

HT22 cells were grown in Dulbecco's modified Eagle medium (DMEM; Sigma Aldrich, Munich Germany) supplemented with 10% (v/v) fetal calf serum (FCS) and 1% (v/v) penicillin–streptomycin. BV-2 cells were grown in low-glucose DMEM (Invitrogen, Carlsbad, CA, USA) supplemented with 10% FCS and 1% (v/v) penicillin–streptomycin. Cells were subcultured every 2 days and incubated at 37 °C with 5% CO_2 in a humidified incubator. Compounds were dissolved in DMSO (Sigma Aldrich, Munich, Germany) as stock solutions and diluted further into culture medium. To determine cell viability, a colorimetric 3-(4,5-dimethylthiazol-2-yl)-2,5-diphenyl tetrazolium bromide (MTT; Sigma Aldrich, Munich, Germany) assay was used. MTT solution (4 mg mL^{-1} in PBS) was diluted 1:10 with medium and added to the wells after removal of the old medium. Cells were incubated for 3 h and then lysis buffer (10% sodium dodecyl sulfide) was applied. The next day, the absorbance at 560 nm was determined with a multiwell plate photometer (Tecan, SpectraMax 250).

Neurotoxicity and neuroprotection (oxytosis)

For the toxicity and oxytosis assay, 5×10^3 cells per well were seeded into sterile 96-well plates and incubated overnight. For the neurotoxicity assay, medium was removed and 1, 5, 10, 25, or 50 μM of the compound diluted with medium from a 0.1 M stock solution was added to the wells. DMSO (0.05%) in DMEM served as a control. Cells were incubated for 24 h if neurotoxicity was determined by using a colorimetric MTT assay.

For the oxytosis assay, 5 mM glutamate (monosodium L-glutamate, Sigma Aldrich, Munich, Germany) together with 1, 2.5, 5, 7.5, or 10 μM of the respective compounds were added to the cells and incubated for 24 h. As a positive control, a mixture of 25 μM quer-

cetin (Sigma Aldrich, Munich, Germany) and 5 mM glutamate was used. After 24 h incubation, cell viability was determined by using a colorimetric MTT assay, as described above. Results are presented as percentage of untreated control cells. Data are expressed as means ± SEM of three independent experiments. Analysis was accomplished by using GraphPad Prism 5 software by applying one-way ANOVA followed by Dunnett's multiple comparison post-test. Levels of significance: $^{*}p<0.05$; $^{**}p<0.01$; $^{***}p<0.001$.

DPPH radical scavenging assay

Stock solutions of standard antioxidant, ascorbic acid, and compounds were prepared in DMSO (3 mM). DPPH solution was freshly prepared in methanol daily and stored in the dark. A dilution row of compound in methanol ranging over nine dilutions (1–500 μM) was prepared in a 96-well plate by using a multichannel pipette. The blank was measured at 517 nm. To 100 μL compound dilution, a solution of DPPH (33.3 μL, 200 μM) in ethanol was added by using a multichannel pipette. The 96-well plate was incubated at room temperature in the dark for 30 min. After incubation, the absorbance was measured at 517 nm. Methanol (100 μL) and DPPH (33.3 μL, 200 μM) served as the negative control. The percentage of DPPH radical scavenging activity (SCV) was calculated by using Equation ():

$$\%\ \mathrm{SCV} = \frac{(A_{\mathrm{neg.control}} - A_{\mathrm{blank1}}) - (A_{\mathrm{sampe1}} - A_{\mathrm{blank2}})}{(A_{\mathrm{neg.control}} - A_{\mathrm{blank1}})} \times 100 \qquad (1)$$

Concentration-dependent SCV curves were calculated by using a nonlinear fit and EC_{50} values were then determined graphically by using GraphPad Prism 5 software.

Microglial activity

For the anti-neuroinflammation assay, 1×10^{6} cells per well were seeded in a sterile six-well plate. After overnight incubation, the medium was exchanged for fresh medium. The cells were pretreated with the respective compounds at the indicated concentrations for 30 min after 50 ng mL^{-1} bacterial LPS was added. After 24 h incubation, the medium was collected, spun briefly to remove floating cells, and the supernatant (100 μL) was assayed for nitrite by using the Griess Reagent (100 μL) in a 96-well plate. After incubation for 10 min at room temperature, the absorbance at 550 nm was read on a microplate reader. Results were normalized to cell number as assessed by the MTT assay, as described above. Analysis was accomplished by using GraphPad Prism 5 software by applying one-way ANOVA followed by Dunnett's multiple comparison post-test. Levels of significance: $^{*}p<0.05$; $^{**}p<0.01$; $^{***}p<0.001$.

Acknowledgements

Financial support by the Graduate School of Life Science (GSLS) Würzburg and the COST action CA15135 (Multitarget Paradigm for Innovative Ligand Identification in the Drug Discovery Process MuTaLig) to J.H. is gratefully acknowledged. We are also grateful for financial support by the Spanish Ministerio de Economía y Competitividad (MDM2017-0767; AEI/FEDER UE) and the Generalitat de Catalunya (2017SGR1746; 2019LLAV00016). The Barcelona Supercomputer Center is acknowledged for providing computational resources (BCV-2021-1-0022). We thank Dr. Pamela Maher (Cellular Neurobiology Laboratory, The Salk Institute for Biological Studies, La Jolla, USA) for providing HT22 and BV-2 cells. We thank Claudia Gehrig and Daniela Bunsen (Biocenter/Theodor-Boveri-Institute) for technical assistance. Open access funding enabled and organized by Projekt DEAL.

Conflict of interest

The authors declare no conflict of interest.

Keywords: amyloid beta · bioisosterism · natural products · neuroprotectivity · replica-exchange molecular dynamics

[1] E. Babusikova, A. Evinova, J. Jurecekova, M. Jesenak, D. Dobrota in *Advanced Understanding of Neurodegenerative Diseases*, IntechOpen, **2011**.
[2] a) G. G. Glenner, C. W. Wong, *Biochem. Biophys. Res. Commun.* **1984**, *120*, 885–890; b) C. L. Masters, G. Simms, N. A. Weinman, G. Multhaup, B. L. McDonald, K. Beyreuther, *Proc. Natl. Acad. Sci. USA* **1985**, *82*, 4245–4249.
[3] C. Haass, D. J. Selkoe, *Nat. Rev. Mol. Cell Biol.* **2007**, *8*, 101–112.
[4] L. M. Sayre, G. Perry, M. A. Smith, *Chem. Res. Toxicol.* **2008**, *21*, 172–188.
[5] M. Prior, C. Chiruta, A. Currais, J. Goldberg, J. Ramsey, R. Dargusch, P. A. Maher, D. Schubert, *ACS Chem. Neurosci.* **2014**, *5*, 503–513.
[6] a) S. Giorgetti, C. Greco, P. Tortora, F. A. Aprile, *Int. J. Mol. Sci.* **2018**, *19*, 2677; b) F. Panza, M. Lozupone, G. Logroscino, B. P. Imbimbo, *Nat. Rev. Neurosci.* **2019**, *15*, 73–88.
[7] a) L. Fang, S. Gou, X. Liu, F. Cao, L. Cheng, *Bioorg. Med. Chem. Lett.* **2014**, *24*, 40–43; b) M. Venigalla, S. Sonego, E. Gyengesi, M. J. Sharman, G. Münch, *Neurochem. Int.* **2016**, *95*, 63–74; c) A. Espargaró, T. Ginex, M. d. M. Vadell, M. A. Busquets, J. Estelrich, D. Muñoz-Torrero, F. J. Luque, R. Sabate, *J. Nat. Prod.* **2017**, *80*, 278–289.
[8] A. A. Reinke, J. E. Gestwicki, *Chem. Biol. Drug Des.* **2007**, *70*, 206–215.
[9] K. M. Nelson, J. L. Dahlin, J. Bisson, J. Graham, G. F. Pauli, M. A. Walters, *J. Med. Chem.* **2017**, *60*, 1620–1637.
[10] J. B. Baell, G. A. Holloway, *J. Med. Chem.* **2010**, *53*, 2719–2740.
[11] a) F. Li, Q. Gong, H. Dong, J. Shi, *Curr. Pharm. Des.* **2012**, *18*, 27–33; b) S. Gunesch, S. Schramm, M. Decker, *Future Med. Chem.* **2017**, *9*, 711–713; c) J. Vrba, R. Gažák, M. Kuzma, B. Papoušková, J. Vacek, M. Weiszenstein, V. Křen, J. Ulrichová, *J. Med. Chem.* **2013**, *56*, 856–866; d) F. Yang, G. P. Lim, A. N. Begum, O. J. Ubeda, M. R. Simmons, S. S. Ambegaokar, P. P. Chen, R. Kayed, C. G. Glabe, S. A. Frautschy, *J. Biol. Chem.* **2005**, *280*, 5892–5901; e) G. Henríquez, A. Gomez, E. Guerrero, M. Narayan, *ACS Chem. Neurosci.* **2020**, *11*, 2915–2934.
[12] F. Pohl, P. Kong Thoo Lin, *Molecules* **2018**, *23*, 3283.
[13] S. Gunesch, C. Kiermeier, M. Hoffmann, W. Fischer, A. F. M. Pinto, T. Maurice, P. Maher, M. Decker, *Redox Biol.* **2019**, 101378.
[14] S. Gunesch, D. Soriano-Castell, S. Lamer, A. Schlosser, P. Maher, M. Decker, *ACS Chem. Neurosci.* **2020**, *11*, 3823–3837.
[15] a) W. Fischer, A. Currais, Z. Liang, A. Pinto, P. Maher, *Redox Biol.* **2019**, *21*, 101089; b) N. Taguchi, M. Yuriguchi, T. Ando, R. Kitai, H. Aoki, T. Kunisada, *Biol. Pharm. Bull.* **2019**, *42*, 1446–1449; c) M. Sato, K. Murakami, M. Uno, H. Ikubo, Y. Nakagawa, S. Katayama, K.-i. Akagi, K. Irie, *Biosci. Biotech. Biochem.* **2013**, *77*, 1100–1103.
[16] M. Singh, M. Arseneault, T. Sanderson, V. Murthy, C. Ramassamy, *J. Agric. Food Chem.* **2008**, *56*, 4855–4873.
[17] T. C. T. Michaels, A. Šarić, G. Meisl, G. T. Heller, S. Curk, P. Arosio, S. Linse, C. M. Dobson, M. Vendruscolo, T. P. J. Knowles, *Proc. Natl. Acad. Sci. USA* **2020**, *117*, 24251–24257.
[18] K. Murakami, K. Irie, *Molecules* **2019**, *24*, 2125.
[19] E. Chainoglou, D. Hadjipavlou-Litina, *Int. J. Mol. Sci.* **2020**, *21*, 1975.
[20] M. Sato, K. Murakami, M. Uno, Y. Nakagawa, S. Katayama, K.-i. Akagi, Y. Masuda, K. Takegoshi, K. Irie, *J. Biol. Chem.* **2013**, *288*, 23212–23224.
[21] F. L. Palhano, J. Lee, N. P. Grimster, J. W. Kelly, *J. Am. Chem. Soc.* **2013**, *135*, 7503–7510.
[22] a) T. Zhang, J. Zhang, P. Derreumaux, Y. Mu, *J. Phys. Chem. B* **2013**, *117*, 3993–4002; b) H. Minh Hung, M. T. Nguyen, P.-T. Tran, V. K. Truong, J.

Chapman, L. H. Quynh Anh, P. Derreumaux, V. V. Vu, S. T. Ngo, *J. Chem. Inf. Model*. **2020**, *60*, 1399–1408.
[23] L. M. Lima, E. J. Barreiro, *Curr. Med. Chem.* **2005**, *12*, 23–49.
[24] a) M. J. Fuchter, *J. Med. Chem.* **2020**, *63*, 11436–11447; b) W. A. Velema, W. Szymanski, B. L. Feringa, *J. Am. Chem. Soc.* **2014**, *136*, 2178–2191; c) D. A. Rodríguez-Soacha, M. Decker, *Adv. Ther.* **2018**, *1*, 1800037; d) L. Agnetta, M. Decker in *Design of Hybrid Molecules for Drug Development* (Ed.: M Decker), Elsevier, Amsterdam, **2017**, pp. 279–311.
[25] A. Espargaró, A. Medina, O. Di Pietro, D. Muñoz-Torrero, R. Sabate, *Sci. Rep.* **2016**, *6*, 23349.
[26] F. Chiti, C. M. Dobson, *Annu. Rev. Biochem.* **2017**, *86*, 27–68.
[27] G. Invernizzi, E. Papaleo, R. Sabate, S. Ventura, *Int. J. Biochem. Cell Biol.* **2012**, *44*, 1541–1554.
[28] S. A. Hudson, H. Ecroyd, T. W. Kee, J. A. Carver, *FEBS J.* **2009**, *276*, 5960–5972.
[29] M. T. Colvin, R. Silvers, Q. Z. Ni, T. V. Can, I. Sergeyev, M. Rosay, K. J. Donovan, B. Michael, J. Wall, S. Linse, R. G. Griffin, *J. Am. Chem. Soc.* **2016**, *138*, 9663–9674.
[30] S. Release, Schrödinger, LLC, New York, NY **2018**.
[31] Amber18, T. Darden, R. Duke, D. Ghoreishi, M. Gilson, H. Gohlke, A. Goetz, D. Greene, R. Harris, N. Homeyer, S. Izadi, University of California, San Francisco **2018**.
[32] T. Ginex, M. Trius, F. J. Luque, *Chem. Eur. J.* **2018**, *24*, 5813–5824.
[33] O. Crescenzi, S. Tomaselli, R. Guerrini, S. Salvadori, A. M. D'Ursi, P. A. Temussi, D. Picone, *Eur. J. Biochem.* **2002**, *269*, 5642–5648.
[34] S. Tan, D. Schubert, P. Maher, *Curr. Top. Med. Chem.* **2001**, *1*, 497–506.
[35] A. Currais, P. Maher, *Redox. Signal*. **2013**, *19*, 813–822.
[36] J. A. Sonnen, J. C. Breitner, M. A. Lovell, W. R. Markesbery, J. F. Quinn, T. J. Montine, *Free Radical Biol. Med.* **2008**, *45*, 219–230.
[37] M. S. Blois, *Nature* **1958**, *181*, 1199–1200.
[38] T. Wyss-Coray, J. Rogers, *Cold Spring Harbor Perspect. Med.* **2012**, *2*, a006346.
[39] a) G. W. Kreutzberg, *Trends Neurosci.* **1996**, *19*, 312–318; b) L. Minghetti, G. Levi, *Prog. Neurobiol.* **1998**, *54*, 99–125.
[40] a) F. González-Scarano, G. Baltuch, *Annu. Rev. Neurosci.* **1999**, *22*, 219–240; b) K. M. Lenz, L. H. Nelson, *Front. Immunol*. **2018**, *9*, .
[41] M. Scheiner, D. Dolles, S. Gunesch, M. Hoffmann, M. Nabissi, O. Marinelli, M. Naldi, M. Bartolini, S. Petralla, E. Poeta, B. Monti, C. Falkeis, M. Vieth, H. Hübner, P. Gmeiner, R. Maitra, T. Maurice, M. Decker, *J. Med. Chem.* **2019**, *62*, 9078–9102.
[42] a) A. J. Doig, P. Derreumaux, *Curr. Opin. Struct. Biol.* **2015**, *30*, 50–56; b) A. Abbott, E. Dolgin, *Nature* **2016**, *540*, 15–16; c) A. J. Doig, M. P. del Castillo-Frias, O. Berthoumieu, B. Tarus, J. Nasica-Labouze, F. Sterpone, P. H. Nguyen, N. M. Hooper, P. Faller, P. Derreumaux, *ACS Chem. Neurosci.* **2017**, *8*, 1435–1437.
[43] J. Broichhagen, J. A. Frank, D. Trauner, *Acc. Chem. Res.* **2015**, *48*, 1947–1960.
[44] K. Lindorff-Larsen, S. Piana, K. Palmo, P. Maragakis, J. L. Klepeis, R. O. Dror, D. E. Shaw, *Proteins* **2010**, *78*, 1950–1958.
[45] J. Wang, R. M. Wolf, J. W. Caldwell, P. A. Kollman, D. A. Case, *J. Comput. Chem.* **2004**, *25*, 1157–1174.
[46] J. Wang, P. Cieplak, P. A. Kollman, *J. Comput. Chem.* **2000**, *21*, 1049–1074.
[47] Gaussian 09, Revision D1, M. J. Frisch, G. W. Trucks, H. B. Schlegel, G. E. Scuseria, M. A. Robb, J. R. Cheeseman, G. Scalmani, V. Barone, B. Mennucci, G. A. Petersson, H. Nakatsuji, M. Caricato, X. Li, H. P. Hratchian, A. F. Izmaylov, J. Bloino, G. Zheng, J. L. Sonnenberg, M. Hada, M. Ehara, K. Toyota, R. Fukuda, J. Hasegawa, M. Ishida, T. Nakajima, Y. Honda, O. Kitao, H. Nakai, T. Vreven, J. A. Montgomery, Jr., J. E. Peralta, F. Ogliaro, M. Bearpark, J. J. Heyd, E. Brothers, K. N. Kudin, V. N. Staroverov, R. Kobayashi, J. Normand, K. Raghavachari, A. Rendell, J. C. Burant, S. S. Iyengar, J. Tomasi, M. Cossi, N. Rega, J. M. Millam, M. Klene, J. E. Knox, J. B. Cross, V. Bakken, C. Adamo, J. Jaramillo, R. Gomperts, R. E. Stratmann, O. Yazyev, A. J. Austin, R. Cammi, C. Pomelli, J. W. Ochterski, R. L. Martin, K. Morokuma, V. G. Zakrzewski, G. A. Voth, P. Salvador, J. J. Dannenberg, S. Dapprich, A. D. Daniels, O. Farkas, J. B. Foresman, J. V. Ortiz, J. Cioslowski, D. J. Fox, Gaussian Inc., Wallingford CT, **2016**.
[48] C. S. Perone, *SIGEVOlution* **2009**, *4*, 12–20.
[49] W. L. Jorgensen, J. Chandrasekhar, J. D. Madura, R. W. Impey, M. L. Klein, *J. Chem. Phys.* **1983**, *79*, 926–935.
[50] I. S. Joung, T. E. Cheatham, *J. Phys. Chem. B* **2008**, *112*, 9020–9041.
[51] J.-P. Ryckaert, G. Ciccotti, H. J. Berendsen, *J. Comput. Phys.* **1977**, *23*, 327–341.
[52] T. Darden, D. York, L. Pedersen, *J. Chem. Phys.* **1993**, *98*, 10089–10092.
[53] H. J. C. Berendsen, J. P. M. Postma, W. F. v. Gunsteren, A. DiNola, J. R. Haak, *J. Chem. Phys.* **1984**, *81*, 3684–3690.
[54] M. Abraham, D. Van Der Spoel, E. Lindahl, B. Hess, *GROMACS user manual version* **2014**, *5*, 1–298.
[55] G. Bussi, D. Donadio, M. Parrinello, *J. Chem. Phys.* **2007**, *126*, 014101.
[56] M. Parrinello, A. Rahman, *J. Appl. Phys.* **1981**, *52*, 7182–7190.
[57] B. Hess, H. Bekker, H. J. C. Berendsen, J. G. E. M. Fraaije, *J. Comput. Chem.* **1997**, *18*, 1463–1472.
[58] W. Kabsch, C. Sander, *Biopolymers* **1983**, *22*, 2577–2637.
[59] K. Murakami, K. Irie, A. Morimoto, H. Ohigashi, M. Shindo, M. Nagao, T. Shimizu, T. Shirasawa, *J. Biol. Chem.* **2003**, *278*, 46179–46187.

Manuscript received: December 9, 2020
Revised manuscript received: January 14, 2021
Version of record online: March 5, 2021

Supporting Information

Azobioisosteres of curcumin with pronounced activity against amyloid aggregation, intracellular oxidative stress and neuroinflammation

Julian Hofmann, Tiziana Ginex, Alba Espargaró, Matthias Scheiner, Sandra Gunesch, Marc Aragó, Christian Stigloher, Raimon Sabaté, F. Javier Luque, and Michael Decker

Supporting Information

Table of contents

1. Parametrization of the C-C-N-N dihedral angle

The capability of the general Amber force field (GAFF) to properly describe the chemistry of the azobioisosteres investigated in this study was evaluated through preliminary MD simulations (data not shown). Accordingly, since no energy barrier was observed for the C*ar*=C*ar*-N=N torsional, a proper parametrization of this torsional was carried out prior to proceed to MD simulations with Aβ42. MM parameters were generated by fitting the MM potential energy of the C*ar*=C*ar*-N=N torsional on the QM-derived potential energy profile for the same torsional, derived from a relaxed scan performed at the M062X/6-31G(d) level in vacuo (see **Table S1**).

Table S1. Energy profiles for the selected torsion in azobenzenes determined by fitting quantum mechanical data. All energy values are in kcal/mol.

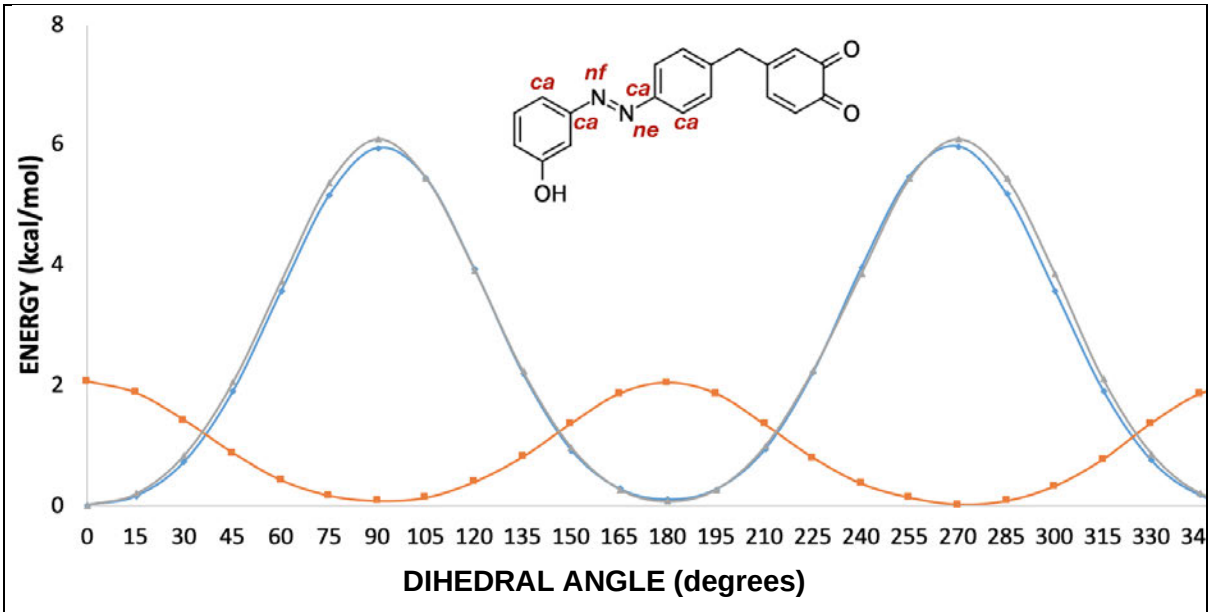

ca-ca-nf-ne dihedral angle (degrees)	ΔE (M062X)	ΔE (MM default)	ΔE (MM fitted)
0	0.00	2.05	0.00
15	0.15	1.86	0.19
30	0.72	1.40	0.83
45	1.89	0.86	2.04
60	3.56	0.40	3.72
75	5.16	0.15	5.36
90	5.94	0.06	6.09
105	5.43	0.11	5.43
120	3.92	0.38	3.91
135	2.19	0.79	2.22
150	0.91	1.35	0.96
165	0.27	1.85	0.26
180	0.09	2.03	0.06
195	0.26	1.85	0.26

210	0.92	1.33	0.97
225	2.21	0.78	2.24
240	3.95	0.35	3.85
255	5.47	0.11	5.43
270	5.97	0.00	6.09
285	5.17	0.06	5.43
300	3.57	0.31	3.85
315	1.90	0.75	2.09
330	0.74	1.36	0.85
345	0.16	1.84	0.20
360	0.00	2.03	0.02

Fitted torsional parameters used in this study for the C-C-N-N torsion:

```
1. ca-ca-ne-nf   2    4.100      180.000      -2.000
1. ca-ca-ne-nf   2    0.300      360.000       4.000

2. ca-ca-nf-ne   2    4.100      180.000      -2.000
2. ca-ca-nf-ne   2    0.300      360.000       4.000
```

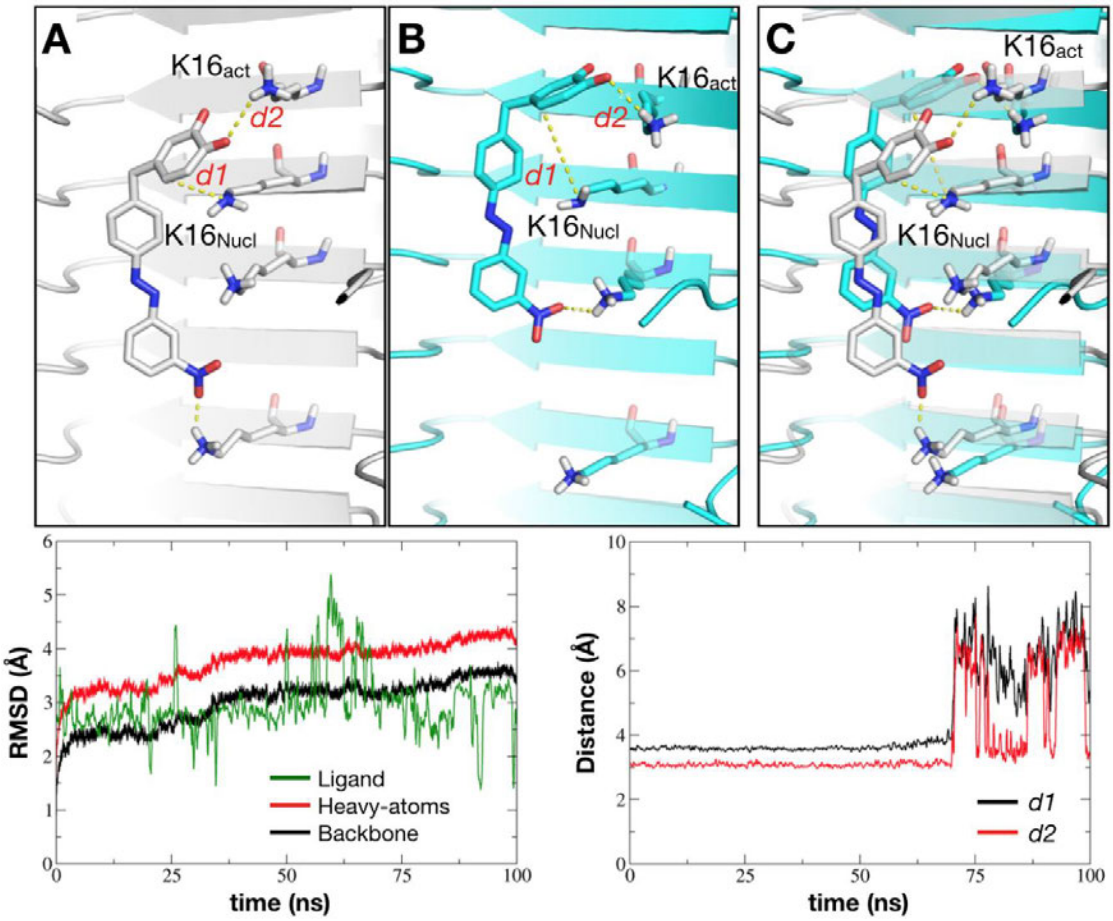

Figure S1. Initial (**A**), final (**B**) complex and their superposition (**C**) from one of the three MD simulation of **8c** with Aβ42. RMSD for protein backbone (in black), heavy atoms (in red) and for the ligand (in green) and distance analysis for Cβ•••NH_2-K16$_{Nucl}$ (*d1*) and C=O•••NH_3-K16$_{Act}$ (*d2*). No data was reported for the other two simulated systems since the ligand left the cavity during the unrestrained MD simulation.

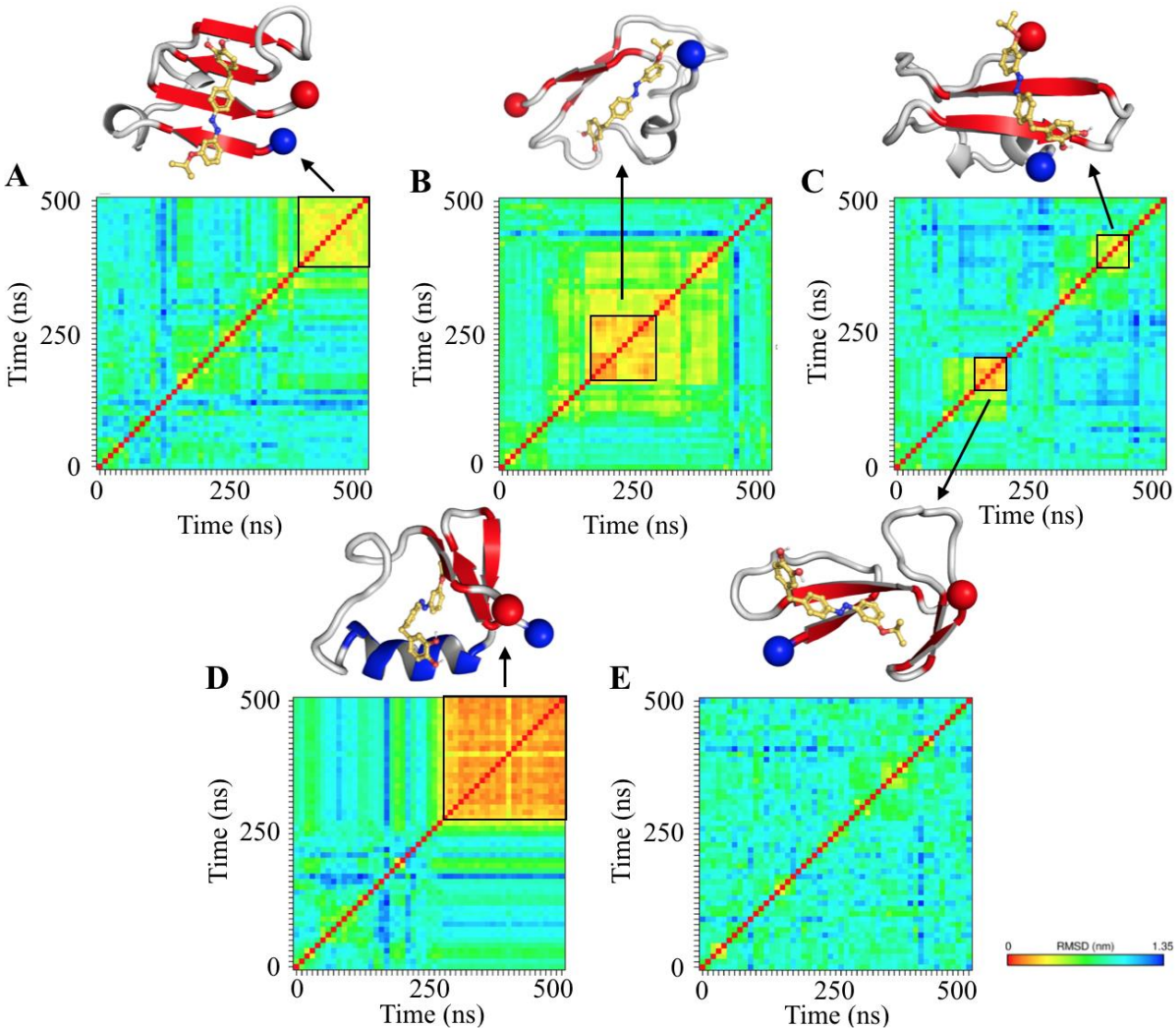

Figure S2. 2D-RMS analysis for the first five T-replicas of Aβ42$_{mon}$-**8f**. representative conformers relative to the most populated clusters are also reported. Colour code for the Aβ42$_{mon}$ sequence is set according to the secondary structure analysis shown in **Figure 2** of the main text while **8f** is reported as yellow sticks. N- and C-terminal edges of the Aβ42$_{mon}$ were reported as blue and red spheres, respectively.

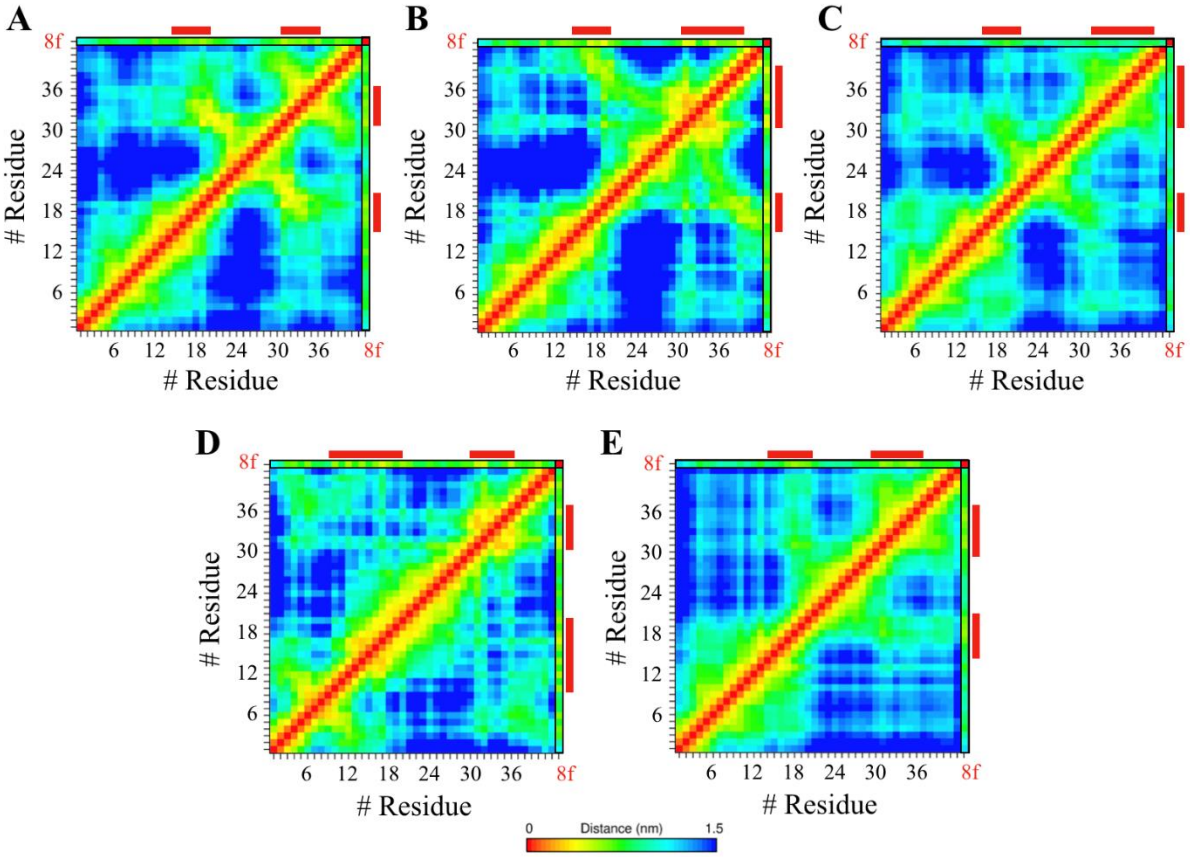

Figure S3. Contact map for the five T-replicas of the Aβ42$_{mon}$-**8f** complex. Contacts between Cβ atoms of Aβ42$_{mon}$ and compound **8f** are marked by red rectangles.

2. HPLC-Chromatograms for purity control

(E)-4-(4-(phenyldiazenyl)benzyl)benzene-1,2-diol ***(8a)***

<Chromatogram>

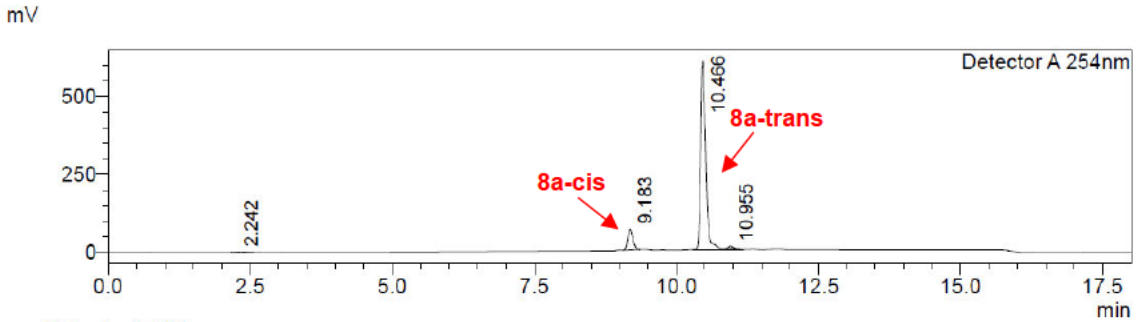

Detector A 254nm

Peak#	Ret. Time	Area	Height	Area%
1	2.242	23546	1450	0.546
2	9.183	420138	66690	9.737
3	10.466	3822013	603335	88.580
4	10.955	49057	8647	1.137
Total		4314754	680122	100.000

(E)-4-(4-((3-ethoxyphenyl)diazenyl)benzyl)benzene-1,2-diol ***(8b)***

<Chromatogram>

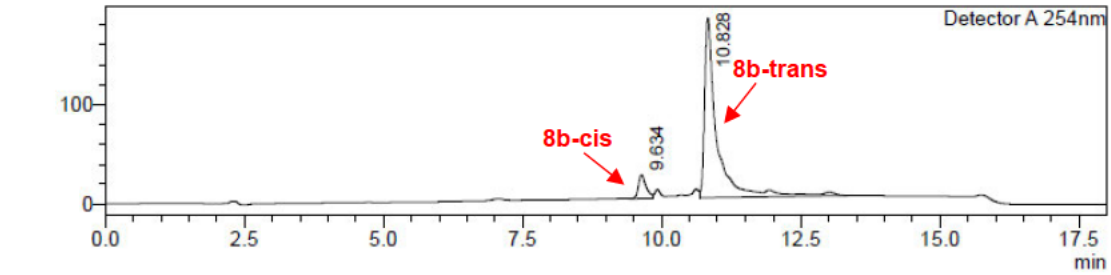

Detector A 254nm

Peak#	Ret. Time	Area	Height	Area%
1	9.634	228633	23643	7.728
2	10.828	2729853	180339	92.272
Total		2958487	203982	100.000

(E)-4-(4-((3-nitrophenyl)diazenyl)benzyl)benzene-1,2-diol ***(8c)***

<Chromatogram>

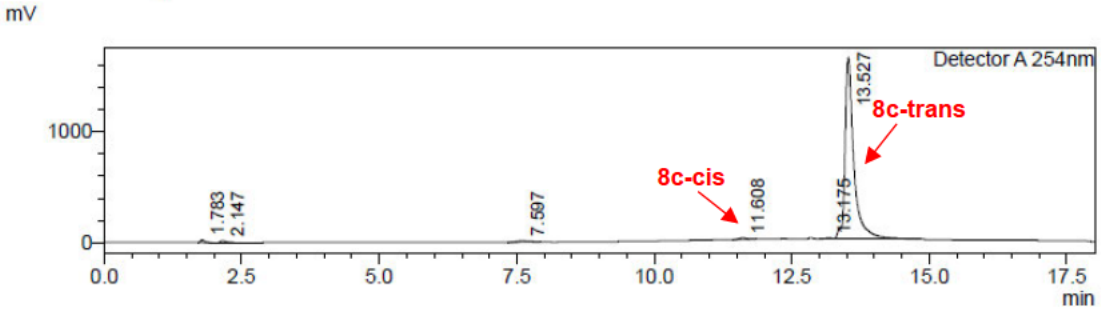

Detector A 254nm

Peak#	Ret. Time	Area	Height	Area%
1	1.783	108048	23313	0.567
2	2.147	139768	19661	0.734
3	7.597	194872	11746	1.023
4	11.608	124705	12670	0.655
5	13.175	116605	11775	0.612
6	13.527	18363965	1633112	96.409
Total		19047961	1712277	100.000

(E)-4-(4-((3-chlorophenyl)diazenyl)benzyl)benzene-1,2-diol ***(8d)***

<Chromatogram>

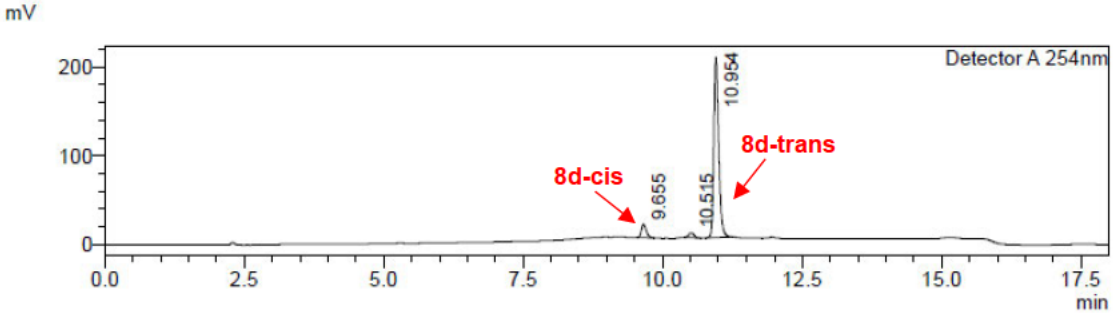

Detector A 254nm

Peak#	Ret. Time	Area	Height	Area%
1	9.655	91003	15057	6.737
2	10.515	35427	5431	2.623
3	10.954	1224333	202168	90.640
Total		1350763	222657	100.000

(E)-4-(4-((3-methoxyphenyl)diazenyl)benzyl)benzene-1,2-diol ***(8e)***

<Chromatogram>

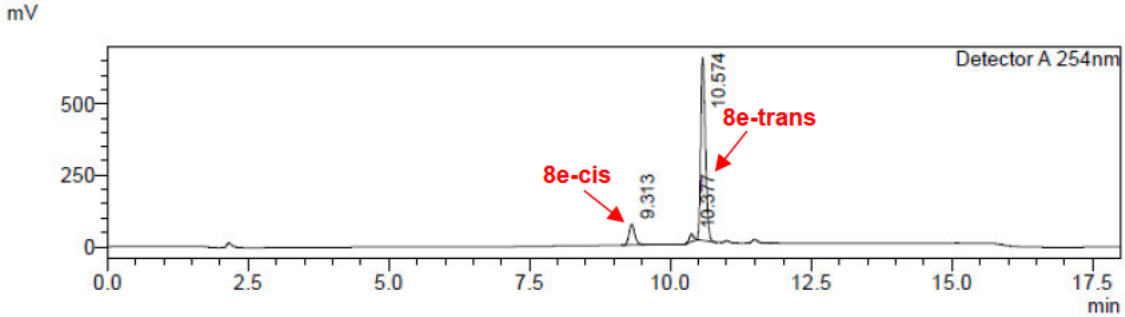

Detector A 254nm

Peak#	Ret. Time	Area	Height	Area%
1	9.313	524822	71424	11.939
2	10.377	142458	26276	3.241
3	10.574	3728487	635583	84.820
Total		4395768	733282	100.000

(E)-4-(4-((3-isopropoxyphenyl)diazenyl)benzyl)benzene-1,2-diol ***(8f)***

<Chromatogram>

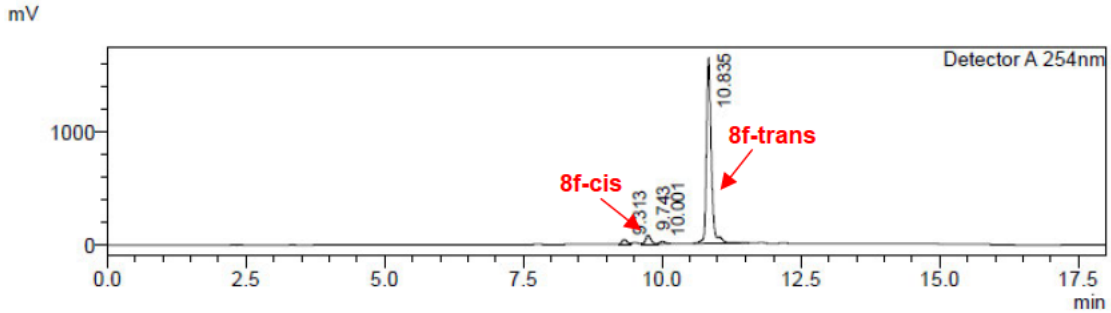

Detector A 254nm

Peak#	Ret. Time	Area	Height	Area%
1	9.313	238187	41003	2.162
2	9.743	483583	76927	4.390
3	10.001	132954	20649	1.207
4	10.835	10160992	1630878	92.241
Total		11015717	1769456	100.000

(E)-1-(4-(3,4-dimethoxybenzyl)phenyl)-2-phenyldiazene ***(8g)***

<Chromatogram>

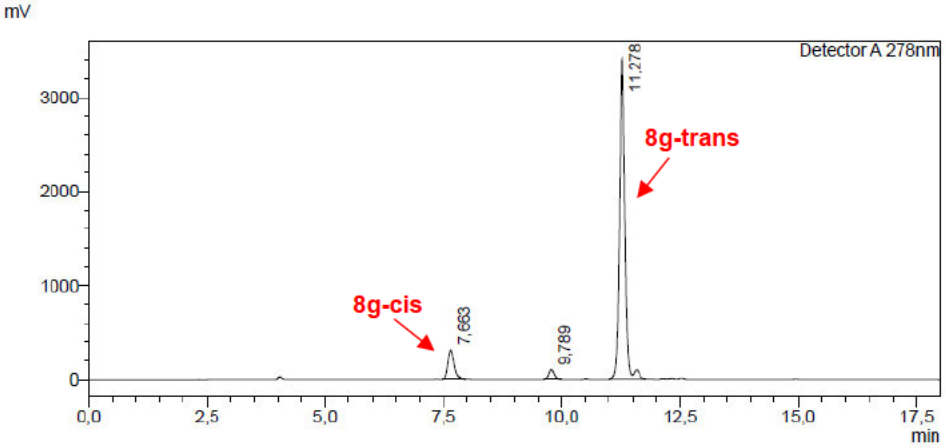

Detector A 278nm

Peak#	Ret. Time	Area	Height	Area%
1	7,663	2688643	310342	9,351
2	9,789	738512	98967	2,569
3	11,278	25324315	3390073	88,080
Total		28751470	3799381	100,000

3. Transmission Electron Microscopy

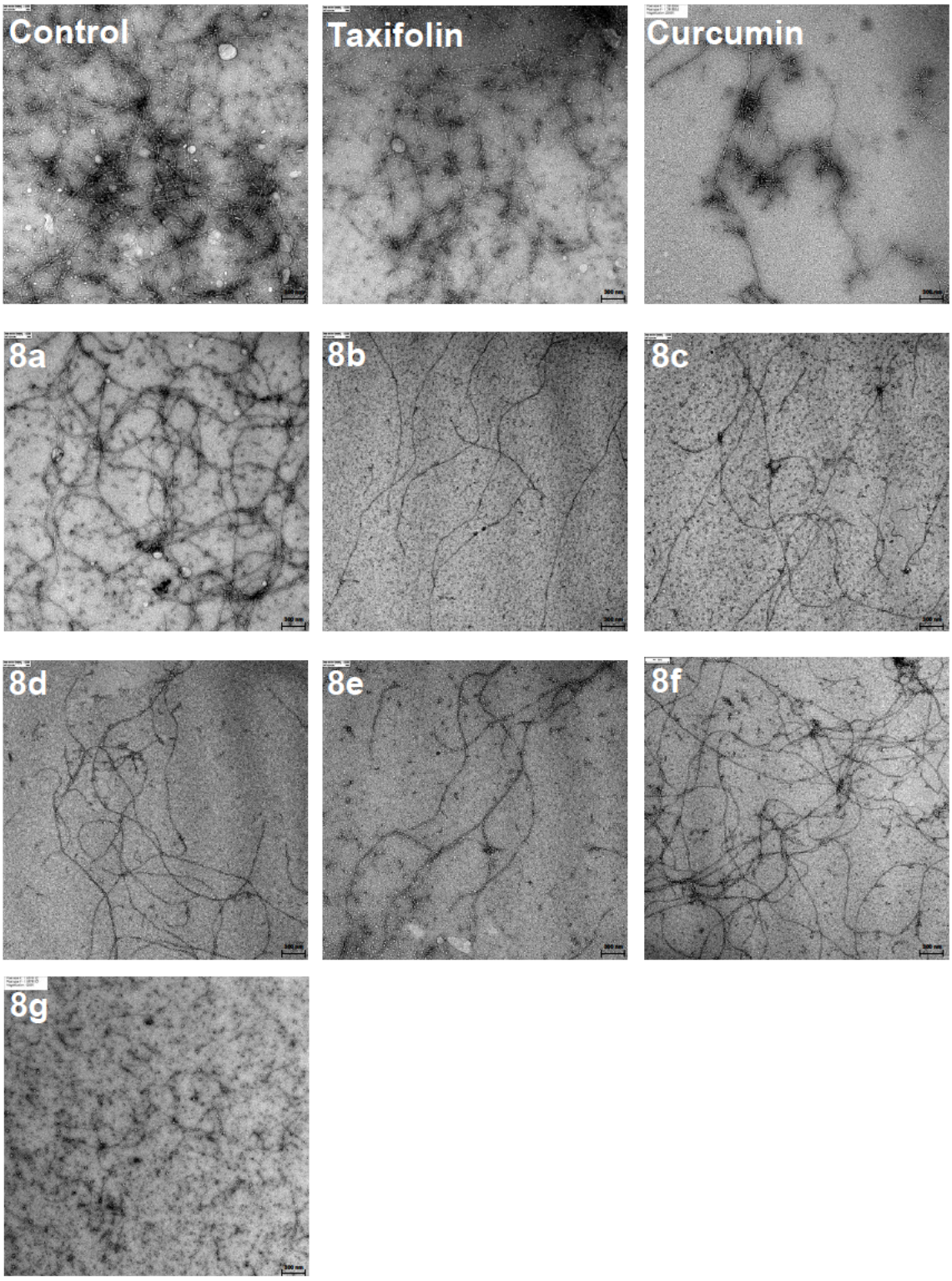

Figure S4. TEM analysis of the inhibitory effect on Aβ42. The Aβ monomer (100 μM) was incubated at 37°C in PBS for 24 h with or without 50 μM of the respective compound. Scale bar 300 nm.

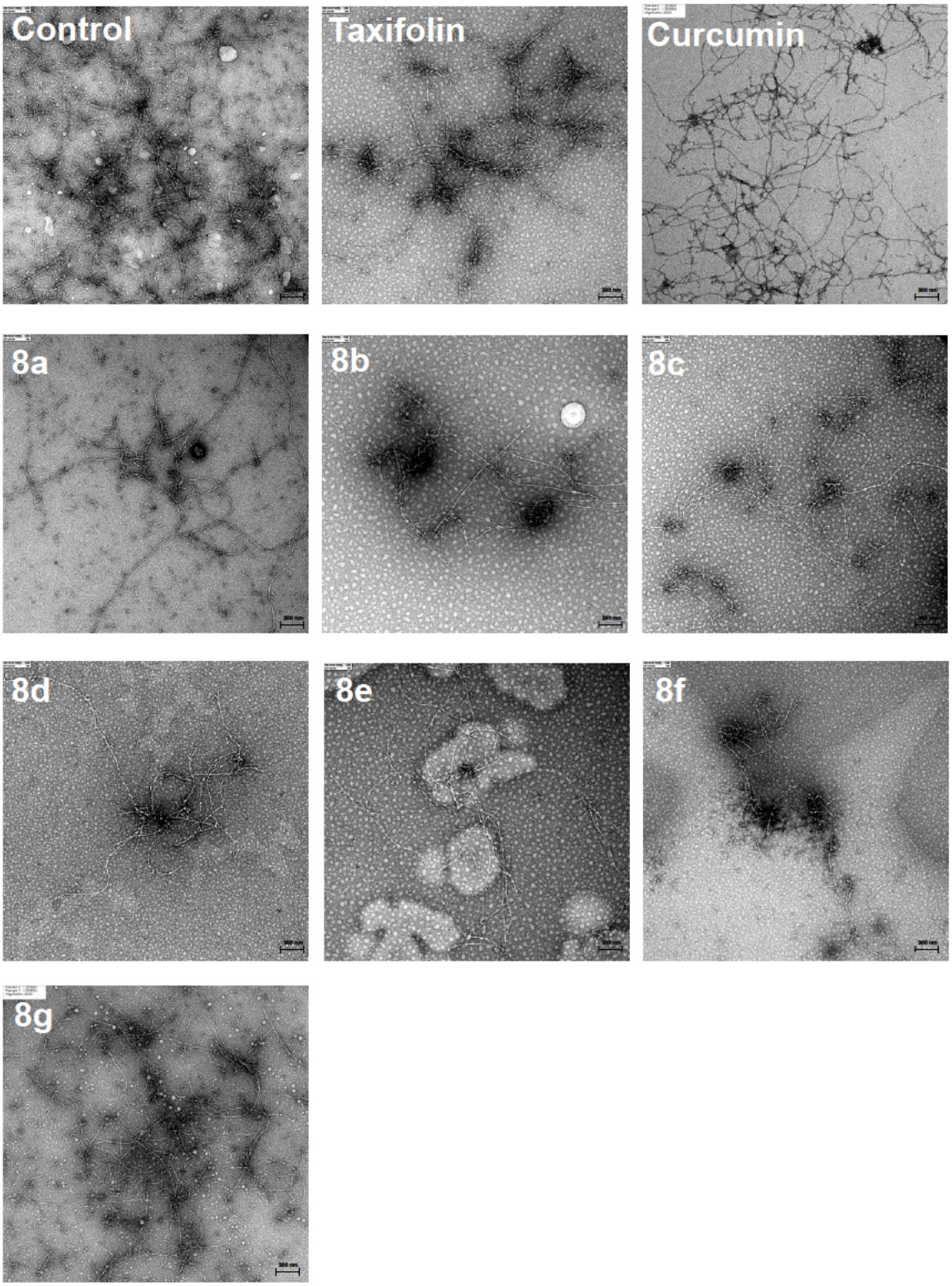

Figure S5. TEM analysis of the inhibitory effect on Aβ42. The Aβ monomer (100 μM) was incubated at 37°C in PBS for 24 h with or without 10 μM of the respective compound. Scale bar 300 nm.

4. Anti-Inflammatory Effect on BV-2 cells

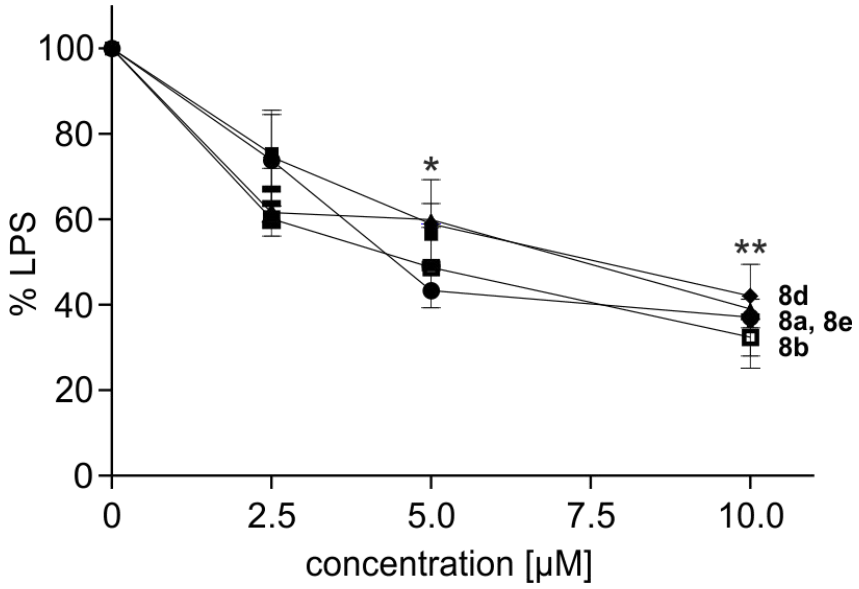

Figure 6: Effect of compounds **8a**, **8b**, **8d** and **8e** on the production of NO as inflammation marker. BV-2 cells were treated with 50 ng/mL LPS alone or with the respective compound. NO was determined by the Griess assay in the supernatant. Data is presented as means ± SEM of three independent experiments and results refer to LPS treated cells. Statistical analysis was performed using One-Way ANOVA followed by Dunnett's multiple comparison posttest using GraphPad Prism 5. Level of significance: ** $p < 0.01$, *$p < 0.05$.